



City Research Online

City, University of London Institutional Repository

Citation: Mylonas, N. (2012). Development of positioning devices for MRI-guided high intensity focused ultrasound (HIFU) for abdominal, thyroid and brain, tumours. (Unpublished Doctoral thesis, City University London)

This is the unspecified version of the paper.

This version of the publication may differ from the final published version.

Permanent repository link: <https://openaccess.city.ac.uk/id/eprint/2417/>

Link to published version:

Copyright: City Research Online aims to make research outputs of City, University of London available to a wider audience. Copyright and Moral Rights remain with the author(s) and/or copyright holders. URLs from City Research Online may be freely distributed and linked to.

Reuse: Copies of full items can be used for personal research or study, educational, or not-for-profit purposes without prior permission or charge. Provided that the authors, title and full bibliographic details are credited, a hyperlink and/or URL is given for the original metadata page and the content is not changed in any way.

City Research Online:

<http://openaccess.city.ac.uk/>

publications@city.ac.uk

Development of positioning devices for MRI-guided high intensity focused ultrasound (HIFU) for abdominal, thyroid and brain, tumours

A thesis submitted to the graduate faculty in partial fulfilment of
the requirements for the Degree of Doctor of Philosophy in
Biomedical Engineering

Nicos Mylonas

School of Engineering and Mathematical Sciences
Electronic and Electrical Engineering

City University London

October 2012

Table of Contents

LIST OF FIGURES.....	IV
LIST OF TABLES.....	IX
ABBREVIATIONS AND SYMBOLS USED	XIV
1 INTRODUCTION.....	1
1.1 AIMS AND OBJECTIVES	3
1.2 CHAPTERS OUTLINE.....	4
2 ABDOMINAL AND THYROID TUMOURS.....	6
2.1 LIVER TUMOURS	6
2.1.1 <i>Non-cancerous liver tumours</i>	7
2.1.2 <i>Cancerous liver tumours</i>	7
2.1.3 <i>Liver cancer statistics</i>	11
2.2 KIDNEY TUMOURS.....	11
2.2.1 <i>Non-cancerous kidney tumours</i>	12
2.2.2 <i>Cancerous kidney tumours</i>	14
2.2.3 <i>Kidney cancer statistics</i>	18
2.3 PANCREATIC TUMOURS.....	19
2.3.1 <i>Pancreatic Cancers</i>	20
2.3.2 <i>Pancreatic cancer statistics</i>	23
2.4 THYROID TUMOURS.....	24
2.4.1 <i>Thyroid benign and malignant tumours</i>	25
2.5 BRAIN TUMOURS	29
2.5.1 <i>Benign and malignant and metastatic brain tumours</i>	31
2.6 CONCLUSION	34
3 HIGH INTENSITY FOCUSED ULTRASOUND (HIFU) TECHNOLOGY	35
3.1 ULTRASOUND THEORY AND ULTRASOUND TRANSDUCERS	35
3.2 HIFU TRANSDUCERS, PHYSICS AND TECHNOLOGY OF HIFU	37
3.3 UTILIZATION OF MRI FOR THE GUIDANCE OF THE THERAPEUTIC ULTRASOUND.....	42
3.4 THERAPEUTIC ULTRASOUND AND HIFU	44
3.4.1 <i>How HIFU can be used to treat tumours</i>	45
3.4.2 <i>MRI compatible HIFU Transducers and safety issues</i>	46
3.5 HISTORY OF THERAPEUTIC HIFU	47
4 APPLICATIONS OF HIFU IN MEDICINE.....	52
4.1 CURRENT STATE OF THE ART OF HIFU FOR TREATING ABDOMINAL TUMOURS AND THYROID TUMOURS.....	52
4.1.1 <i>Disadvantages of the current methods for treating abdominal tumours</i>	54
4.2 ADVANTAGES OF HIFU	55
4.3 LIMITATIONS AND DRAWBACKS OF HIFU	57
4.4 MAGNETIC RESONANCE GUIDED HIGH INTENSITY FOCUSED ULTRASOUNDS (MRGHIFU) SYSTEMS.....	57
4.5 IMAGE GUIDED ROBOTS AND HIFU SYSTEMS WITH MRI GUIDANCE	59
4.6 EXISTING IMAGING POSITIONING DEVICES	59
5 DEVELOPMENT OF HIFU SYSTEM WITH MRI GUIDANCE.....	64
5.1 DESIGN CRITERIA AND REQUIREMENTS.....	64
5.2 HIFU/ MRI SYSTEM.....	65
5.2.1 <i>HIFU system</i>	65
5.2.2 <i>Positioning device (Robot)</i>	68
5.2.3 <i>Cavitation detector</i>	74
5.2.4 <i>MRI compatible camera</i>	74
5.2.5 <i>Software</i>	74
5.3 ADVANTAGES AND LIMITATIONS OF THE THREE VERSIONS OF POSITIONING DEVICES.....	75
6 DEVELOPMENT OF THE POSITIONING DEVICE VERSION 1	78

6.1	DESCRIPTION OF THE POSITIONING DEVICE – 1 ST VERSION.....	78
6.2	DESIGN AND IMPLEMENTATION OF POSITIONING DEVICE VERSION 1	79
6.2.1	<i>Parts and materials used for the positioning device</i>	80
6.2.2	<i>Description of the operation of the positioning device</i>	86
6.2.3	<i>Coupling mechanism</i>	88
6.3	CONCLUSION AND DISCUSSION	89
7	DEVELOPMENT OF THE POSITIONING DEVICE VERSION 2	91
7.1	PARTS AND SPECIFICATIONS OF POSITIONING DEVICE VERSION 2	92
7.2	DESIGN AND DEVELOPMENT OF THE 2 ND VERSION OF THE POSITIONING DEVICE	93
7.3	CONCLUSION AND DISCUSSION	99
8	DEVELOPMENT OF THE POSITIONING DEVICE VERSION 3	101
8.1	PARTS AND SPECIFICATIONS OF POSITIONING DEVICE VERSION 3	102
8.2	DESIGN AND DEVELOPMENT OF THE 3 RD VERSION OF THE POSITIONING DEVICE	103
8.3	CONCLUSION AND DISCUSSION	114
9	SOFTWARE AND PERIPHERAL DEVICES OF A HIFU SYSTEM DEVELOPMENT.....	116
9.1	SOFTWARE DEVELOPMENT AND SETUP OF THE PERIPHERAL DEVICES USED FOR CAPTURING TEMPERATURE, PHOTOGRAPHS AND VIDEO DISPLAYED IN THE USER INTERFACE.....	117
9.2	DEVELOPMENT OF THE DIGITAL THERMOMETER	121
9.3	THE COMPLETE END-USER INTERFACE.....	124
9.4	CONCLUSION	126
10	EVALUATION OF THE MRI COMPATIBLE POSITIONING DEVICES.....	128
10.1	MEASURING THE EFFICIENCY OF THE HIFU TRANSDUCERS	128
10.2	<i>IN VITRO AND IN VIVO EXPERIMENTS TO EVALUATE THE MRI GUIDED HIFU SYSTEM</i>	129
10.2.1	<i>Material and methods</i>	129
10.2.2	<i>In vitro experiments</i>	130
10.2.3	<i>In vivo experiments</i>	131
10.2.4	<i>Evaluation of MRI compatibility</i>	131
10.2.5	<i>Results</i>	131
10.2.6	<i>Discussion</i>	136
10.2.7	<i>Conclusion</i>	137
10.3	TESTING THE MRI COMPATIBILITY OF ROBOT V2 ON PHANTOM.....	138
10.3.1	<i>Material and methods</i>	138
10.3.2	<i>Conclusion</i>	140
10.4	TEST MRI COMPATIBILITY OF POSITIONING DEVICE VERSION 3.....	140
10.4.1	<i>Material and methods</i>	140
10.4.2	<i>Conclusion</i>	142
10.5	ABLATE A PORCINE MUSCLE TISSUE USING THE POSITIONING DEVICE VERSION 3.	142
10.5.1	<i>Material and methods</i>	142
10.6	VISUALIZE THE COUPLING METHOD OF ROBOT V3 USING MRI.	144
10.6.1	<i>Material and methods</i>	144
10.6.2	<i>Conclusions</i>	146
10.7	MRI COMPATIBLE CAMERA USING GEL.....	146
10.7.1	<i>Material and methods</i>	146
10.7.2	<i>Conclusions</i>	148
11	EXPERIMENTS USING HIFU/MRI SYSTEM	149
11.1	HIFU ABLATION OF PORCINE LIVER GUIDED BY MRI	149
11.1.1	<i>In vitro experiments</i>	149
11.1.2	<i>Experiments on liver</i>	150
11.2	EVALUATION OF FAST SPIN ECHO MRI SEQUENCE FOR AN MRI GUIDED HIGH INTENSITY FOCUSED ULTRASOUND SYSTEM FOR <i>IN VIVO</i> RABBIT LIVER ABLATION.....	161
11.2.1	<i>Introduction</i>	161
11.2.2	<i>Methods</i>	163
11.2.3	<i>In vivo experiments</i>	164
11.2.4	<i>Results</i>	165

11.2.5	<i>Discussion</i>	168
11.3	MRI MONITORING OF LESIONS CREATED AT TEMPERATURE BELOW THE BOILING POINT AND OF LESIONS CREATED ABOVE THE BOILING POINT USING HIGH INTENSITY FOCUSED ULTRASOUND.	170
11.3.1	<i>Materials and Methods</i>	172
11.3.2	<i>In vitro experiments</i>	174
11.3.3	<i>In vivo experiments</i>	174
11.3.4	<i>Results</i>	175
11.3.5	<i>Discussion</i>	182
12	CONCLUSION AND FUTURE ENHANCEMENTS	184
12.1	FUTURE ENHANCEMENTS	188
13	APPENDIX	191
13.1	JOURNAL AND CONFERENCES PUBLICATIONS	191
13.1.1	<i>Journal papers</i>	191
13.1.2	<i>Conference papers</i>	192
13.2	ANIMAL EXPERIMENTS ISSUES	193
13.2.1	<i>Licenses from Ministry of Agriculture, animal services</i>	195
13.3	CANCER STATISTICS	197
13.3.1	<i>Liver cancer Statistics</i>	197
13.3.2	<i>Kidney cancer statistics</i>	198
13.3.3	<i>Pancreatic cancer statistics</i>	199
13.3.4	<i>Thyroid cancer statistics</i>	201
13.3.5	<i>Brain and other nervous system</i>	202
US Mortality	203
13.3.6	<i>World Health Organization: International Agency for research on Cancer; World statistics for liver, pancreas, kidney and thyroid cancer</i>	204
13.4	SOFTWARE CODING	208
14	REFERENCES AND BIBLIOGRAPHY	237

List of figures

Figure		Page
2.1	The Biliary system. The figure shows the liver location in the abdominal cavity.	7
2.2	The Anatomy of the Kidney	11
2.3	The Front View of Urinary Tract. The figure shows the kidneys' location in the abdominal cavity.	12
2.4	The Anatomy of the Pancreas	19
2.5	The anatomy of thyroid. The figure shows the thyroid location.	24
2.6	The brain is composed of three parts, the cortex the brain stem the basal ganglia the cerebellum	30
2.7	The brain is divided into several lobes, the frontal, the parietal, the temporal and occipital	30
3.1	A cross-section of an ultrasonic transducer	37
3.2	A diagram of a spherical HIFU Transducer with focal length of 100mm.	39
3.3	A photo of a typical HIFU Transducer.	39
3.4	How the ablation causes necrosis of tissue at the targeted area.	40
5.1	Block diagram of high intensity focused ultrasound (HIFU) system with the MRI guidance. This diagram shows the arrangement of the devices used in the HIFU system	66
5.2	Setup of the actual devices used for the HIFU system with the MRI guidance (The positioning device shown is the third version)	67
5.3	Diagram of the mechanism of the ultrasonic motor	69
5.4	Traveling Wave Formation	69
5.5	Inside structure of USM (USR60-S4)	70
5.6	A photo of piezoelectric ultrasonic motor by Shinsen USR60E3N	70
5.7	A photo of dedicated driver for Shinsei USR60 series, Shinsei D6060E.	71
5.8	Basic connection diagram of the dedicated driver for Shinsei USR60 series, Shinsei D6060E	71
5.9	Wiring diagram of the motor drivers for 3 degrees of freedom positioning device.	72
5.10	The photograph shows the cavitation detector.	74
5.11	The photograph shows the MRI compatible camera	75
6.1	Corner part used to support the rods and the pulleys. This part is also used to support the different stages of the robot.	80
6.2	The brass rod used to support and guide the surface plates of the stages X, Y and Z.	81
6.3	Position of the brass screw which is used to mount the rod on the angular part.	81
6.4	The brass screws used to mount the parts of the positioning device.	81
6.5	Brass rod mounted on two angular parts which are attached on the base of the positioning device.	82
6.6	Diagrams and photos of surface plates of the base, X-Stage and Y-Stage.	83
6.7	Pulleys, timing belt, and the piezoelectric ultrasonic motor attached on the base with an angular part which is driving the timing belt to achieve the motion of a surface plate of the X-axis.	84
6.8	The pulleys on the other end of the timing belt hold with two angular parts.	84
6.9	Top view of the base with the brass rods that support and guide the X-axis plate. The timing belt is mounted on the X-axis plate (not shown here) with a brass screw.	85
6.10	The angular parts attached at the bottom of the X-axis plate are sliding along the brass rod which acts as a support and guide.	85

6.11	Drawings of the various mechanical stages of the positioning device.	87
6.12	Schematic of the robot showing all of its stages.	88
6.13	Photograph of the complete positioning device.	88
6.14	Coupling methods, A. <i>In vitro</i> or <i>in vivo</i> (tissue outside the water container). B. <i>In vitro</i> (tissue inside the water container).	89
7.1	CAD design and photograph of the base of the positioning device: A. CAD drawing, B. actual photo (with zooming in the guide).	93
7.2	A. CAD design of the X-axis plate and B. photograph of the X-axis plate base of the positioning device.	94
7.3	A photograph of the groove and the guide used for the motion of all axis plates.	94
7.4	A. CAD drawing of the X-axis plate mounted on the base and B. photograph of the X-axis plate mounted on the base.	95
7.5	A. the CAD drawing of the Y-axis plate of the positioning device and B. a photograph of the Y-axis plate of the positioning device.	95
7.6	A. the 3D drawing of the base and the X and Y-axis plates assembled together and B. the corresponding photograph of the base, X and Y-axis plates. The piezoelectric ultrasonic motor shown between the X and Y plates drives the Y-axis plate.	96
7.7	A. the 3D drawing of the holder of the Z-axis plate, the Z-axis plate with the PUM motor which moves the Z-axis plate and B. a photograph of the actual part of 7.7.A as developed and assembled.	96
7.8	A. the CAD drawing of the HIFU transducer holder attached on the Z-axis plate and B. a photograph of the HIFU transducer holder attached on the Z-axis plate.	97
7.9	A. the CAD drawing of the top plate of the positioning device and B. a photograph of the top plate of the positioning device. The piezoelectric motor shown moves the X-axis plate.	97
7.10	A. the final 3D drawing and B. the developed positioning device.	98
7.11	A photograph of the positioning device inside the gantry of the MRI scanner with a phantom gel target inside the tank which is filled with degassed water.	98
7.12	A. the base of the positioning device can be easily modified and B. the device as attached on the top of the gantry of the MRI scanner.	89
8.1	A. the CAD design of the base of the positioning device with the PUM motor attached to it and B. a photograph of the produced base of the positioning device with zooming in the groove in which the X-axis plate will slide in. The brass pinion attached to the PUM motor will drive the X-axis plate (back – forward motion).	104
8.2	A. the CAD design of the X-axis plate responsible for the back and forward motion and B. a photograph of the formed X-axis plate with zooming on the male guide which will slide in the corresponding groove of the base. The brass pinion shown here, will drive the Y-axis plate.	104
8.3	A. the CAD drawing of the base with the X-axis plate attached and B. a photograph of the base together with the X-axis plate. The X-axis plate will slide back and forward within the groove of the base. The piezoelectric ultrasonic motor shown here on the top of the X-axis plate is the motor that drives the Y-axis plate.	105
8.4	A. the CAD design of the Y-axis plate and B. a photograph of the ABS Y-axis plate.	106
8.5	A. the 3D drawing of the base and the X and Y-axis plates assembled together and B. the corresponding photograph of the ABS base, X and Y-axis plates.	106
8.6	A. the 3D drawing of the holder of the Z-axis plate with the PUM motor which moves the Z-axis plate and B. a photograph of corresponding ABS Z-axis holder and the PUM motor with the brass pinion that drives the Z-axis plate.	106
8.7	A. the CAD drawing of the Z holder attached on the support holder of the Y-axis plate and B. a photograph of corresponding ABS Z-axis holder attached on the Y-axis plate.	107

8.8	A. the CAD extension of the base that hosts the coupling and B. a photograph of the produced ABS extension of the base.	108
8.9	A. the CAD drawing of the base extension attached on the base of the robot and B. a photograph of the ABS base extension joined with the base of the robot.	108
8.10	A. the CAD drawing of the Z-axis plate and B. a photograph of the ABS Z-axis plate.	108
8.11	A. the CAD drawing of the Z-axis plate attached on the Z holder and B. the corresponding photograph of the ABS Z-axis plate positioned on the Z holder.	109
8.12	A. the CAD drawing of the water tank holder used for the coupling of the HIFU transducer with the targeted tumour and B. the corresponding photograph of the ABS water tank holder.	109
8.13	A. the CAD drawing of the degassed water container and B. a photograph of the acrylic glass container covered with milar bag.	110
8.14	A. the CAD drawing of the water tank holder fitted on the base extension and the water container placed inside the water tank holder and B. a photograph of the ABS water tank holder mounted on the ABS base extension and the acrylic glass container fitted inside the water tank holder.	110
8.15	A. the CAD drawing of the vertical HIFU transducer holder and B. the photograph of the corresponding ABS vertical HIFU transducer holder.	111
8.16	A. the CAD drawing of the horizontal HIFU transducer holder and B. the photograph of the corresponding ABS horizontal HIFU transducer holder.	111
8.17	A. the CAD drawing of the complete positioning device with the vertical HIFU transducer holder attached in the slot of the Z-axis plate and B. the photograph of the ABS vertical HIFU transducer holder mounted in the slot of the Z-axis plate.	112
8.18	A. the CAD drawing of the complete positioning device with the horizontal HIFU transducer holder attached in the slot of the Z-axis plate and B. the photograph of the ABS horizontal HIFU transducer holder mounted in the slot of the Z-axis plate.	112
8.19	A photograph showing how the robot can be used for brain tumours.	112
8.20	The CAD drawing of the robot inside the gantry of a typical MRI scanner.	113
8.21	A. a photograph of the robot with the MRI compatible camera outside the gantry of an MRI and B a photograph of the robot inside the gantry of an MRI scanner with the HIFU transducer immerse in the degassed water saline.	113
8.22	Photographs A and B show the robot placed in the gantry of an MRI scanner and are taken from the MRI compatible camera which is also placed in the gantry of the MRI scanner.	114
9.1	Photograph of the power supply and the three dedicated drivers (X, Y and Z)	118
9.2	Photograph of the rear panel of the enclosure that holds the dedicated drivers.	119
9.3	Photograph of the three dedicated drivers of the PUM motors mounted inside the enclosure	119
9.4	Photograph of the data acquisition board. National Instruments 6251	120
9.5	Photograph of the setup of the MR compatible camera	121
9.6	The thermocouple is connected directly to the analogue input of the data acquisition card.	121
9.7	The thermocouple is connected as shown in the diagram to the analogue input of the data acquisition card.	122
9.8	Omega thermocouple-to-analogue connector.	122
9.9	Data acquisition set up	123
9.10	The end-user interface used to capture the temperature fluctuations at the focal point of the HIFU transducer at specified time intervals.	123
9.11	Part of the temperature file stored during an experiment.	124
9.12	The user interface for the software of the HIFU system.	125

10.1	The photograph shows the ultrasound power meter, a device used to measure the ultrasound power of the transducers.	128
10.2	A. an MRI image of phantom without the presence of the motor. B. an MRI image of phantom with the presence of the motor. C an MRI image of the subtraction of the two images showing no shift.	132
10.3	Lesions created in pig kidney demonstrating the excellent repeatability of the positioning device.	132
10.4	Large lesion in pig kidney <i>in vitro</i> by moving the transducer in grid formation (8 X 8) (top view)	133
10.5	A Axial MR images of HIFU ablation using T2-weighted FSE (TE=32ms) pulse sequence. B Photograph after slicing.	133
10.6	MR images showing the focal beam during a 3 X 3 scanning using low intensity ultrasound using T1 weighted FSPGR.	134
10.7	MR images (in plane perpendicular to the transducer beam) of large lesions (full coverage of the intended target) using T2-Weighted FSE with TE = 32ms. The spatial average intensity was 1,500 W/cm ² for 5s	135
10.8	MR images (in plane perpendicular to the transducer beam) of large lesions (partial coverage of the intended target) using T2-Weighted FSE with TE = 32ms. The spatial average intensity was 2,000 W/cm ² for 5s	136
10.9	Photograph of the positioning device version 2 in the gantry of the MRI scanner. The gel phantom is immersed in the degassed water saline.	138
10.10	The MRI image shows the HIFU transducer, the phantom gel and the tank filled with degassed water saline using T2 W FSE.	139
10.11	The MRI image shows the HIFU transducer, the phantom gel and the tank filled with degassed water saline using FSPGR. The red arrow indicates the focal spot A. at position 1 B. at position 2 and C at position 3.	139
10.12	A Photograph of the positioning device version 3 on the table of the MRI scanner, B the positioning device version 3 in the gantry of the MRI scanner.	141
10.13	A the MRI image shows the HIFU transducer, and the phantom gel this image was captured using T1 W FSE, B the MRI image shows the phantom gel and the tube passes through the gel. The image was also captured using T1 W FSE.	141
10.14	The MRI image shows the phantom gel mounted within the plastic holders. The image captured using FSPGR in a plane inside the gel.	142
10.15	Photograph shows the positioning device version 3 with the porcine muscle placed under the tank filled with degassed water saline.	143
10.16	Exposure A, the cross section – depth	144
10.17	Exposure B, A is the top view of the lesion, B cross section showing the depth of the lesion.	144
10.18	A photograph of the positioning device on the table of the MRI with the tank filled with degassed water saline and the gel phantom at the bottom of the tank, B photograph of the positioning device inside the gantry of the MRI scanner.	145
10.19	An MRI image showing the coupling between the milar bag which is filled with degassed water saline and the gel phantom.	145
10.20	Photograph of the experiment setup showing the positioning device version 3 and the MRI compatible camera.	146
10.21	Photograph of the positioning device version 3 inside the gantry of the MRI scanner, taken from the MRI compatible camera.	147
10.22	Photograph of the MRI Gel inside the gantry of the MRI scanner taken from the MRI compatible camera	147
10.23	A MRI image with T1 FSE with the MRI camera in the gantry of the MRI scanner, B MRI image with T1 FSE without the MRI compatible camera.	148
11.1	A. show a photograph of large lesion created in the phantom at a plane perpendicular to the transducer beam axis. B. shows the corresponding photograph in a parallel plane. C. shows the MRI image of the result of A using T2–W FSE (for MRI parameters see Table 10.1, row 2), and D. shows the same result using T1-W FSE.	149

11.2	MRI guided HIFU system with cavitation detection system using the actual photos of the instruments.	151
11.3	POC as a function of in situ spatial average intensity for 5s pulse duration in liver.	154
11.4	A CNR between lesion and liver plotted against TR using T1-weighted FSE, B CNR between lesion and liver plotted against TE using T2-weighted FSE, C CNR between lesion and liver plotted against TR using T1-weighted FSPGR.	155
11.5	A MR images (in a plane perpendicular to the transducer beam) of large lesion using T2-weighted FSE showing cavitation lesions, B cavitation map of the above large lesion, C typical frequency spectrum acquired during the occurrence of a cavitation lesion.	156-157
11.6	MR images (in a plane parallel to the transducer beam) of large lesion using A T2-weighted FSE with TE=15ms. B Photograph after slicing.	157
11.7	Large lesion in liver <i>in vivo</i> using T1-w FSE	166
11.8	Photograph of the lesion shown in Figure 10.30	166
11.9	CNR vs TR	167
11.10	MRI image of the lesion of Figure 10.30 using T1W FSE	167
11.11	MRI images of the same lesion as in Figure 10.30 using T2W FSE.	168
11.12	CNR vs TE for the MRI image shown in 10.35	168
11.13	MR images (in a plane perpendicular to the beam) of four lesions (intensities 1000, 1500, 2000 and 2500 W/cm ²) in kidney <i>in vitro</i> using A. T1-weighted FSE, B. T2-weighted FSE, C. T1-weighted FSPGR. With intensities above 2000 W/cm ² the lesions exhibit boiling activity. The discrimination between boiling and non-boiling lesion is best monitored using T2-W FSE.	176
11.14	MR images (in a plane parallel to the beam) of 3 lesions in kidney <i>in vitro</i> using a) T1-weighted FSE, b) T2-weighted FSE, c). T1-weighted FSPGR. With intensities above 2000 W/cm ² the lesions exhibit boiling activity. The discrimination between boiling and thermal lesion is best monitored using T2-W FSE.	177
11.15	CNR vs. TE for the lesion, kidney and cavity for the lesion of Fig. 8B with intensity of 3000 W/cm ²	178
11.16	MRI image using T2-weighted FSE of 3 lesions in rabbit kidney <i>in vivo</i> at different intensities (1000, 2000, and 2500 W/cm ²) for a 5 s pulse. The lesion with intensity of 2500 W/cm ² is affected by tissue boiling	178
11.17	A. MR image (in a plane perpendicular to the beam) of large lesion in kidney <i>in vitro</i> using T1-weighted FSPGR (TR=50 ms), showing one cavitation lesion. B. Photograph of the kidney showing the cavitation lesion within the large thermal lesion, C. Frequency spectrum of the HIFU transducer exhibiting cavitation activity	179
11.18	Temperature evolution <i>in vitro</i> kidney using T1-weighted FSPGR (thermal mechanism). Each image was acquired in 5 s. a) Ultrasound is OFF b-f) applied spatial average intensity: 1000 W/cm ² (for 25 s), g-h) ultrasound is OFF	180
11.19	Temperature elevation <i>in vitro</i> kidney using T1-weighted FSPGR (boiling). a) Ultrasound is OFF b-f) applied spatial average intensity: 3500 W/cm ² (for 25 s)	181
11.20	MR image using proton density of lesion in liver created under the influence of boiling. The lesion was created using low intensity (1000 W/cm ²) for long time (30 s)	181

List of tables

Table		Page
3.1	The main historical events in the development of medical ultrasonic	49
3.2	Active companies in image guided ultrasound robotic systems	50-51
5.1	Design criteria and requirements for the development of the HIFU-MRI system.	64-65
9.1	The table above describes all the elements of the user interface of figure 9.12	125-126
11.1	Parameters used for the various MRI pulse sequences.	160
11.2	Parameters used for the various MRI pulse sequences	177
11.3	Recommended pulse sequences for discriminating between a) normal and thermal lesions and b) normal tissue, lesions created with temperature below boiling and lesions created with temperature above boiling	183
13.1	Incidence rates by race of cancer of the liver and intrahepatic bile duct.	198
13.2	Death rates by race of cancer for the liver and intrahepatic bile duct.	199
13.3	Incidence rates by race of cancer for the kidney and renal pelvis in 2009	200
13.4	Death rates by race of cancer for kidney and renal pelvis in 2009.	200
13.5	Incident rates by race of pancreatic cancer 2009.	201
13.6	Death rates by race of pancreatic cancer 2009.	201
13.7	Incident rates by race of thyroid cancer 2009	202
13.8	Death rates by race of thyroid cancer 2009	203
13.9	Incident rates by race of brain and nervous system 2009	204
13.10	Estimated incidence, mortality and 5-year prevalence: Liver Cancer.	206
13.11	Estimated incidence, mortality and 5-year prevalence: Pancreatic Cancer.	206
13.12	Estimated incidence, mortality and 5-year prevalence: Kidney Cancer	206
13.13	Estimated incidence, mortality and 5-year prevalence: Thyroid Cancer.	207
13.14	Estimated incidence, mortality and 5-year prevalence: Brain and nervous system Cancer.	207
13.15	Summary cancer statistics.	207-208

Acknowledgements

Sincere thanks to my principal supervisor Dr P. Kyriacou for his on-going support and guidance. I truly and appreciate his patience and understanding.

I am more than grateful and I truly appreciate the support and help from my external supervisor Dr C. Damianou, who gave me the idea of this research and guidance and support throughout the completion of this report.

Many thanks to my friends and colleagues Mr V. Hatdisavvas, Mr A. Kouppis for their help and support and they were always there ready to help me without any price.

Finally I appreciate the help and support of Mr Kleanthis Ioannides who patiently spent many hours in front of the MRI monitor to achieve the best results in our experiments.

DECLARATION FORM



THESIS DEPOSIT AGREEMENT

COVERED WORK

I Nicos Mylonas-Ariou Pagou 11, 4042, Yermasoyia, Lemesos, Cyprus ,“the Depositor”, would like to deposit “**Development of positioning devices for MRI-guided high intensity focused ultrasound (HIFU) for abdominal, thyroid and brain, tumours**”, hereafter referred to as the “Work”, in the City University Institutional Repository and agree to the following:

NON-EXCLUSIVE RIGHTS

Rights granted to the City University Institutional Repository through this agreement are entirely non-exclusive and royalty free. I am free to publish the Work in its present version or future versions elsewhere. I agree that the City University Institutional Repository administrators or any third party with whom the City University Institutional Repository has an agreement to do so may, without changing content, translate the Work to any medium or format for the purpose of future preservation and accessibility.

DEPOSIT IN THE CITY UNIVERSITY INSTITUTIONAL REPOSITORY

I understand that work deposited in the City University Institutional Repository will be accessible to a wide variety of people and institutions - including automated agents - via the World Wide Web. I also agree to an electronic copy of my thesis being included in the British Library Electronic Theses On-line System (EThOS).

I understand that once the Work is deposited, a citation to the Work will always remain visible. Removal of the Work can be made after discussion with the City University Institutional Repository, who shall make best efforts to ensure removal of the Work from any third party with whom the City University Institutional Repository has an agreement.

I AGREE AS FOLLOWS:

- That I am the author or co-author of the work and have the authority on behalf of the author or authors to make this agreement and to hereby give the City University Institutional Repository administrators the right to make available the Work in the way described above.
- That I have exercised reasonable care to ensure that the Work is original, and does not to the best of my knowledge break any UK law or infringe any third party's copyright or other Intellectual Property Right. Where I have included third party copyright material, I have fully acknowledged its source.
- The administrators of the City University Institutional Repository do not hold any obligation to take legal action on behalf of the Depositor, or other rights holders, in the event of breach of intellectual property rights, or any other right, in the material deposited.

Signature:

A handwritten signature in blue ink, appearing to read "Nicos Mylonas-Ariou", written over a horizontal line.

Abstract

This research focuses on the design and the development of three positioning devices with the ability to accurately move a High Intensity Focused Ultrasound (HIFU) transducer guided by a Magnetic Resonance Imaging (MRI) scanner in order to create discrete and overlapping lesions in biological tissue such as a brain, thyroid, kidney, liver and pancreas.

The positioning devices were designed and fabricated using construction materials selected for compatibility with high magnetic fields and fast switching magnetic field gradients encountered inside MRI scanners. The positioning devices incorporate only MRI compatible materials such as piezoelectric ultrasonic motors, plastic sheets, brass screws, plastic pulleys, brass racks and pinions and timing belts.

The MRI compatibility of the system was successfully demonstrated in a clinical high field MRI scanner. The robots have the ability to accurately move the transducer thus creating discrete and overlapping lesions in biological tissue and this was also tested successfully.

The main goals during the design and implementation of all three positioning devices were similar and these were to implement a positioning device which is simple, cost effective, portable, and can be used in virtually any clinical MRI scanner either sited on the scanner's table or mounted on the top of the gantry of the MRI.

Additionally the developed positioning devices incorporate a flexible coupling system and thus they can be used in all the anatomies accessible by HIFU like liver, kidney, breast, brain, pancreas and thyroids of for experiments in small and large animals.

The three different positioning devices were developed either as an improvement of one another, as in case of the first and third positioning devices, or to be used for different application, as in case of the second and third versions of positioning devices.

The applications of each version of positioning device are described below.

- a. The first positioning device can be used for brain tumours.
- b. The second version can be applied for experiments on large animals like pig, sheep and dog and small animals like rabbit and rat. However, with a slight modification of the base of this positioning device and with the collaboration an MRI vendor can be attached on the top of the gantry of the MRI scanner. Therefore, more space will be left for the target body and as a result this positioning device will be suitable for abdominal tumours (kidney, liver, and pancreas), brain and thyroid.
- c. The third device which is an upgrade of the first positioning device can be also used for treating brain tumours and additionally under certain conditions it would be suitable for treating abdominal tumours, and thyroid.

The positioning devices were evaluated for their MRI compatibility, reliability, accuracy and functionality, with several experiments on phantom gel, pork kidney, porcine muscle and rabbit liver.

Furthermore, other experiments were conducted to evaluate the effects of the HIFU / MRI system. The effectiveness of MRI to monitor therapeutic protocols of HIFU in freshly excised pig liver and in rabbit liver *in vivo* were investigated. The detection of large lesions using MRI was evaluated as well as the possibility to create both thermal and cavitation lesions. MRI sequences where best contrast between liver and lesion is obtained were also studied. The range of repetition time (TR) and range of echo time (TE) which maximizes the contrast to noise ratio (CNR) were investigated. Additionally, MRI was utilized to monitor lesions created at temperature below the boiling point and lesions created at temperature above the boiling point using HIFU in freshly excised kidney, liver and *in vivo* rabbit kidney.

Results from 1942 since today have proved that HIFU is a very promising technology and recent studies convince many experts that HIFU is the future in medicine. Furthermore MRI guidance of a positioning device that guides HIFU transducer for non-invasive interventions offers accuracy and reliability and it appears to be very encouraging approach for treating tumours. The evaluation of the proposed positioning devices is very optimistic for MRI guided HIFU applications.

Abbreviations and symbols used

	Abbreviation	Expansion
1	ABS	Acrylonitrile Butadiene Styrene
2	A/D	Analogue to Digital
3	AI	Analogue Input
4	AO	Analogue Output
5	ALARA	As Low As Reasonably Achievable
6	AVR	Aortic Valve Replacement
7	BPH	Benign Prostatic Hyperplasia
8	BW	Bandwidth- a measure of frequency range, the range between the highest and lowest frequency allowed
9	CAD	Computer-Aided Design
10	CE	Conformité Européene, meaning "European Conformity"
11	CAM	Computer-Aided Manufacturing
12	CEA	Carcinoembryonic Antigen
13	CNR	Contrast to Noise Ratio
14	CPU	Central Processing Unit
15	CT or CAT	Computed Tomography scan
16	DIO	digital input/output
17	DoF	Degrees of Freedom
18	ETL	Echo Train Length
19	ERCP	Endoscopic retrograde cholangiopancreatography
20	FDA	Food and Drug Administration
21	FOV	Field of View
22	FSE	Fast Spin Echo
23	FSPGR	Fast Spoiled Gradient echo
24	GI	Gastrointestinal
25	HCC	Hepatocellular carcinoma
26	HIFU	High Intensity Focused Ultrasound
27	ICU	Intensive Care Unit
28	IV	Injection into a vein
29	IVP	intravenous pyelogram
30	LTA	Laser thermal ablation
31	MI	Mechanic index
32	MRgHIFU	Magnetic Resonance Image guided HIFU
33	MRI	Magnetic Resonance Imaging
34	MRgFUS	Magnetic Resonance Guided Focused Ultrasound
35	MTC	Medullary thyroid carcinoma
36	NCI	National Cancer Institute
37	NDT	Non-Destructive Testing
38	NEX	Number of Excitations
39	PET	Positron Emission Tomography
40	PMI	Profound Medical Inc.
41	PMMA	Polymethyl methacrylate
42	POC	Probability of Cavitation

43	PFI	Programmable Function Interface
44	PSA	Prostate-Specific Antigen
45	PTC	Percutaneous Transhepatic Cholangiography
46	PUM	Piezoelectric ultrasonic motors
47	RCC	Renal Cell Carcinoma
48	ROI	Region of Interest
49	SEER	Surveillance, Epidemiology and End Results
50	SPECT	Single Photon Emission Computed Tomography
51	SPTA	Spatial Peak Temporal Average
52	TI	Thermal index
53	TIB	Bone Thermal Index
54	TIS	Tissue Thermal Index
55	T1	The longitudinal relaxation time
56	T2	The transverse relaxation time
57	TE	Time to Echo
58	TR	Repetition Time
59	USP	United States Plastic Company
60	WHO	World Health organization

1 Introduction

High intensity focused ultrasound (HIFU) is a promising technology for a variety of therapeutic applications. This concept initiated in 1942 by Lynn Zwemer [1]. HIFU has long been known as a minimal invasive or non-invasive procedure that destroys tissue through ablation. However, it is only in recent years that clinical applications are becoming feasible, with the development of high power ultrasound transducers compatible with the MRI scanner which is used to monitor these non-invasive HIFU applications. New technologies, combined with more sophisticated treatment methods and monitoring methods allow non-invasive procedures in many areas such as the brain, eye, breast, kidney, liver, pancreas, thyroid, uterine fibroids and pancreas. Meanwhile, new investigations are underway for treating cardiac arrhythmia, strokes, palliative pain treatment of bone metastases and brain disorders such as Parkinson's disease, essential tremor, and neuropathic pain. These optimistic investigations have encouraged physicians and provided them new valuable tools for medical research.

After the introduction of the concept of HIFU in 1942 by Lynn Zwemer the first complete system for the use of HIFU was developed by Fry Mosberg [2] in 1954. However, at that time Magnetic Resonance Imaging (MRI) did not exist and therefore the previous systems were not guided effectively, and therefore had not survived in the clinical setting.

Jolesz and Jakab [3] in 1991 demonstrated that the MRI scanner can be used to guide the HIFU transducer and about a year later Hynynen et al. [4], [5] produce necrosis in a canine muscle using a HIFU transducer and monitored by an MRI. After these first studies of producing lesions on tissues using a HIFU transducer guided by an MRI, this concept was carried on in the following years [6], [7] and they have proven that the contrast between necrotic tissue and normal tissue was clearly observable. Therefore, MRI became the only modality of guiding HIFU to create lesions.

Through the years it has been proven that HIFU can be used to accurately heat the targeted biological tissues and therefore proven suitable for applications for destroying cancerous tissues with non-invasive or minimal invasive procedures

guided either by ultrasound or by MRI to provide, to the operator performing the procedure, images of a region within the subject being heated [2].

Furthermore, HIFU was explored in almost every tissue that is accessible by ultrasound. The propagation of HIFU can successfully generate discrete and large lesions with reproducible results. The following literature represents some examples of some applications explored: prostate [8], liver [9], brain [2], [10]-[11], eye [12], kidney [13]-[14], pancreas [15], [16], breast [17] and thyroid [18]-[22].

In the recent commercial systems (for example, [8], [23] and [24]) HIFU is either guided by ultrasound or MRI. Although, ultrasonic imaging is the simplest and most inexpensive method to guide HIFU, it is not as good as MRI as MRI offers superior contrast than ultrasound. Also, the thermometry capability provided by the MRI is unique and is used for the localization and the effect of the HIFU beam at any time. However, the disadvantages of MRI are mainly its cost and the fact that MRI imaging is not real time and this makes it difficult to point an organ which is moving due to breathing.

Several examples of MRI compatible positioning devices (robot) have been developed for other applications. Systems have been developed to perform breast interventions [25]-[28], to perform brain biopsies [29], to perform prostate procedures [30], [32], and one to perform general purpose procedures with the “doubledonut” scanner [33]. Although these studies have demonstrated the technical feasibility of MR compatible manipulators, these devices are highly specialized for a certain anatomy or MR scanner design.

The proposed positioning devices are prototypes magnetic resonance imaging (MRI) compatible positioning devices used to move an MRI-guided high intensity focused ultrasound (HIFU) transducer for the treatment of tumours by producing lesions on the targeted areas. The future application of these systems is to treat brain tumours (positioning devices versions 1 and 3) abdominal tumours (liver, kidney and pancreas with versions 2 and 3) and thyroid tumours (positioning devices version 2 and 3). Also, the positioning devices can be used to perform experiments in large animals like pig, sheep and dog and small animals like rabbit and rat.

1.1 Aims and objectives

The aims and objectives of the thesis are listed below:

- i. Design and implement a positioning device which will guide the HIFU transducer to effectively destroy the targeted tumour and avoiding lesions to healthy tissues
- ii. The positioning device must be MRI compatible since it will be used inside the gantry of an MRI scanner
- iii. The positioning device must be small in size and light in weight and therefore, portable
- iv. Design and develop a universal positioning device which will be capable to operate in the gantry any MRI scanner.
- v. The positioning device should be flexible and should be easily modified for many different applications
- vi. Design and develop a user friendly interface software application to be used to guide the positioning. Furthermore, the software application will provide the user with several other functions like,
 - digital thermometer to capture the temperature variations at the HIFU transducer focal point,
 - store patient treatment history,
 - set the ultrasound treatment protocol, settings of the HIFU treatment, i.e. the parameters of the given therapy like intensity, frequency, starting and ending times,
 - maintain patient database with data of the patients treated which can be used for statistical purposes,
 - display of MRI images The MRI images of each treatment will be stored and the user has the ability to load any image stored,
 - display video or pictures captured from the MR compatible camera An MRI compatible camera is connected on the system. The camera was interfaced by means of a video capture card. With the aid of the MRI compatible camera, the researcher can monitor the welfare of the animal or human.

1.2 Chapters Outline

This section gives an overview of each chapter in this report.

Chapter 2: Abdominal and thyroid tumours

Kidney, liver and pancreatic tumours are the abdominal tumours considered in this report. Thyroid tumours are also considered and therefore this chapter covers the most common tumours of these organs as well as the symptoms, diagnostic methods and treatments used. Treating these tumours using HIFU is not explained in this chapter since this method is described in details in chapter 3.

Chapter 3: High Intensity Focused Ultrasound (HIFU) technology and therapeutic applications

This chapter gives an overview of the physics and technology of HIFU and HIFU transducers. Also, describes how HIFU can be used for treating tumours and how Magnetic Resonance Imaging (MRI) can be utilized for the guidance of HIFU transducers. Furthermore, MRI compatibility and safety issues as well as therapeutic HIFU applications and historical events of therapeutic HIFU are also described.

Chapter 4: Applications of HIFU in medicine

The current state for treating abdominal and thyroid tumours using HIFU technology experimentally and commercially is described in this chapter.

Also, in this chapter HIFU technology for treating abdominal and thyroid tumours is compared with the current treatment methods for treating these tumours and advantages and limitations are summarized. This chapter also gives an overview of MRI guided HIFU (MRgHIFU) systems and MRI compatible positioning devices and exhibits the existing MRgHIFU positioning devices.

Chapter 5: Development of HIFU system with MRI guidance

This chapter describes the parts and the setup of a HIFU system. MRI compatible materials like piezoelectric motors, piezoelectric ultrasonic transducer MRI compatible camera and cavitation detector are also discussed here.

- Chapter 6: Development of the positioning device version 1**
The description, the application, the parts and materials used, the designs, the development of the different components as well as the integration of the first version of the proposed positioning device are given in this chapter.
- Chapter 7: Development of the positioning device version 2**
This chapter gives an overview of the applications, the materials, the designs of the different components used and the development and integration of the second version of the proposed MRI compatible positioning device.
- Chapter 8: Development of the positioning device version 3**
This third version of the proposed positioning device, as mentioned earlier, is an advancement of the first version. In this chapter the applications, the materials used, the design of the different parts, the development and the integration of the third positioning device are explained in details.
- Chapter 9: Software development**
This chapter explains the development of the software that will be used to control the HIFU system. The digital thermometer, transducer movement, treatment history, ultrasound treatment protocol, and patient database, are the main functions of the software and these are presented in this chapter.
- Chapter 10: Evaluation of the MRI compatible positioning devices**
This chapter describes how the MRI compatible devices are tested and evaluated. All the experiments made to evaluate HIFU ablation and the MRI compatibility of the HIFU system are analysed.
- Chapter 11: Conclusion and future enhancements**
Conclusions and future enhancements are described in this last chapter.

2 Abdominal and thyroid tumours

This research primarily focuses on the design and development of three positioning devices which will be used in an MRI to guide the HIFU transducer to treat the brain, the thyroid and abdominal tumours. More specific, the abdominal tumours are tumours appearing on organs such as the liver, kidney and pancreas. These organs are the abdominal organs where HIFU has been tested by previous researchers, liver [9], [34]-[47], kidney [13], [14], [34], [46]-[49] and pancreas [15], [16]. Thyroid tumours were also studied and tested by previous researchers [18]-[22]. Abdominal or thyroid tumour is an abnormal growth of mass in the abdominal region of the body and this is a result of an abnormal growth of the cells in this area. The positioning device will guide the HIFU transducer to ablate the tumour area with and this process will be monitored by an MRI scanner.

In this chapter the basic anatomy and physiology of these abdominal organs, and the thyroid will be described. Also, in brief there will be description of the tumours manifested in these organs together with a synopsis of the current main treatment regimes.

2.1 Liver tumours

The liver is located in the upper right-hand portion of the abdominal cavity, beneath the diaphragm, and on top of the stomach, right kidney, and intestines [50]. The anatomy of the liver is shown in figure 2.1.

The liver regulates most chemical levels in the blood and excretes a product called bile, which helps carry away waste products from the liver. All the blood leaving the stomach and intestines passes through the liver. The liver processes this blood and breaks down the nutrients and drugs into forms that are easier to use for the rest of the body.

Important to note is that the liver can lose three-quarters of its cells before it stops functioning. In addition, the liver is the only organ in the body that can regenerate.

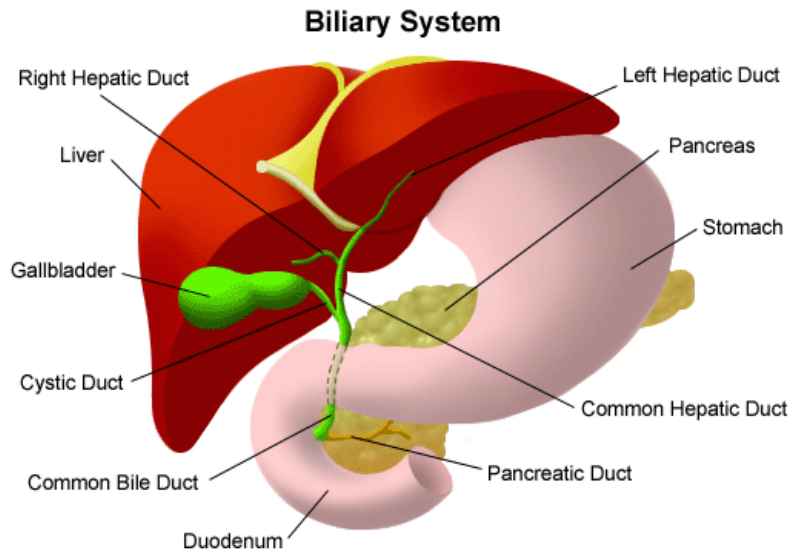


Figure 2.1: The Biliary system. The figure above shows the liver location in the abdominal cavity [50].

Liver tumours are divided to two categories, the non-cancerous and the cancerous (malignant). In this section the different types of tumours are discussed.

2.1.1 Non-cancerous liver tumours

The symptoms of these tumours usually are not noticeable and they are only detected incidentally when an ultrasound scan, or computer tomography or CT scan or Magnetic Resonance imaging (MRI) is performed on the patient. Hepatocellular adenoma which appears usually in women at young age and the hemangioma which is a mass of abnormal blood vessels. There are no treatment for these, apart for some cases of infants with large liver hemangiomas who might require surgery to prevent clotting and heart failure [50]-[54].

2.1.2 Cancerous liver tumours

Cancerous (malignant) liver tumours are also subdivided to primary liver cancer and secondary liver cancer. Primary liver cancer is one that starts in the liver where secondary liver cancer is one that spreads into the liver from cancer of

another part of the body (metastatic liver cancer). Most cancerous liver tumours are secondary [53]-[59].

a. Primary liver cancers

Hepatoma is a type of primary liver cancer and is also called hepatocellular carcinoma. Hepatoma is the most common form of primary liver cancer. Some of the causes of this primary liver cancer are chronic infection hepatitis B and C, alcoholism and chronic liver cirrhosis.

b. Diagnostic methods for liver hepatoma

Diagnosis of hepatoma is done through the medical history of the patient and a physical examination.

The following are some diagnostic procedures for liver hepatoma [50]-[54]:

- **Liver function tests**, a series of special blood tests that can determine if the liver is functioning properly.
- **Abdominal ultrasound (also called sonography)**, a diagnostic imaging technique which uses high-frequency sound waves to create an image of the internal organs. Ultrasounds are used to view internal organs of the abdomen such as the liver, spleen, and kidneys and to assess blood flow through various vessels.
- **Computed Tomography scan (CT or CAT scan)**, a diagnostic imaging procedure using a combination of x-rays and computer technology to produce cross-sectional images (often called slices), both horizontally and vertically, of the body. A CT scan shows detailed images of any part of the body, including the bones, muscles, fat, and organs. CT scans are more detailed than general x-rays.
- **Hepatic arteriography**, x-rays taken after a substance is injected into the hepatic artery.
- **Liver biopsy**, a procedure in which tissue samples from the liver are removed (with a needle or during surgery) from the body for examination under a microscope.

c. Treatment methods for liver hepatoma

For the treatment of liver hepatoma several approaches are used some of which are listed below [50]-[54]:

- **Surgical resection** can only be used in some cases to remove cancerous tissue from the liver. However, the tumour must be small and confined.
- **Radiation therapy** that uses high-energy rays to kill or shrink cancer cells.
- **Chemotherapy** that uses anticancer drugs to kill cancer cells.
- **Liver transplantation**
- **Thermal ablation** methods using HIFU are also used and these are discussed in detail later in this report.

d. Other Types of primary liver cancers

Other types of primary liver cancers which are less common are the following:

- **Cholangiocarcinoma**, a cancer that originates in the lining of the bile channels in the liver or in the bile ducts.
- **Hepatoblastoma**, a cancer in infants and children, sometimes causing the release of hormones that result in early puberty.
- **Angiosarcoma**, a rare cancer that originates in the blood vessels of the liver.

According to the National Cancer Institute primary liver cancer passes through the following stages:

- **localized resectable.** Cancer is in one place and can be removed completely with surgery.
- **localized unresectable.** Cancer is in one place, but cannot be totally removed.
- **Advanced.** Cancer has spread through the liver and other parts of the body.
- **Recurrent.** Cancer has come back after it was treated.

e. Secondary Liver cancers (metastatic liver cancers)

As explained earlier in section 2.1.2 secondary liver cancer is one that has spread from other areas in the body to the liver. These metastatic cancers infecting the liver usually start from the lung, breast, colon, pancreas, and stomach. Blood cancers including Leukemia are also spread to the liver sometimes.

f. Diagnostic methods for metastatic liver cancer

Diagnosis of metastatic liver cancer is done through the medical history of the patient and a physical examination.

The diagnostic procedures used for metastatic liver cancer are very similar as the one described above for liver hepatoma.

g. Treatment methods for metastatic liver

For the treatment of metastatic liver cancer several approaches are used some of which are listed below:

- **Surgical resection** as mentioned previously for primary liver cancers can only be used in some cases to remove cancerous tissue from the liver. However, the tumour must be small and confined.
- **Radiation therapy** which uses high-energy rays to kill or shrink cancer cells.
- **Chemotherapy** that uses anticancer drugs to kill cancer cells.
- **Thermal ablation** methods using HIFU are also used and these are discussed in detail later in this report.

Hepatocellular carcinoma (HCC), a primary liver cancer described above in primary liver cancers section is considered to be one of the most common malignancies worldwide, and metastatic liver cancers are the most common cause of death in cancer patients [46].

2.1.3 Liver cancer statistics

The statistical information shown in appendix 12.3 was taken from the National Cancer Institute (NCI) [51] and from the World Health Organization-International Agency for research on Cancer [55].

2.2 Kidney tumours

Renal is the Latin word for kidneys and therefore the word renal is common when referring to kidneys. The kidneys are two dark-red, bean-shaped organs one on each side of the backbone, above the waist. There is a cavity attached to the indented side of the kidney, called the renal pelvis which extends into the ureter [50]-[54]. Each kidney is enclosed in a transparent membrane called the renal capsule which helps to protect them against infections and trauma. Nephrons are about one million of microscopic structures inside each kidney responsible for filtering the blood removing waste products and making urine. The urine passes from each kidney into the bladder through a long tube called a ureter. The bladder stores the urine until it is passed from the body.

Blood is delivered to the kidneys through the renal artery and over 180 litres of blood pass through the kidneys every day. When this blood enters the kidneys it is filtered and returned to the heart via the renal vein. Figure 2.2 shows the anatomy of the kidney.

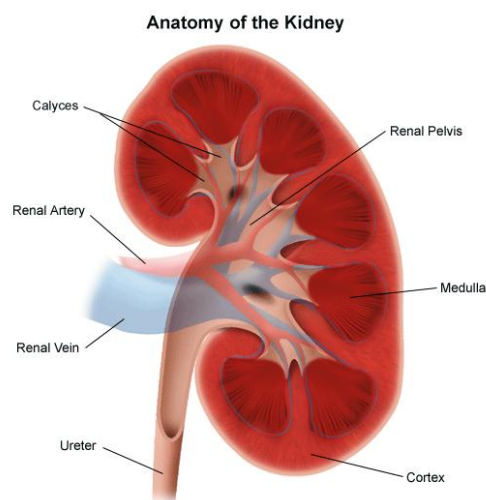


Figure 2.2: The Anatomy of the Kidney [50]

Kidneys are located towards the back of the abdominal cavity, just above the waist. One kidney is normally located just below the liver, on the right side of the abdomen and the other is just below the spleen on the left side. Figure 2.3 shows the kidneys' location in the abdominal cavity.

The kidney is full of blood vessels since every function of the kidney involves blood; therefore, it requires a lot of blood vessels to facilitate these functions. Together, the two kidneys contain about 160 km of blood vessels.

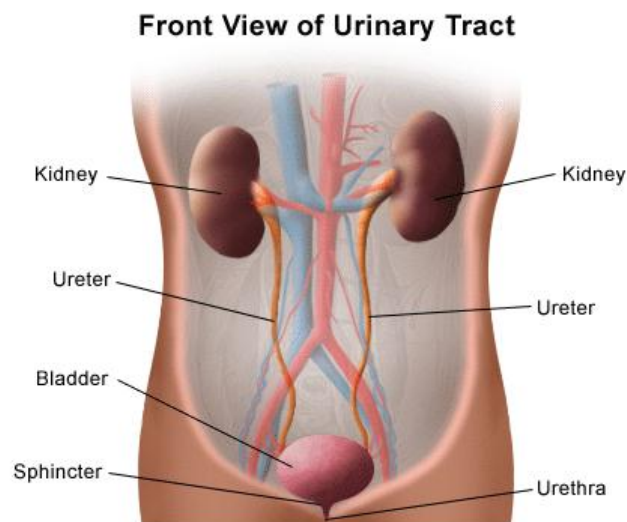


Figure 2.3: The Front View of Urinary Tract. The figure above shows the kidneys' location in the abdominal cavity [50].

The size of an adult human kidney is about 10 to 13 cm long and about 5 to 7.5 cm wide and weighs approximately 150 grams. Kidneys weigh about 0.5% of total body weight.

Kidney cancers are also called renal cancers. Kidney cancers are also divided to different types. These types of cancers, their symptoms and the method used for the treatment of these tumours are explained below.

2.2.1 Non-cancerous kidney tumours

Benign kidney tumours are noncancerous. The symptoms of these tumours are not noticeable and usually are detected incidentally. These tumours are not threatening the life of the patients' [53].

Renal adenomas are the most common form of benign, solid kidney tumour, and are typically small, low-grade growths. Their cause is unknown. Because they usually are asymptomatic, their incidence is unknown, although one study found them present in 7% to 22% of autopsy cadavers. In rare cases, when they have grown large enough to affect kidney function or adjacent vessels, symptoms similar to those of renal cell carcinoma (RCC) may occur.

Renal Oncocytoma is a benign, usually asymptomatic tumour that can grow quite large. They can develop throughout the body and are not unique to the kidneys. Their cause is unknown, and they appear with greater frequency in men than in women. Typically, they are discovered incidentally by ultrasound, IVP, CT, or MRI scan for an unrelated health problem.

Under a microscope, many oncocytomas resemble early-stage RCCs. Many physicians regard them as precancerous growths to be surgically removed unless the patient's age or overall health condition dictates otherwise.

Angiomyolipoma also known as renal hamartoma, angiomyolipomas are rare benign tumours usually caused by an inherited genetic mutation. They can occur on an isolated, individual basis, but most often are associated with a rare genetic disease called tuberous sclerosis, which can cause tumours in the skin, kidneys, brain, and other organ systems. About 80% of persons diagnosed with tuberous sclerosis also have angiomyolipoma.

In patients without tuberous sclerosis, these tumours most often occur in middle-aged women. Most cases are discovered when the patient undergoes a CT scan for an unrelated abdominal problem, suffers gastrointestinal discomfort, or suffers a sudden hemorrhage caused by the rupture of a large tumour.

Management of the condition depends on the size of the tumours and the severity of the symptoms they produce. Asymptomatic patients and those with small tumours usually are not treated; instead, they are observed periodically with an eye toward surgery if the tumours grow or produce symptoms. Because of the potential for spontaneous rupture and life-threatening hemorrhage, patients with large tumours usually are considered candidates for some form of surgical treatment, ranging from partial nephrectomy to arterial embolization.

Fibromas are tumours of the fibrous tissue on, in, or surrounding the kidney. They are rare and are more common in women. Their cause is unknown and most do not cause symptoms. Usually they grow on the periphery of the kidney and can become large before becoming clinically obvious. While generally benign, these tumours have no special characteristics to differentiate them from malignant tumours of the kidney. Because of this uncertainty of diagnosis, partial or radical nephrectomy is the standard treatment.

Lipomas are rare renal tumours that originate in the fat cells within the renal capsule or surrounding tissue. They typically occur in middle-aged women, can grow very large, and produce pain and hematuria. Like many benign tumours, they may become cancerous and usually are treated with total nephrectomy.

2.2.2 Cancerous kidney tumours

Several types of cancer can start in the kidney. When kidney cancer spreads outside the kidney, cancer cells are often found in nearby lymph nodes. Kidney cancer also may spread to the lungs, bones, liver or even from one kidney to the other [51], [57]-[59].

a. Types of cancerous kidney tumours

Kidney cancerous tumours include renal cell cancer, the most common type of kidney cancer in adults and the transitional cell carcinoma which affect the renal pelvis. Wilms tumour is another kidney cancer which is the most common type of childhood kidney cancer. It also includes renal sarcoma a rare type of kidney cancer that starts in the kidney's blood vessels. These kidney cancer types are described below [51], [57]-[59].

Renal cell cancer (RCC) is the most common type of kidney cancer in adults and it is also called renal adenocarcinoma or hypernephroma. More than 8 in every 10 kidney cancers diagnosed in the UK are RCC. In renal cell cancer the cancerous cells start in the lining of very small tubes in the kidney that help filter the blood and remove waste products through urine.

Below there is a list of several subtypes of renal cell cancer (RCC):

- **Clear cell renal cell carcinoma:** This is the most common form of RCC. About 7 out of 10 people with RCC have this kind of cancer. When seen under a microscope, the cells that make up clear cell RCC look very pale or clear.
- **Papillary renal cell carcinoma:** This is the second most common subtype – about 1 out of 10 people with RCC have this kind. These cancers make little finger-like projections (called papillae) in some, if not most, of the tumor. Some doctors call these cancers chromophilic because the cells take up certain dyes used to prepare the tissue to be looked at under the microscope. The dyes make them look pink.
- **Chromophobe renal cell carcinoma:** This subtype accounts for a few cases of RCCs. The cells of these cancers are also pale, like the clear cells, but are much larger and differ in other ways.
- **Collecting duct renal cell carcinoma:** This subtype is very rare. The major feature is that the cancer cells can form irregular tubes.
- **Unclassified renal cell carcinoma:** In rare cases, renal cell cancers are called as “unclassified” because they don’t fit into any of the other groups or because more than one type of cell is present.

Transitional cell carcinoma are tumours that begin in the renal pelvis, the point where the kidney joins the tube that carries urine from the kidney to the bladder (ureter), and not in the kidney itself. About 7 or 8 out of every 100 (7 to 8 %) kidney cancers diagnosed in the UK are transitional cell carcinomas, also known as urothelial carcinomas.

The symptoms of transitional cell carcinoma are quite similar to those of RCC, and include haematuria and back or flank pain.

At early stage these cancers have a 90% cure rate. Treatment usually involves surgical removal of the kidney, ureter, and portion of the bladder connecting to the ureter. Depending on the stage of the cancer, chemotherapy and radiation may be used as adjuvant treatments.

Wilms' Tumour is a type of kidney cancer that usually develops in children under the age of 5. About 5% of all kidney cancers are Wilms tumours also called nephroblastomas. Wilms' tumour can arise anywhere within the kidney's

tissues. If left untreated, it can spread to the veins, lymph nodes, adrenal glands, large or small bowel, and liver. Wilms' tumour is one of the most curable of all childhood cancers. Today the 5-year survival rate approaches 90%.

Renal sarcoma: Renal sarcomas are a rare type of kidney cancer that starts in the kidney's connective tissue or blood vessels. Less than 1% of all kidney tumours are of this type. In most cases, it is impossible to differentiate renal sarcoma from RCC externally, so the diagnosis usually is made after examination of a CT scan or MRI procedure.

Such tumours will grow and spread to adjacent organs, bones, and lymph nodes if left untreated. The only potentially curative form of treatment is surgery, usually radical or partial nephrectomy, sometimes with radiation or chemotherapy.

b. Diagnostic methods for Kidney cancer (renal cell cancer)

Diagnostic procedures for kidney cancer may include the following [50]-[54]:

- blood and urine laboratory tests
- intravenous pyelogram (IVP) - a series of x-rays of the kidney, ureters, and bladder with the injection of a contrast dye into the vein - to detect tumours, abnormalities, kidney stones, or any obstructions, and to assess renal blood flow.
- renal angiography (Also called arteriography.) - a series of x-rays of the renal blood vessels with the injection of a contrast dye into a catheter, which is placed into the blood vessels of the kidney, to detect any signs of blockage or abnormalities affecting the blood supply to the kidneys.
- other imaging tests (to show the difference between diseased and healthy tissues), including the following:
 - computed tomography scan (Also called a CT or CAT scan.) - a non-invasive procedure that takes cross-sectional images of the brain or other internal organs; to detect any abnormalities that may not show up on an ordinary x-ray.

- magnetic resonance imaging (MRI) - a non-invasive procedure that produces two-dimensional view of an internal organ or structure, especially the brain and spinal cord.
- ultrasound (Also called sonography.) - a diagnostic imaging technique which uses high-frequency sound waves and a computer to create images of blood vessels, tissues, and organs. Ultrasounds are used to view internal organs as they function, and to assess blood flow through various vessels.

Biopsy is the only sure way to diagnose cancer.

c. Treatment methods for kidney cancer

Specific treatment for kidney cancer will be determined by your physician based on [50]-[54]:

- your age, overall health, and medical history
- extent of the disease
- your tolerance for specific medications, procedures, or therapies
- expectations for the course of the disease
- your opinion or preference

Treatment may include:

- **Surgery:** Surgery to remove the kidney is called a nephrectomy and it is the most common treatment for kidney cancer. The following are different types of nephrectomy procedures:
 - **radical nephrectomy**, the whole kidney is removed along with the adrenal gland, tissue around the kidney, and, sometimes, lymph nodes in the area.
 - **simple nephrectomy**, only the kidney is removed.
 - **partial nephrectomy**, only the part of the kidney that contains the tumour is removed.

The remaining kidney is generally able to perform the work of both kidneys.

- **Radiation therapy (also called radiotherapy):** Radiation therapy uses high-energy x-rays to kill cancer cells, and is also sometimes used to relieve pain when kidney cancer has spread to the bone.
- **Biological therapy (also called immunotherapy):** Biological therapy is a treatment that uses the body's own immune system to fight cancer.
- **Chemotherapy:** Chemotherapy is the use of drugs to kill cancer cells.
- **Hormone therapy:** Hormone therapy is used in a small number of patients with advanced kidney cancer to try to control the growth of cancer cells.
- **Arterial embolization:** Arterial embolization is a method where small pieces of a special gelatine sponge, or other material, are injected through a catheter to clog the main renal blood vessel. This procedure shrinks the tumour by blocking the oxygen and other substances it needs to grow. It may also be used before an operation to make surgery easier, or to provide relief from pain when removal of the tumour is not possible.
- New **chemotherapy drugs** and targeted therapies are also under development being used to treat kidney cancer.
- A **vaccine** for treatment is under study.

2.2.3 Kidney cancer statistics

The statistical information shown in appendix 12.3 was taken from the National Cancer Institute (NCI) [51] and from the World Health Organization-International Agency for research on Cancer [55].

2.3 Pancreatic tumours

The pancreas is located in the abdomen. It is surrounded by the stomach, intestines, and other organs. The pancreas is about 6 inches long and is shaped like a long, flattened pear wide at one end and narrow at the other. The wide part of the pancreas is called the head, the narrow end is the tail, and the middle section is called the body of the pancreas [54]. Figure 2.3 shows the pancreas.

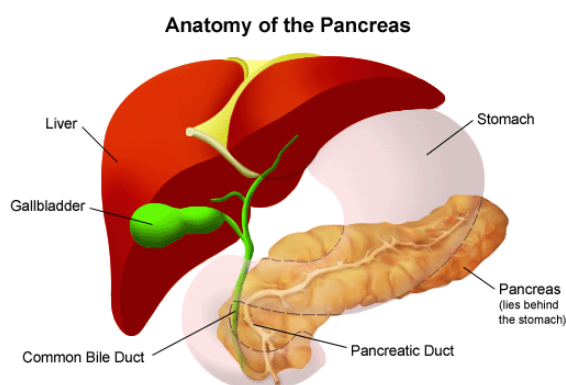


Figure 2.4: The Anatomy of the Pancreas [50].

Pancreas has two main functions, it makes pancreatic juices, and it produces several hormones, including insulin. Pancreatic juices contain proteins called enzymes that help digest food. The pancreas releases these juices, as they are needed, into a system of ducts. The main pancreatic duct joins the common bile duct from the liver and gallbladder. The common bile duct carries bile, a fluid that helps digest fat. Together these ducts form a short tube that empties into the duodenum, the first section of the small intestine [50].

Pancreatic cancer has been called a "silent" disease because the symptoms do not appear at an early stage. The cancer may grow for some time before it causes noticeable symptoms. When symptoms do appear, they may be so vague that they are ignored at first. For these reasons, pancreatic cancer is hard to find early. In many cases, the cancer spreads outside the pancreas by the time it is found [54]. Also, advanced pancreatic cancer patients will only survive for about four months.

The treatment for these patients as for many other cancer patients is mainly chemotherapy and radiotherapy. These therapies can relieve the pain to some degree but their efficacy is poor and they also bring side effects.

The pancreas, its operation, pancreatic tumours their symptoms and the common treatments are discussed in this section.

2.3.1 Pancreatic Cancers

Cancer of the pancreas is also called pancreatic cancer or carcinoma of the pancreas. Most pancreatic cancers begin in the ducts that carry pancreatic juices. A rare type of pancreatic cancer begins in the cells that produce insulin and other hormones. These cells are called islet cells, or the islets of Langerhans. Cancers that begin in these cells are called islet cell cancers [53], [54], [56]-[58].

As pancreatic cancer grows, the tumour may invade organs that surround the pancreas, such as the stomach or small intestine. Pancreatic cancer cells also may break away from the tumour and spread to other parts of the body. When pancreatic cancer cells spread, they often form new tumours in lymph nodes and the liver, and sometimes in the lungs or bones. The new tumours have the same kind of abnormal cells and the same name as the primary (original) tumour in the pancreas. For example, if pancreatic cancer spreads to the liver, the cancer cells in the liver are pancreatic cancer cells. The disease is metastatic pancreatic cancer; it is not liver cancer.

a. Diagnostic methods for pancreatic cancers

Diagnosis of pancreatic cancers is through physical examination, patient's medical history in addition to checking general signs of health, blood, urine, and stool tests [50].

The doctor usually orders procedures that produce images of the pancreas and the area around it. Images can help the doctor diagnose cancer of the pancreas. They also can help the doctor determine the stage, or extent, of the disease by showing whether the cancer affects nearby organs. Images that

show the location and extent of the cancer help the doctor decide how to treat it. Procedures to produce images of the pancreas and nearby organs may include:

- An **upper gastrointestinal (GI)** series, sometimes called a barium swallow. A series of x-rays of the upper digestive system is taken after the patient drinks a barium solution. The barium shows an outline of the digestive organs on the x-rays.
- **Computed Tomography scan (CT or CAT)** scanning, the use of an x-ray machine linked with a computer. The x-ray machine is shaped like a doughnut with a large hole. The patient lies on a bed that passes through the hole, and the machine moves along the patient's body, taking many x-rays. The computer puts the x-rays together to produce detailed pictures.
- **Magnetic Resonance Imaging (MRI)**, the use of a powerful magnet linked to a computer. The MRI machine is very large, with space for the patient to lie in a tunnel inside the magnet. The machine measures the body's response to the magnetic field, and the computer uses this information to make detailed pictures of areas inside the body.
- **Ultrasound** (also called sonography or ultrasonography), the use of high-frequency sound waves that cannot be heard by humans. An instrument sends sound waves into the patient's abdomen. The echoes that the sound waves produce as they bounce off internal organs create a picture called a sonogram. Healthy tissues and tumours produce different echoes.
- **Endoscopic retrograde cholangiopancreatography (ERCP)**, a method for taking x-rays of the common bile duct and pancreatic ducts. The doctor passes a long, flexible tube (endoscope) down the throat, through the stomach, and into the small intestine. The doctor then injects dye into the ducts and takes x-rays.
- **Percutaneous Transhepatic Cholangiography (PTC)**, in which a thin needle is put into the liver through the skin on the right side of the abdomen. Dye is injected into the bile ducts in the liver so that blockages in the ducts can be seen on x-rays.
- **Angiography**, x-rays of blood vessels taken after the injection of dye that makes the blood vessels show up on the x-rays.

- **Pancreas biopsy**, a procedure in which a sample of pancreatic tissue is removed (with a needle or during surgery) for examination under a microscope.
- **Positron Emission Tomography (PET)**, a type of nuclear medicine procedure. This means that a tiny amount of a radioactive substance, called a radionuclide (radiopharmaceutical or radioactive tracer), is used during the procedure to assist in the examination of the tissue under study.

Images of the pancreas and nearby organs provide important clues as to whether a person has cancer. However, doing a biopsy is the only sure way for the doctor to learn whether pancreatic cancer is present.

b. Pancreatic cancer treatment methods

Pancreatic cancers are not treated easily unless they have been identified at an early stage, before spreading to other organs. However, treatment can improve the quality of a person's life by controlling the symptoms and complications of this disease [15].

The choice of treatment of these tumours depends on the type of cancer, the location and size of the tumours, the extent (stage) of the disease, the person's age and general health, and other factors.

Cancer that begins in the pancreatic ducts may be treated with surgery, radiation therapy, or chemotherapy. Doctors sometimes use combinations of these treatments. Researchers are also studying biological therapy (also called immunotherapy or biotherapy, is a type of treatment that uses the body's immune system to fight cancer or help to lessen the side effects that maybe caused from other cancer treatments like chemotherapy) to see whether it can help when pancreatic cancer has spread to other parts of the body or has recurred.

- Surgery may also be done to remove all or part of the pancreas and other nearby tissue. A total pancreatectomy is surgery to remove the entire pancreas as well as the duodenum, common bile duct, gallbladder, spleen, and nearby lymph nodes. Sometimes, the cancer cannot be

completely removed. However, surgery can help to relieve symptoms that occur if the duodenum or bile duct is blocked. To relieve such symptoms, the surgeon creates a bypass around the blockage.

Other therapies for pancreatic cancer include, radiation therapy (also called radiotherapy), chemotherapy, biological therapy (also called immunotherapy).

It is hard to limit the effects of treatment so that only cancer cells are removed or destroyed. Because treatment also damages healthy cells and tissues, it often causes unpleasant side effects. The side effects of cancer treatment vary. They depend mainly on the type and extent of the treatment. Also, each person reacts differently.

2.3.2 Pancreatic cancer statistics

The statistical information shown in appendix 12.3 was taken from the National Cancer Institute (NCI) [51] and from the World Health Organization-International Agency for research on Cancer [55].

2.4 Thyroid tumours

Thyroid is located in the neck, just above the collarbone, around the windpipe below the Adam's apple and is a soft, butterfly-shaped gland. Thyroid anatomy is shown in figure 2.5. The thyroid gland has two main types of cells: thyroid follicular cells and C cells (also called parafollicular cells). The follicular cells produce thyroid hormone used to regulate metabolism i.e. it controls the process of converting the food we eat to energy C cells make calcitonin, a hormone that helps regulate how the body uses calcium. Other, less common cells in the thyroid gland include immune system cells (lymphocytes) and supportive (stromal) cells [56]-[60].

Thyroxine, known as T4 and triiodothyronine, known as T3 are the two essential hormones produced by the thyroid. These two hormones are similar and are called thyroid hormones. T4 hormone acts as a reserve for T3 since most T3 circulating in the blood stream is a transformation of T4. Thyroid hormone regulates the metabolic rate of almost all the cells of the body, and influences the health of the heart, brain and bones. It is also needed for normal development of the brain in children and for normal reproductive functioning.

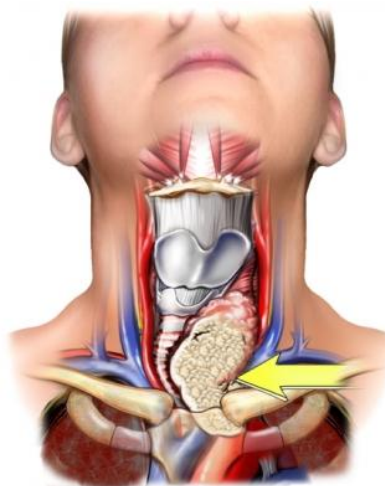


Figure 2.5: The anatomy of thyroid. The figure above shows the thyroid location [50].

Millions of people worldwide most of them women suffer from thyroid disease which causes the body uses energy more slowly and called hypothyroidism or quickly than it should and called hyperthyroidism. Hypothyroidism is the most common and it can make you gain weight, feel fatigued and have difficulty

dealing with cold temperatures. Hyperthyroidism has a result of producing too much thyroid hormone and this can make you lose weight, speed up your heart rate and make you very sensitive to heat.

Hypothyroidism and hyperthyroidism although important, are not to be considered here in this study but instead the thyroid cancer and the treatment methods available today, are concerned and analysed below.

2.4.1 Thyroid benign and malignant tumours

Thyroid cancer is a disease that you get when abnormal cells, often appear as bumps in the neck, begin to grow in your thyroid gland and these are called nodules. Thyroid cancer is an uncommon type of cancer and in most cases, thyroid nodules are not cancerous. Those that are cancerous have the potential to spread throughout the body [50]. Thyroid cancer is usually found at early stages and therefore it can be treated very well. Care must be taken after the treatment of a thyroid tumour since it is possible to come back some time after the treatment.

Thyroid cancer occurs in all age groups, although its incidence increases with age, especially after 30 years of age. More aggressive forms of thyroid cancer are found in older patients. Thyroid cancer occurs three times more frequently in women than in men [61]. Different cancers develop from each kind of cell. The differences are important because they affect how serious the cancer is and what type of treatment is needed.

Many types of tumours can develop in the thyroid gland. Most of them are benign (non-cancerous) but others are malignant (cancerous), which means they can spread into nearby tissues and to other parts of the body [59].

a. Benign thyroid enlargement and nodules

Changes in the thyroid gland's size and shape can often be felt or even seen by patients or by their doctor.

Some goiters (abnormally large thyroid gland) are diffuse, meaning that the whole gland is large. Other goiters are nodular, meaning that the gland is large and has one or more bumps in it. There are many reasons the thyroid gland might be larger than usual, and most of the time it is not cancer. Both diffuse and nodular goitres are usually caused by an imbalance in certain hormones. For example, not getting enough iodine in the diet can cause changes in hormone levels and lead to a goitre [59].

Lumps or bumps in the thyroid gland are called thyroid nodules. Most thyroid nodules are benign, but about 1 in 20 is cancerous. Sometimes these nodules make too much thyroid hormone and cause hyperthyroidism.

People can develop thyroid nodules at any age, but they occur most commonly in older adults. Fewer than 1 in 10 adults have thyroid nodules that can be felt by a doctor. But when the thyroid is looked at with an ultrasound test, up to half of all people are found to have nodules that are too small to feel [59].

Solid nodules have little fluid or colloid, and these nodules are likely to be cancerous than are fluid-filled nodules. Still, most solid nodules are not cancer. Some solid nodules, such as hyperplastic nodules and adenomas, have too many cells, but the cells are not cancer cells. Moreover, benign thyroid nodules can sometimes left untreated as long as they're not growing or causing symptoms [59].

b. Malignant (cancerous) thyroid tumours

The two most common types of thyroid cancer are papillary carcinoma and follicular carcinoma. Hurthle cell carcinoma is a subtype of follicular carcinoma. Other types of thyroid cancer, such as medullary thyroid carcinoma, anaplastic carcinoma, and thyroid lymphoma, occur less often [59].

Differentiated thyroid cancers develop from thyroid follicular cells. In these cancers, the cells look a lot like normal thyroid tissue when looked at under a microscope [59].

Papillary carcinoma: About 8 of 10 thyroid cancers are papillary carcinomas (also called papillary cancers or papillary adenocarcinomas). Papillary carcinomas typically grow very slowly. Usually they develop in only one lobe of

the thyroid gland, but sometimes they occur in both lobes. Even though they grow slowly, papillary carcinomas often spread to the lymph nodes in the neck. But most of the time, these cancers can be successfully treated and are rarely fatal [59].

Follicular carcinoma: Follicular carcinoma is the next most common type of thyroid cancer. It is also sometimes called follicular cancer or follicular adenocarcinoma. Follicular cancer is much less common than papillary thyroid cancer, making up about 1 out of 10 thyroid cancers. Unlike papillary carcinoma, follicular carcinomas usually don't spread to lymph nodes, but some can spread to other parts of the body, such as the lungs or bones. The prognosis for follicular carcinoma is probably not quite as good as that of papillary carcinoma, although it is still very good in most cases [59].

Hurthle cell carcinoma, also known as oxyphil cell carcinoma, is actually a kind of follicular carcinoma. It accounts for about 3% of thyroid cancers. The prognosis may not be as good as that of typical follicular carcinoma because this type is harder to find and treat. This is because it is less likely to absorb radioactive iodine, which is used both for treatment and to look for the spread of differentiated thyroid cancer [59].

c. Other types of thyroid cancers

Medullary thyroid carcinoma: Medullary thyroid carcinoma (MTC) accounts for about 4% of thyroid cancers. It develops from the C cells of the thyroid gland. Sometimes this cancer can spread to lymph nodes, the lungs, or liver even before a thyroid nodule is discovered.

Anaplastic carcinoma: Anaplastic carcinoma (also called undifferentiated carcinoma) is a rare form of thyroid cancer, making up about 2% of all thyroid cancers. It is thought to sometimes develop from an existing papillary or follicular cancer.

Thyroid lymphoma: Lymphoma is very uncommon in the thyroid gland. Lymphomas are cancers that develop from lymphocytes, the main cell type of the immune system.

Thyroid sarcoma: These rare cancers start in the supporting cells of the thyroid. They are often aggressive and hard to treat.

Parathyroid cancer: Behind, but attached to, the thyroid gland are 4 tiny glands called the parathyroids. The parathyroids glands help regulate the body's calcium levels. Cancers of the parathyroid glands are very rare.

d. Diagnostic methods for thyroid cancers

The doctor will ask about your symptoms and medical history, and perform a physical exam. This may include a careful examination of your neck to look for lumps or abnormalities.

Tests:

- **Fine needle aspiration**, removal of fluid and cells from a thyroid nodule with the use of a very thin needle
 - This test can be done in the doctor's office and may or may not require a local anaesthetic.
- **Blood test**
- **Thyroid scan**, x-rays taken after radioactive iodine is injected into the blood
 - The iodine is absorbed by the thyroid gland. This causes it to light up and be more visible on x-ray.
- **Ultrasound**, a test that uses sound waves to examine thyroid nodules
- **Surgical biopsy**, removal of a sample of thyroid tissue to test for cancer cells

e. Thyroid cancer treatment methods

Once thyroid cancer is found, staging tests (possibly including CT scans and PET scans) are done to find out if the cancer has spread. Treatment depends on the stage of the cancer. The treatment methods for thyroid cancer are surgery, radioactive iodine therapy, external radiation therapy, chemotherapy and laser thermal ablation (LTA). LTA method is under study and suggested that light may be delivered interstitially by implanting a laser fibre directly into body tissues [63]. In this study US-guided needle inserted into thyroid lesions

and an optical fibre positioned in the target area. Hence a laser irradiation is performed on the area being treated.

f. Thyroid cancer statistics

The statistical information shown in appendix 12.3 was taken from the National Cancer Institute (NCI) [51] and from the World Health Organization-International Agency for research on Cancer [55].

2.5 Brain tumours

The brain is a large and complex human organ located in the skull which protects the brain from injury. Brain is the organ that controls all the processes of the human body. All of our thoughts, emotions, senses, skills and memories are controlled by the brain by receiving and interpreting information [64], [65].

The anatomy of the brain is very complex and is separated in four specialized areas that work together. Figure 2.6 shows the different specialized areas of the brain and these areas are listed below:

- the **cortex** is the outermost layer of brain cells. Thinking and voluntary movements begin in the cortex.
- the **brain stem** is between the spinal cord and the rest of the brain. Basic functions like breathing and sleep are controlled here.
- the **basal ganglia** are a cluster of structures in the centre of the brain. The basal ganglia coordinate messages between multiple other brain areas.
- the **cerebellum** is at the base and the back of the brain. The cerebellum is responsible for coordination and balance.

The brain is also divided into several lobes. These lobes are shown in figure 2.7 and listed below:

- The **frontal lobe** is located in front of the central sulcus associated reasoning, planning, parts of speech and movement (motor cortex), emotions, and problem-solving.

- The **parietal lobe** is located behind the central sulcus and manages sensation, perception of stimuli such as touch, pressure, temperature and pain handwriting, and body position.
- The **temporal lobe** Located below the lateral fissure concerned with perception and recognition of auditory stimuli (hearing) and memory are involved with memory and hearing.
- The **occipital lobe** is located at the back of the brain behind the parietal lobe and temporal lobe contain the brain's visual processing system.

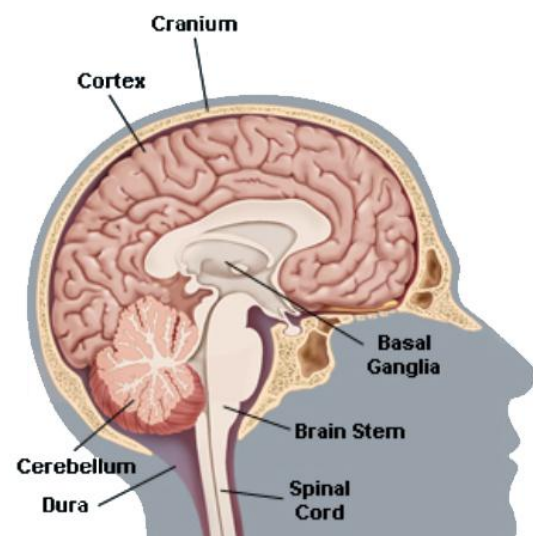


Figure 2.6: The brain is composed of three parts, the cortex the brain stem the basal ganglia the cerebellum [50].

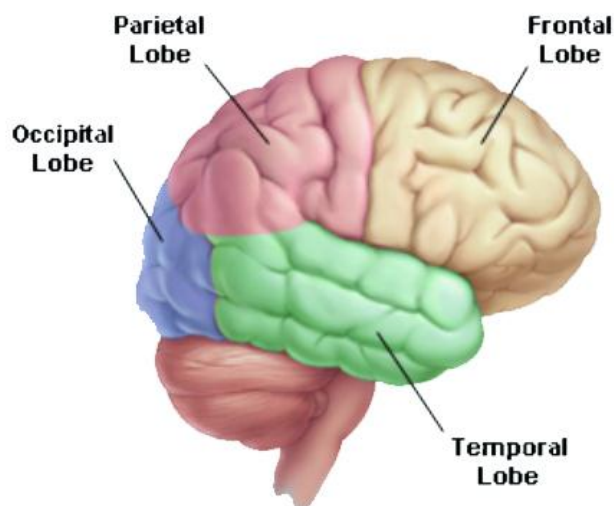


Figure 2.7: The brain is divided into several lobes, the frontal, the parietal, the temporal and occipital [50].

2.5.1 Benign and malignant and metastatic brain tumours

A brain tumour is an abnormal growth of tissue in the brain. The tumour can either originate in the brain itself, or come from another part of the body and travel to the brain [64], [65].

a. Benign brain tumour

A benign tumour does not contain cancer cells and usually, once removed, does not recur. Most benign brain tumours have clear borders, meaning they do not invade surrounding tissue. These tumours can, however, cause symptoms similar to cancerous tumours because of their size and location in the brain.

b. Malignant (cancerous) thyroid tumours

Malignant brain tumours contain cancer cells. Malignant brain tumours are usually fast growing and invade surrounding tissue. Malignant brain tumours very rarely spread to other areas of the body, but may recur after treatment. Sometimes, brain tumours that are not cancer are called malignant because of their size and location, and the damage they can do to vital functions of the brain.

c. Metastatic brain tumours

Metastatic brain tumours are tumours that begin to grow in another part of the body and then spread to the brain through the bloodstream. Common types of cancer that can travel to the brain include lung cancer, breast cancer, melanoma (a type of skin cancer), and colon cancer. All of these cancers are considered malignant once they have spread to the brain.

d. Types of brain tumours

There are many different types of brain tumours. They are usually categorized by the type of cell where the tumour begins, or they are categorized by the area of the brain where they occur.

Gliomas are the most common type of primary brain tumour. There are several type of gliomas and these begin from glial cells, which are the supportive tissue of the brain. Several types of brain tumours are given below:

- **Astrocytomas** are glial cell tumours that are derived from connective tissue cells called astrocytes. These cells can be found anywhere in the brain or spinal cord. Astrocytomas are the most common type of childhood brain tumour, and the most common type of primary brain tumour in adults. Astrocytomas are generally subdivided into high-grade, medium-grade or low-grade tumours. High-grade astrocytomas are the most malignant of all brain tumours.
- **Brain stem gliomas** are tumours found in the brain stem. Most brain stem tumours cannot be surgically removed because of the remote location and delicate and complex function this area controls. Brain stem gliomas occur almost exclusively in children.
- **Glioblastoma multiforme (GBM)** is the most common glioma. It represents nearly one fourth of all primary brain tumours. This cancer starts in the glial cells, which are cells that help nerve cells work.
- **Ependymomas** are also glial cell tumours. They usually develop in the lining of the ventricles or in the spinal cord. This type of tumours mostly occurs in children younger than 10 years of age. Ependymomas can be slow growing, compared to other brain tumours, but may recur after treatment is completed. Recurrence of ependymomas results in a more invasive tumour with more resistance to treatment. Two percent of brain tumours are ependymomas.
- **Hemangioblastomas** are tumours usually located in the cerebellum and spinal cord. They can cause significant problems, for example angiomas in the brain or spinal cord may press on nerve or brain tissue. The tumours can occur as the result of von Hippel-Lindau disease.
- **Optic nerve gliomas** are found in or around the nerves that send messages from the eyes to the brain. They are frequently found in persons who have neurofibromatosis, a condition a child is born with that makes him/her more likely to develop tumours in the brain. These are typically difficult to treat because of the surrounding sensitive brain structures.
- **Oligodendrogliomas** is a type of tumour also arises from the supporting cells of the brain. They are found commonly in the cerebral hemispheres (cerebrum). This tumour is more common in persons in their 40s and

50s. These tumours have a better prognosis than most other gliomas, but they can become more malignant with time.

- **Uveal melanoma** is cancer (melanoma) of the eye. Common surgical treatment for uveal melanomas is enucleation (removal of the eye), and other therapeutic options include radium plaque therapy and proton beam therapy.

e. Diagnostic methods for brain cancers

In addition to a complete medical history and physical examination, diagnostic procedures for brain tumours may include the following:

- Neurological examination
- Computed tomography scan
- Magnetic resonance imaging (MRI)
- X-ray
- Bone scan
- Arteriogram (also called an angiogram)
- Myelogram
- Spinal tap (also called a lumbar puncture)
- Positron emission tomography (PET)
- Magnetic resonance spectroscopy (MRS)
- Surgical biopsy

f. Brain cancer treatment methods

- Surgery is usually the first step in the treatment of brain tumors
- Chemotherapy
- Radiation therapy
- Steroids are used to treat and prevent swelling, especially in the brain.
- Anti-seizure medication treats and prevents seizures associated with intracranial pressure.
- Placement of a ventriculoperitoneal shunt (also called a VP shunt), which is a tube that is placed into the fluid filled spaces of the brain called ventricles. The other end of the tube is placed into the abdomen to help drain excess fluid that can build up in the brain and cause an increase in pressure in the brain.
- Bone marrow transplantation
- Supportive care minimizes the side effects of the tumor or treatment.
- Rehabilitation may be necessary to regain lost motor skills and muscle strength; speech, physical, and occupational therapists may be involved in the healthcare team.
- Antibiotics treat and prevent infections.
- Continuous follow-up care helps manage disease, detect recurrence of the tumour, and to manage late effects of treatment.

g. Brain cancer statistics

The statistical information shown in appendix 12.3 was taken from the National Cancer Institute (NCI) [51] and from the World Health Organization-International Agency for research on Cancer [55].

2.6 Conclusion

In this chapter the abdominal organs liver, kidney, and pancreas as well as thyroid were described and the different types of cancers on these organs were considered. Furthermore, the current treatments for these tumours were stated. However, through research HIFU has proven to be very optimistic method for treating many cancers like brain tumours [2], [10]-[11], breast interventions [17],[24]-[26], brain biopsies [29], prostate procedures [8], [30]-[32], including those discussed in this chapter liver [9], [34]-[47], kidney [13], [14], [34], [46]-[49], pancreas [15], [16], and thyroid [18]-[22].

Before these studies are discussed. It will be very useful for the reader to receive an overall description of HIFU, and this will be the subject of the next chapter.

3 High intensity focused ultrasound (HIFU) technology

The concept of using ultrasound to treat cancer was not possible in 1930s-1940s but this conception started to change gradually in 1950s – 1960s and today it seems to be a very promising method for treating tumours and is the only non-invasive intervention [63]. Many researchers on the field strongly believe that HIFU will be the modality of the future when it comes to treating tumours although it has been proven that HIFU could also be used for other applications. HIFU applications for treating abdominal and thyroid tumours are concerned in this report and these applications are non-invasive and therefore a guidance system is a necessity. For the guidance of the HIFU transducers two methodologies are suitable, the MRI scanner and ultrasound. These two methodologies are discussed and compared in this chapter as well as why MRI was selected for these applications. Furthermore, the development of the positioning device was initiated by the need to precisely move the HIFU transducer inside the gantry of an MRI scanner to treat tumours up to 12 cm deep by selectively heating them and therefore causing necrosis with HIFU. Therefore, in this chapter the basic theory of ultrasound, and HIFU technologies, including MRI compatible ultrasound transducers are presented.

3.1 Ultrasound theory and ultrasound transducers

Sound is a physical phenomenon that produces vibrations or sound waves which propagate through matter and these sound waves transfer energy from one point to another. Important to consider here is that sound waves cannot travel through vacuum. The frequency is a basic characteristic of sound which specifies the number of vibrations per second. Humans can only hear sounds of frequencies between 20Hz and 2KHz, any sound of a higher frequency of the upper boundary is said to be ultrasound and cannot be heard by humans [69]-[71].

Prior to World War II, sound/sonar, was used to detect submerged objects in water and this initiate the study to apply the concept to medical diagnosis. After

World War II, researchers in Japan began to explore the medical diagnostic capabilities of ultrasound. In 1950s researchers managed to use ultrasound to detect gallstones, breast masses, and tumours. Japan was also the first country to apply Doppler ultrasound, an application of ultrasound that detects internal moving objects such as blood coursing through the heart for cardiovascular investigation. Later, ultrasound was applied to detect potential cancers and to visualize tumours in living subjects and in excised tissue.

The concept of producing ultrasounds relies on the conversion of electrical pulses to mechanical vibrations and the conversion of returned mechanical vibrations back into electrical energy is the basis for ultrasonic testing. Ultrasound transducer is the device used for converting the electrical pulses to mechanical energy (sound) and the returned sound (echo) back to electrical signals.

The heart of the transducer that converts the electrical energy to acoustic energy, and vice versa is the active element which basically is a piece of polarized material (i.e. some parts of the molecule are positively charged, while other parts of the molecule are negatively charged) with electrodes attached to two of its opposite faces. When an electric field is applied across the material, the polarized molecules will align themselves with the electric field, resulting in induced dipoles within the molecular or crystal structure of the material. This alignment of molecules will cause the material to change dimensions. This phenomenon is known as electrostriction. In addition, a permanently-polarized material such as quartz (SiO_2) or barium titanate (BaTiO_3) will produce an electric field when the material changes dimensions as a result of an imposed mechanical force. This phenomenon is known as the piezoelectric effect.

The active element of most acoustic transducers used today is a piezoelectric ceramic, which can be cut in various ways to produce different wave modes. A large piezoelectric ceramic element can be seen in the image of a cut away of a typical transducer in figure 3.1. Preceding the advent of piezoelectric ceramics in the early 1950's, piezoelectric crystals made from quartz crystals and magnetostrictive materials were primarily used. The active element is still sometimes referred to as the crystal by old timers in the non-destructive testing (NDT) field. When piezoelectric ceramics were introduced, they soon became

the dominant material for transducers due to their good piezoelectric properties and their ease of manufacture into a variety of shapes and sizes. They also operate at low voltage and are usable up to about 300°C. The first piezoceramic in general use was barium titanate, and that was followed during the 1960's by lead zirconate titanate compositions, which are now the most commonly employed ceramic for making transducers. New materials such as piezopolymers and composites are also being used in some applications.

The thickness of the active element is determined by the desired frequency of the transducer. A thin wafer element vibrates with a wavelength that is twice its thickness. Therefore, piezoelectric crystals are cut to a thickness that is 1/2 the desired radiated wavelength. The higher the frequency of the transducer, the thinner the active element. The primary reason that high frequency contact transducers are not produced is because the element is very thin and too fragile.

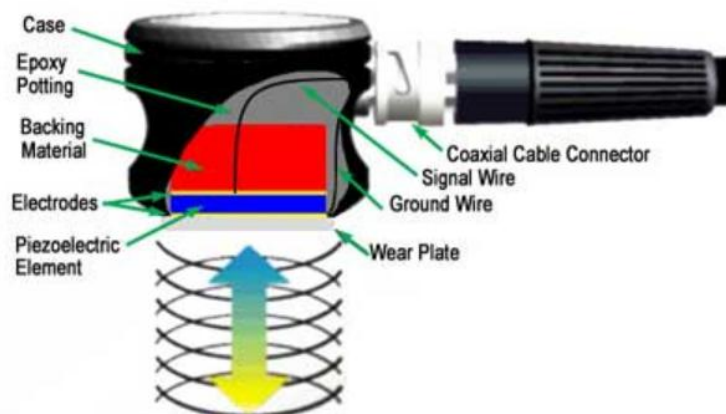


Figure 3.1: A cut away of a typical piezoelectric ceramic transducer.

The ultrasound technology was adopted by medical science initially for the diagnostic capabilities and for diagnostic ultrasound the frequencies used are in the range of 2 MHz to 20 MHz.

3.2 HIFU transducers, physics and technology of HIFU

High Intensity Focused Ultrasound (HIFU) transducer is like an ordinary ultrasound transducer with its area cut from a sphere and in this way the ultrasound pulses focus in the centre of the sphere from which the transducer is

made of. Due to the spherical geometry of the construction of the HIFU transducers, they can be used to precisely ablate the targeted area producing inducing necrosis at any depth from zero to focal length of the selected transducer and this can be done without harming the surrounding healthy tissues. Figure 3.2 shows a diagram of a HIFU transducer as a part of a sphere, with radius of 100mm targeting a tumour seated deeply into a healthy tissue. Figure 3.3 shows a photo of a typical HIFU transducer.

HIFU makes use of the bioeffects that occur with the insonation of human tissue with HIFU waves. The basic effects are the change of sonographic energy into heat and cavitation. Heat energy is caused by the friction that results from vibrating tissues interacting over time.

Exposing a tissue to HIFU energy for long time will cause cavitation [72], [73]. Cavitation is developed from gas bubbles generated within tissues when the HIFU energy hits the target for a long time. A bubble is formed from gas extracted from a tissue due to the pressure of the expansion or rarefaction. If the ultrasound beam continues to hit this bubble then the probability of cavitation is rising. The inertial cavitation is the cavitation that occurs when the bubble collapses after a rapid growth during the rarefaction phase. Transient cavitation is the bursting of these bubbles within the tissue planes and this causes significant cellular damage [74].

Furthermore, when targeting a tumour with HIFU there is a returned echo. This returned echo is not important absorption. However, it might be of a great importance when detecting cavitation. HIFU differs from diagnostic sonography exposure by the intent to maximize these biological effects to cause destruction of tumour cells and tissue planes.

HIFU Transducer with focal length of 100 mm

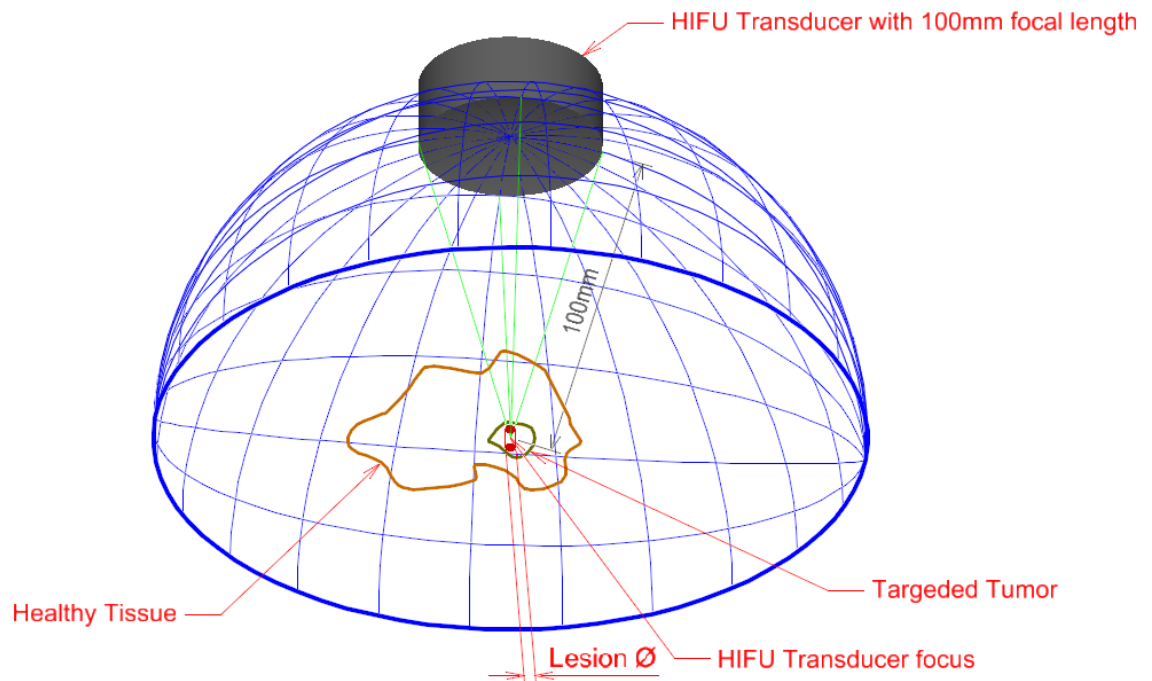


Figure 3.2: A diagram of a spherical HIFU Transducer with focal length of 100mm.

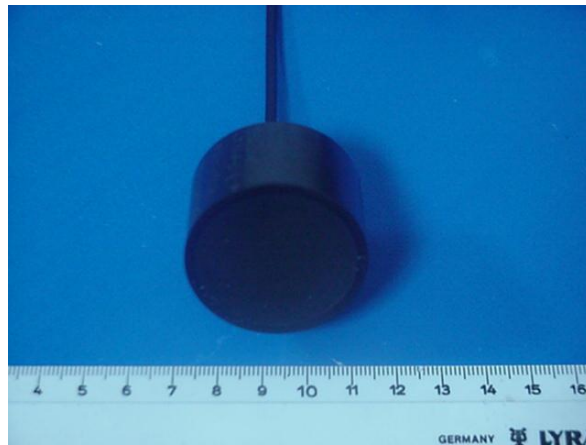


Figure 3.3: A photo of a typical HIFU Transducer.

The destruction of the targeted area is achieved by the HIFU Transducer. The HIFU transducer incorporates a piezoelectric element, which converts electrical signals into mechanical vibrations (transmit mode) [75]. These mechanical vibrations are concentrated at the focal point of the transducer and heat energy is developed by the friction of vibrating tissues interacting over time. Tissue temperature increases in the focal area resulting in a finite necrotic area. The area dimension is related to the firing duration and the necrotic area starts at

the transducer focus and progresses toward the transducer during the firing sequence as shown in figure 3.4.

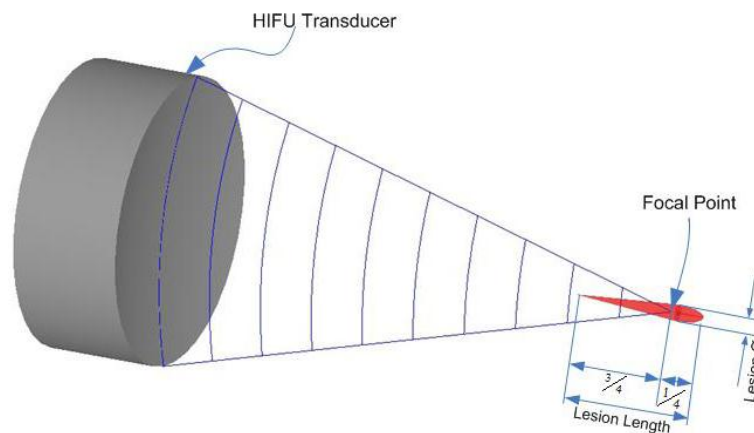


Figure 3.4: How the ablation causes finite necrosis of tissue at the targeted area.

Innovations in HIFU transducer construction in the recent years provide as better designs of transducers, acoustic materials. These advancements of HIFU transducers construction have improved the beam control, treatment times, and the ability to control beam distortion. In our days scientists have a choice of HIFU systems to administer for different applications. The choice is between treating tumours with a single transducer that focuses the beam at the centre of the sphere from which the transducer surface was cut from or a phased-array transducer that is electronically steered.

The single-transducer approach uses frequencies between 0.5 and 10 MHz, with the average around 1.5 MHz. With focusing intensity varies per procedure between 10,000 and 100,000 W/cm^2 , over a time period of 1 to 30 seconds.

Depending on the application of HIFU and the area of the body, many of the studies reviewed have built transducers and delivery systems that are unique to their research. A comparison between systems becomes difficult due to the variability of many of these experimental configurations.

HIFU delivery does have the commonality of maximizing biological effects, which are governed by certain physical properties to provide direct treatment. The fundamental concepts on which sonographic procedures are based include

the transmission frequency and the spatial peak temporal average (SPTA) intensity. The transducer itself has a specific range of output capability. An increase in frequency and/or output will have a direct effect on the temperature of the local tissue. As expected, heating increases as intensity and frequency are increased. It is equally important to note that, because of the attenuation, tissue located at a greater depth from the surface will heat to a lesser degree. This occurs because of the tissue's ability to absorb energy and the tendency for this energy to diffuse to a lower strength as it travels farther away from the source. The intensity of the beam is also governed by the density of the tissue that it is traveling through. As it is known, bone absorbs more energy than soft tissues, which is critical when determining the dosage required for therapeutic effects. These differences are accounted for in the mathematical index calculations for the soft tissue thermal index (TIS) and bone thermal index (TIB). These indices are the foundation for the as low as reasonably achievable (ALARA) principle, used in diagnostic sonographic practice. A conclusion drawn from research is that if temperature elevation exceeding 2°C, in diagnostic ultrasound, will cause damage on the tissue. This threshold is achieved at an energy level of 100 mW/cm² [76].

In addition to thermal effects in tissue caused by the sonographic process, it is vital to recognize the related pressure effects. A sound wave creates pressure changes as it propagates through a medium; in this case, the medium is tissue. Depending on the intensity and frequency at which the transducer is operating, the amplitude of the sound wave is directly related to increasing pressure against the tissue. Because the tissues are largely composed of fluids, cavitation can occur as the sound wave propagates. As the amplitude/pressure of the sound wave increases, transient cavitation can occur and cause rather significant destruction of cells and, ultimately, the tissue. As with the thermal aspect of sonography, thermal index (TI), there is a mechanic index (MI) used to measure the threshold at which the pressure becomes destructive, which is still under research.

3.3 Utilization of MRI for the guidance of the therapeutic ultrasound.

The available techniques for imaging are the following [77]:

- i. Ultrasound
- ii. Computer Tomography (CT)
- iii. Optical tomography
- iv. Positron emission tomography (PET)
- v. Single-photon emission computed tomography (SPECT)
- vi. Magnetic Resonance Imaging (MRI)

Ultrasonic imaging is small in size, simple and inexpensive method and can also create a real-time moving image of what you are looking at. An ultrasound transducer sends sound waves (1 to 10 MHz) into the body and receives the reflected sounds and this way creates a real-time moving image. Because sound waves are highly scattered at bone and air interfaces, many parts of the body are inaccessible, and effective imaging depth is limited in most organs to approximately 10 cm.

Computed tomography (CT) is an imaging technique for producing 2D and 3D cross-sectional images of soft tissue or bone from flat X-ray images. However CT exposes the patients to far more radiation than traditional X-ray in order to produce the 3D images.

Optical tomography is still under development and it seems to be a powerful technique for detecting tissue abnormalities and it works best on soft tissues such as breast and brain tumours. Most optical methods use relatively simple instrumentation to image-reflected excitation light, or fluorescence emission light, from a surface. Tissue reflectance imaging has high resolution and is fast, but because of multiple light scattering, sensitivity is limited by the $1/e$ optical penetration, and contrast is derived primarily from superficial structures, typically up to approximately 3 mm in depth.

Positron emission tomography (PET) is a technology in which radioactive isotopes are injected into the patient's bloodstream and it is mainly used to evaluate the extend of tumour metastasis, evaluation of the response to

treatment tumour and is considered to be the only imaging test that can distinguish a benign tumour from a malignant tumour.

SPECT is a powerful tool for quantifying the distribution of a radioactive compound (i.e., radiotracer) in humans. SPECT is similar to PET in its use of radioactive tracer material and detection of gamma rays. In contrast with PET, however, the tracer used in SPECT emits gamma radiation that is measured directly, whereas PET tracer emits positrons that annihilate with electrons up to a few millimetres away, causing two gamma photons to be emitted in opposite directions.

MRI uses magnetic fields to align protons inside our bodies and scans the rates at which protons change their orientation and creates static cross-sectional images of the body which can be combined to create 3D view.

Given the available techniques for imaging CT, PET and SPECT were excluded due to the harm that can cause to patients due to the radiation the patients are exposed to (CT), and the injected radioactive isotopes (PET and SPECT). Optical tomography is still under development and is currently used for brain and breast tumours, therefore is also excluded for abdominal organs or thyroid.

Comparing ultrasound with MRI both technologies are considered to cause no harm to the health of the patients and therefore tumour treatment can be repeated any number of times.

Furthermore, according to Yoav Medan, Chief Systems Architect of InSightec and Visiting Associate Professor, Biomedical Engineering at the Technion Institute of Technology, in an interview [78], with the current technology MR guided HIFU (MRgHIFU) operations on moving organs like liver and pancreas are performed while the patient is anesthetized something which should be avoided. Therefore MRI should undergo through major improvements in order to track moving organs in real time like ultrasound technology. Also MRI is a huge machine and very expensive compared to ultrasound.

Although MRI implies three main drawbacks compared to ultrasound technology, the limitation on the materials that can be used for the positioning devices, the significant higher cost [79] and the difficulty of tracking moving

organs, yet is the only available technology that fulfils the requirements of MR guided FUS (MRgFUS). MRI will provide the anatomy of soft tissues, the location of the FUS beam using the thermal imaging capabilities of the MRI scanner and the feedback of the effect of the FUS on the targeted organ which gives the physician a full control over its therapeutic outcome. Therefore MRI is the only modality available today for MRgFUS.

Moreover MRI guidance of robotic systems will fulfil the expectations of more precise interventions with minimal invasive procedures and reduced recovery time and additionally MRI provides us with high contrast images of soft tissues and without any ionizing radiation or injection of radioactive liquids.

As a result, in the last fifteen years MRgFUS and intraoperative MRI are penetrating the market as tools for various interventions and biopsy procedures on various organs [80].

3.4 Therapeutic ultrasound and HIFU

In our days many professionals in healthcare rely on ultrasound as a diagnostic tool but our concern in this research is not the diagnostic property of ultrasound but its therapeutic capabilities.

HIFU has the property to deliver heat to targeted tissues and therefore it is used extensively for medical applications. Nowadays HIFU is utilized to selectively heat biological tissues mainly for oncological applications with minimal invasiveness guided either by ultrasound or by MRI to provide, to the operator performing the procedure, images of a region within the subject being heated [3], [4], [5]. The main advantage of using HIFU to treat tumours compared to other recent treatment technologies, is that HIFU technology is non-invasive since the HIFU transducers can be applied to achieve necrosis of the targeted area, the tumour, without affecting the surrounding healthy tissue. This enables patients to walk home right after the operation and rehabilitation time is much shorter as they do not have to spend time in the intensive care unit (ICU) as usually patients do after a traditional operation. Therefore, this means that the cost of the operation will be much lower. Also, HIFU treatment technology has

none or minimal side effects and therefore it can be repeated any number of times if necessary.

Furthermore, HIFU has been proposed as a possible therapy treatment for several types of tumours that are complicated to treat using other methods. However, due to the nature of HIFU which doesn't pass through either solid bone or air it can be applied only for treatment of tumours of solid organs in some areas of the body. Also, HIFU is not suitable for people with cancer that has spread to more than one place in their body. Therefore, HIFU is not a candidate treatment technology for all cancers.

HIFU is considered investigational as a therapeutic option; the ability to provide non-invasive treatment for tumours is advantageous, and clinical trials that have been performed worldwide are very promising [75], [81].

In the future, HIFU could be the non-invasive therapeutic choice to treat tumours. This advanced technology would destroy the tumour centrally and any migrating cells without compromising the host organ and intervening tissues between the transducer and the mass [75].

3.4.1 How HIFU can be used to treat tumours

The concept of a HIFU system is to maintain a temperature between 50-100°C for few seconds to create tissue necrosis. This can be achieved with focal peak intensity between 1.000 and 10.000 W/cm² at frequency of 1-5 MHz and duration between 1-10 seconds.

Furthermore this ultrasonic energy can be applied from outside of the subject's body as shown in figure 3.2 [81]. The applied energy can be focused to a small spot (few millimetres, between 1 and 3mm) within the body so as to heat the biological tissue to a temperature sufficient to create a desired therapeutic effect. Therefore, to create tissue necrosis on larger areas, the HIFU transducer should be moved and with overlapping lesions larger areas will also be covered. This is shown *in vitro* experiments using clear synthetic gel [83]. This technique can be used to selectively destroy unwanted tissue within an

organ. The transducer must be immersed in a fluid container so that acoustical coupling is achieved between the transducer and the subject's body.

3.4.2 MRI compatible HIFU Transducers and safety issues

The idea of Fry brothers [2] half a century ago is now leading the way towards non-invasive operations. The main problem of this concept was the ability of the physicians to observe where the HIFU beam is at any time as well as the feedback or the effect of the HIFU application. Fortunately this problem was resolved by Jolesz, Jakab in 1991 [3] and as explained in section 3.3 MRI with the thermometry capability is the only modality that provides the physician the location of the HIFU beam at any time and the required feedback on the effect of the HIFU beam. Therefore, the HIFU transducers suitable for HIFU applications must be MRI compatible and safe. Lack of compatibility of the transducer with its MRI environment causes distortion of the images used for the guidance of the procedure. Moreover, careful selection of materials for the HIFU transducers operating inside the gantry of an MRI is of vital importance [84].

Moreover, in the recent years HIFU technologies are moving from research to commercial applications, therefore, the safety of patients during HIFU treatments is also important and need to be considered. The main safety issues to be considered when using HIFU to treat tumours are the following [85]:

- control of the acoustic power,
- control of the duty cycle (excitation time intervals),
- control of the acoustic beam to hit the targeted area,
- and the coupling of the transducer with the patient,

Excessive acoustic power may result in lesions larger than expected destroying healthy tissues or cavitation which causes significant cellular damage and possible burns at interface. Also, higher acoustic power may cause overheat resulting to damage of the transducer. On the other hand if the acoustic power is low, necrosis will not be achieved on the targeted area and this will result to inappropriate treatment of the targeted tumour.

Failure to control the duty cycle might also cause cavitation or inappropriate treatment of the targeted area.

Furthermore, controlling the HIFU beam to hit the targeted area (localization) is also very important for HIFU treatment. Defective transducers due to excessive heating may modify the focal point causing the beam to hit healthy tissues. This can be avoided with the use of MRI thermometry which gives us the exact location of the beam at any time.

Finally, poor coupling of the transducer with the patient will damage the transducer and would be impossible to have an effective treatment of the targeted area.

3.5 History of therapeutic HIFU

The development of ultrasound transducers started with the work of P. Langevin who used the piezoelectric properties of quartz crystal for the development of active sound devices for detecting submarines in 1915.

The first investigations of HIFU for non-invasive ablation were reported by Lynn et al. [1] in the early 1940s and later in the 1950s by the Fry brothers, Francis and William [2], at the University of Illinois and Carl Townsend, Howard White and George Gardner at the Interscience Research Institute of Champaign, pioneered the first medical application of ultrasonic waves.

This concept was related to the treatment of neurologic disorders such as Parkinson's disease. Using a set of ultrasound transducers, they were able to focus the energy deep inside the cerebral cortex. In particular, High Intensity ultrasound and ultrasound visualization was accomplished stereotaxically with a Cincinnati precision milling machine to perform accurate ablation of brain tumours. Until recently, clinical trials of HIFU for ablation were few (although significant work in hyperthermia was performed with ultrasonic heating), perhaps due to the complexity of the treatments and due to the lack of necessary imaging technology devices required for targeting the beam noninvasively. With recent advances in medical imaging and ultrasound

technology, interest in HIFU ablation of tumours has increased. Irradiation of experimental tumours using HIFU followed in the late 1970s and early 1980s.

In the 1980s, Lizzi, with a more advanced technology, set up a device for the treatment of glaucoma and intra-ocular tumours. This approach has been rapidly replaced by laser technology [12].

At the end of the 1980s, the INSERM - French National Institute for Medical Research of Lyon Hospitals and EDAP Technomed, engaged in a research program on the interaction of High Intensity Focused Ultrasound (HIFU) on tissues. The main purpose of this work was to develop applications to treat malignant tumours and the result of this joined venture was the prototype Ablatherm, the first High Intensity Focused Ultrasound device for the treatment of localized prostate cancer [86].

The first commercial HIFU machine, called the Sonablate 200, was developed by the American Company Focus Surgery, Inc. (Milipitas, CA) and launched in Europe in 1994 after receiving CE (Conformité Européene, meaning "European Conformity) approval, bringing a first medical validation of the technology for benign prostatic hyperplasia (BPH). Comprehensive studies by practitioners at more than one site using the device demonstrated clinical efficacy for the destruction of prostatic tissue without blood loss or long term side effects [79].

Although, the Ablatherm first patient was treated in 1993 with the first Ablatherm HIFU system, the CE mark was only received in 2000. Later studies on localized prostate cancer by Murat and colleagues at the Edouard Herriot Hospital in Lyon in 2006 showed that after treatment with the Ablatherm, progression-free survival rates were very high for low and intermediate risk patients with recurrent prostate cancer (70% and 50% respectively) [86]. HIFU treatment of prostate cancer is currently an approved therapy in Europe, Canada, South Korea, Australia, and elsewhere. Prostate cancer trials for the new Sonablate 500 in the U.S.A. are currently held for prostate cancer patients and those who have experienced radiation failure.

Magnetic Resonance Guided Focused Ultrasound MRgFUS was first developed by Harvey Cline and Ronald Watkins at GE Corporate R&D lab in Niskayuna NY and Kullervo Hynynen at the University of Arizona, Tucson AZ. starting in

1991. The technology was later transferred to InsignTec in Haifa Israel in 2000. The InsignTec ExAblate 2000 was the first MR Guided focused ultrasound system to obtain FDA market approval and sold commercially in the United States [79], [86].

Haifu Model JC and JC200 by ChongQing Haifu Ltd [88], [89] are complete ultrasound guided tumour treatment systems, and they are only CE approved for benign and malignant tumours. HIFU-2001(By Sumo Corporation Ltd) is an enhanced technology treatment system which doesn't require anaesthesia and is used extensively in Asia countries.

Table 3.1 summarizes the main historical events in the development of therapeutic HIFU and table 3.2 lists the active companies in the area of image guided ultrasound robotic systems and their medical applications.

Num.	Year	Event
1	1912	Sonar
2	1914	First sonar (sound navigation and ranging) apparatus
3	1916	Sonar to locate submarines in World War I
4	1920	Piezoelectric Transducers
5	1927	Bioeffects
6	1933	Cancer Therapy (Intensity)
7	1937	Flow Direction
8	1939	Physiotherapy
9	1942	HIFU for non-invasive ablation
10	1945	World War II -'reflectoscope' for non-destructive testing. This was used in the testing of aircraft wings.
11	1949	Erlangen Resolution
12	1954	Clinical treatments of neurological disorders
13	1989	EDAP TMS and INSERM jointly develop HIFU technology
14	1991	Magnetic Resonance Guided Focused Ultrasound MRgFUS
15	1994	First commercial HIFU machine, called the Sonablate 200
16	1995	First MRI compatible robot for the guidance of HIFU Transducer
17	2000	EDAP TMS - Ablatherm HIFU receives the CE mark and industrial production starts
18	2004	First MR Guided focused ultrasound system ExAblate 2000 to obtain FDA market approval in the United States, by InsignTec
19	2009	Sonallevé MR-HIFU by Philips Healthcare Philips received the CE mark for clinical use

Table 3.1: The main historical events in the development of medical ultrasonic are listed in the above table [90].

Num	Company country of origin and Foundation year	Model	Application
1	<ul style="list-style-type: none"> • INSERM – French Institute of Medical Research • EDAP TMS • Lyon - France • founded in 1979 	<ul style="list-style-type: none"> • Ablatherm • CE mark in 2000 • Ultrasound image guided 	<ul style="list-style-type: none"> • Treatment of localized prostate cancer
2	<ul style="list-style-type: none"> • Focus Surgery, Inc. subsidiary of US HIFU • Indianapolis, Indiana, US • Founded in 1996 	<ul style="list-style-type: none"> • Sonablate 200 • CE approval in 1994 • Ultrasound image guided 	<ul style="list-style-type: none"> • Benign prostatic hyperplasia
		<ul style="list-style-type: none"> • Sonablate 500 • CE Mark in Europe • MHW approval in Japan • Ultrasound image guided 	<ul style="list-style-type: none"> • Prostate cancer
3	<ul style="list-style-type: none"> • InsignTec • Tirat Carmel, Israel • Founded in 1999 	<ul style="list-style-type: none"> • ExAblate 2000 • CE mark in 2002 • 1st HIFU System obtained FDA market in 2004 • MR image guided 	<ul style="list-style-type: none"> • Prostate cancer • Breast cancer • Adenomyosis • Pain palliation of bone metastases.
4	<ul style="list-style-type: none"> • Philips Healthcare, • Netherland • Founded in 1895 	<ul style="list-style-type: none"> • Sonalleve • CE mark in 2009 • MR image guided 	<ul style="list-style-type: none"> • Uterine fibroids • Non-invasive palliative pain treatment of bone metastases
5	<ul style="list-style-type: none"> • ChongQing Haifu Ltd • Chongqing, China • Founded in 1999 	<ul style="list-style-type: none"> • Haifu Model JC • CE mark in 2005, China: SFDA, Korea: KFDA, Russian Federation approval • Ultrasound image guided 	<ul style="list-style-type: none"> • Primary and metastatic liver cancer • Breast • Kidney • Pancreas • Primary and metastatic malignant bone tumours • Soft tissue sarcomas • Uterine fibroids • Breast fibroadenomas • Pain relief of patients with advanced-stage malignant tumours.
		<ul style="list-style-type: none"> • Haifu Model JC200 • CE mark in 2005 • Ultrasound image guided 	<ul style="list-style-type: none"> • Uterine fibroids • Uterine adenomyosis
6	<ul style="list-style-type: none"> • Supersonic Imagine • Aix-en-Provence, France • Founded in 2005 	<ul style="list-style-type: none"> • Brain therapy system • MR image guided 	<ul style="list-style-type: none"> • Neurological diseases • Brain therapy
7	<ul style="list-style-type: none"> • Medsonic • Lemesos, Cyprus • Founded in 2005 	<ul style="list-style-type: none"> • Medsonic HIFU Robotic System • MR image guided 	<ul style="list-style-type: none"> • Brain • Stroke • Liver • Kidney • Pancreas
8	<ul style="list-style-type: none"> • Image Guided Therapy • Pessac-Bordeaux, France • Founded in 2001 	<ul style="list-style-type: none"> • TargetedFUS • MR image guided 	<ul style="list-style-type: none"> • Uterine Fibroma • Breast
9	<ul style="list-style-type: none"> • Theraclion The sound Therapy • France • Founded in 2004 	<ul style="list-style-type: none"> • TH-One • CE mark in 2005 • Ultrasound image guided 	<ul style="list-style-type: none"> • Breast fibroadenoma, • Thyroid nodules • Primary and secondary hyperparathyroidism

Num	Company country of origin and Foundation year	Model	Application
10	<ul style="list-style-type: none"> • Profound Medical Inc. (PMI) • Toronto, Canada, • Founded in 2008 	<ul style="list-style-type: none"> • high-energy ultrasound beam with a number of very small transducers (not focused) • Ultrasound image guided 	<ul style="list-style-type: none"> • Treatment of prostate cancer
11	<ul style="list-style-type: none"> • National Institute of Advanced Industrial Science and Technology • Tsukuba and Tokyo, Japan • Founded in 2001 	<ul style="list-style-type: none"> • AIST • MR compatible surgical assist robot • 2000 • MR image guided 	<ul style="list-style-type: none"> • Prostate biopsy
12	<ul style="list-style-type: none"> • Innomotion • Herxheim, Germany • Founded in 2004 	<ul style="list-style-type: none"> • Innomotion MR compatible Robotic Arm • CE mark in 2005 • MR image guided 	<ul style="list-style-type: none"> • Spinal diseases • Biopsy • Insertion of cannula and probes • Drainage • Drug delivery • Energetic tumour destruction • Aortic valve replacement
13	<ul style="list-style-type: none"> • China Medical Technologies, Inc, operated through subsidiary Beijing Yuande Bio-Medical Engineering Co., Ltd • Beijing, China • Founded in 1999 	<ul style="list-style-type: none"> • FEB-BY • Ultrasound Image guided 	<ul style="list-style-type: none"> • Liver, • Breast, • Kidney • Tumours in the pelvic cavity
14	<ul style="list-style-type: none"> • Shanghai A&S • Shanghai, China • Founded in 2001 	<ul style="list-style-type: none"> • HIFUNIT9000 • CE mark in 2005, China SFDA in 2002 and Korea KFDA in 2007 • Ultrasound Image guided 	<ul style="list-style-type: none"> • Treatment of abdominal and pelvic benign or malignant tumours
		<ul style="list-style-type: none"> • HIFUNIT9000P • Ultrasound Image guided 	<ul style="list-style-type: none"> • Treatment of abdominal and pelvic benign or malignant tumours

Table 3.2: Active companies in image guided ultrasound robotic systems [79], [86].

4 Applications of HIFU in medicine

As explained in previous chapters due to the nature of HIFU (ultrasound doesn't pass through bones or air) it can be applied only for treatment of tumours of solid organs in some areas of the body. For this reason HIFU is not a candidate for lungs for example.

Moreover, recent studies show that the contrast between necrotic tissue and normal tissue in MRI images is very good [7], [91]-[93] and therefore MRgFUS is becoming one of the best candidates when using HIFU treatment.

Nowadays apart from the treatment of tumours in abdominal organs considered in this report, liver, kidney, and pancreas researchers are studying application of HIFU to treat brain tumours [11], [83], [94], [95], cardiac arrhythmia [96], [97], strokes [98]-[100], breast interventions [17], [24]-[26], brain biopsies [29], and prostate procedures [30]-[32].

Moreover, in a study in 2008 sixteen patients were treated with HIFU and the results show that symptoms like pain were significantly alleviated and the quality of life of the patients in terms of eating, sleeping and mental status was markedly improved in most of the patients. They also claim that no serious complications were observed [15], [56].

However, this chapter focuses only on the utilization of HIFU technology to treat tumours of the abdominal area and thyroid. Furthermore, pros and cons of the HIFU technology as well as magnetic resonance image guided robots used to guide the ultrasonic transducers are also discussed in this chapter.

4.1 Current state of the art of HIFU for treating abdominal tumours and thyroid tumours

The current methods used for treating abdominal and thyroid tumours are described in chapter 2.

The traditional methods for treating tumours found in liver, kidney, pancreas and thyroid are described in chapter 2. Over the last two decades, non-invasive and minimally invasive procedures have been developed to provide means for the ablation of solid tumours in the liver, kidney, pancreas and thyroid. On-going research on these therapies have developed more efficient methods for treating tumours, laser [101]-[104] cryotherapy-cryosurgery [105]-[107], radiofrequency [108]-[112], ethanol injection [113], [114], and microwave [115]-[117] and comparison of these methods [118]-[121], have open the doors towards the non-invasive surgeries. However, HIFU remains the only modality to be completely extracorporeal [47].

Apart from the image guided ultrasound robotic systems models appeared in table 3.2, Siemens Medical Solutions and Chongqing Haifu Technology Co., Ltd have signed a contract to jointly develop an MRI guided High Intensity Focused Ultrasound (HIFU) therapy system. This collaboration aims to combine Haifu's therapy technology with Siemens' expertise in high field Magnetic Resonance Imaging (MRI) to develop a new MRgHIFU system which will focus on women's health treatments like benign uterine fibroids and cancer as well as malignant and benign tumours of liver, kidney, pancreas and bone.

Another partnership which aims to develop a HIFU system to treat prostate cancer is the US HIFU and Riverside Research Institute (RRI). This partnership claims to develop a system that will combine the advanced tissue-type imaging with ultrasound energy from the Sonablate 500 medical device in order to more reliably detect and evaluate cancerous tissue and make treating only the cancerous prostatic tissue instead of the entire gland possible.

The third partnership that aims to penetrate the market of MRI Guided HIFU is the cooperation of Siemens, German Cancer Research Center (D.K.F.Z.) and Heidelberg University. This partnership aims to develop an MRgFUS system for the treatment of localized tumours, whether in the prostate, the breast, or in any ultrasound accessible organ.

Furthermore, the treatment of abdominal and thyroid tumours using HIFU systems were also studied and tested by previous researchers during the last two decades like liver [9], [34]-[47], kidney [13], [14], [34], [46]-[49], pancreas

[15], [16] and thyroid [18]-[22]. However, as shown in table 3.2 only seven out of seventeen commercial image guided ultrasound robotic systems are using MRI for the image guidance, but it seems that in the near future more and more companies will invest on MRgFUS systems and few of them are currently under development. Moreover, from these seventeen models displayed in table 3.2 apart from the robotic systems under development of Medsonic Ltd. (presented in this report) only four models are applied on liver tumours, (Haifu Model JC, FEB-BY, HIFUNIT9000 and HIFUNIT9000P), the same four for kidney tumours, one for pancreatic tumours (Haifu Model JC), and one for thyroid tumours (TH-One). Finally from the seventeen commercial image guided ultrasound robotic systems presented in table 3.2 none of these is using MR for the image guidance for treating tumours located in liver, kidney, pancreas and thyroid.

As mentioned previously this research concerns with HIFU technology and in particular on the positioning devices that can be utilized to guide the HIFU transducers inside the gantry of an MRI scanner to treat liver, kidney, pancreas and thyroid tumours.

4.1.1 Disadvantages of the current methods for treating abdominal tumours

All of the current treatments have several disadvantages. These disadvantages are listed below:

- With the current treatments it is hard to limit the effects of treatment so that only cancer cells are removed or destroyed. In surgical resection for example, the surrounding healthy tissue is also removed to prevent cancer spreading. Chemotherapy also kills healthy cells.
- Because treatment also damages healthy cells and tissues, it often causes unpleasant side effects. The side effects of cancer treatment may vary. They depend mainly on the type and extent of the treatment. Also, each person reacts differently. Chemotherapy for some persons causes tragic side effects.
- Most of these methods have several side effects.
- Patients suffer from pain after surgical resection.

- Patient after surgery they entered the intensive care unit and after the intensive unit care they need some time for recovery at home. Thus implies higher cost.
- The psychological effects on the patients caused by the side effects, the pain and the recovery time of traditional treatment methods is also a major limitation of these therapies.
- Treatments cannot be repeated if necessary.

4.2 Advantages of HIFU

High Intensity Focused Ultrasound is often considered a promising technology within the non-invasive or minimally invasive therapy segments of medical technology. HIFU's capacity to generate in-depth precise tissue necrosis using an external applicator, with no effect on the surrounding structures, is unique. The history of using therapeutic ultrasound dates back to early in the 20th century. Technology has continually improved and additional clinical applications, both diagnostic and therapeutic, have become an integral part of medicine today.

Furthermore, an important difference between HIFU and many other forms of focused energy, such as radiation therapy or radio surgery, is that the passage of ultrasound energy through intervening tissue has no apparent cumulative effect on that tissue [122]. Also, treatment with HIFU is minimally invasive; in-depth as well it generates precise tissue necrosis. There is no effect on the surrounding areas. Another advantage of HIFU is the repetition of the treatment.

HIFU can also be administered to older patients as well. "When patients in their 70s are diagnosed with prostate cancer, this is the only technique we recommend. It is also recommended for young patients who suffer from high blood pressure, diabetes and cardiac diseases," shares Dr Desai [122].

Explaining the advantages, Dr Ramana Murthy adds, "The use of HIFU is quite effective showing no sign of cancer in biopsies taken following the procedure.

The levels of Prostate-Specific Antigen (PSA), drop dramatically after the treatment. "He adds that in general cases, no hormones are required. Also, people who have been treated with HIFU so far have had very few side effects [122].

Experts consider HIFU as a promising technology and recent studies prove that HIFU is the future in medicine. The healthy tissue through which the ultrasound passes is not affected and therefore HIFU is not invasive therapy.

The benefits of HIFU treatment are listed below:

- With HIFU the tumour is targeted and ablated precisely and therefore healthy tissues are not destroyed. Furthermore, the pain is minimized since only the cancerous cells are ablated.
- HIFU treatment causes far less damaging side-effects than conventional treatments.
- HIFU can avoid chemotherapy.
- HIFU does not involve radiotherapy.
- With HIFU technology surgery is not required since it is non-invasive. Therefore, the pain and the recovery time are minimized.
- Patient after HIFU treatment they don't entered the intensive care unit. Therefore, this will lower the cost to the patient.
- The recovery time after HIFU treatment is minimized and patients can go to work the day after the treatment. Therefore, the cost is lower and also the psychological effects on the patient are minimized.
- Not limited by tumour size
- HIFU treatment may result in a strengthening of the patient's immunity to cancer [123]-[125].
- HIFU treatment can be repeated, if necessary, any number of times with no any effects on the patient.

Therefore HIFU technology with so many advantages it seems to be very promising in future medicine and especial in treating tumours.

4.3 Limitations and drawbacks of HIFU

HIFU may cause some pain for three to four days post-surgery. In some cases, HIFU also causes sore skin in the area treated.

Generally, HIFU is used for treating small tumours on solid organs it cannot be used in case the tumours are more widespread. This means that HIFU is not suitable for people with cancer that has spread to more than one place in their body.

HIFU cannot propagate through either solid bone can absorb or reflect an ultrasound beam or air." This also means that it is not suitable to treat every type of cancer.

Although it has been showed that pancreatic and liver tumours can be treated with today's technology, in such cases the patient needs to be anesthetised. Anesthetising the customer is not desirable, however this cannot be avoided with the current state of MRI. As mentioned earlier, MRI cannot track organs in real time like ultrasound and therefore, moving organs are hard to be treated. To solve this problem either MRI will have to go through major improvement so imaging will be in real time and this will enable physicians to point an organ which is moving or though research we will be able to control breathing and moving organs [126], [127].

4.4 Magnetic Resonance guided High Intensity Focused Ultrasounds (MRgHIFU) systems

HIFU, as explained in the previous chapters is a promising technology with many advantages when compared with other available methodologies for treating tumours. The fact that the number of scientist devoted in this area is rising exponentially in the recent years proves that HIFU is considered to be the future solution for treating tumours. However since HIFU is a non-invasive technique the main gap that Fry brothers faced is the targeted organ anatomy and the feedback on the effect of the applied HIFU beam. Without these, it is like a physician trying to perform a surgery blindfolded. The solution to the real

time guidance and the necessary feedback is provided by the MRI scanner and its thermometry capability.

Moreover, as explained in chapter 3 in order to treat large areas by creating tissue necrosis, the HIFU transducer should be maneuvered to create overlapping lesions of a diameter 1 to 3mm, leaving no untreated tissues. The positioning device of the HIFU transducer is responsible for this motion and should be placed inside the MRI scanner and monitored using a software interface from a distance. Therefore a positioning device which will guide the HIFU transducer to cover large regions of tumours is necessary in order to assure that the movement of the HIFU transducer is more precise creating the overlapping necrosis of the tumour. Furthermore, as the positioning device is placed inside the MRI scanner and this can cause interference with the RF field and therefore can cause some corruption of the images. Thus, care must be taken when selecting materials for its construction as all the components must be MRI compatible and small enough as to fit in the gantry of a typical MR scanner with diameter of 55 cm and length between 150 cm and 200 cm. MRI compatible robotic system refers to a system that is not hazardous in any way and neither generates any interference to the MRI scanner nor affected by the strong electromagnetic field of the MRI scanner [128], [129].

The development of a positioning device compatible with MRI is revolutionary since such applications will be guided by the three dimensional (3D) technology provided by the MRI. During the last decade the concept and the development of MRI compatible robots is moving with an accelerated pace and the number of the involved groups and funding is increasing [128]. The MRI guidance of a robot provides reliability and accuracy necessary for non-invasive or minimally invasive interventions [79].

The robots proposed in this study will be used to accurately move the HIFU transducer inside the gantry of an MRI scanner to create necrosis on the tissue where a tumour is identified.

The next section explains the choice of MRI guidance and gives an overview of image guided robots and HIFU systems with MRI guidance. Furthermore existing MRI compatible positioning devices are reviewed.

4.5 Image guided robots and HIFU systems with MRI guidance

The concept of using MRI to guide a real time non-invasive surgery with HIFU, as described earlier, proved to be feasible since the early nineties with clearly visible lesions produced by HIFU beams on a canine muscle *in vivo* inside the gantry of an MRI. Studies followed this concept [6], [7] showed that the contrast between necrotic tissue and normal tissue is superior when compared with ultrasound technology and this proves that MRI is an excellent tool for HIFU systems guidance. As a result the use of MRI to guide HIFU systems increased rapidly in recent years.

The advantages of using MRI compatible positioning device for different medical applications are the following:

- i. non or minimal invasive methods,
- ii. use of 3D view provided by the MRI scanner during the intervention,
- iii. the use of a robot assures high precision and repeatability,
- iv. and the main advantage of MRI over ultrasound imaging is the better anatomical information and is the only modality to show thermal lesions and temperature maps which will provide feedback to a physician for controlling the non-invasive procedure.

4.6 Existing imaging positioning devices

The concept of image guided robots using CT was introduced by Minerva system [130] for placing a needle precisely during stereotactic brain biopsy in 1993. The concept transferred to the gantry of the MRI scanner with the first MRI compatible robot developed by Masamune et al. [29] in 1995. This robot was made of polymers and MRI compatible material. However, the robot would not maneuverer during scan time.

As described in the previous section the combination of focused ultrasound with MRI imaging for the guidance of non-invasive procedures, was proposed in the early nineties by Jolesz and Jakab [3] and after that Harvey Cline and Ronald Watkins at the GE Corporate R&D lab and Kullervo Hynynen at the University of

Arizona joined Jolesz to develop the first focused ultrasound prototype [131]. The early MRgFUS developed by General Electric in the years 1993-1994 [132]-[133] used hydraulic principles to move the transducer. Several studies were done with these systems [134]. These MRgFUS systems place the transducer directly beneath the targeted tumour. Additionally, the hydraulic positioning systems have serious repeatability and reliability problems, and have never reached the clinics. The motors used in the hydraulic positioning systems interfere with the MRI scanner, and therefore are placed far from the MRI scanner, thus requiring the use of long motor drive shafts, which result to a large and complicated positioning system.

Another patent of MRgFUS by General Electric in 1995 [135] uses threaded shafts and screw drives through universal joints. This patent also requires the ultrasonic transducer to be placed directly beneath the object to be treated. The motors of this positioning system are made out of magnetic material and therefore they are placed at a distance from the MRI scanner.

This group of Hynynen, Jolesz and GE Healthcare in collaboration with Brigham and Women's Hospital and Elbit Medical Imaging continue successfully together until 1999. At that time their proprietary transferred to the newly formed company InSightec which had started as InSight Therapeutics and was based in Tirat Carmel, near Haifa Israel. The robotic system of patent [136] uses piezoelectric motors to move the transducer inside an MRI scanner. InSightec is considered to be the leader in the market of MRgFUS and system ExAblate 2000 was the first commercial MRgFUS for the treatment of uterine fibroids received the Food and Drug Administration (FDA) approval in 2004. InSightec claims that more than 8.000 patients have been treated with the ExAblate system worldwide since 2011 [86]. Furthermore, according to InSightec the ExAblate system can also be used to treat prostate cancer, breast cancer, adenomyosis, and for pain palliation of bone metastases. The ExAblate 2000 MRgFUS system is embedded on the patient's table which is compatible with the bore of both 1.5 Tesla and 3 Tesla MRI Systems.

In 1999 Chinzei et al. [84] delivered a study on the criteria to design MR compatible mechatronic devices and in the year 2000 a five degrees of freedom (DoF) MR compatible surgical assist robot [137] was developed by Chinzei et

al. This robot is placed outside the bore of the General Electric signa SP double-doughnuts intraoperative MRI, is actuated by ultrasonic motors and used for prostate biopsy.

Chongqing Haifu (HIFU) Technology Co., Ltd. founded in 1999 [88], [89] in Chongqing China have developed two models of HIFU therapeutic systems. The Haifu Model JC, which offers a non-invasive treatment of solid tumours including primary and metastatic liver cancer, breast cancer, primary and metastatic malignant bone tumours, soft tissue sarcomas, and benign tumours such as uterine fibroids and breast fibroadenomas and the Haifu Model JC200 Focused Ultrasound Tumour Therapeutic System which offers non-invasive treatment of uterine fibroids to reserve the patients' uterus and ablate the fibroids extracorporeally.

Another commercial robotic device for precise needle insertion during MR-guided therapy of spinal diseases [138], [139] was developed by Hempel et al. in 2003. This MR-guided robotic system was commercialized by the start-up company Innomedic. This MR guided robotic system was made to perform biopsy, insertion of cannula and probes, drainage, drug delivery and energetic tumour destruction [140], [141]. In 2008 Mazilu et al. use this MR guided robotic system of Innomotion for aortic valve replacement (AVR) [96]. The Innomotion MR guided robotic arm which has 6 DoF is moving along an arch which is mounted on the MRI patient table. An arm sitting on the arch takes advantage of the clearance between the patient and the bore. Further evaluation and different applications of the Innomotion robotic system are performed until today [80], [142]-[144].

Sonallevé MR-HIFU is also a commercial MRgFUS by Philips Healthcare Philips Healthcare, Netherland [145]. This MR guided robotic system is 5 DoF positioning system and is integrated with the HIFU transducer on the patient's table. According to the Focused Ultrasound Surgery Foundation the Sonallevé MR-HIFU system, received the CE mark for clinical use in December 2009, and offers a non-invasive alternative to the traditional surgical treatments for uterine fibroids in women. The Sonallevé MR-HIFU system has also received CE marking for non-invasive palliative pain treatment of bone metastases in 2011.

Another company that innovates in therapeutic products using High Intensity Focused Ultrasound and ultrasonic image guidance for the treatment of solid cancers and benign tumours is China Medical Technologies, Inc. FEB-BY is a non-invasive HIFU tumour therapy system and it was approved for sale by the Chinese State Food and Drug Administration (SFDA) in 1999 for the treatment of a wide variety of cancerous and benign solid tumours including: liver, breast, and kidney tumours and tumours in the pelvic cavity. According to China Medical Technologies, Inc. this HIFU tumour therapy system has been used in over 40,000 cases in China.

Theraclion is a French company, founded in 2004. Theraclion develops, manufactures and markets the TH-One, used in the non-invasive and ambulatory treatment of breast fibroadenoma, as well thyroid nodules and primary and secondary hyperparathyroidism [18], [22]. TH-One combines HIFU technology guided by real-time ultrasound imaging. It's an online step-by-step procedure through a touch screen monitor with a mobile unit and a robotic arm.

Profound Medical Inc. (PMI) - Prostate Focus Ultrasound is based in Toronto, Canada, and founded in 2008 [86]. PMI has developed an MRI-compatible ultrasound energy wand to deliver controlled thermal therapy to the regions of the prostate gland via a trans-urethral approach. This PMI system is not using the HIFU technology but is using high-energy ultrasound beam with a number of very small transducers (not focused) aligned on a probe introduced through the urethra.

Image Guided Therapy (IGT) founded 2001 based in Pessac, Bordeaux, France. Their HIFU system, the TargetedFUS, is a totally non-invasive MR guided thermal ablation device based on Focused Ultrasound (MRgFUS). The TargetedFUS model can be fitted with two different tabletop positioning systems optimized for different anatomies.

Focus Surgery is subsidiary of US HIFU, a US company in Indianapolis, Indiana who commercialized the Sonablate 500 system for non-invasive treatment of prostate cancer. Sonablate 500 system combines proprietary multi-focal length transducer technology in a custom transrectal imaging and therapy probe

[146]. The Sonablate 500 system is not using MRI for image guidance but it uses ultrasound imaging for treatment planning and monitoring.

The MR guided HIFU robotic system proposed by Damianou et al. [81] has three DoF and is small and portable and it can be seated on the table of any MRI scanner. This positioning device is to be used to treat brain tumours.

The patent [147] describes a manual positioning system, which can be used only in an open MRI system. Despite the fact that open MRI offers several advantages, it is not widely used because of its poor image quality. Moreover, the manual system is user dependent, whereas the system we propose is not user- dependent.

Another positioning system developed by Tsekos et al. [148], also utilizes piezoelectric motors in order to guide a biopsy needle. However, this system cannot be used in combination with a HIFU system, because there are no means to provide acoustical coupling between the transducer holder and the targeted tissue.

MR compatible robotic systems are very attractive for non-invasive surgeries where the physician will get continuous feedback from the MRI in order to have full control over the procedure. In the past fifteen years MRgHIFU robotic devices have been developed for a variety of applications like breast intervention [17], [24]-[26], [27], [149]-[150], prostate procedures [30]-[32], interventional spinal procedure [138], neurosurgery [29], [151], interventional liver therapy [152], cardiac intervention [96] and for experimental work on small animals [153].

Although these MRgHIFU robotic systems have demonstrated the technical feasibility of MR compatible manipulators, these devices are highly specialized for a certain anatomy or MR scanner design. Some of these robots are very complicated, expensive, not portable due to their complicated structure or size, and not compatible with all MRI scanners. Moreover, most of these robotic systems are not flexible to perform a variety of applications.

5 Development of HIFU system with MRI guidance

The importance of the MRI compatible positioning device which will guide the HIFU transducer was explained earlier. In this chapter three positioning devices are proposed for use in different MRI scanners for different applications and with several improvements from version to version. All three were designed and developed to be small, light, portable, cost effective, flexible and universal.

5.1 Design Criteria and requirements

The required devices for the implementation of the proposed HIFU-MRI system are summarized in table 5.1 and described in the following sections.

Commercially Available Components		
Num	Required Devices	Devices Used
1	RF amplifier	250 W, AR, Souderton, PA, USA
2	Signal generator	HP 33120A Hewlett Packard, now Agilent technologies, Englewood, CO, USA
3	High intensity focused ultrasound transducer	Etalon, Lebanon, IN, USA, 4 MHz, focal length of 10 cm and diameter of 3 cm.
4	Piezoelectric Ultrasonic Motors (PUM)	Shinsei USR60E3N
5	Dedicated driver for Shinsei PUM	Piezo Systems/Shinsei D6060E
6	Data acquisition Card	National instruments 6251 DAQ
7	MRI compatible camera	MRC Systems GmbH, Heidelberg, Germany
9	MRI compatible cavitation detector	Onda Corporation, Sunnyvale, CA
10	Thermocouple-to-analogue converter	Omega M2813-1205
11	Personal computer	Sony Vaio PCG-6W2M
12	MRI scanner	Signa 1.5 T, by General Electric, Fairfield, CT, USA
Componets used for Positioning Device Version 1		
1	Brass rods	0.95 cm diameter brass rod
2	Timing belt	<ul style="list-style-type: none"> the material of the band is Neoprepene width of 9 mm, pitch 5.8 mm length 60 cm (120 teeth)
3	Pulleys	The pulley has a width of 9.5 mm, and a pitch 5.8 mm and is made of Polycarbonate.
4	Plastic parts of the positioning device	<ul style="list-style-type: none"> polyethelyne supplied by United States Plastic Company (USP)
5	Brass Screws	-

Componets used for Positioning Devices Version 2 and 3		
1	Plastic parts of the positioning device	<ul style="list-style-type: none"> • Acrylonitrile Butadiene Styrene (ABS) • Design using CAD software, Microstation V8, Bentley Systems, Inc. • Produced by 3D printer, Stratasys, FDM400, 7665 Commerce Way Eden Prairie, MN 55344 U.S.A.
2	Brass racks and pinions	supplied by Sterling instrument NY USA
3	Brass screws	-
Design and Implemented Components		
1	Positioning Device	Design and implemented with MRI compatible materials and it will be used to guide the HIFU transducer inside the gantry of the MRI.
2	Coupling System	This is the container filled with the degassed water within which the transducer will operate and is attached on the positioning device. Is the media used for the focused ultrasound beam to travel through to the targeted area.
3	Software	<ul style="list-style-type: none"> • the application software to be developed for the user interface of the system. This software application will be used to control and guide the therapy. • software used for the development of the user interface application is MATLAB (The Math works Inc., Natick, MA, USA)

Table 5.1: Design criteria and requirements for the development of the HIFU-MRI system.

5.2 HIFU/ MRI system

The block diagram of the HIFU/MRI system used for the development of the MRI compatible positioning device is shown in figure 5.1. Figure 5.2 shows the actual components and devices used for the proposed positioning device. The HIFU/MRI system devices are summarized in the table 5.1 above.

5.2.1 HIFU system

The HIFU system consists of a signal generator (HP 33120A Hewlett Packard, now Agilent technologies, Englewood, CO, USA), an RF amplifier (250 W, AR, Souderton, PA, USA), and a spherically shaped bowl transducer (Etalon, Lebanon, IN, USA) made from piezoelectric ceramic which is non-magnetic. The transducer operates at 4 MHz, has focal length of 10 cm and diameter of 3 cm. The transducer is rigidly mounted on the MR compatible positioning device.

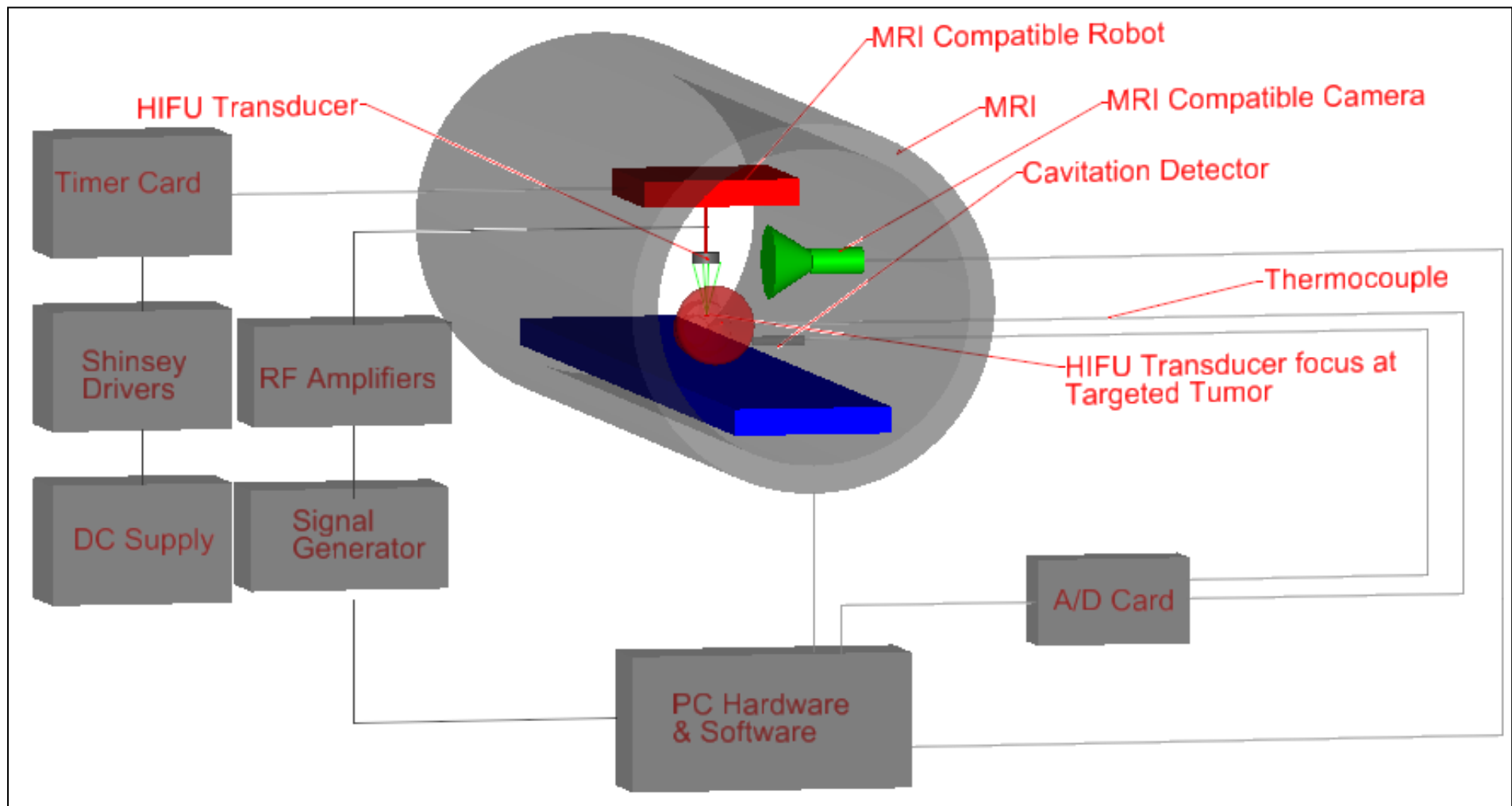


Figure 5.1: Block diagram of high intensity focused ultrasound (HIFU) system with the MRI guidance. This diagram shows the arrangement of the devices used in the HIFU system.

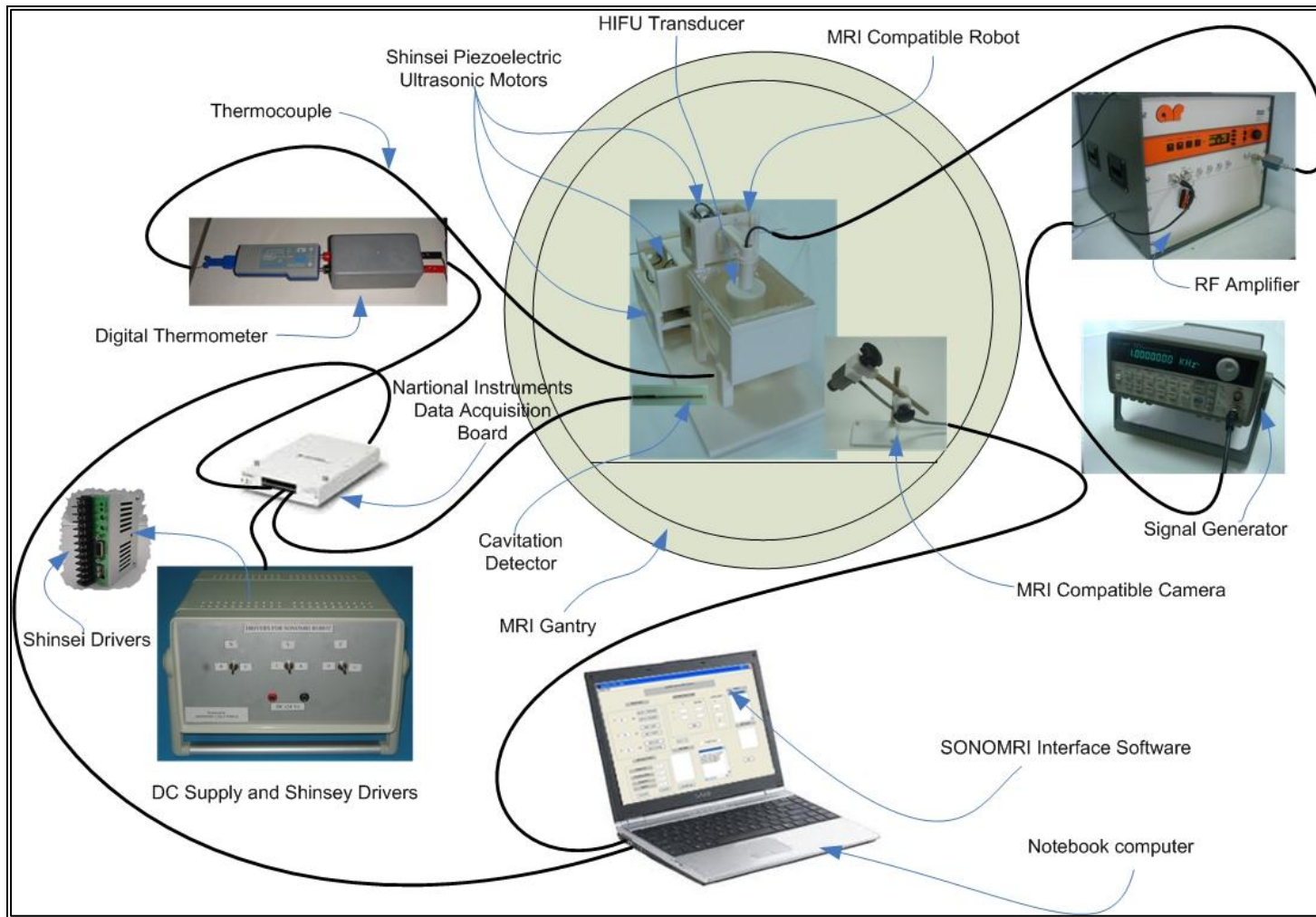


Figure 5.2: Setup of the actual devices used for the HIFU system with the MRI guidance (The positioning device shown is the third version).

5.2.2 Positioning device (Robot)

As explained previously the positioning device will operate inside the MRI scanner and therefore all the materials to be used for the construction of the robot should be MRI compatible (non-magnetic). This section here describes the devices and the materials used for the positioning device.

a. Piezoelectric Ultrasonic Motors (PUM) and their drivers

Piezoelectric ultrasonic motors (PUM) are used in various MRI compatible robotic systems [25], [29], [81], [137]. These motors are driven by the ultrasonic vibration of a piezoelectric transducer when high-frequency voltage is applied. Therefore PUMs do not interfere with the magnetic fields of the MRI scanner. However, according to Chinzei et al. [84], some commercially available PUM are prone to cause image artifacts and significant signal-to-noise ratio (SNR) loss [80].

The actuators of the robot apart from being non-magnetic in order to be used in the MRI must also be accurately controlled. The accuracy, by which the actuators are control to guide the HIFU transducer is of great importance and should be considered very carefully. The reason for this is due to the fact that actuators should precisely move the robot to cover the targeted area only avoiding lesions to healthy tissues. Furthermore, actuators must be small to save space inside the gantry of the MRI and must also be light to contribute to the portability of the robot.

Piezoelectric ultrasonic motors (PUM) have several advantages for space-based robot applications. These motors are MRI compatible, small, light in weight, bidirectional with high torque output, accurately driven and mechanically simple. Therefore PUM are well-suited to these requirements. PUM can achieve high precision as a result of low speed, lack of gears and transmissions, and freedom from backlash [154]. They are quite simple mechanically, consisting of a single moving part that provides the same functionality as motor, transmission, and brake in a conventional motor-driven system.

A typical piezoelectric ultrasonic motor consists of a toothed piezoelectric disk (stator) in contact with a metal disk (rotor) as shown in figure 5.3. Time-varying electric fields applied to the piezoelectric stator induce a travelling wave which is mechanically rectified, causing the rotor to rotate. This mechanism produces relatively high torque at low rotor angular velocities, obviating the need for gearing. The friction between rotor and stator provides a passive holding torque typically larger than the rotating torque, eliminating the need for mechanical brakes or active holding torque. These motors can be built such that they neither produce nor are affected by magnetic fields, making them useful in highly magnetic environments and applications in which magnetic fields are harmful.

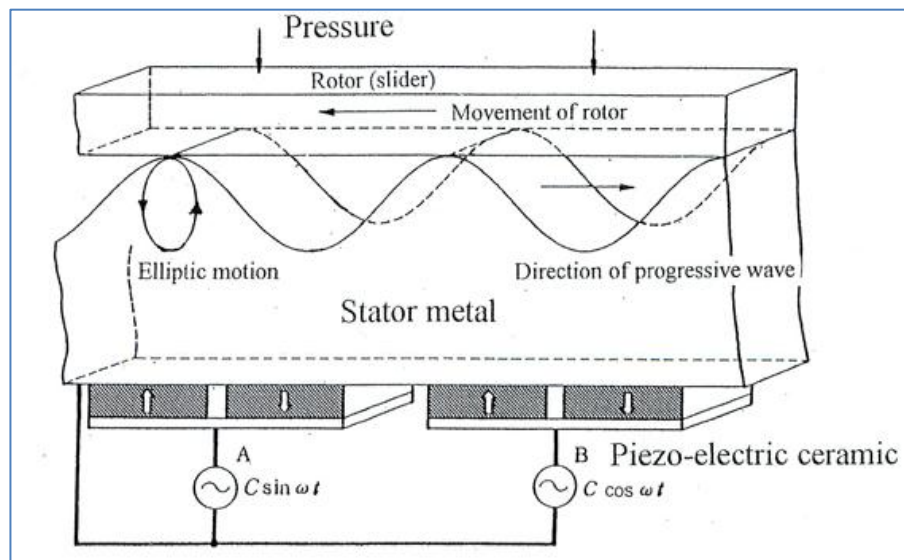


Figure 5.3: Diagram of the mechanism of the ultrasonic motor. The diagram above was taken from the manual of Shinsei motors.

Figure 5.4 shows the traveling wave formation and the direction of the rotor. The photo of figure 5.5 is a cross-section of a Shinsei PUM motor and shows the structure inside the motor.

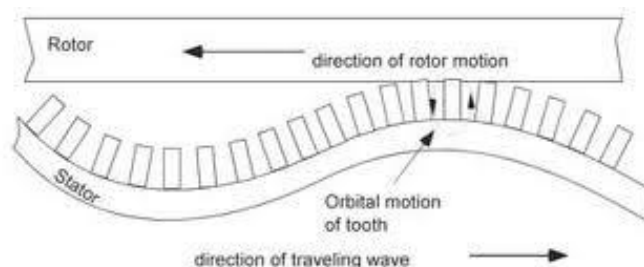


Figure 5.4: Traveling Wave Formation

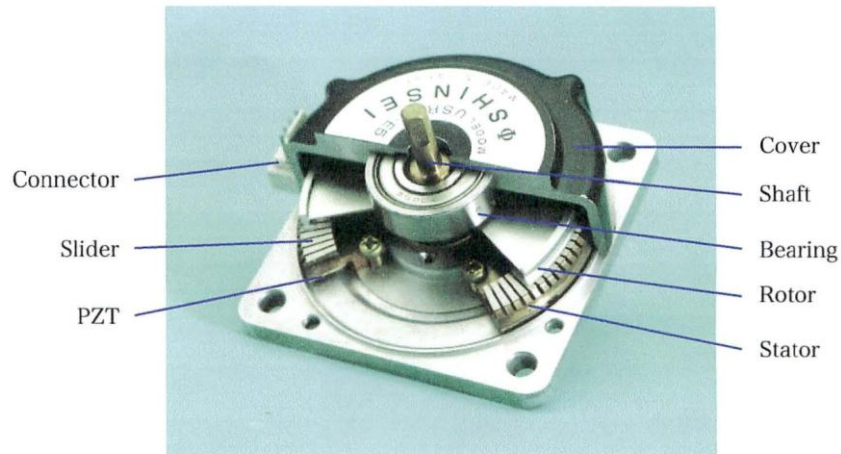


Figure 5.5: Inside structure of ultrasonic motor (USR60-S4)

The production of drive signals for the PUM requires special circuitry that produces a pair of phased sinusoidal signals of variable frequency. The motor was supplied with a standard commercial driver (Piezo Systems/Shinsei D6060E) that permits open-loop speed control via an analogue input signal and direction control via a pair of discrete input signals. Figure 5.6 shows a photo of piezoelectric ultrasonic motor by Shinsei USR60E3N and Figure 5.7 a photo of dedicated driver for Shinsei USR60 series, Shinsei D6060E.

b. Robot drivers

The box hosting the motor drivers is placed outside the MRI room since magnetic materials are involved. The diagram of figure 5.8 shows the basic connection diagram of the dedicated driver for Shinsei USR60 series, Shinsei D6060E and the diagram of figure 5.9 shows the wiring diagram of the driving electronics and computer-controlled interface.



Figure 5.6: A photo of piezoelectric ultrasonic motor by Shinsei USR60E3N.



Figure 5.7: A photo of dedicated driver for Shinsei USB60 series, Shinsei D6060E.

A DC supply (24 V, 6 A) is used to drive the Shinsei drivers. Wires from the Shinsei drivers are connected to a PCI 6602 interface card (National instruments, Austin, Texas, USA) via a connecting block. The PCI 6602 interface card includes timing and digital I/O modules. The interface is connected in a PC (Dell Inc. Round Rock, Texas, USA).

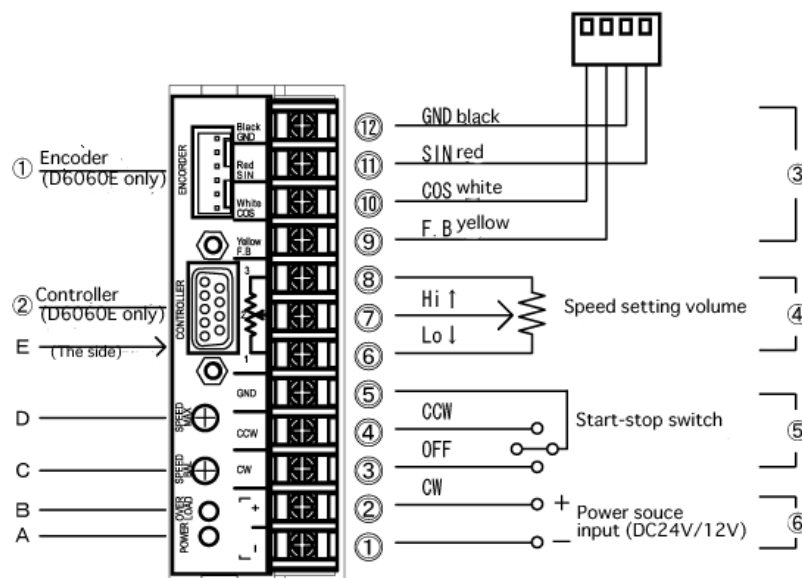


Figure 5.8: Basic connection diagram of the dedicated driver for Shinsei USB60 series, Shinsei D6060E

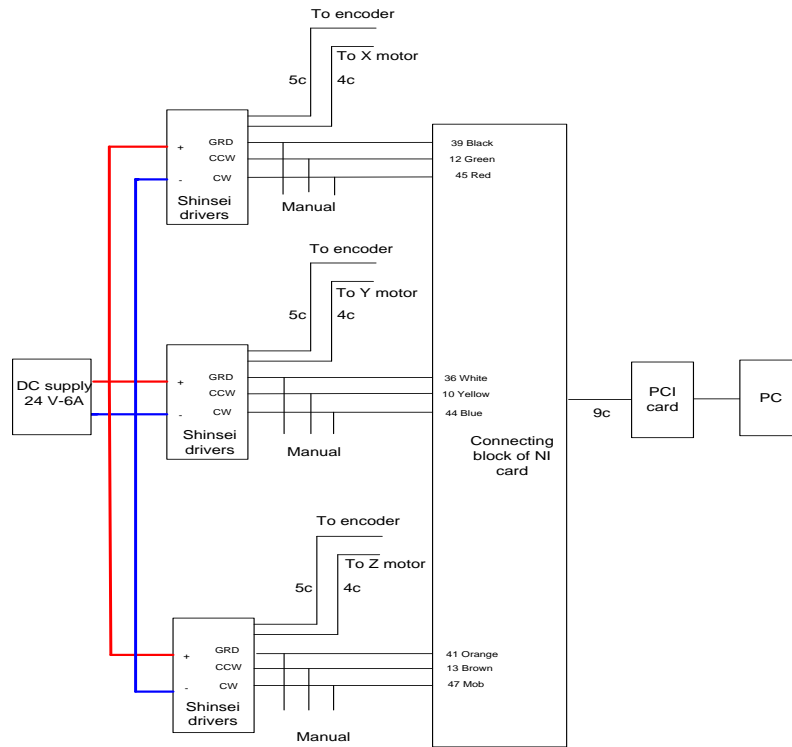


Figure 5.9: Wiring diagram of the motor drivers for 3 degrees of freedom positioning device.

The motors are driven when the ground and clockwise terminals of the Shinsei drivers are connected (clockwise rotation) or when the ground and anti-clockwise terminals of the Shinsei drivers are connected (anti-clockwise rotation). This is achieved by initiating a command from the software which places 2 digital output terminals of the PCI card (for example ground and clockwise) in the same potential. Movement of a certain axis can be achieved also manually by means of an ON-OFF-ON switch.

c. Temperature measurement at the focal point of the HIFU

The development of the digital thermometer was one of the first tasks of this research since this thermometer is of vital importance for all the experiments. The importance of the digital thermometer arises from the fact that necrosis of biological tissues is achieved through the induction of thermal dose only in the targeted area which is situated at any depth between 0cm and 10cm. Therefore this digital thermometer can be used during the experimental work to locate the focus of the HIFU transducer by emerging its thermocouple into the targeted biological tissue and measure the heat produced inside the tissue. Also it will

be used to store in a text file the variation of temperature with respect to time as heat is generated with the use of the HIFU transducer. This text file can then be used for the analysis of the thermal dose in to the tissue and these can give useful conclusions related to frequency, exposure time and cool off period and the intensity used.

d. Data Acquisition Card-National instruments 6251 DAQ

The data acquisition board used for the development of this project is the National Instruments 6251 DAQ model which feature 16 analogue input (AI) channels, two analogue output (AO) channels, up to 8 lines of digital input/output (DIO), Programmable Function Interface (PFI) or Digital I/O. As an input, each PFI terminal can be used to supply an external source for AI, AO, DI, and DO timing signals or counter/timer inputs. As a PFI output, you can route many different internal AI, AO, DI, or DO timing signals to each PFI terminal. You also can route the counter/timer outputs to each PFI terminal. As a Port 1 or Port 2 digital I/O signal, you can individually configure each signal as an input or output.

The digital input/output lines are used to drive the motors of the robot, and one of the analogue lines is used to capture the temperature into the computer. Also this card will be used for the localization of the robot.

e. Driving the piezoelectric motors with the Data Acquisition Board

The driver (Shinsei D6060 E) provided for the piezoelectric motors (Shinsei USR 60-E3N) permits speed control via an analogue input signal and the direction is controlled via a pair of discrete input signals. The analogue input signal is provided by the data acquisition card used by National instruments 6251 DAQ which is connected to the PC and driven by the software to be developed. This arrangement is shown in figures 5.1 and 5.2. This driver of piezoelectric motor also accepts a feedback from the motor and this will be fed back to the software through the data acquisition card to verify the localization of the motors.

5.2.3 Cavitation detector

From a scientific point of view it will be useful to separate lesions developed based on thermal and based on cavitation mechanisms. In this system we use a passive MRI compatible cavitation detector (Onda Corporation, Sunnyvale, CA), shown in figure 5.10, which is placed perpendicularly to the beam of the HIFU transducer. Since the HIFU protocol is applied inside the magnet of an MRI scanner, the detector must be MRI compatible. The diameter of the detector was 1 cm, its radius of curvature was 10 cm and operated between 1 and 13 MHz (centre frequency is 7 MHz). The detector was mechanically coupled to the HIFU transducer. The voltage from the detector was fed to an analogue to digital (A/D). The signal was then displayed in order to visualize whether cavitation occurs or not.



Figure 5.10: The photograph shows the cavitation detector.

5.2.4 MRI compatible camera

In order to monitor the condition of the animal or humans (future use), a MRI compatible camera (MRC Systems GmbH, Heidelberg, Germany) shown in figure 5.11, was mounted on the system. The camera was interfaced by means of a video card. With the aid of the MRI compatible camera, the researcher can monitor the welfare of the animal.

5.2.5 Software

A user-friendly program written in MATLAB (The Mathworks Inc., Natick, MA) has been developed in order to control the system. The software serves the following main tasks:

- i. Displaying of MR images

- ii. Transducer movement (the user may move the robotic arm in a specific direction or customize the automatic movement of the robotic arm in any rectangular formation by specifying the pattern, the step and the number of steps)
- iii. Messaging (starting time, treatment time left etc.)
- iv. Patient data (age, weight, etc.)
- v. Display of motor position
- vi. Display of the contents of the MR compatible camera
- vii. Cavitation detection window
- viii. Temperature measurement



Figure 5.11: The photograph shows the MRI compatible camera.

5.3 Advantages and limitations of the three versions of positioning devices

This thesis report proposed three versions of positioning devices each of which has several benefits and limitations. In this section the pros and cons of all three versions are outlined. The first version of positioning device was designed and implemented to overcome some of the limitations of the existing MRI guided HIFU positioning devices. The design requirements of the first version positioning device are listed below:

- i. to be used in experimental work to treat brain tumours in small animals *in vivo* or *in vitro* and hence transfer this concept to treat human brain tumours
- ii. to be portable therefore, small in size and light in weight
- iii. to be used in all commercially available MRI Design
- iv. to be flexible in order to be used for a variety of HIFU applications
- v. to be guided and controlled easily and effectively with a user friendly interface software. The requirements of the end user application are described in section 1.1

The completion of the first version of positioning device revealed some limitations and that's why the second version was considered. These limitations are listed below:

- i. the positioning device is driven with the timing belts and timing belts will not provide the robot with the best accuracy and stability.
- ii. the positioning device is applicable mainly for brain tumour and therefore, it's considered flexible multi-tool.
- iii. many parts of the robot are fabricated and assembled manually and thus makes the reproduction of the robot very difficult.

Designing the second version of positioning device all the advantages of the first version were retained with some additional features and some advantages. These new features and advantages are outlined below:

- i. the timing belts were replaced with racks and pinions and this granted better stability and accuracy
- ii. the second version of positioning device was designed with detachable HIFU transducer holders and this makes this robot a more flexible tool in the hands of the physicians. This robot can be utilized to treat tumours on liver, kidney, pancreas and thyroid tumours. This robot can also be used to perform experiments in large animals like pig, sheep and dog and small animals like rabbit and rat
- iii. related to the above advantage the capability of attaching different HIFU transducer holders of different length, height, and pointing direction or angle provide the robot the advantage to accept HIFU transducers from

different manufacturers or with different focal length and different diameter, for different applications

- iv. this robot was designed on CAD software and manufactured from a 3D printer and this will give smoother edges more accurate design and the reproduction of the robot will be possible.
- v. the production material and the new design made this version lighter and more compact compared to version one.

This second version also has some limitations the main of which is the effective working space for the targeted objects which is limited if it is to be sited on the table of the MRI. An alternative for this positioning device is to be attached on the top of the gantry of the MRI providing more effective operational area. However, this approach requires the cooperation with the MRI manufacturers.

The third version of positioning device adopted all the advantages of the second version of positioning device and resolves the limitation given above. All advances of this version compared to version two are listed below:

- i. the robot can operate on any MRI scanner available without any modification of the MRI
- ii. can be utilized treat brain liver, kidney, pancreas and thyroid tumours as well as to perform experiments in large animals like pig, sheep and dog and small animals like rabbit and rat.

6 Development of the positioning device version 1

This first version robot was to design to overcome the limitation of other existing similar devices. Therefore, the focus was to design a robot that is small, light, cost effective, universal and flexible positioning device which will be used to accurately guide the HIFU transducer inside the gantry of any MRI scanner to provide in medicine a non-invasive alternative to the traditional surgical treatments to treat tumours by creating overlapping lesions to the targeted area. This positioning device was designed and implemented for experimental work on small animals *in vivo* or *in vitro* and to treat brain tumours.

Furthermore, the proposed positioning device will be used inside the gantry of an MRI scanner and therefore care must be taken when considering any part to be attached to the positioning device to be MRI compatible. For this reason the screws, the timing belts and the material for the construction of the robot are all selected having this in mind as described in chapter 5.

This section describes the design and development stages of the positioning device version 1.

6.1 Description of the positioning device – 1st version

The proposed positioning device is a prototype magnetic resonance imaging (MRI)-compatible positioning device used to move an MRI-guided high intensity focused ultrasound (HIFU) transducer. The positioning device has 3 user-controlled degrees of freedom that allow access to various targeted lesions. However, it can be easily developed for 5 degrees of motion.

The main component of an ultrasonic system guided by MRI is the positioning device. The positioning devices and HIFU transducers cause problems when used inside an MRI scanner. Any interference with the RF field will reduce the quality of the image. The imaging will occur if the robotic system and transducer or any other therapeutic object does not interfere with the magnetic and RF fields needed by the MRI system. Therefore these devices must be made out

of non-magnetic materials and the proposed positioning device incorporates only MRI compatible materials such as piezoelectric motors, plastic sheets, brass screws, plastic pulleys and timing belts.

Moreover, since the positioning device is placed on the table of the MRI scanner its height and length should be less than 55 cm (diameter of the gantry of the MRI scanner). The height of the proposed positioning device is 34 cm, its length is 45 cm and its width is 30 cm. The weight of the positioning device is only 6 kg and therefore it can be considered portable. Furthermore the positioning device was not designed based on any specific MRI scanner and can be positioned on the bed of any MRI scanner, therefore it is also considered universal.

This chapter describes the non-magnetic materials and parts acquired for the development of the positioning device, the designs based on the limitations and considerations gathered for this application, and photographs of the different stages and the final product developed.

6.2 Design and implementation of positioning device version 1

As mentioned previously the selection of the materials and parts for the development of this positioning device are restricted to be compatible to operate within the gantry of an MRI scanner. The devices of an integrated HIFU system are shown in figure 5.2 and described in chapter 5. The piezoelectric ultrasonic motors and their drivers are described in sections 5.1.3 and the photographs of these are shown in figures 5.6 and 5.7. Apart from the piezoelectric ultrasonic motors and their drivers which are described earlier, the following sections describe the rest of the selected parts and materials used as well as the designs of the three stages of the robot.

6.2.1 Parts and materials used for the positioning device

Figure 6.1 shows the angular part which is useful in order to support the rods and the pulleys. It is also used to hold the surface plate of the other axis as shown in figure 6.10. Figure 6.1.A shows the side view of the angular part and the top view is shown in figure 6.1.B. The top view of the angular part of figure 6.1.B shows the brass screws used for mounting this part on the other plates. Figure 6.1.C shows a photograph of the actual part. This angular part of figure 6.1 is made of polyethylene and is 90° . Its thickness is 0.65cm and the two sides are 3.8cm long. This part is supplied by the company named United States Plastic Company (USP) and comes in length of 120cm.

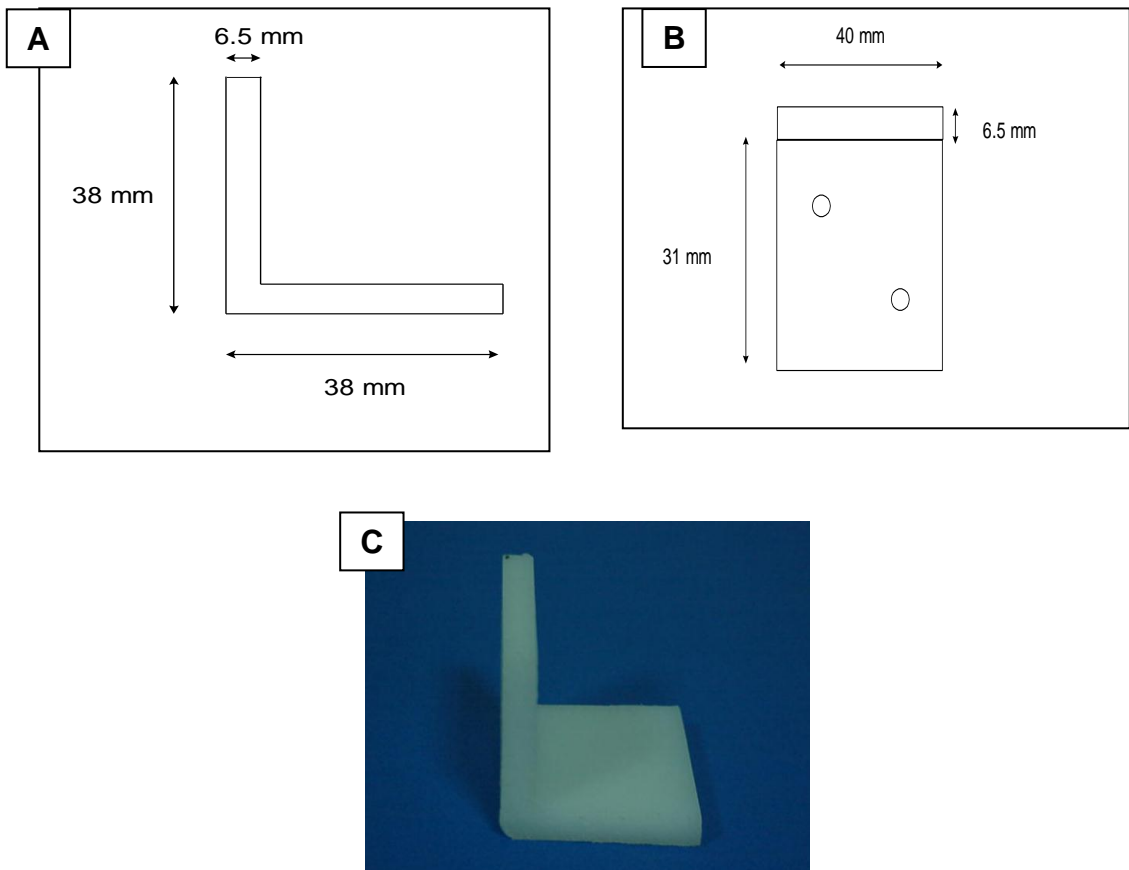


Figure 6.1: Corner part used to support the rods and the pulleys. This part is also used to support the different stages of the robot.

Figure 6.2.A. shows the diagram of the rod used to guide and support the surface plate of the stages X, Y and Z and figure 6.2.B. shows a photo of the rod. Each stage/dimension it's supported by two rods. The rod shown in figure

6.2 is of 0.95cm diameter. The length of the rod is 30cm and this is the length used for supporting and guiding the X-stage responsible for the back and forward motion. The material used for the rod is brass.

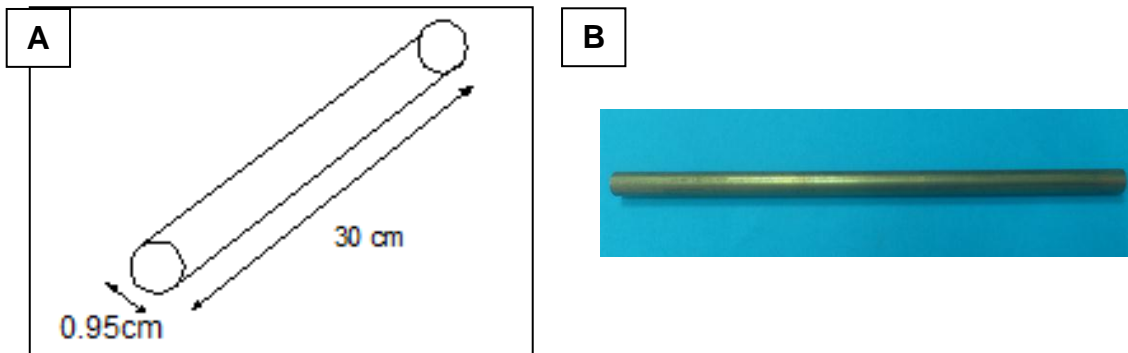


Figure 6.2: The brass rod used to support and guide the surface plates of the stages X, Y and Z.

The rod mounted with a brass screw on the angular part is shown in Figure 6.3.

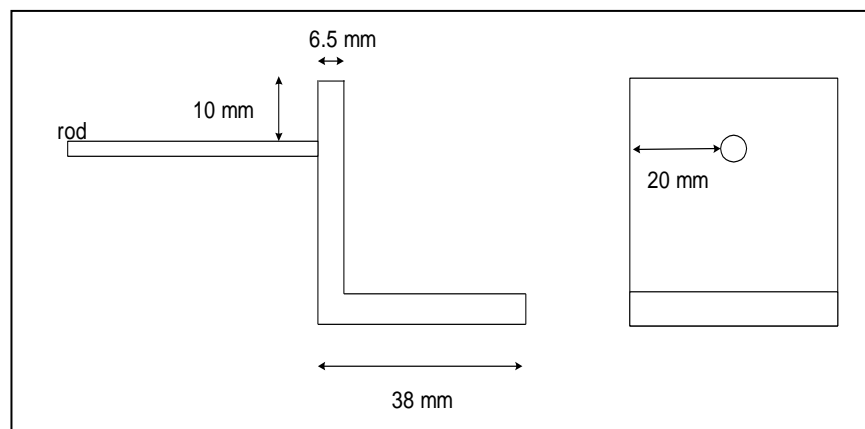


Figure 6.3: Position of the brass screw which is used to mount the rod on the angular part.

The brass screws used for mounting the parts of the positioning device are shown in figure 6.4.



Figure 6.4: The brass screws used to mount the parts of the positioning device.

Three surface plates were used each of which is used to hold the guidance mechanism of each of the three stages (X, Y, Z). Two angular parts are mounted on a surface plate, facing each other and a rod is attached across the two plates to serve as a guide for the next stage. As mentioned previously two rods are used to support and guide a stage surface plate as shown in figure 6.5.

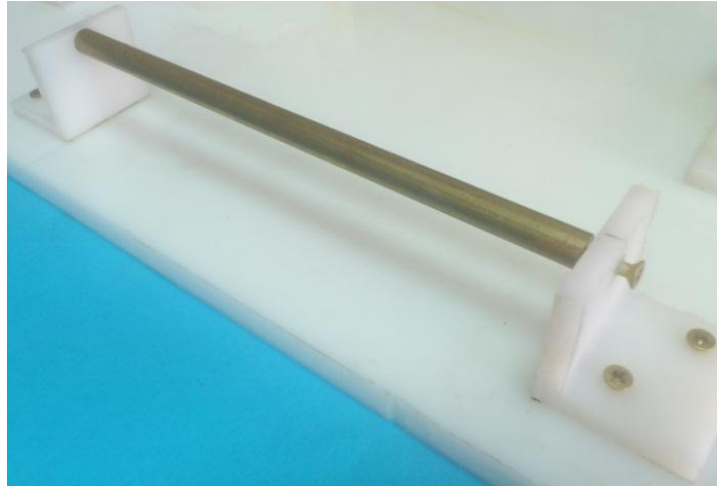


Figure 6.5: Brass rod mounted on two angular parts which are attached on the base of the positioning device.

The surface plate of figure 6.6.A. is the diagram of the base of the positioning device and figure 6.6.B. shows a photo of this plate. The diagram and the photo of the surface plates for X-stage and Y-stage are shown in figures 6.6.C., 6.6.D and 6.6.E., 6.6.F respectively. The thickness of all surface plates is 1.27cm and the material used is polyethelyne.

The timing belt and the pulley are shown in figure 6.7.A and 6.7.B respectively. The belt has a width of 9 mm, a pitch 5.8 mm and length 60 cm (120 teeth) and the material of the band is Neoprepene. The pulley has a width of 9.5 mm, and a pitch 5.8 mm and is made of Polycarbonate.

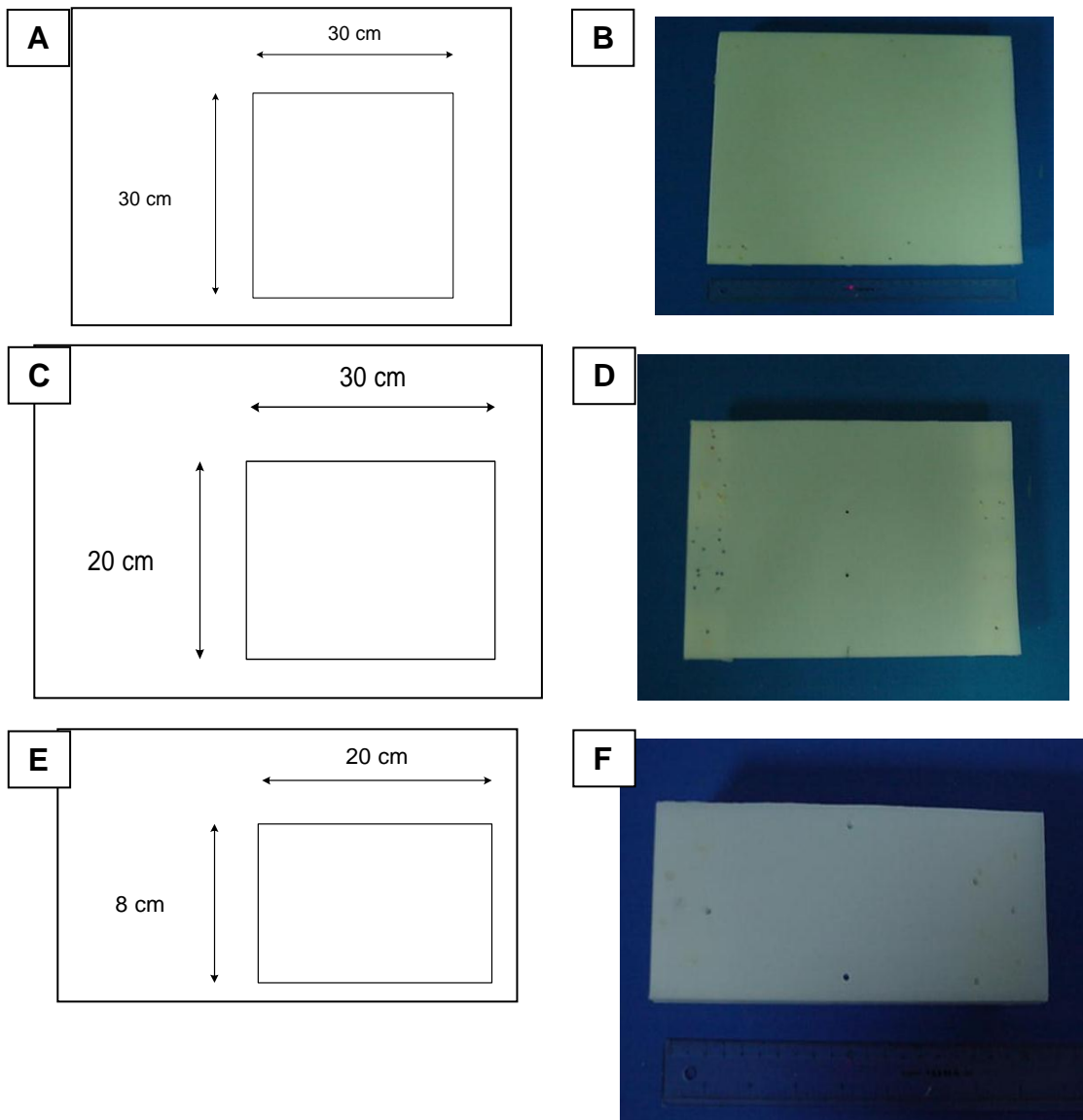


Figure 6.6: Diagrams and photos of surface plates of the base, X-Stage and Y-Stage.

The timing belt is attached between two pulleys and is also mounted on a surface plate of the stage which it moves. One of the pulleys is attached on a Piezoelectric Ultrasonic Motor shown in figure 6.7.C and 6.7.C, and when the motor spins the pulley attached to it rotates and that's how the motion of the surface plate is achieved.

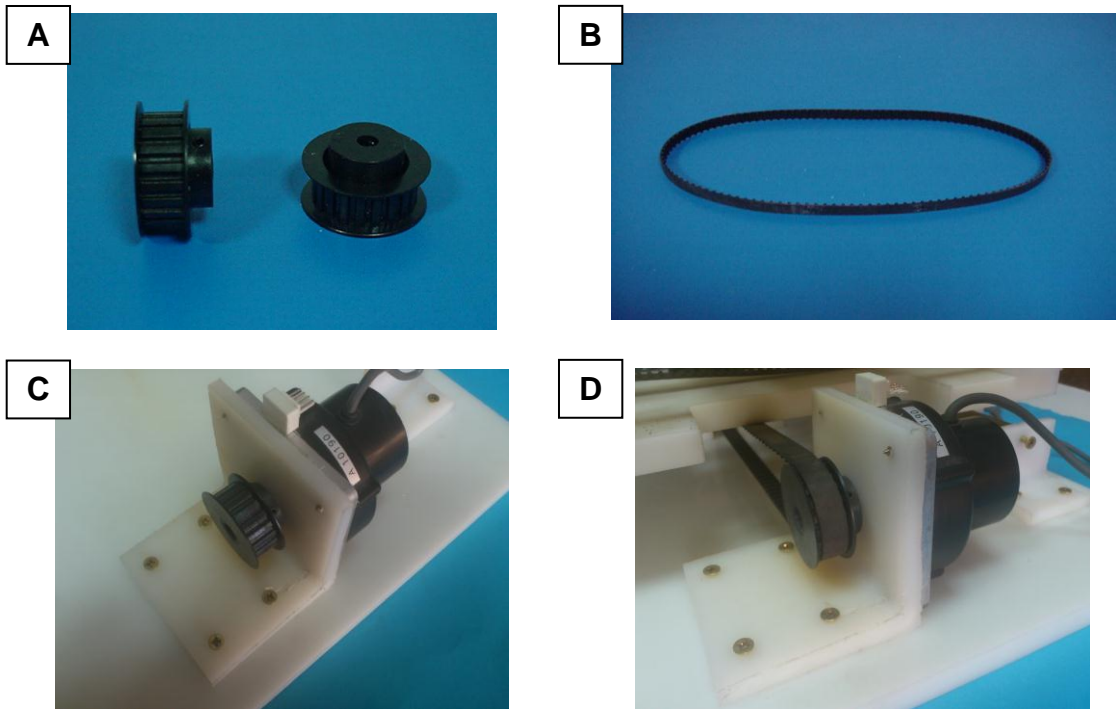


Figure 6.7: Pulleys, timing belt, and the piezoelectric ultrasonic motor attached on the base with an angular part which is driving the timing belt to achieve the motion of a surface plate of the X-axis.

The pulley on the other end of the timing belt is held within two angular parts as shown in figure 6.8.



Figure 6.8: The pulleys on the other end of the timing belt held with two angular parts.

The base of the positioning device with the two brass rods used for supporting and guiding the X-axis plate is shown in figure 6.9. The timing belt shown in figure 6.9 is driven by the pulley which is attached on the piezoelectric

ultrasonic motor. This timing belt is anchored on the X-axis plate with a brass screw and that's how the X-axis plate moves back and forth.

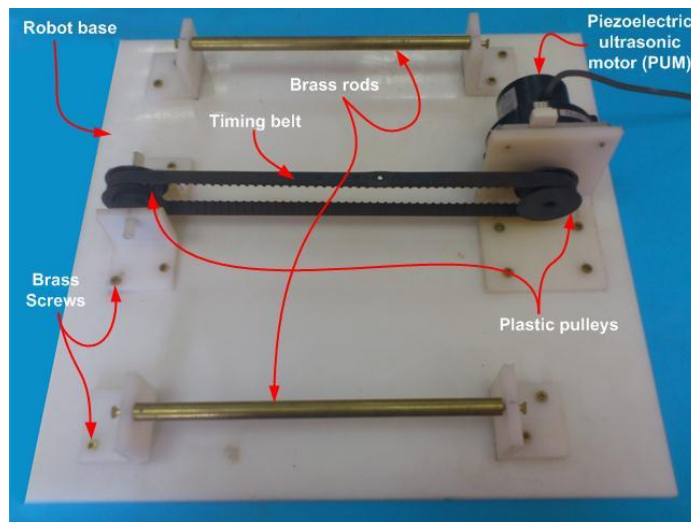


Figure 6.9: Top view of the base with the brass rods that support and guide the X-axis plate. The timing belt is mounted on the X-axis plate (not shown here) with a brass screw.

The photograph of figure 6.10 shows the angular parts attached with brass screws at the bottom of the X-axis plate and the brass rod which how the X-axis plate moves the angular parts

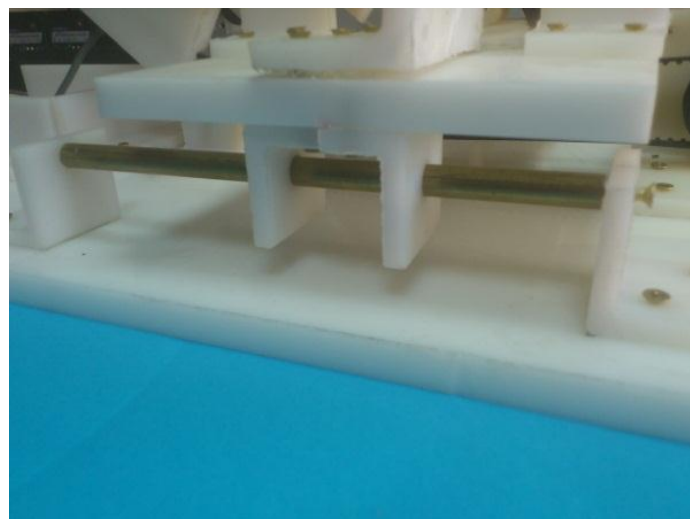


Figure 6.10: The angular parts attached at the bottom of the X-axis plate are sliding along the brass rod which acts as a support and guide.

6.2.2 Description of the operation of the positioning device

Figure 6.11.A shows the rectangular base of the positioning device made out of polyethylene. This plastic base holds the 3 stages that establish motion in the X, Y and Z direction. Four polyethylene angles are placed on the base. Two brass rods are attached to the 4 angles (see figure 6.9). A fixed polycarbonate pulley is supported on polyethylene angles through a plastic rod. A piezoelectric motor (USR60-S3N, Shinsei Kogyo Corp., Tokyo, Japan) is fixed on another polyethylene angle. A neoprene belt is placed around the fixed pulley and the pulley which is coupled to the motor. This figure shows also the water container that hosts the transducer. The transducer is immersed in the water container which is filled with degassed water or saline. The water is poured in a mylar bag. The mylar bag is made thin enough to conform to the contours of the target. A circular window is opened in the water container in order to allow ultrasound energy to be applied through the body. For the purpose of brain ablation, the head of the subject is placed inside an open MRI coil.

Figure 6.11.B shows the bottom side of the polyethylene sheet that establishes motion in the X-direction. If the motor is energized, the belt which is coupled to this sheet will rotate, and eventually linear motion of this sheet is established. This sheet is coupled to the brass rods of the base (Figure 6.11.A).

Figure 6.11.C shows the rectangular sheet (top side) which is used to provide motion in the Y-axis. The same principles as in Figure 6.11.A are implemented. The only difference is the smaller size of this sheet. Figure 6.11.D shows the bottom side of the polyethylene sheet that establishes motion in the Y-direction.

Figure 6.11.F shows the rectangular sheet made out of polyethylene for moving the transducer in the Z axis (same principles are applied as in Figure 6.11.A). Figure 6.11.G shows the bottom side of the polyethylene sheet that establishes motion in the Z-direction.

Figure 6.11.H shows the holder of the transducer. A plastic rod is attached on the Z –axis sheet. A brass rod is coupled to the plastic rod. The transducer holder is attached to the brass rod. The HIFU transducer is coupled to the holder.

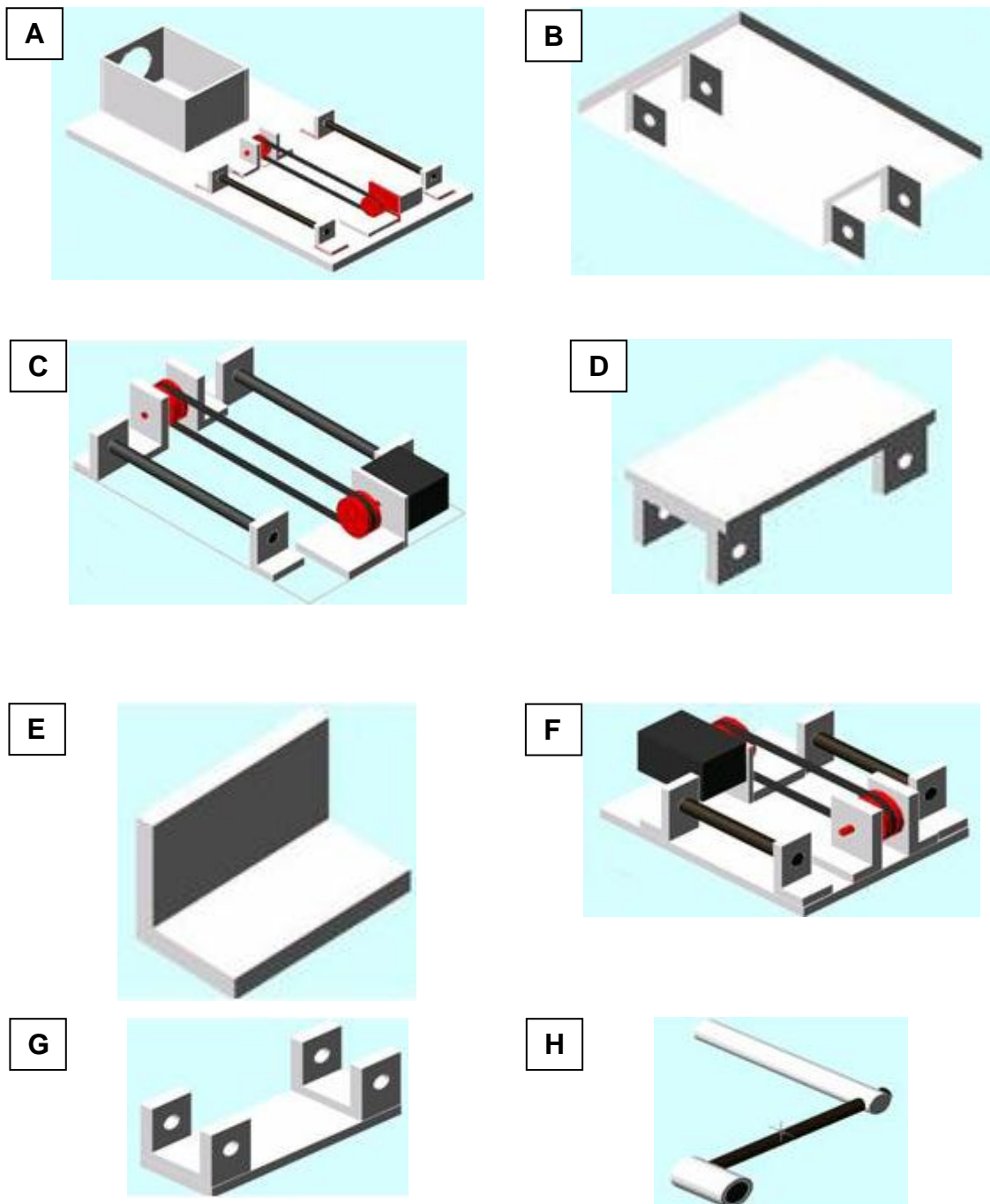


Figure 6.11: Drawings of the various mechanical stages of the positioning device.

Figure 6.12 shows the complete positioning system with all the components described in Figure 6.11. The movement of the positioning device is monitored by an MRI compatible camera (not shown in the figure) which is placed on a non-magnetic holder.

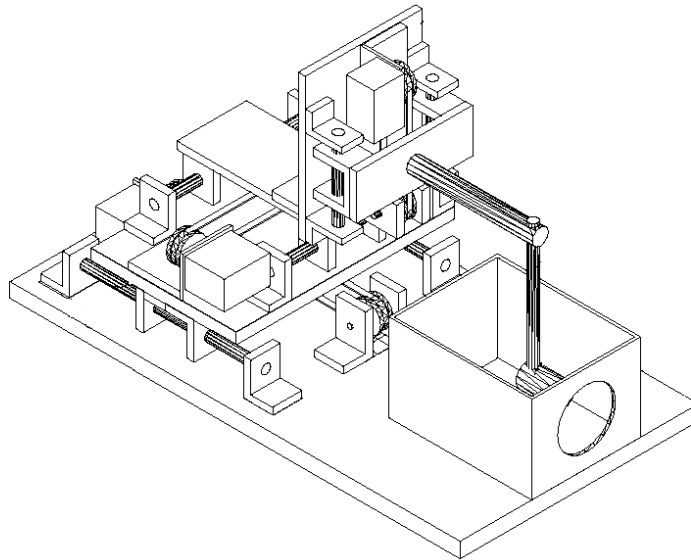


Figure 6.12: Schematic of the robot showing all of its stages.

Finally the photograph of the positioning device is shown Figure 6.3.

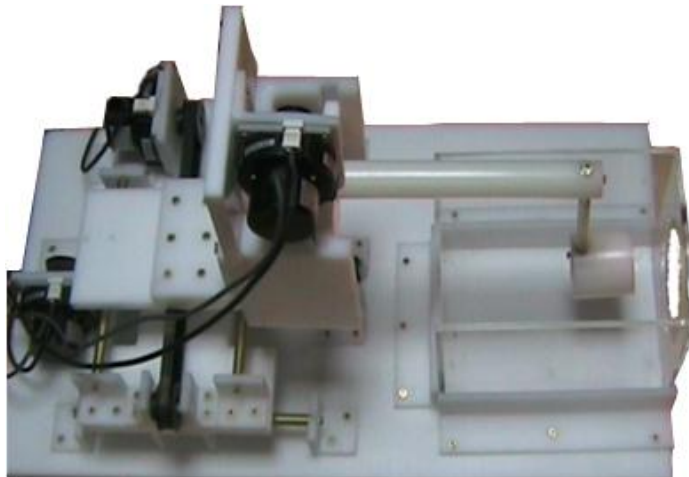


Figure 6.13: Photograph of the complete positioning device.

6.2.3 Coupling mechanism

The system provides three main mechanisms for achieving coupling to tissues. Figure 6.14 illustrates the two mechanisms. In Figure 6.14.A the tissue (*in vitro* or *in vivo*) is placed outside the container which is filled with degassed water. Due to the weight of the water container, the coupling with this method is very good. This method can be described as a top to bottom approach, meaning that the transducer is on top of the tissue. In the commercial system described by Yehezkeli et al. [136] the approach used is bottom to top, meaning that the transducer is below the tissue. In Figure 6.14.B the tissue is placed inside the container which is filled with degassed saline. The use of saline is needed for

this method in order to preserve the excised tissue, which is placed inside the saline bath. This method which provides good coupling since the tissue is placed inside the container can be used only for tissues *in vitro*. In both methods the liquid in the container (water or saline) was maintained at 37 °C.

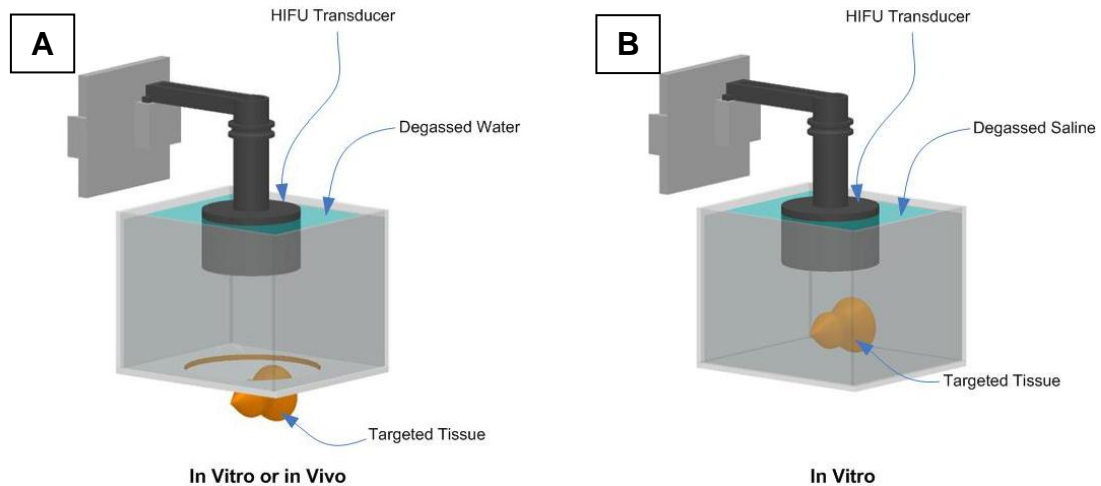


Figure 6.14: Coupling methods, **A.** *In vitro* or *in vivo* (tissue outside the water container). **B.** *In vitro* (tissue inside the water container).

6.3 Conclusion and Discussion

The First version positioning device described in this chapter seems to fulfil the requirements set prior its design. The robot proves to move the transducer accurately with both methods available for the end user, manual and automatic, and thus discrete and large thermal lesions can be formed reliably and repeatedly on the targeted tissue. This has been proven in both *in vitro* and *in vivo* tissues. The evaluation of the positioning device can be found later in chapter 10.

Furthermore this device is much simpler, smaller and inexpensive than the existing systems, while maintaining high standards of repeatability and readability. Also, this positioning device is flexible since it can be easily reduced or increased in size. This can be adjusted easily by modifying the length of the rods, the length of polyethylene sheets used as base for each level and the length of the belts. All the other components remain fixed in size. Thus, easily any size of positioning device can be designed and manufactured. There is limitation though based on the diameter of the MRI scanner. Moreover, the transducer holder can be easily replaced and this will make the robot suitable

for a variety of tissues targets. Also, this positioning device is lightweight (approximately 6 Kg) and therefore it can be transported and placed on the table of any MRI scanner. Thus the positioning device is considered portable and universal.

Furthermore, this system has the potential to be marketed as a cost effective solution for performing experiments in large animals (pig, sheep and dog) and small animals (rabbit and rat).

However, this positioning device is driven with the timing belts and timing belts will not provide the robot with the best accuracy and stability. In addition, the robot described in this chapter cannot be reproduced precisely. Many parts of the robot are fabricated and assembled manually and thus makes the reproduction of the robot difficult.

These limitations of the first version brought the idea of the next version of the positioning device. For the second version of the robot the timing belts will be replaced with racks and pinions and is expected that this will result better stability and accuracy. Moreover, the new robot will be design on CAD software and manufactured from a 3D printer and this will give smother edges more accurate design and the reproduction of the robot will be possible.

7 Development of the positioning Device version 2

The second version of the positioning device is a simple, cost effective, and portable, and it has been developed to be used in virtually any clinical MRI scanner since it can be placed on the scanner's table. This system has the potential to be marketed as a cost effective solution for performing experiments in large animals (pig, sheep and dog) and small animals (rabbit and rat). Moreover, with a slight modification of its base as shown in figure 7.11, this positioning device can be attached on top of the gantry of an MRI scanner and this will maximize the space of the targeted body. Also, this positioning device can be used in a double-donut MRI scanner which offers a 50cm vertical gap between the two facing superconductive magnets. The proposed positioning device can be accommodated in this gap. Finally the base of the positioning device can be modified to be placed on a side table of an open C-shape MRI scanner. With the modifications described above the positioning device can be used to treat abdominal tumours on kidney, liver and pancreas, as well as for thyroid tumours.

The main constrain when designing a positioning device to be used inside the gantry of an MRI scanner is the space. With the new generation of scanners (Siemens MAGNETOM Espree 1.5T) with short bore of 125cm and increased diameter of 70cm offers better patient access and comfort and makes intervention access and interventional robot assistance within the magnet more feasible. Philips MR Ingenia also features a 70 cm gantry in order to decrease anxiety of the patient and provides additional space for MR guided robotic systems.

This positioning device also incorporates only MRI compatible materials such as piezoelectric ultrasonic motor by Shinsei USR60E3N, Acrylonitrile Butadiene Styrene (ABS) plastic, brass screws, and the motion of the X, Y, and Z plates is accomplished with brass racks and pinions replacing the pulleys and timing belts of the first version. The system is manufactured automatically using a rapid prototyping system (FDM400, Stratasys, 7665 Commerce Way, Eden Prairie, Minnesota, 55344, USA).

The MRI compatibility of the system was successfully demonstrated in a clinical high field MRI scanner. The robot has the ability to accurately move the transducer thus creating discrete and overlapping lesions in biological tissue.

The following sections describe the mechanical parts and the specifications as well as the details of how the proposed positioning device was design and implemented.

7.1 Parts and specifications of positioning device version 2

The ABS parts of the robot were first designed using Computer-Aided Design (CAD) software (Microstation V8, Bentley Systems, Inc.) and exported to Computer-Aided Manufacturing (CAM) software (Insight V. 6.4.1, Stratasys Inc.) and finally were send to a 3D printer (FDM400, Stratasys, 7665 Commerce Way, Eden Prairie, Minnesota, 55344, USA) for production. Therefore, the manufacturing of the positioning device is absolutely reproducible.

Brass rack, and pinions (Sterling instrument, NY, USA) were used to convert the rotational motion of the three piezoelectric ultrasonic motors (USR60-S3N, Shinsei Kogyo Corp., Tokyo, Japan) into linear motion for the three degrees of freedom. The three racks were attached on the ABS plates with brass screws. The positioning device is controlled by a user friendly interface application developed in MATLAB (The Math works Inc., Natick, MA, USA).

The positioning device can be placed on the table of any MRI scanner and therefore its height is 32.5 cm (diameter of the gantry of a typical MRI scanner is about 55 cm). The length of the positioning device is 25 cm and its width 25 cm. The weight of the positioning device is only 2.9 kg and therefore it is considered portable. The range of the robot is, X: 135mm, Y: 112mm, Z: 68mm.

7.2 Design and development of the 2nd version of the positioning device

The CAD drawing of the base of the positioning device is shown in figure 7.1.A. Figure 7.1.B shows the corresponding photograph of the base shown in figure 7.1.A. This base was needed in order to hold the robot for conducting experiments and for demonstration purposes outside an MRI. In real life the robot can be fixed inside the bore of an MRI scanner, which requires the collaboration with MRI vendors. The tracks in which the X-axis plate slides in are located on the left and right side of the base as shown in figure 7.1.B.

The plate, responsible for the movement in the X-axis is shown in figure 7.2. Figure 7.2.A shows the 3D CAD drawing and figure 7.2.B shows the corresponding photo of the produced part of the 3D printer. The PUM motor attached at the bottom of the plate is the motor which will guide the Y-axis plate. The brass rack shown on the top of this plate will be driven by the pinion which is attached on the PUM motor of the top cover of the robot as shown in figure 7.9. The length of the brass rack is 150mm however; the effective range of the X-axis plate is 135mm because of the two brass screws at the two ends of the rack necessary to mount the rack on the ABS plate. The X-axis plate of figure 7.2 will slide in the grooves shown in figure 7.1. The form of the guides sliding in the grooves used for the motion of all axis plates is shown in the photograph of figure 7.3. Figure 7.4.A and 7.4.B shows the CAD drawing and photograph of the X-axis plate attached in the guiding slot of the base.

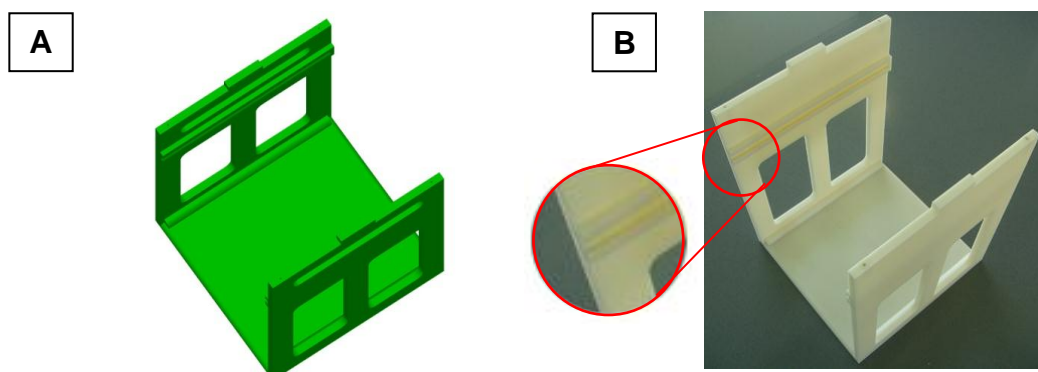


Figure 7.1: CAD design and photograph of the base of the positioning device: **A.** CAD drawing, **B.** actual photo (with zooming in the guide).

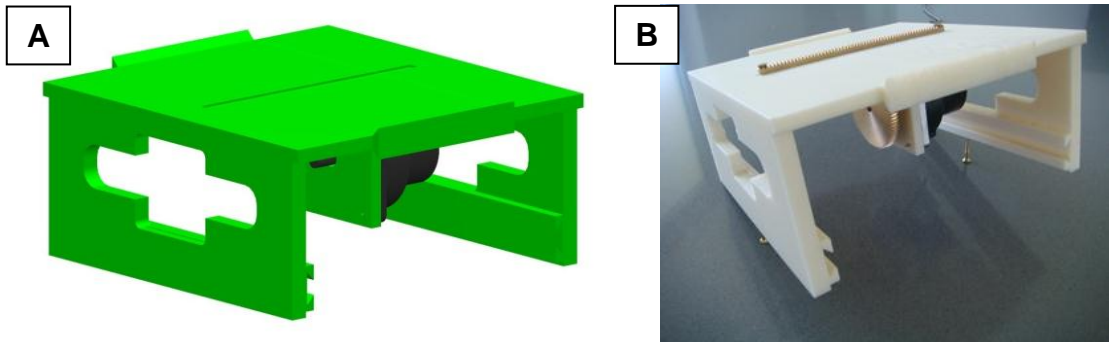


Figure 7.2: **A.** CAD design of the X-axis plate and **B.** photograph of the X-axis plate base of the positioning device.

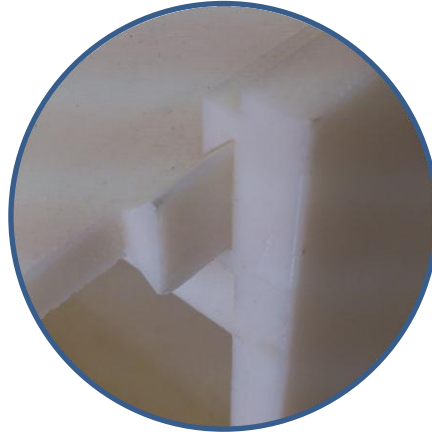


Figure 7.3: A photograph of the groove and the guide used for the motion of all axis plates.

The CAD drawing of the plate responsible for the Y-axis motion of the guided HIFU transducer is shown in figure 7.5.A and the corresponding photograph of the resulting product is shown in figure 7.5.B. This Y-axis plate will slide in the grooves of the X-axis plate and the brass rack mounted on the top of the Y-axis plate will be driven by the brass pinion attached on the PUM motor mounted at the bottom of the X-axis plate as shown in figure 7.6. Although the length of the brass rack for the Y-axis plate is 130mm, the effective range for the Y-axis is 112mm because of the brass screws used to mount the rack on the ABS plate as shown in figure 7.5.B. The Y-axis plate mechanism carries the Z holder together with the PUM motor and associated brass pinion which drives the Z-axis plate, which is also assembled to slide within the guiding slot of the Z-holder (shown in figure 7.7). The 3D drawing of the Z holder with the PUM motor and the Z-axis plate is shown in figure 7.7.A. Figure 7.7.B shows the corresponding photograph of the Z-axis plate. The brass rack mounted on the back side of the Z-axis plate is 83mm long but the effective range is only 68mm since 15mm were used for the brass screws used to support the rack on the ABS Z-axis plate.

Several designs were made for the y-axis plate in order to deliver enough strength to support the Z holder and provide stability for the HIFU transducer. Fortunately the positioning device was design for flexibility and changing the design of any part will not affect the other parts. Therefore, redesigning the Y-axis plate to reach the final form, which is stable, did not affect the other parts of the robot.

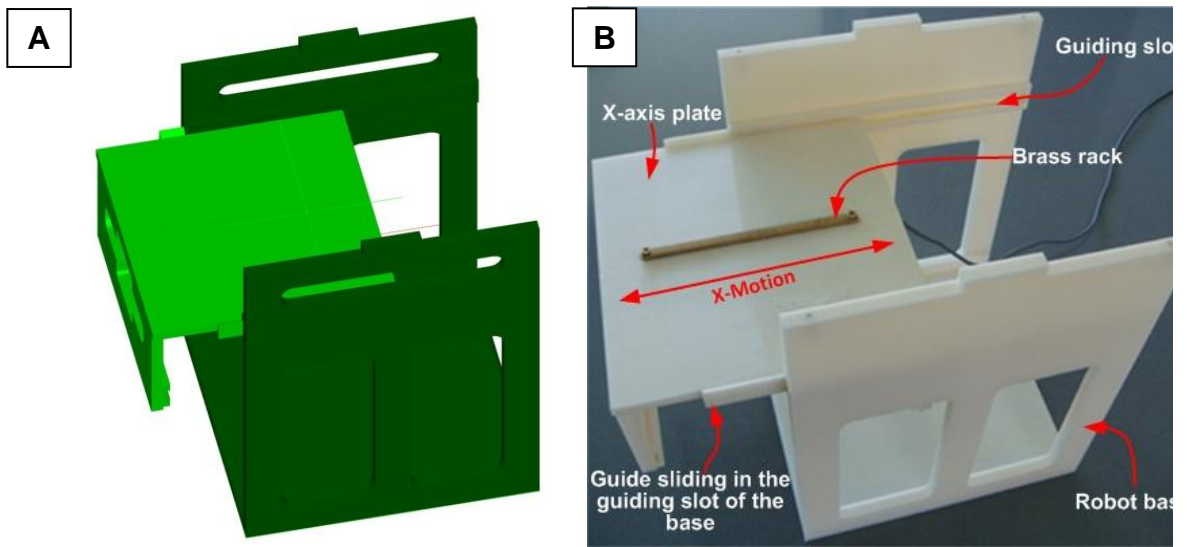


Figure 7.4: A. CAD drawing of the X-axis plate mounted on the base and B. photograph of the X-axis plate mounted on the base.

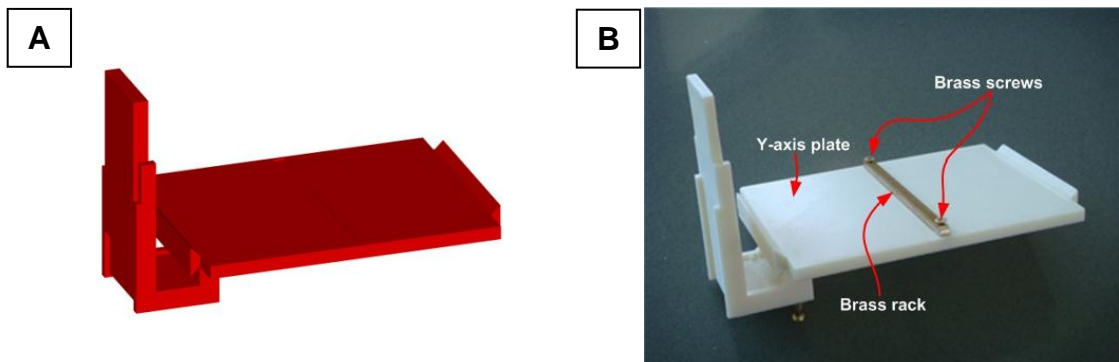


Figure 7.5: A. the CAD drawing of the Y-axis plate of the positioning device and B. a photograph of the Y-axis plate of the positioning device.

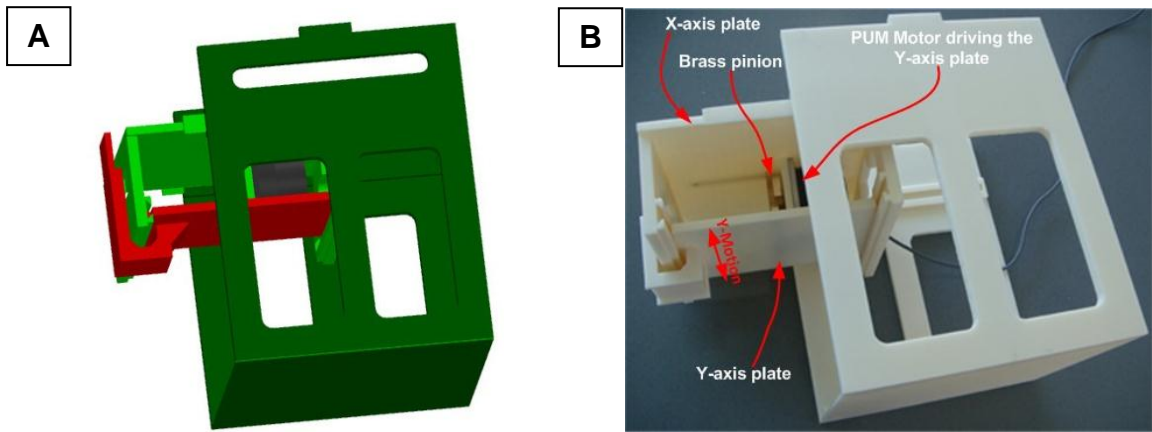


Figure 7.6: **A.** the 3D drawing of the base and the X and Y-axis plates assembled together and **B.** the corresponding photograph of the base, X and Y-axis plates. The piezoelectric ultrasonic motor shown between the X and Y plates drives the Y-axis plate.

On the front side of the Z-axis plate of figure 7.7 there is a slot. This slot will be used to attach a variety of HIFU transducer holders for different applications as shown in figure 7.8. The CAD drawing of the HIFU transducer holder attached on the Z-axis plate is shown in figure 7.8.A. Figure 7.8.B shows the corresponding photograph of this part as produced by the 3D printer and assembled together.

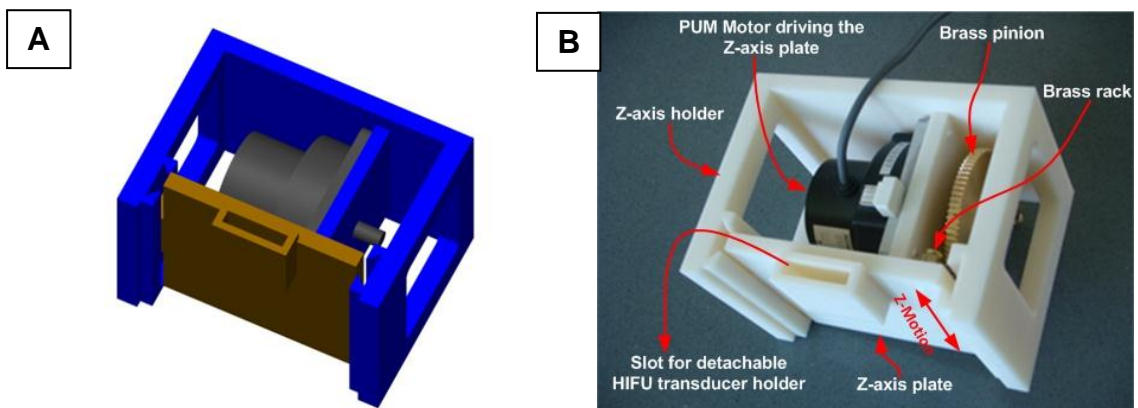


Figure 7.7: **A.** the 3D drawing of the holder of the Z-axis plate, the Z-axis plate with the PUM motor which moves the Z-axis plate and **B.** a photograph of the actual part of 7.7.A as developed and assembled.

The CAD drawing of the top plate of the robot with the PUM motor which drives the X-axis plate via the brass rack shown in figure 7.2 is shown in figure 7.9.A. The produced part is shown in the photograph of figure 7.9.B. The brass pinion attached on the PUM motor shown in the photograph of figure 7.9.B will drive the brass rack mounted on the top of the X-axis plate.

Figure 7.10.A shows the isometric view of the CAD drawing of the developed positioning device and figure 7.10.B shows a photograph of the developed positioning device. The photograph of figure 7.11 shows the positioning device placed on the bed inside the MRI scanner for testing.

The degassed water container that hosts the transducer is shown in the CAD drawing of Figure 7.10.A. This container is also shown in the photograph of Figure 7.11 and is made of Polymethyl methacrylate (PMMA), sometimes called acrylic glass. The transducer is immersed in the container which is filled with degassed water. The water is poured in a milar bag. The milar bag is made thin enough to conform to the contours of the target. A circular window is opened in the water container in order to allow ultrasound energy to be applied through the body.

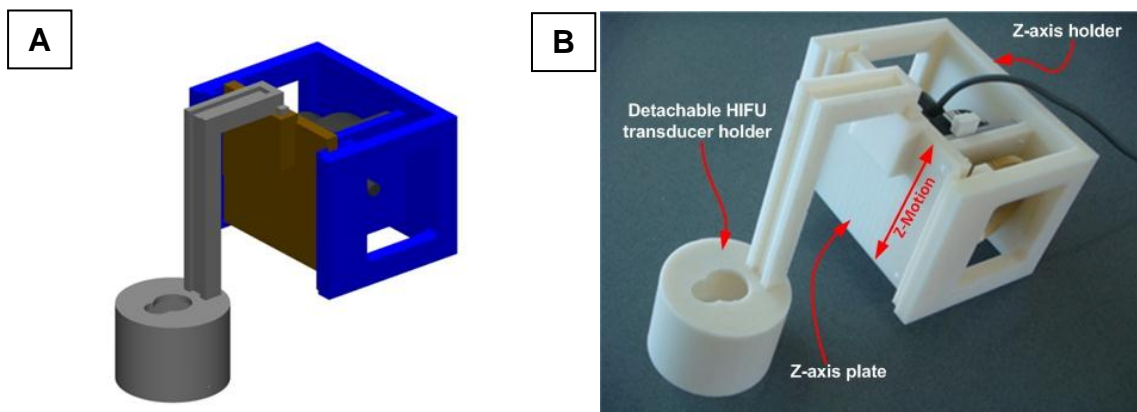


Figure 7.8: **A.** the CAD drawing of the HIFU transducer holder attached on the Z-axis plate and **B.** a photograph of the HIFU transducer holder attached on the Z-axis plate.

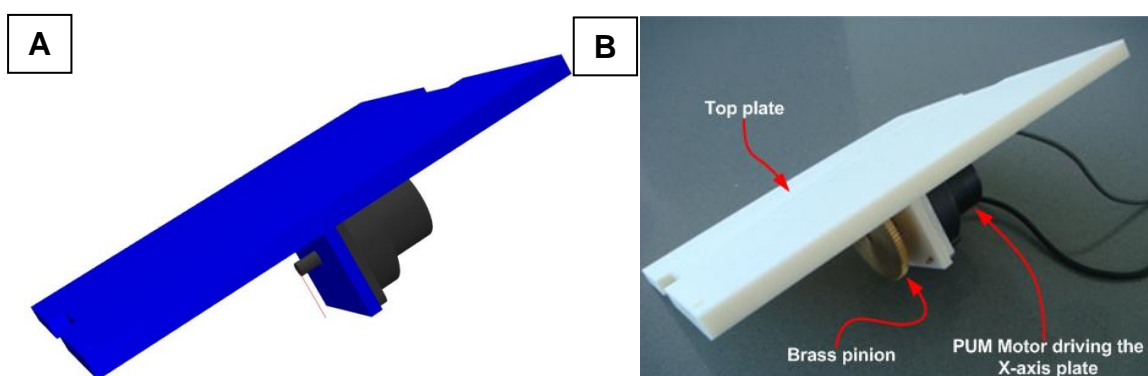


Figure 7.9: **A.** the CAD drawing of the top plate of the positioning device and **B.** a photograph of the top plate of the positioning device. The piezoelectric motor shown moves the X-axis plate.

As described at the beginning of this chapter the base of the proposed positioning device is designed in order to hold the robot for conducting experiments and for demonstration purposes outside the MRI. Figure 7.12.A shows how this base can be modified and with the collaboration with the vendor(s) of MRI scanners this can be mounted inside the bore of an MRI scanner as shown in figure 7.12.B. This modification will qualify the robot to perform lesions on:

- i. abdominal organs like kidney, liver and pancreas and
- ii. also used for treating thyroid tumours.

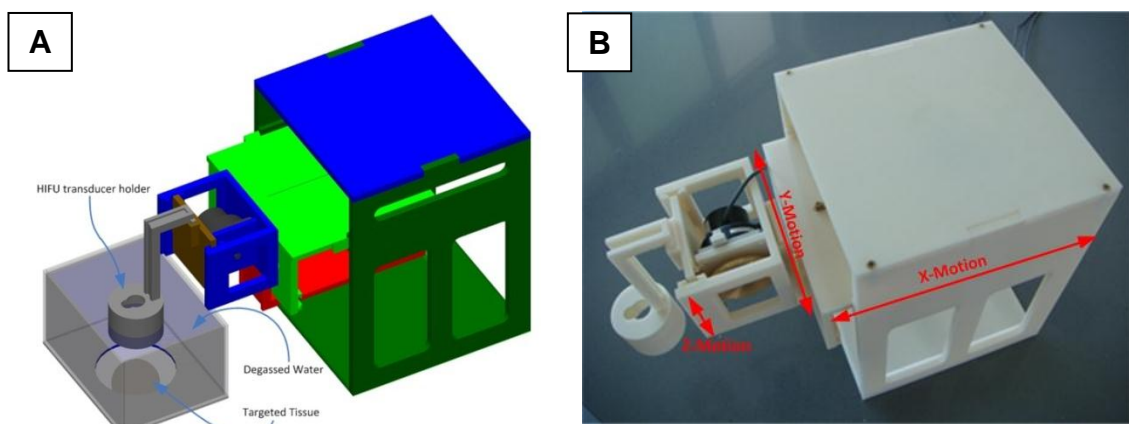


Figure 7.10: A. the final 3D drawing and B. the developed positioning device.

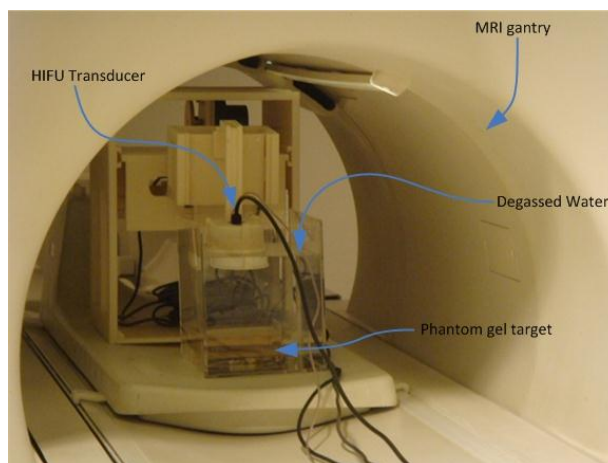


Figure 7.11: A photograph of the positioning device inside the gantry of the MRI scanner with a phantom gel target inside the tank which is filled with degassed water.

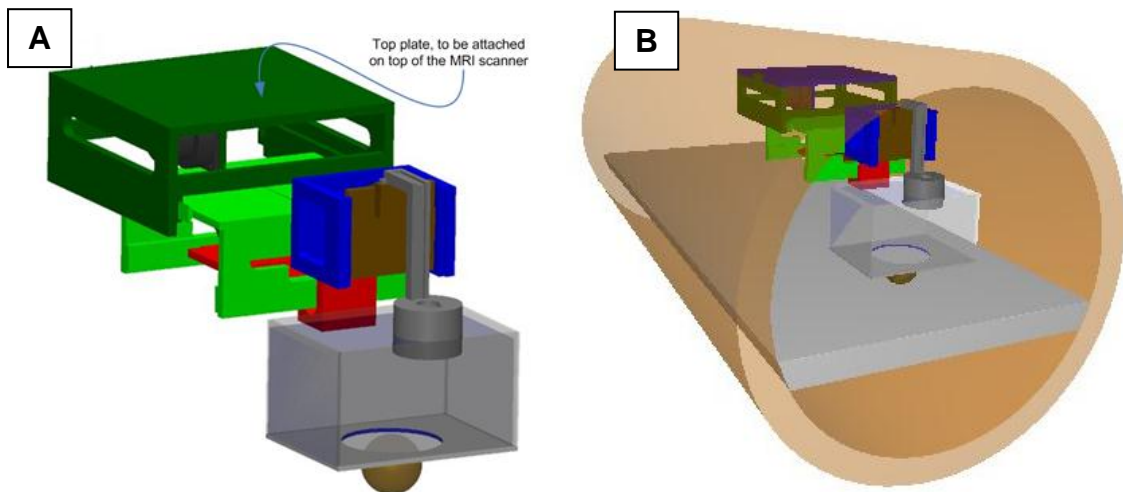


Figure 7.12: A. the base of the positioning device can be easily modified and **B.** the device as attached on the top of the gantry of the MRI scanner.

7.3 Conclusion and Discussion

The proposed second version of the positioning device it's proved to be MRI compatible, lightweight, cost effective, reproducible and universal since with slight modifications can be used in most MRI scanners available. Furthermore this second version of the positioning device is more stable and accurate and approximately half weight when compared with the first version.

An important improvement of this version is that it was designed to be as flexible as possible. All the parts of the positioning device can be easily detached and this provides better portability but even more important is that any part of the robot can be redesigned and/or replaced at no time and this will have no effect on the rest of the parts of the robot. During the development phase most of the parts although seemed to be operational on the 3D drawing (Microstation V8), but in reality when these parts were manufactured and assembled together showed that they needed some modification. Fortunately due to the flexible design these modifications on the individual parts caused no effect on the rest of the parts of the positioning device. Also, the slot on the Z-axis plate of figure 7.6 allows attaching different HIFU transducer holders of different length, height, and pointing direction or angle. Moreover, HIFU transducers from different manufacturers or with different focal length and different diameter, for different applications can be easily mounted on the positioning device. In such modifications the only part that needs to be remanufactured will be the HIFU transducer holder.

Finally this is the first demonstration of showing that a robot can be attached on the top of the gantry thus providing top-to-bottom access to patients. This robot can be used for several organs such as liver, kidneys, pancreas and especially thyroid. Especially for thyroid a similar mechanism has been designed-developed [18]. This method does not involve an MRI scanner, but employs the HIFU principle which is emitting a beam of converging high intensity ultrasound from an external applicator attached on a robotic arm. The process is controlled with a diagnostic ultrasound probe, integrated into the applicator and this allows designing the protocol and conducting follow up treatment in real time.

The limitations of this second version of the positioning device are that although it is a flexible device suitable for a variety of applications, yet this device cannot be applied for all tissues where HIFU can be applied. The second limitation is that at this moment it is not feasible to attach it on the top of the gantry of the MR scanner as shown in figure 7.12 since this requires cooperation with the manufacturer of the MRI scanner. Therefore, at present will only be used for experiments *in vitro* tissues and gel phantom or on animals. Therefore the idea of the new third positioning device came to resolve the limitations of the second version robot.

8 Development of the positioning Device version 3

The proposed third version of positioning device is a flexible MR compatible positioning device for treating multiple tumours. This positioning device is suitable for *in vitro* targets like kidney, liver, turkey fillet, porcine muscle etc. as well as *in vivo* targets like small animals as rabbits and rats. Furthermore, by attaching the appropriate HIFU transducer holder the positioning device is qualified to treat brain tumours and strokes.

This positioning device was also designed and constructed using materials selected for compatibility with high magnetic fields and fast switching magnetic field gradients encountered inside MRI scanners. The positioning device incorporates only MRI compatible materials such as piezoelectric ultrasonic motors by Shinsei USR60E3N, ABS plastic, brass screws, brass racks and pinions.

As mentioned previously, a main constrain of such positioning devices is the limited working space available in the bore of an MRI scanner. Therefore, during the design process great effort was taken to achieve a minimum size device and as a result maximize the useful operational space. Even though different designs and many different attempts were made, the useful operational space in a conventional 55-60cm bore diameter of MRI is still limited. An alternative approach to extend the operating space of this positioning device is to accommodate it in the 50cm vertical gap between the two facing superconductive magnets of a double-donut MRI scanner. The open C-shape MRI scanner provides another solution to this constrain and the new generation of scanners (Siemens MAGNETOM Espree 1.5T) with short bore of 125cm and increased diameter of 70cm will also provide more space for the robot to operate within the magnet.

Another major consideration when designing a positioning device that will guide a HIFU transducer inside the gantry of an MRI is the coupling mechanism described in chapter 6 and shown in figure 6.14. Since sound waves cannot travel through vacuum, the HIFU transducer has to be immersed in degassed saline where sound waves can propagate through and transfer the energy to

the transducer's focal point (the targeted area). As a result of this property of sound waves, it makes it necessary that liquid should surround the HIFU transducer inside the bore core of the MRI scanner. Therefore, the container in which the HIFU transducer will operate is unavoidable and this raises two important issues to be addressed. The first issue to be addressed is the protection of degassed saline to avoid spills inside the MRI, and the second is the space required by the container in a situation where space is limited.

This third version of the positioning device was designed in such a way so it could be placed on the table of any MRI scanner (diameter of the gantry of a typical MRI scanner is about 55 cm) and therefore it's also considered portable and universal.

Furthermore, this robot employs detachable HIFU transducer holders for different transducers as well as, for a variety of applications demonstrated in the following sections. This feature of the proposed robot makes it even more flexible.

The following sections describe the parts, specifications and a description of the operation of the third positioning device.

8.1 Parts and specifications of positioning device version 3

The ABS parts of this positioning device as for the second version, were designed using Computer-Aided Design (CAD) software (Microstation V8, Bentley Systems, Inc.) and exported to Computer-Aided Manufacturing (CAM) software (Insight V. 6.4.1, Stratasys Inc.) and then produced by the 3D printer (Stratasys FDM400 7665 Commerce Way Eden Prairie, MN 55344 U.S.A.). Therefore this positioning device is also one hundred per cent reproducible.

Brass racks and pinions (Sterling instrument NY USA) were used to convert the rotational motion of the three piezoelectric motors (USR60-S3N, Shinsei Kogyo Corp., Tokyo, Japan) into linear motion for the three degrees of freedom. The three brass racks were attached on the ABS plates with brass screws. The

positioning device is controlled by a user friendly interface application developed in MATLAB (The Math works Inc., Natick, MA, USA).

The dimensions of the third version of the positioning device are as follows, height 33.5 cm, length 55 cm and its width 25 cm. The weight of the positioning device is only 3.0 kg. Therefore, this is a cost effective solution, portable and universal since it can be placed on the table bed of any MRI scanner. Furthermore this positioning device is flexible since different transducer holders, shown in figures 8.16 and 8.17 can be attached on the Z-axis plate for different applications. The effective range of the positioning device is, X: 135mm, Y: 110mm, Z: 68mm.

8.2 Design and development of the 3rd version of the positioning device

The CAD drawing of the base of this positioning device and the PUM motor that drives the X-axis plate is shown in figure 8.1.A and figure 8.1.B shows a photograph of the produced by the 3D printer ABS base. The PUM motor of figure 8.1.B is used for the motion on the X-axis plate through the brass pinion attached on the motor which is driving the brass rack at the bottom of the X-axis plate of figure 8.2.A. The length of the brass rack responsible for the motion of the X-axis plate is 150mm and the effective range for the X-axis is 135mmsince 15mm were used for the brass screws supporting the rack on the X-axis plate. The groove in which the guide of the X-axis plate will slide in a forward-backward motion is expanded as shown in figure 8.1.B. This groove and guide were used for the motion of all three plates of X, Y, and Z axis. A close-up photograph of this guiding mechanism is show in figure 7.3 of the previous chapter. Figure 8.2.A shows the CAD drawing of the X-axis plate and the corresponding photograph of the ABS X-axis plate along with the PUM motor with the brass pinion which will drive the Y-axis plate are shown in figure 8.2.B.

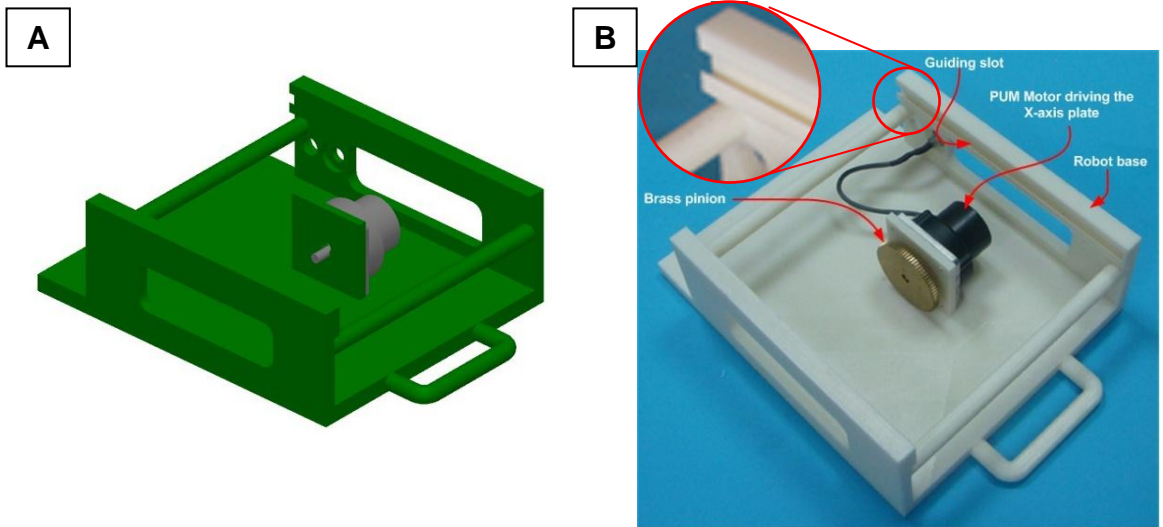


Figure 8.1: **A.** the CAD design of the base of the positioning device with the PUM motor attached to it and **B.** a photograph of the produced base of the positioning device with zooming in the groove in which the X-axis plate will slide in. The brass pinion attached to the PUM motor will drive the X-axis plate (back – forward motion).

The X-axis plate of figure 8.2 is attached on the grooves of the base of figure 8.1 and the CAD drawing of this assembly is shown in figure 8.3.A. The photograph of the X-axis sliding in the guiding slots of the base is shown in figure 8.3.B.

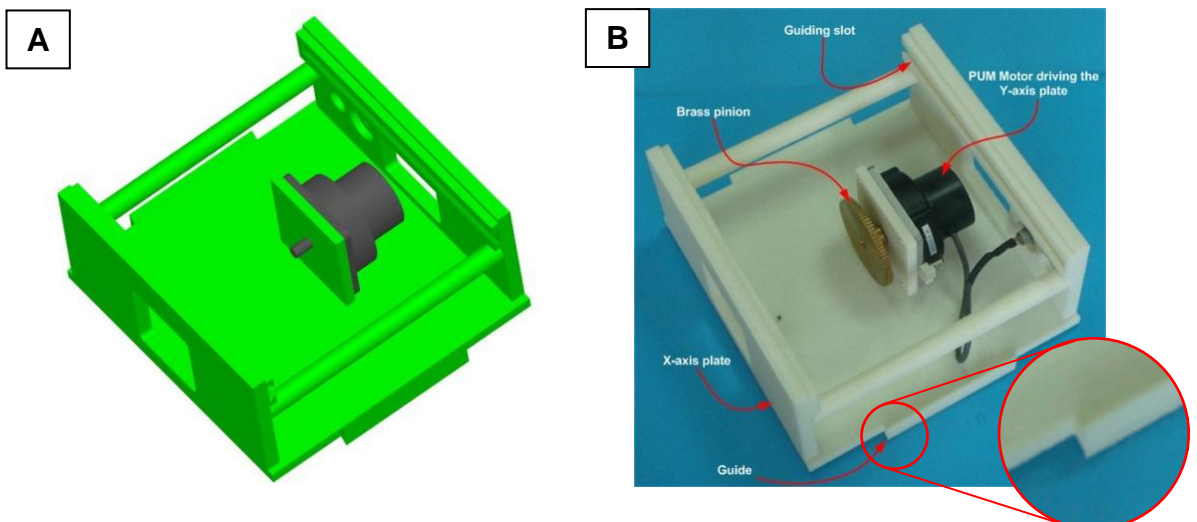


Figure 8.2: **A.** the CAD design of the X-axis plate responsible for the back and forward motion and **B.** a photograph of the formed X-axis plate with zooming on the male guide which will slide in the corresponding groove of the base. The brass pinion shown here, will drive the Y-axis plate.

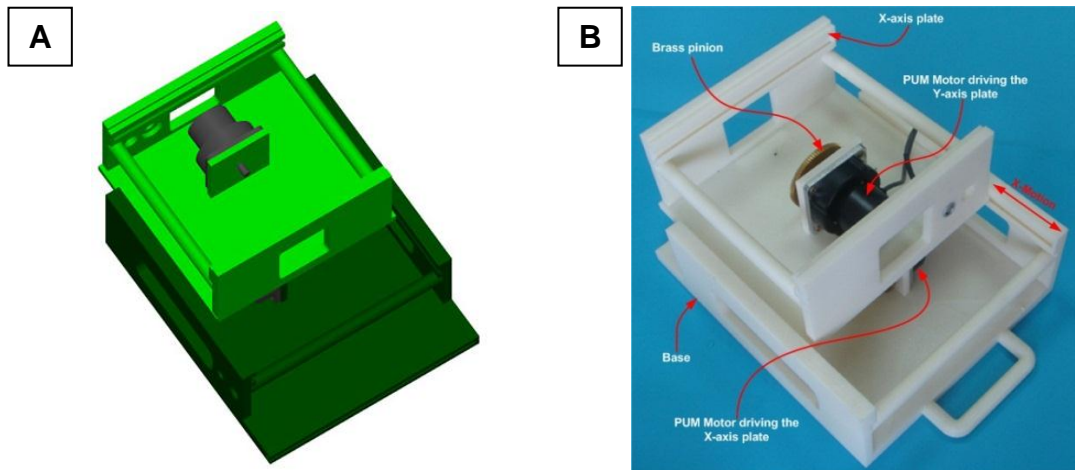


Figure 8.3: **A.** the CAD drawing of the base with the X-axis plate attached and **B.** a photograph of the base together with the X-axis plate. The X-axis plate will slide back and forward within the groove of the base. The piezoelectric ultrasonic motor shown here on the top of the X-axis plate is the motor that drives the Y-axis plate.

Figure 8.4.A shows the CAD drawing of the Y-axis plate and the photograph of the ABS Y-axis plate is shown in figure 8.4.B. This Y-axis plate is attached in the guiding slots of the X-axis plate and the CAD drawing of this assembly and the photograph of the ABS parts are shown in figures 8.5.A and 8.5.B respectively. The Y-axis plate will be driven by the brass pinion which is attached on the PUM motor of the X-axis plate of figure 8.2.B. The brass rack used for the Y-axis plate motion is mounted with brass screws at the bottom of the Y-axis plate of figure 8.4.B. The length of the brass rack is 130mm and the effective range of the Y-axis plate is 110 since 20mm were used for the brass screws supporting the rack on the ABS Y-axis plate.

For the Y-axis plate several designs were made in order to achieve the final stable design. The main problem was the accumulated weight of the Z holder, Z-axis plate, PUM motor driving the Z-axis plate, brass pinion, transducer holder and the HIFU transducer that had to be carried by the support holder mounted on the Y-axis plate shown in the photograph of figure 8.5.B. This accumulated weight made the motion of the HIFU transducer unstable and this problem was finally resolved after several attempts, by modifying the design of the support holder on the Y-axis plate and by adding extra supporting ABS material on the base of the support holder. The CAD drawing of the Z holder supported by the Y-axis plate discussed previously is shown in figure 8.6.A and the photograph of the corresponding ABS part is shown in figure 8.6.B. The Z holder is attached on the support holder of the Y-axis and the CAD drawing of the assembly is

shown in figure 8.7.A and figure 8.7.B shows the photograph of ABS parts assembled together.

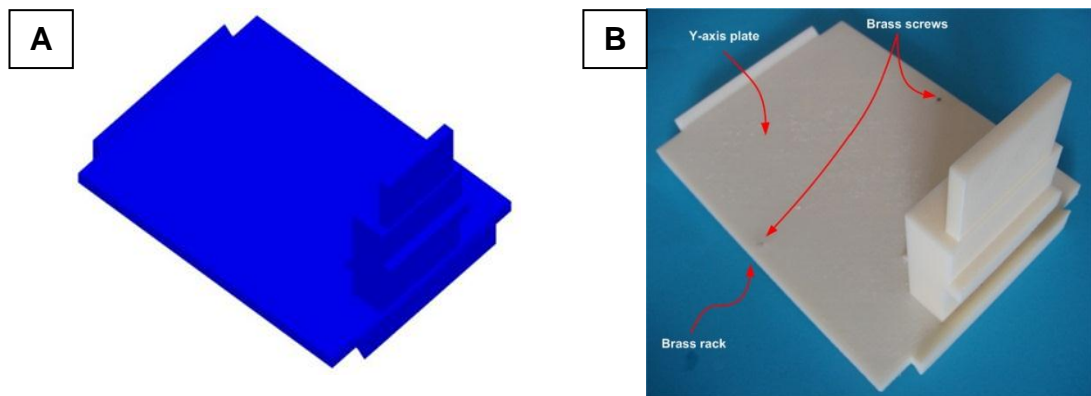


Figure 8.4: **A.** the CAD design of the Y-axis plate and **B.** a photograph of the ABS Y-axis plate.

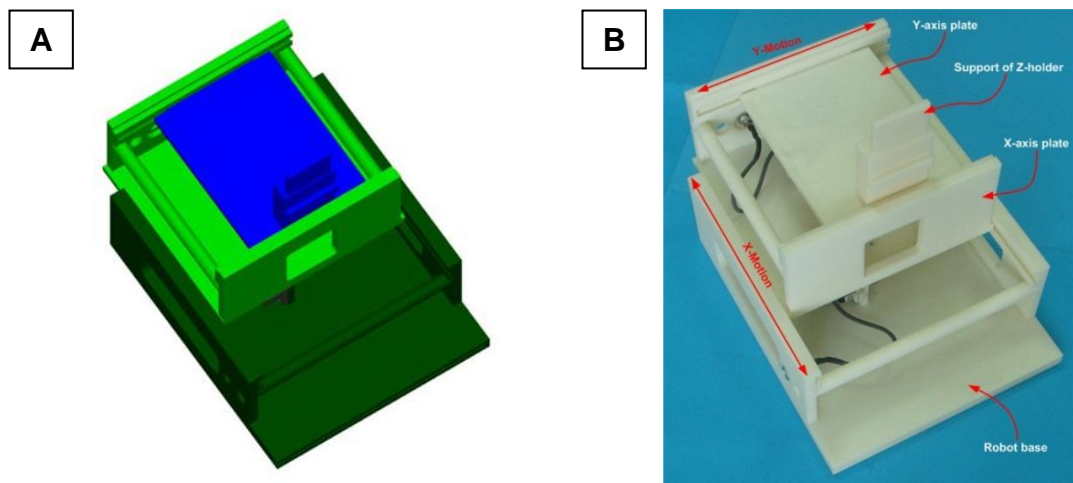


Figure 8.5: **A.** the 3D drawing of the base and the X and Y-axis plates assembled together and **B.** the corresponding photograph of the ABS base, X and Y-axis plates.

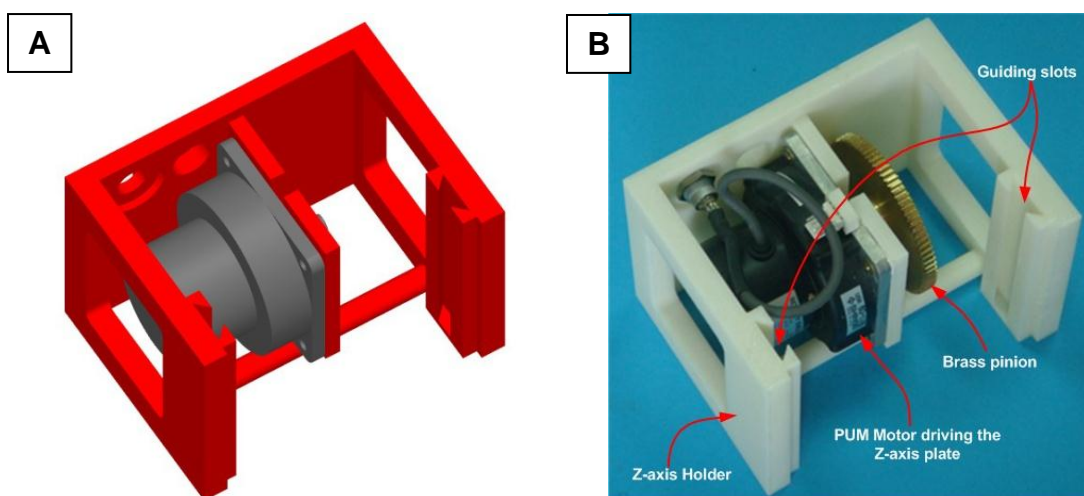


Figure 8.6: **A.** the 3D drawing of the holder of the Z-axis plate with the PUM motor which moves the Z-axis plate and **B.** a photograph of corresponding ABS Z-axis holder and the PUM motor with the brass pinion that drives the Z-axis plate.

Figure 8.8.A shows the CAD drawing of the base extension which will accommodate the water container used for the coupling mechanism and figure 8.8.B shows the photograph of the ABS base extension. This base extension is attached on the slot of the robot base and the CAD drawing of this joint is shown in figure 8.9.A. The photograph of the ABS extension base attached on the base of the robot is shown in figure 8.9.B. The extension of the base is also designed to be detachable and this contributes to the portability and flexibility of the robot. The robot can be easily disassembled to offer portability and the extension of the base can be easily modified to accommodate different coupling parts for different targets.

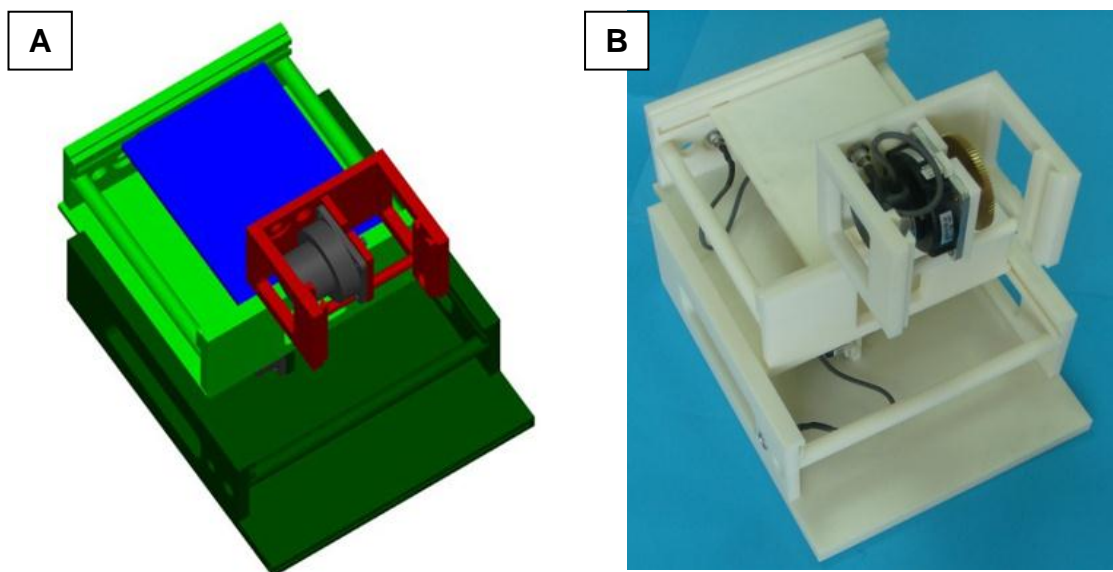


Figure 8.7: **A.** the CAD drawing of the Z holder attached on the support holder of the Y-axis plate and **B.** a photograph of corresponding ABS Z-axis holder attached on the Y-axis plate.

The CAD drawing of the Z-axis plate which will slide in the grooves of the Z-holder, shown in figure 8.6.A and 8.6.B is shown in figure 8.10.A and the corresponding photograph of the ABS Z-axis plate is shown in figure 8.10.B. The brass rack attached on the Z-axis plate will be driven by the PUM motor of figure 8.6 and is 83mm long and this gives an effective range for the Z-axis 68mm since 15mm are used for the brass screws supporting the rack on the ABS Z-axis plate shown in figure 8.10.B.

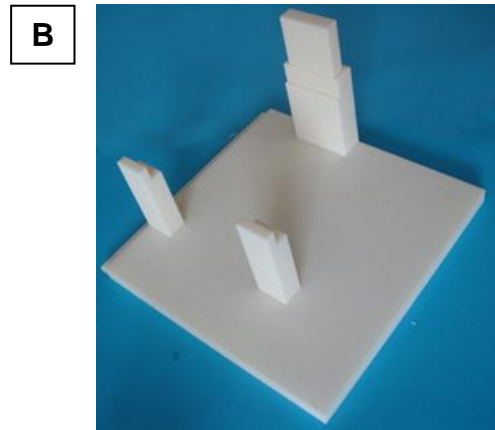
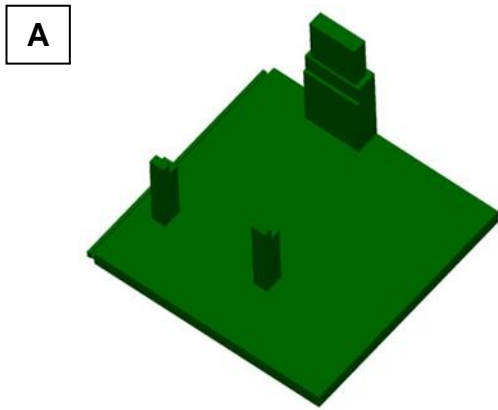


Figure 8.8: **A.** the CAD extension of the base that hosts the coupling and **B.** a photograph of the produced ABS extension of the base.

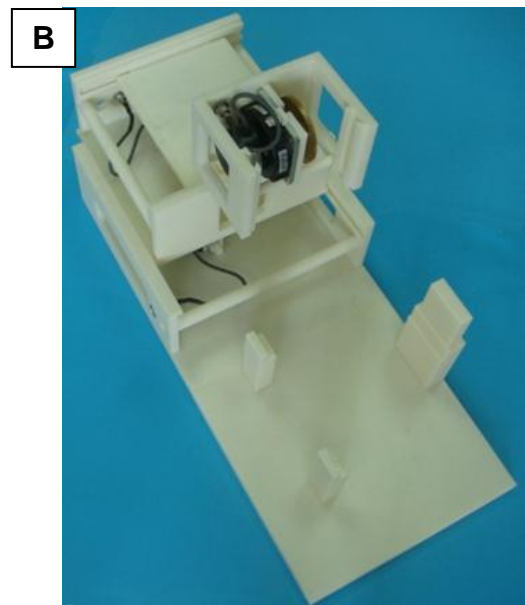
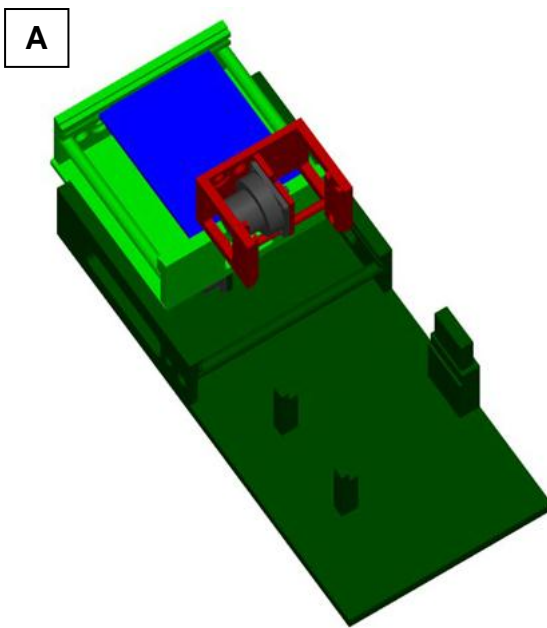


Figure 8.9: **A.** the CAD drawing of the base extension attached on the base of the robot and **B.** a photograph of the ABS base extension joined with the base of the robot.

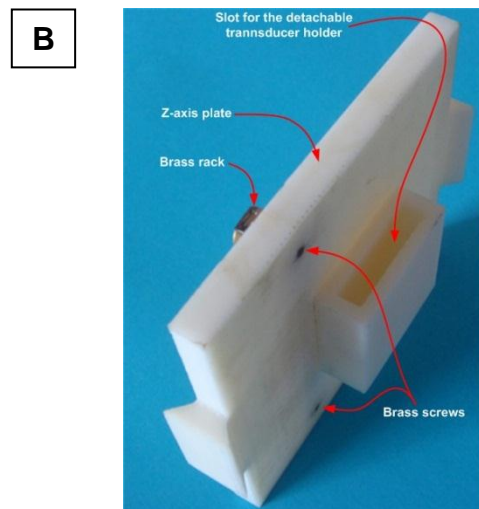
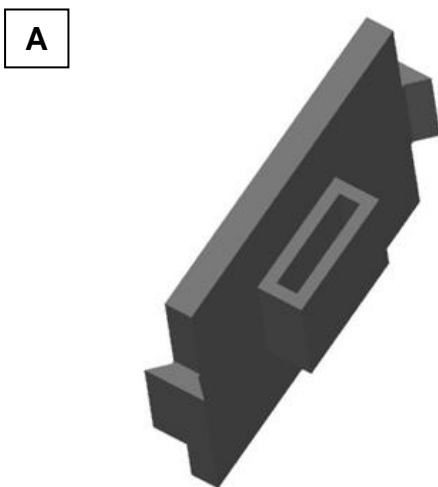


Figure 8.10: **A.** the CAD drawing of the Z-axis plate and **B.** a photograph of the ABS Z-axis plate.

The Z-axis plate is attached in the sliding grooves of the Z-holder and the CAD drawing of this is shown in figure 8.11.A. The photograph of the corresponding ABS construct is shown in figure 8.11.B.

Figure 8.12.A shows the CAD drawing of the water tank holder which is attached on the base extension of figure 8.8 and a photograph of the ABS construct of this water tank holder is shown in figure 8.12.B. The CAD drawing of the water container which is fitted inside the water tank holder is shown in figure 8.13.A and the acrylic glass container is shown in figure 8.13.B.

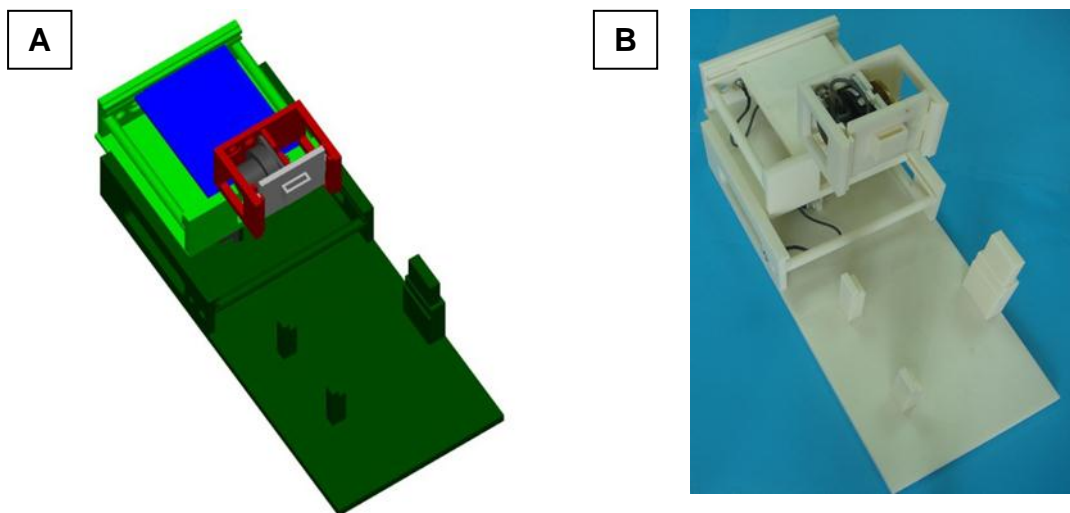


Figure 8.11: **A.** the CAD drawing of the Z-axis plate attached on the Z holder and **B.** the corresponding photograph of the ABS Z-axis plate positioned on the Z holder.

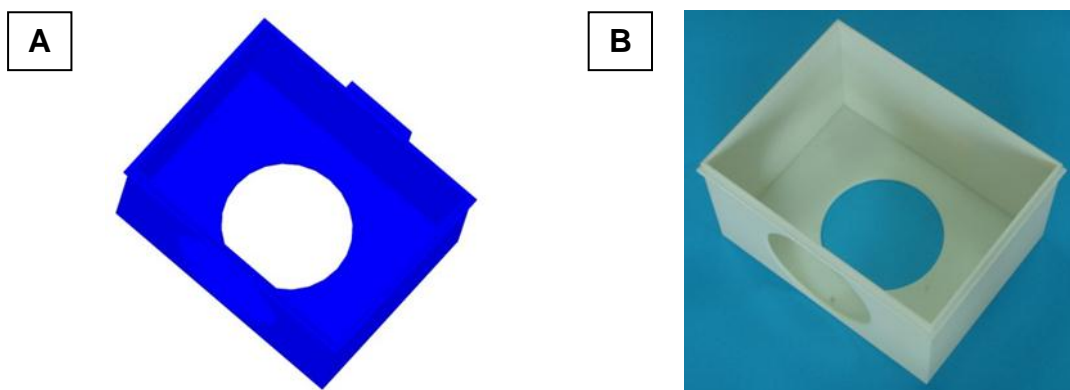


Figure 8.12: **A.** the CAD drawing of the water tank holder used for the coupling of the HIFU transducer with the targeted tumour and **B.** the corresponding photograph of the ABS water tank holder.

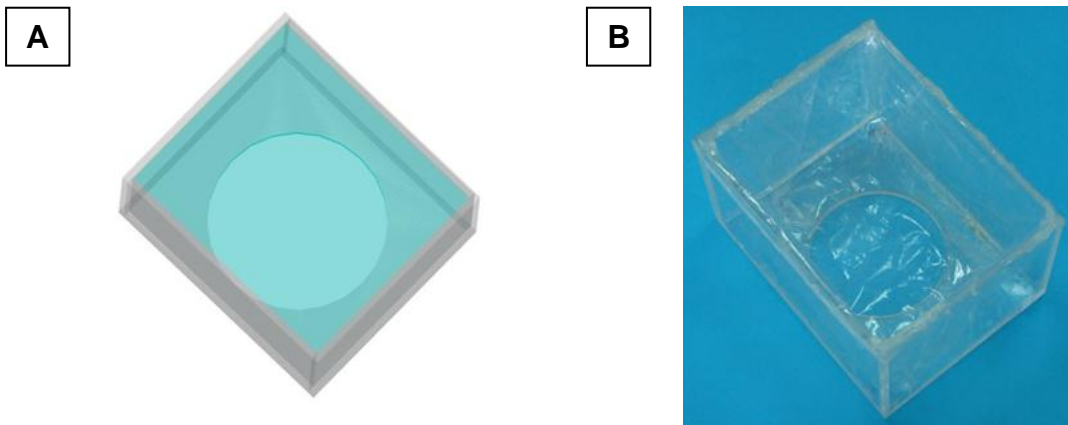


Figure 8.13: **A.** the CAD drawing of the degassed water container and **B.** a photograph of the acrylic glass container covered with milar bag.

Figure 8.14.A shows the CAD drawing of the water tank holder mounted on the base extension and the water container fitted inside the water tank holder and figure 8.14.B shows a photograph of the construct arrangement of the water tank holder and the water container fixed on the base extension.

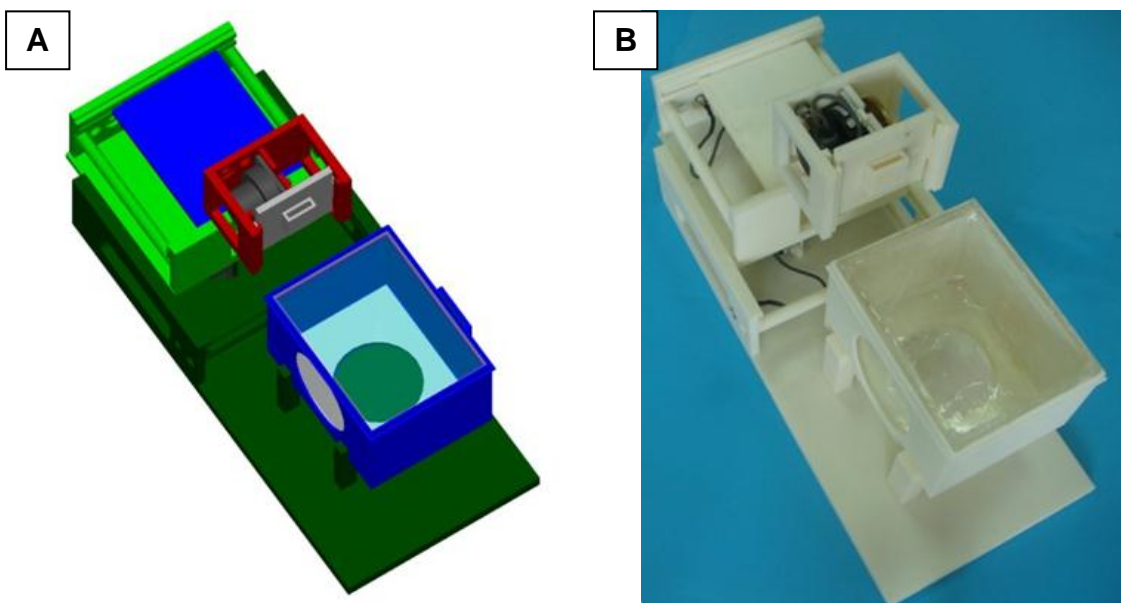


Figure 8.14: **A.** the CAD drawing of the water tank holder fitted on the base extension and the water container placed inside the water tank holder and **B.** a photograph of the ABS water tank holder mounted on the ABS base extension and the acrylic glass container fitted inside the water tank holder.

The CAD drawing of the detachable vertical and horizontal HIFU transducer holders are shown in figure 8.15.A and 8.16.A respectively and the ABS constructs of these HIFU transducer holders are shown in the photographs of figure 8.15.B and 8.16.B respectively. The different types of HIFU transducer holders could be constructed to accommodate different types and/or sizes of

HIFU transducers and also for different applications. The HIFU transducer holders can be easily attached on the slot of the Z-axis plate shown in figure 8.10.B. Figure 8.17.A shows the CAD drawing of the complete robot with the vertical HIFU transducer holder attached in the slot of the Z-axis plate and figure 8.17.B shows a photograph of the ABS robot with the vertical HIFU transducer holder mounted in the slot of the Z-axis plate. The CAD drawing of the horizontal HIFU transducer holder fitted on the slot of the Z-axis plate of the positioning device is shown in figure 8.18.A and the corresponding ABS construct is shown in figure 8.18.B. The photograph of figure 8.19 shows how the proposed positioning device can be used for brain tumours.

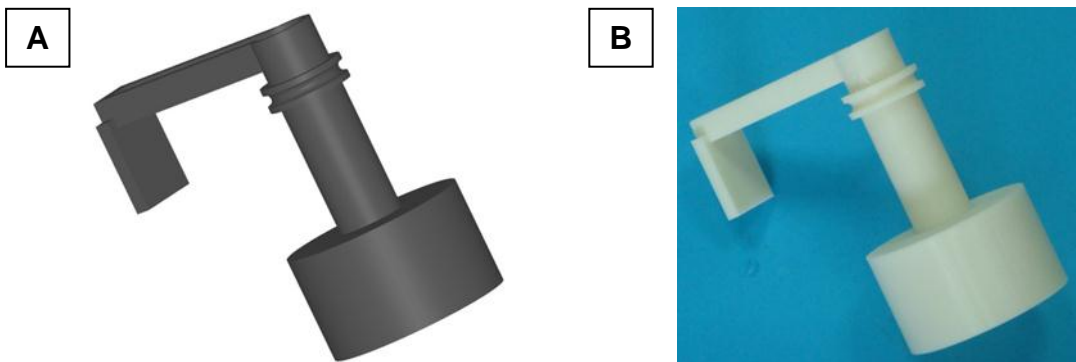


Figure 8.15: **A.** the CAD drawing of the vertical HIFU transducer holder and **B.** the photograph of the corresponding ABS vertical HIFU transducer holder.

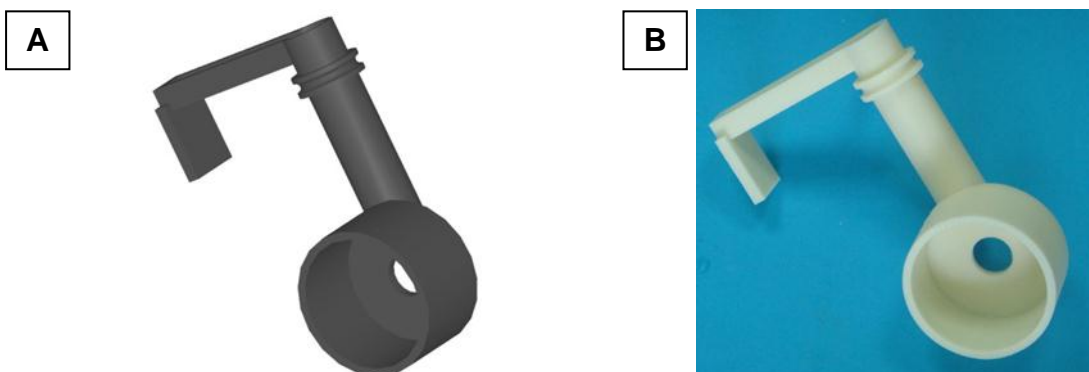


Figure 8.16: **A.** the CAD drawing of the horizontal HIFU transducer holder and **B.** the photograph of the corresponding ABS horizontal HIFU transducer holder.

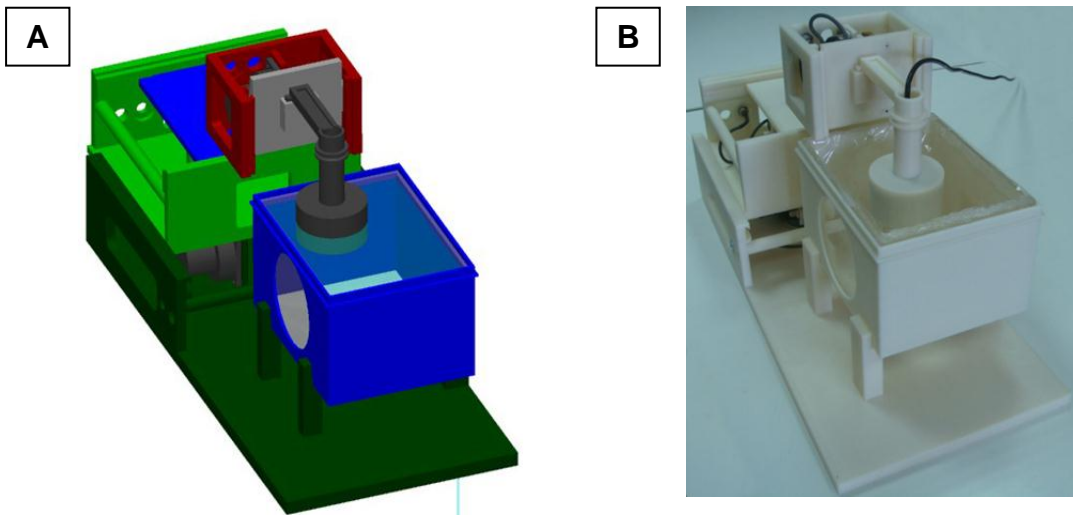


Figure 8.17: **A.** the CAD drawing of the complete positioning device with the vertical HIFU transducer holder attached in the slot of the Z-axis plate and **B.** the photograph of the ABS vertical HIFU transducer holder mounted in the slot of the Z-axis plate.

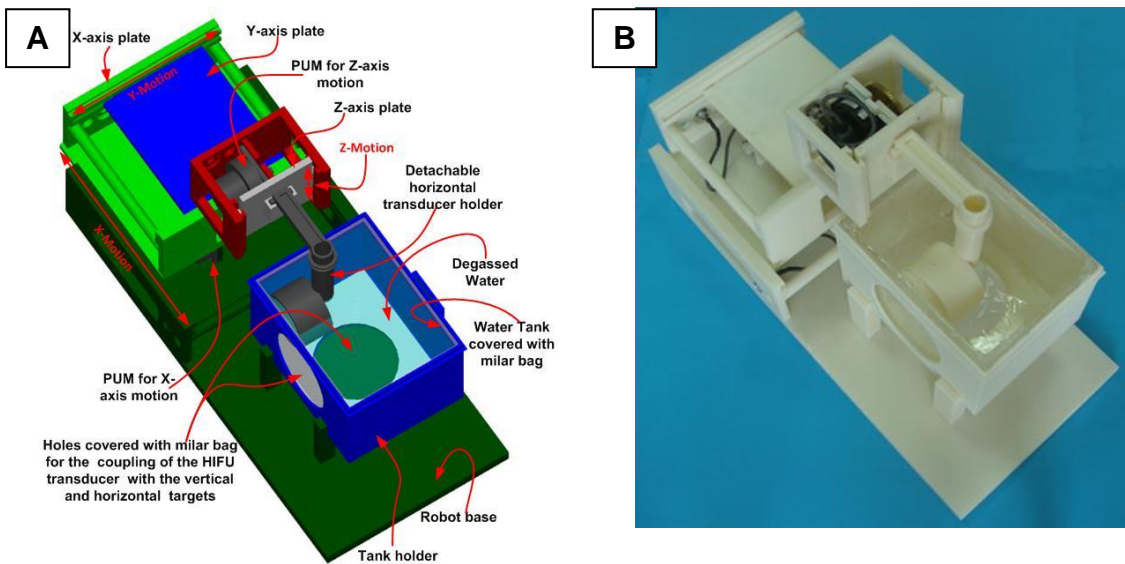


Figure 8.18: **A.** the CAD drawing of the complete positioning device with the horizontal HIFU transducer holder attached in the slot of the Z-axis plate and **B.** the photograph of the ABS horizontal HIFU transducer holder mounted in the slot of the Z-axis plate.



Figure 8.19: A photograph showing how the robot can be used for brain tumours.

Figure 8.20 shows the CAD drawing of the robot inside the gantry of a typical MRI scanner and figures 8.21.A and 8.21.B shows photographs of the positioning device placed on the table of an MRI scanner.

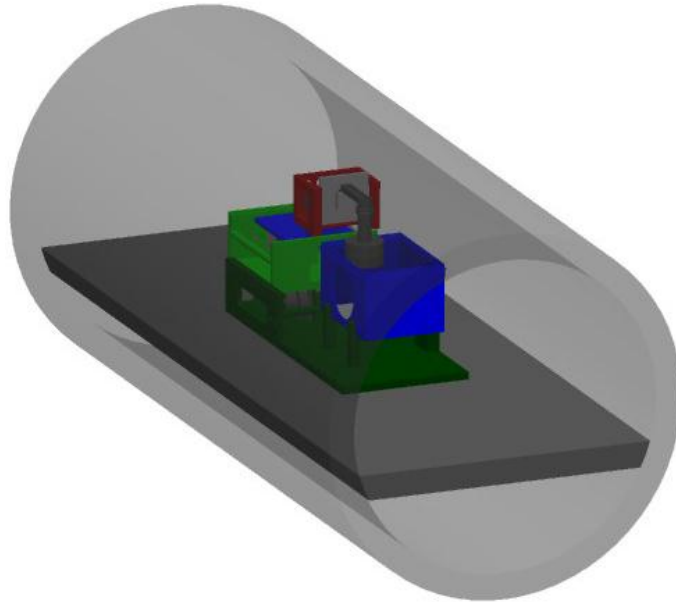


Figure 8.20: The CAD drawing of the robot inside the gantry of a typical MRI scanner.

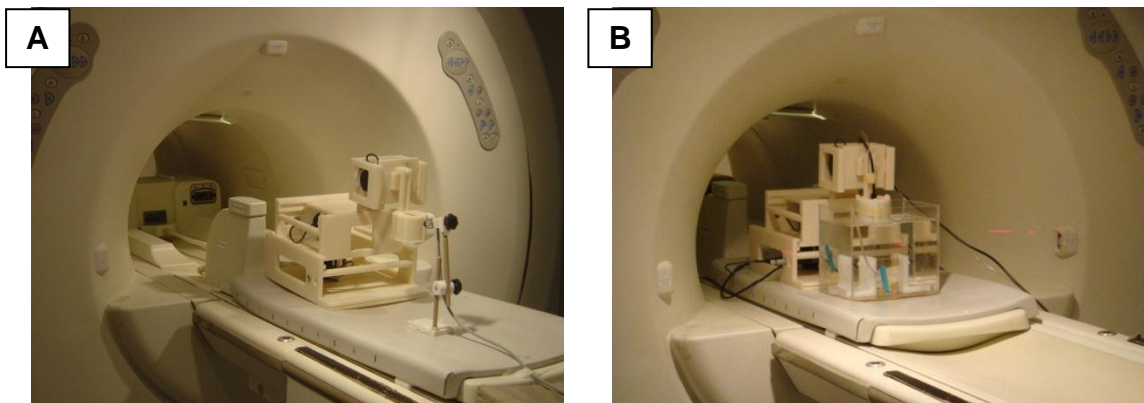


Figure 8.21: **A.** a photograph of the robot with the MRI compatible camera outside the gantry of an MRI and **B.** a photograph of the robot inside the gantry of an MRI scanner with the HIFU transducer immerse in the degassed water saline.

The photographs of figures 8.22.A and 8.22.B show the positioning device placed on the table inside the gantry of an MRI and were taken from the MRI compatible camera which is also placed on the table of the MRI scanner as shown in figure 8.21.A.

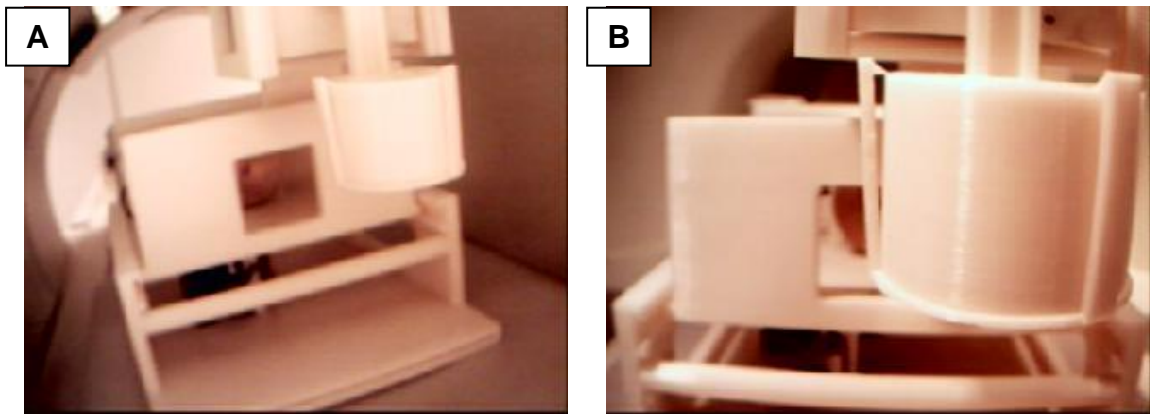


Figure 8.22: Photographs **A** and **B** show the robot placed in the gantry of an MRI scanner and are taken from the MRI compatible camera which is also placed in the gantry of the MRI scanner.

8.3 Conclusion and Discussion

The third version of the positioning device inherited all of the characteristic advantages of the second version since it is also designed on CAD software (Microstation V8, Bentley Systems, Inc.) and exported to a CAM software (Insight V. 6.4.1, Stratasys Inc.) and then produced by the 3D printer (Stratasys FDM400 7665 Commerce Way Eden Prairie, MN 55344 U.S.A.). Therefore, this third version is also MRI compatible, lightweight, cost effective, reproducible, and universal. Moreover this robot is as stable and accurate as the second version since the PUM motors, the brass racks and pinions, the guiding mechanism, as well as the software routines used for the guidance are identical with the second version robot.

The proposed third version of the positioning device can be used for brain tumours as shown in figure 8.19 with the horizontal HIFU transducer holder. Furthermore the water container holder shown in figure 8.12.B, is suitable for *in vitro* targets placed inside or underneath the water tank (kidney, liver, turkey fillet, porcine muscle etc.) by attaching the appropriate vertical HIFU transducer holder and also for *in vivo* targets (small animals like rabbit and rats).

This third version of the positioning device is also designed to be as flexible as possible. As in the case of the 2nd version of the robot all the parts can be easily detached and this provides better portability and any part of the robot can be redesigned and/or replaced at no time and this will have no effect on the rest

of the parts of the robot. During the development phase many parts had to be redesigned for better stability or for more efficient and smooth movement of the robot. However, due to the flexible design these modifications on the individual parts cause no effect on the rest of the parts of the positioning device. Furthermore, this positioning device can also accept different HIFU transducer holders of different length, height, and pointing direction or angle as well as HIFU transducers from different manufacturers or with different focal length and therefore different diameter, for different applications.

9 Software and peripheral devices of a HIFU system development

This chapter describes the software that provides the user interface that drives the motors of the positioning device. Furthermore, this software keeps the history of the steps of each treatment, stores and retrieves MRI images captured during the treatment, and captures images from the MRI compatible camera. The MR compatible camera which is placed on the table of the MRI scanner monitors the welfare of the person/animal being treated and displays and stores the temperature at the focus of the HIFU transducer which is necessary for the experimental work. This latest feature will not be used in clinical trials since it involves the insertion of a thermocouple in to the targeted biological tissue and as mentioned earlier our method is non-invasive. The software also controls the signal generator driving the ultrasound transducer. For the development of the software several attempts were made to use different programming languages such as visual basic and visual C#, but finally MATLAB (The Mathworks Inc., Natick, MA) was found to be more suitable for this purpose. Moreover the individual parts of the software were implemented separately and they were embedded together, after their completion, to the main user interface.

The features of the software developed are listed below:

i. Transducer movement

The user may move the robotic arm in a specific direction manually, or customize the automatic movement of the robotic arm in any formation by specifying the pattern, the step and the number of steps.

ii. Treatment History

A database is used to keep records of treatments and displays the starting time, elapsed treatment time, treatment time remaining, etc.

iii. Ultrasound treatment parameters

Settings of the ultrasound treatment parameters i.e. the intensity, frequency, treatment starting and ending times

iv. Patient database

A database was developed to store and retrieve the records of patients. A patient record keeps the first name, last name, date of birth, weight, height and gender.

v. Feedback from the encoders

This will be used to verify that the HIFU transducer is at the right location at any moment during the treatment.

vi. Display of MRI images

The MRI images of each treatment will be stored and the user has the ability to load any image stored.

vii. Display video or pictures captured from the MR compatible camera

An MRI compatible camera is connected on the system. The camera was interfaced by means of a video capture card. With the aid of the MRI compatible camera, the researcher can monitor the welfare of the animal or human.

viii. Temperature monitor along the beam of the HIFU transducer

This feature will capture and store in a text file the temperature at the focal point of the HIFU transducer at given time intervals.

9.1 Software development and setup of the peripheral devices used for capturing temperature, photographs and video displayed in the user interface.

For the movement of the PUM motors the main problem was to associate the CPU clock with the millimetres of the linear motion. For all three axis the same rack and pinions were used to convert the rotational motion of the piezoelectric ultrasonic motors into linear motion. The only difference for the three axis versions is the length of the rack. The length of the rack will define the range of the motion of the specified stage. Therefore, once the distance of the motion was associated with the duration of powering a motor, the same concept was applied for all three axis PUM motors.

Figure 9.1 shows a photograph of the power supply, the data acquisition board (National Instruments 6251 DAQ) and the enclosure designed to host the three dedicated drivers of the PUM motors. The power supply feeds the dedicated drivers of the motors with 24V DC. The robot may move forward, backward, left, right, up and down, manually using the three switches fixed on the front panel of the enclosure as shown in figure 9.1. These dedicated drivers are also connected to the three PUM motors and to the data acquisition board as shown in the photograph of figure 9.2. Each motor is connected to its dedicated driver with two cables. These cables are provided by the manufacturer of the PUM motors and one is used to send the signal to the motor so it can move and the other is to return through the encoder of the dedicated driver, a signal that the motor has moved to the right direction at the distance specified.

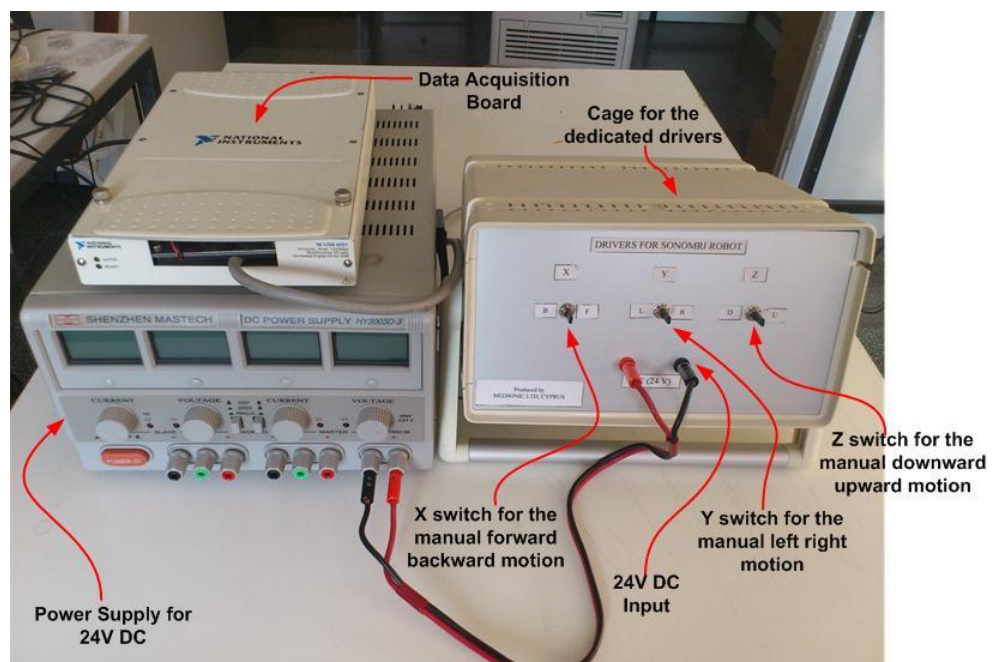


Figure 9.1: Photograph of the power supply and the three dedicated drivers (X, Y and Z)

The data acquisition board is connected at the rear panel of the enclosure as shown in figure 9.2 and is used to drive the PUM motors by sending the right signal from the PC to the dedicated driver. The data acquisition board will also receive a feedback signal from the dedicated driver which is then fitted to the PC. The data acquisition board is connected to the PC through a USB port. The photograph of Figure 9.3 shows how the three dedicated drivers are mounted insight the enclosure.

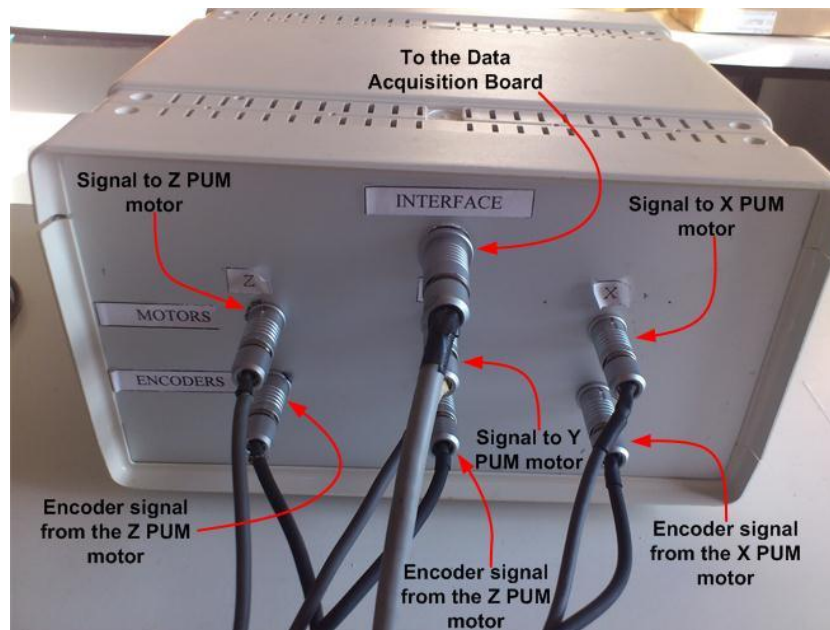


Figure 9.2: Photograph of the rear panel of the enclosure that holds the dedicated drivers.

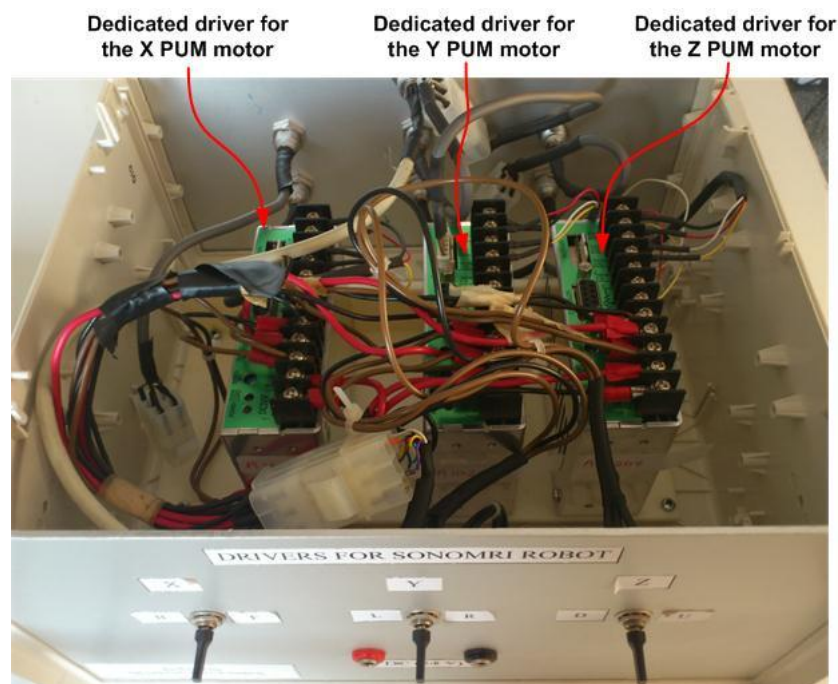


Figure 9.3: Photograph of the three dedicated drivers of the PUM motors mounted inside the enclosure

The connections in the data acquisition board are shown in the photograph of figure 9.4. On the left side of the data acquisition board of figure 9.4 the red and black wires are connected to the analogue input of the board and they are coming from the Omega thermocouple-to-analogue connector. This analogue input is converted to digital signal and entered in the computer to capture in real time the temperature at the focal point of the HIFU transducer. More details on

this digital thermometer can be found in section 9.2. The grey cable on the right side of the data acquisition board of figure 9.4 hosts the wires coming from the dedicated drivers of the PUM motors mounted in the enclosure shown in the photographs of figures 9.2 and 9.3. These wires are used to transmit the signal from the PC to the dedicated drivers to drive the PUM motors and also receive the signal from the encoder of the dedicated drivers.

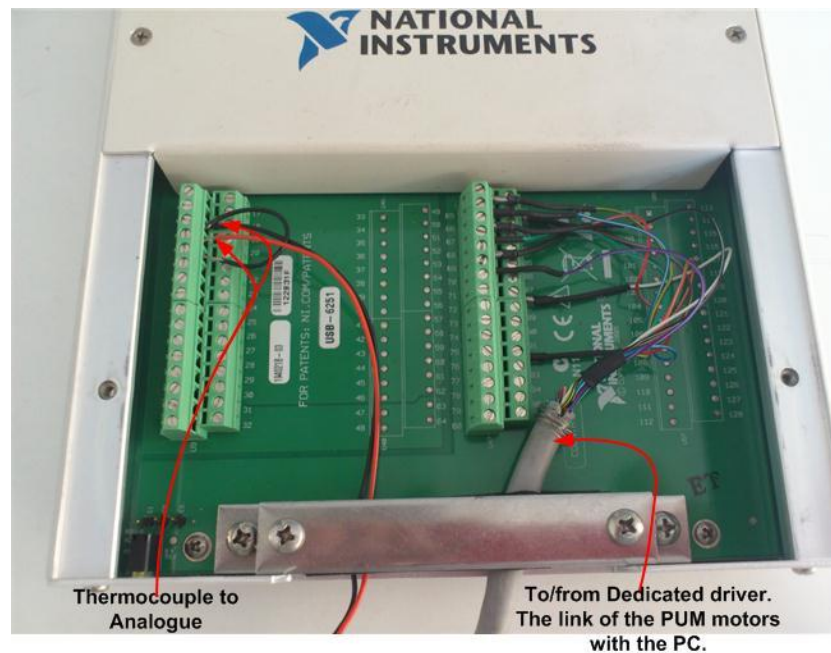


Figure 9.4: Photograph of the data acquisition board (DAQ) National Instruments 6251

The photograph of figure 9.5 shows the setup arrangement of the MR compatible camera (MRC Systems GmbH, Heidelberg, Germany). The filter box comes from the manufacturer and includes power and signal lines as well as shielding. The filter box includes a low pass filter that suppresses frequencies higher than 1 MHz with over 100 db. This filter prevents damage and interferences caused by the high frequency signals of the MR scanner.

The camera is connected to the filter box and the output video signal from the filter is entered in to the video capture card and hence the output video signal of the video capture card enters the PC.

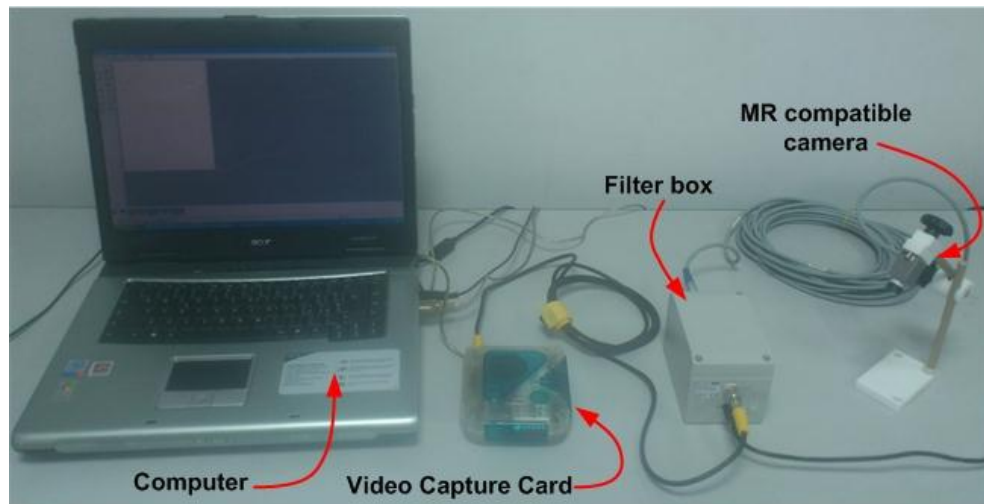


Figure 9.5: Photograph of the setup of the MR compatible camera.

9.2 Development of the digital thermometer

The digital thermometer will be used for capturing the variations of temperature at the focal point of the HIFU transducer at specified time intervals and store them in a text file in order to be used later for further analysis.

The first attempt to read the temperature is shown in figure 9.6 where the thermocouple was connected directly to the analogue input of the data acquisition board. It appeared that the signal was too weak and noise was interfering and therefore the temperature was not entered correctly in to the software.

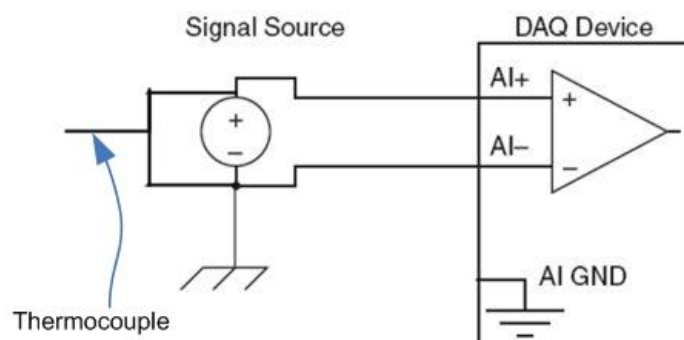


Figure 9.6: The thermocouple is connected directly to the analogue input of the data acquisition card.

Figure 9.7 shows the second attempt used to acquire the temperature which was better but the signal was too weak and therefore we had some temperature fluctuations.

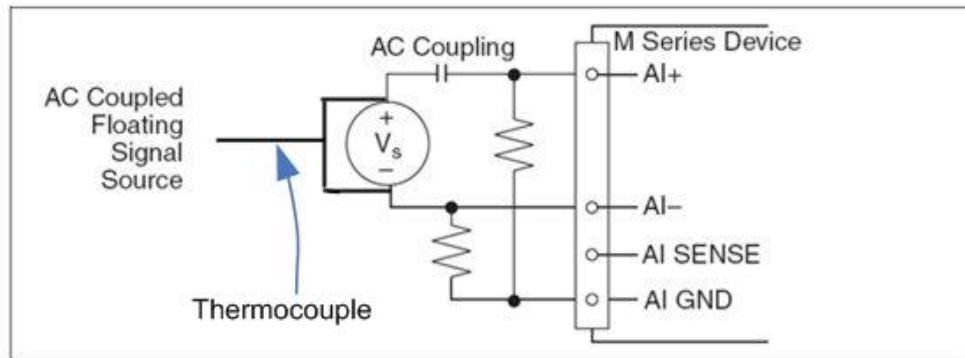


Figure 9.7: The thermocouple is connected as shown in the diagram to the analogue input of the data acquisition card.

Finally a commercial readymade thermocouple-to-analogue proved to work fine for our purposes. With the Omega M2813-1205 thermocouple-to-analogue connector shown in figure 9.8, the process was much more accurate. The thermocouple-to-analogue connector gives analogue output 1mv per degree °C and this was entered in to the data acquisition card and read by the software.



Figure 9.8: Omega thermocouple-to-analogue connector.

Figure 9.9 shows the National Instrument acquisition card used to drive the Shinsen dedicated drivers for the motors of the positioning device mounted in the white box (to the right of the PC) and also to capture the temperature from the Omega thermocouple-to-analogue connector.

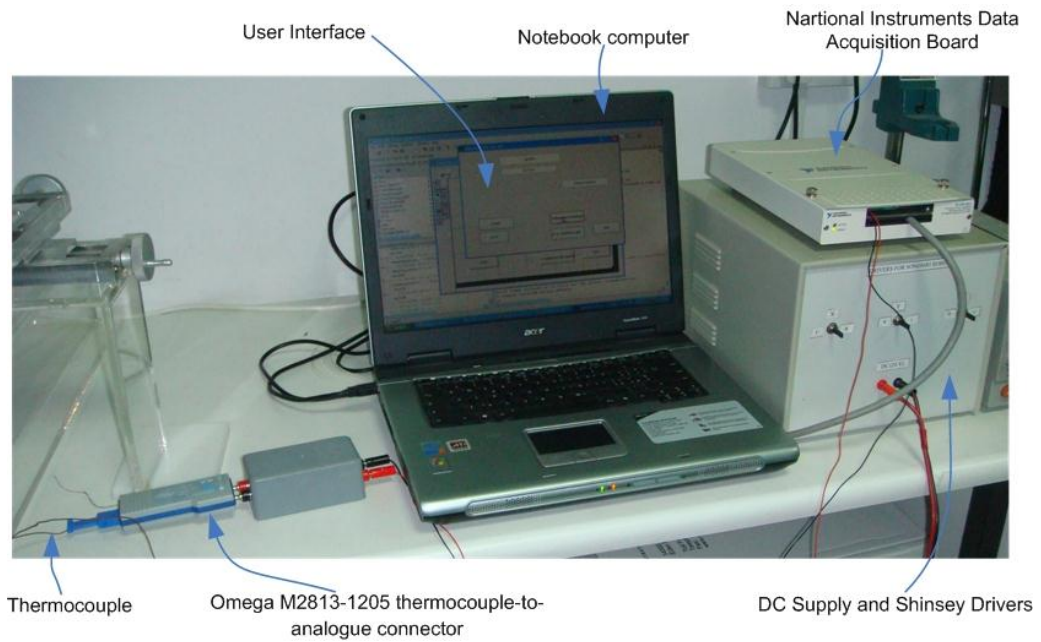


Figure 9.9: Data acquisition set up

Figure 9.10 shows a snap shot of the end user interface of the digital thermometer. The temperature readings will be displayed in textbox 1 and stored in a text file the name of which is given by the end user in textbox 3 along with the time taken shown as Elapsed Time 2. Button 4, *temperature readings* will start the timer and the temperature values will be stored in the file and button 5, *stop temperature* will stop the process. The *exit*, button 6, will terminate the application. Part of the text file that keeps the temperature readings along with the time taken is shown in figure 9.11.

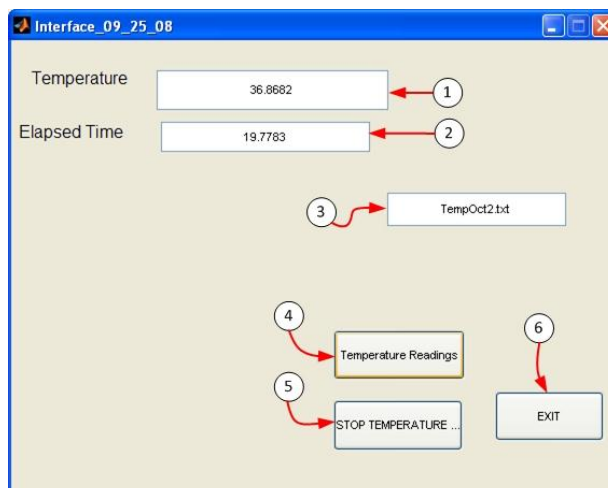
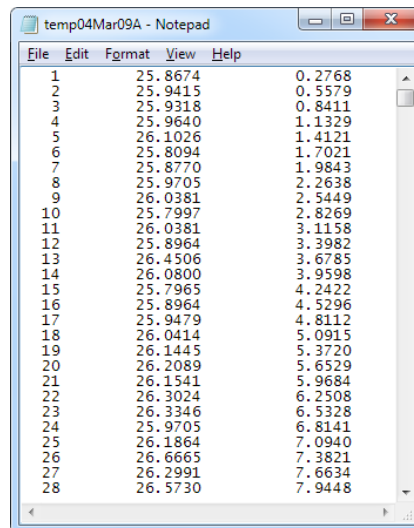


Figure 9.10: The end-user interface used to capture the temperature fluctuations at the focal point of the HIFU transducer at specified time intervals.

The digital thermometer module was designed, implemented and tested extensively in isolation from the other modules of the software and then the final version was embedded in the main software as shown in the lower right corner of figure 9.12 with labels 30 to 34.



Line	Temperature	Value
1	25.8674	0.2768
2	25.9415	0.5579
3	25.9318	0.8411
4	25.9640	1.1329
5	26.1026	1.4121
6	25.8094	1.7021
7	25.8770	1.9843
8	25.9705	2.2638
9	26.0381	2.5449
10	25.7997	2.8269
11	26.0381	3.1158
12	25.8964	3.3982
13	26.4506	3.6785
14	26.0800	3.9598
15	25.7965	4.2422
16	25.8964	4.5296
17	25.9479	4.8112
18	26.0414	5.0915
19	26.1445	5.3720
20	26.2089	5.6529
21	26.1541	5.9684
22	26.3024	6.2508
23	26.3346	6.5328
24	25.9705	6.8141
25	26.1864	7.0940
26	26.6665	7.3821
27	26.2991	7.6634
28	26.5730	7.9448

Figure 9.11: Part of the temperature file stored during an experiment.

9.3 The complete end-user interface

Two methods were implemented to move the robot in the space. The first method is manual and this can be done by entering the number of millimetres desired for each axis, X, Y and Z shown in figure 9.12 shown as labels 1, 2 and 3 respectively. The resolution of all 3 axes of the positioning device is 0.1 mm.

The software apart from driving the positioning device provides the user, the physician, with other useful features described at the beginning of this chapter. The complete end-user interface is shown in Figure 9.12. Table 9.1 describes all the elements and the features of the user interface of figure 9.12.

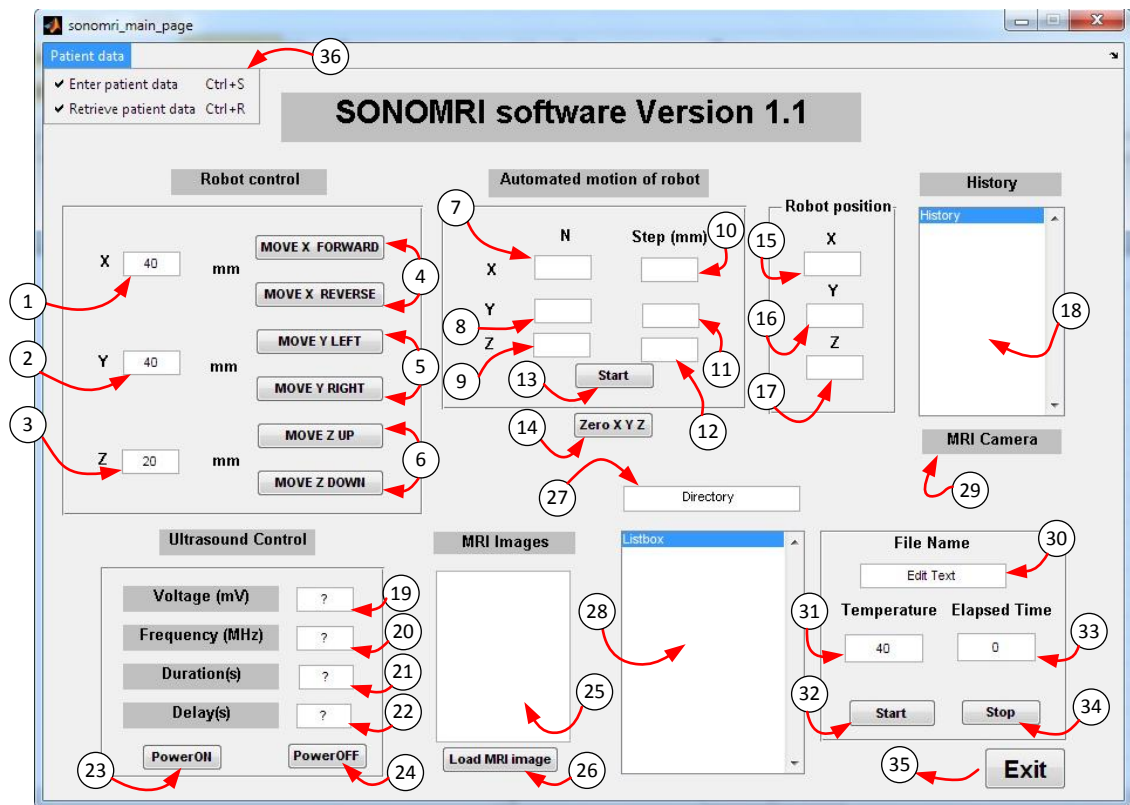


Figure 9.12: The user interface for the software of the HIFU system.

User Interface functions	
Num	Function Description
1	Textbox for the user to enter the number of millimetres for the manual movement of X-plate
2	Textbox for the user to enter the number of millimetres for the manual movement of Y-plate
3	Textbox for the user to enter the number of millimetres for the manual movement of Z-plate
4	Buttons that will move the X-plate forward and backward a number of millimetres specified by the number entered in the textbox 1
5	Buttons that will move the Y-plate forward and backward a number of millimetres specified by the number entered in the textbox 2
6	Buttons that will move the Z-plate forward and backward a number of millimetres specified by the number entered in the textbox 3
7	The user will use this textbox to enter the number of steps for the motor of the X-axis plate
8	The user will use this textbox to enter the number of steps for the motor of the Y-axis plate
9	The user will use this textbox to enter the number of steps for the motor of the Z-axis plate
10	This textbox will be used by the end user to enter the step of the automatic motion of the X-axis plate in millimetres
11	This textbox will be used by the end user to enter the step of the automatic motion of the X-axis plate in millimetres
12	This textbox will be used by the end user to enter the step of the automatic motion of the X-axis plate in millimetres
13	This button will start the automatic motion with the settings of 7, 8, 9, 10, 11 and 12.
14	This button will reset the robot to its origin, 0, 0, 0
15	The encoder of the dedicated driver will return the position of the X PUM motor after its movement

16	The encoder of the dedicated driver will return the position of the Y PUM motor after its movement
17	The encoder of the dedicated driver will return the position of the Z PUM motor after its movement
18	This listbox will display all past movements of the three motors
19	The user will use this textbox to enter the voltage for the signal generator in millivolts
20	The user will use this textbox to enter the frequency in MHz for the signal generator
21	The user will use this textbox to enter the duration of sonification in seconds
22	The user will use this textbox to enter the delay between sonifications in seconds
23	This button will turn the on the power of the RF amplifier and set the settings of the signal generator as specified by textboxes 19, 20, 21 and 22.
24	This button will turn the off the power of the RF amplifier
25	A selected MRI image from the listbox 28 will be displayed in this area
26	This button will load the selected MRI image to the area 25
27	The user will enter the full path for the MRI images to be loaded in the listbox 28
28	The listbox will display a list of all the MRI images found in the directory specified in 27
29	This function will open a window to display a real time video or images captured during the treatment of a patient or an animal from the MRI compatible camera placed on the table of the MRI scanner to monitor the welfare of the person/animal being treated
30	The user will enter the name of the text file in which the temperature readings and the time of each reading will be stored
31	This textbox will display the current temperature reading
32	This button will start the timer and display the current temperature captured from the digital thermometer and elapsed time in textboxes 31 and 33 respectively. These values will be stored in the file specified in 30
33	This textbox will display the elapsed time in seconds
34	This button will stop the timer and the readings from the digital thermometer.
35	This button will terminate the application
36	The patient data menu has two options. The first option will be used to open a form to enter the personal data of the patient and save them in the patients file and the second option will display the personal data of a selected patient.

Table 9.1: The table above describes all the elements of the user interface of figure 9.12

The MatLab R2007b code written for this application can be found in appendix 12.3

9.4 Conclusion

The software developed to drive the robot is user friendly and provides the user two methods for moving the robot in the gantry of the MRI. The user may move the robotic arm in a specific direction or customize the automatic movement of the robotic arm in any rectangular formation by specifying the pattern, the step and the number of steps. Furthermore, the software has additional useful features that can be used by the physician during or after the procedure. These features include, displaying of MR images, monitoring the time of the processes (starting time, treatment time left etc.), stores patient records, display the

position of the motor, display images captured from an MR compatible camera, cavitation detection window, and temperature measurement.

The user interface was tested extensively and proved to be reliable, stable and accurate. The software tested thoroughly in a complete HIFU/MRI system and the results provided in section 10.2. The software was also used and tested in all the experiments executed for the evaluation of this study and the results can be found in the evaluation section, chapter 10. Additionally, the software can be easily updated and modified to fulfil any future requirements.

10 Evaluation of the MRI compatible positioning devices

MRI compatible robotic system design is a challenging task due to the strong magnetic field of the MRI scanner. Therefore, there are many obstacles to overcome. These limitations concern the selection of the materials, the HIFU transducer, the sensors, the actuators and the wiring of the motors and transducer. The challenge is to assemble a robot which will cause no interference to the MRI scanner nor affected by the strong electromagnetic field of the MRI scanner. Moreover, tight geometric limitations, 55-60 cm diameter of bore core of a typical MRI cylindrical scanner, builds up to the challenge of designing and implementing an MRI compatible robot.

The compatibility of the parts of the proposed HIFU system, the functionality, and the accuracy were tested and evaluated. The experiments and the results of these are described here in this chapter.

10.1 Measuring the efficiency of the HIFU transducers

The efficiency of any transducer needs to be measured prior to its use. Figure 10.1 shows a photograph of the apparatus (UPM-DT100N, Ohmic Instruments Co. Easton MD 21601) used to measure the power of the HIFU transducers.



Figure 10.1: The photograph shows the ultrasound power meter, a device used to measure the ultrasound power of the transducers.

To measure the power of a HIFU transducer the cylindrical part is filled with degassed saline water. Hence the spherical area at the bottom of the HIFU transducer is immersed in the degassed saline water facing the metal silver cone of the photograph of figure 10.1. Then the transducer is firing on this metal cone and the device shows the reading. Several measurements had to be made in order to verify the power of the transducer.

10.2 *In vitro* and *in vivo* experiments to evaluate the MRI Guided HIFU system

The MRI compatible positioning device version 1 is used to move an MRI-guided high intensity focused ultrasound (HIFU) transducer. This device includes a flexible coupling system, and thus it can be used in all the anatomies accessible by HIFU (liver, kidney, breast, brain and pancreas). However, in this research only the superior top to inferior approach is utilized i.e. the HIFU transducer is firing the beam from the top of the target. Moreover, details of this positioning device can be found in chapter 6.

10.2.1 Material and methods

a. HIFU/ MRI system:

The HIFU/MRI system is described in chapter 5. Figure 5.1 shows the block diagram of all the components required for a typical HIFU system with the MRI guidance and figure 5.2 shows setup the actual components of the HIFU/MRI system. These components of figure 5.2 were used for most the laboratory experiments. However, for different experiments and for the clinical experiments in MRI room some parts were substituted.

b. HIFU system

The HIFU system consists of a signal generator (HP 33120A Hewlett Packard, now Agilent technologies, Englewood, CO, USA), RF amplifier (250 W, AR, Souderton, PA, USA), and a spherically shaped bowl transducer (Etalon, Lebanon, IN, USA) made from piezoelectric ceramic which is non-magnetic. The transducer operates at 4 MHz, has focal length of 10 cm and diameter of 3 cm. The transducer is rigidly mounted on the MR compatible positioning device version 1 which is described in chapter 6.

c. *MRI Imaging*

The positioning device and the transducer were tested inside a MRI scanner (Signa 1.5 T, by General Electric) at Ygia Polyclinic Private Hospital, Lemesos, Cyprus. A spinal or a brain coil was used to acquire the MRI signal.

d. *Coupling mechanism*

The system provides two main mechanisms for achieving coupling to tissues. Fig. 6.14 illustrates the two mechanisms. In Fig. 6.14.A the tissue (*in vitro* or *in vivo*) is placed outside the container which is filled with degassed water. Due to the weight of the water container, the coupling with this method is excellent. This method can be described as a top to bottom approach, meaning that the transducer is on top of the tissue. In the commercial system by [136] the approach used is bottom to top, meaning that the transducer is below the tissue. In Fig 6.14.B the tissue is placed inside the container which is filled with degassed saline. The use of saline is needed for this method in order to preserve the excised tissue, which is placed inside the saline bath. This method which provides perfect coupling since the tissue is placed inside the container can be used only for tissues *in vitro*. In both methods above the liquid in the container (degassed water or saline) was maintained at 37 °C.

10.2.2 *In vitro* experiments

Various *in vitro* experiments were carried out in order to assess the motion of the positioning devices. The tissue under ablation was placed in a degassed saline water tank (Figure 6.14B). The tissue was placed on top of an absorbing material in order to shield adjacent tissue from stray radiation from the bottom of the plastic water tank. The transducer was placed on the arm of the positioning device and was immersed in the saline tank, thus providing good acoustical coupling between tissue and transducer. Any bubbles that may have collected under the face of the transducer face were removed in order to eliminate any reflections. In all experiments the tissues used were extracted from freshly killed lamb, and the experiment was conducted 1-2 hours after the animal was killed.

10.2.3 *In vivo* experiments

For the *in vivo* experiments, adult rabbits from Cyprus were used weighing approximately 3 kg. The rabbits were anaesthetized using a mixture of 500 mg of ketamine (100 mg/mL, Aveco, Ford Dodge, IA), 160 mg of xylazine (20 mg/mL, Loyd Laboratories, Shenandoah, IA), and 20 mg of acepromazine (10 mg/mL, Aveco, Ford Dodge, IA) at a dose of 1 mL/kg. The animal experiments protocol was approved by the national body in Cyprus responsible for animal studies (Ministry of Agriculture, animal services) and all licenses are found in the appendix. The coupling method of Figure 6.14A was used.

10.2.4 Evaluation of MRI compatibility

The robot motion should not have any adverse effect on the imaging, and it should not be affected by the acquisition of images. The MR safety of the robot requires that it is not moved unintentionally from any activity of the MRI scanner such as eddy currents or radio frequency (RF) pulses. The loss of homogeneity of the magnetic field, and the signal to-noise ratio (SNR) of the image has been examined when the robot is moving inside the MRI scanner. The presence and motion of the robot can distort the image by decreasing the homogeneity of the magnetic field. The images with the presence of the positioning device or not were evaluated using a rectangular phantom that contained CuSO₄ solution. A reference image is taken without the presence of the material under evaluation. Then the material under evaluation is placed in very close proximity to the phantom. Then the two images are subtracted and if the resulted image is dark, it means that the material does not affect the MRI image at all.

10.2.5 Results

Figure 10.2A shows the MRI image of the phantom without the presence of the motor, and Figure 10.2B shows the MRI image of the phantom with the presence of the motor. Finally, Figure 10.2C shows the subtraction of the two images showing no shift. Similar procedure was applied to evaluate the effect of all the system's materials (plastics, pulleys, belts, piezoelectric materials, and brass screws and rods). None of the tested materials resulted in any distortion of the MRI images.

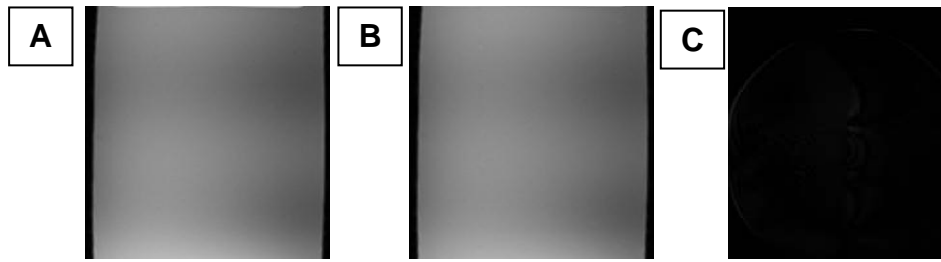


Figure 10.2: **A.** an MRI image of phantom without the presence of the motor. **B.** an MRI image of phantom with the presence of the motor. **C.** an MRI image of the subtraction of the two images showing no shift.

Figure 10.3 shows various discrete lesions (more detailed results can be found in [155]) created by moving the transducer using the robot (2000 W/cm^2 in-situ average spatial intensity for 5 s). The thermal lesions measured were between 2.8-3.4 mm (average was 3.0 mm and standard deviation was 0.3 mm). The lesions are repeatable for a given acoustic exposure. Some differences that are observed are attributed to the variation of focal depth arising from the kidney curvature. On the flat surface of the kidney the lesion width varied from 3.0 to 3.2 mm (average was 3.1 mm and standard deviation was 0.04 mm). This figure demonstrates the excellent repeatability of the HIFU system for creating well controlled discrete lesions.



Figure 10.3: Lesions created in pig kidney demonstrating the excellent repeatability of the positioning device.

Figure 10.4 shows a lesion created by moving the transducer in a patterned movement (square grid of 8x8 with 3 mm step) in both directions. The intended target was the round shape in red colour. The same intensity as in Figure 10.4 was used for each firing. The dimensions of the large lesion clearly demonstrates that the robot can move the transducer as instructed, thus creating well controlled ablation.

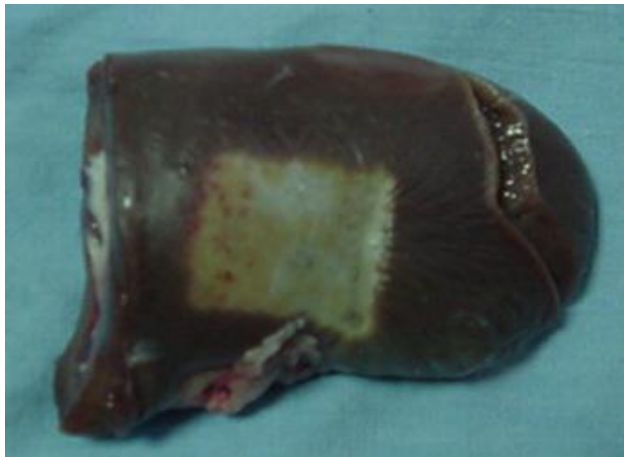


Figure 10.4: Large lesion in pig kidney *in vitro* by moving the transducer in grid formation (8 X 8) (top view)

A very important aspect of this system is the ability to monitor thermal lesions created by HIFU using MRI. Figure 10.5A shows MR images of lesions in kidney using T2-weighted, Fast Spin Echo (FSE) (TE=32 ms, TR=3000 ms, NEX=1, FOV=16 cm, slice=5 mm, 256x256, BW=32 KHz, ETL=8). This image shows the lesion in a plane parallel to the ultrasonic beam. This large lesion volume was created by moving the transducer using a 4x4 grid pattern with step of 3 mm. Figure 10.5A shows the photograph of the kidney after slicing.

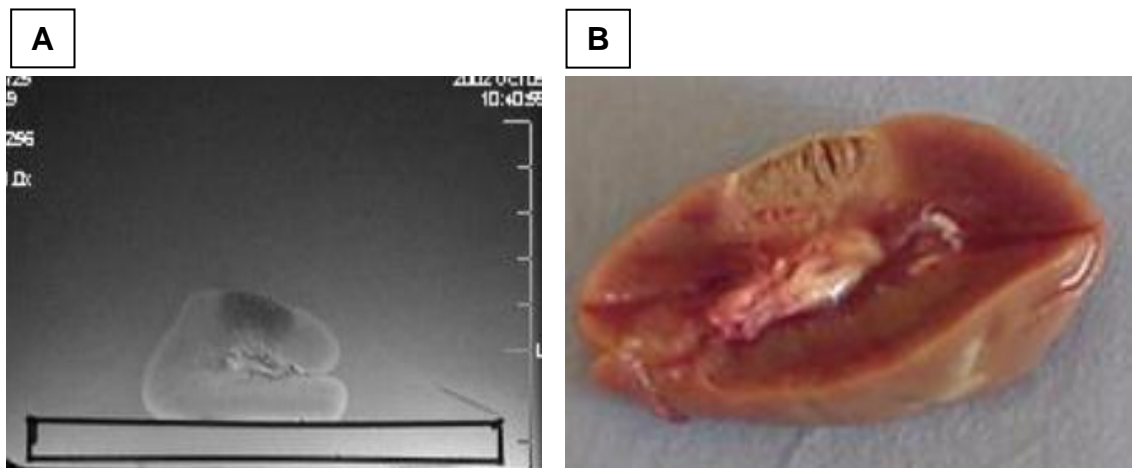


Figure 10.5: **A.** Axial MR images of HIFU ablation using T2-weighted FSE (TE=32ms) pulse sequence. **B.** Photograph after slicing.

Figure 10.6 shows nine MRI images in a plane perpendicular to the beam acquired by using T1-weighted, Fast Spoiled Gradient echo (FSPGR) (TR=50 ms, TE=2.7 ms, FOV=16 cm, matrix=256x256, flip angle=50°, BW=62.5 KHz,

NEX=1). The transducer was moved in a 3x3 pattern and the in situ average spatial intensity used was 100 W/cm^2 for 10s. This intensity was used previously *in vitro* [155] and the temperature measured using a thermocouple was around $2\text{-}5 \text{ }^\circ\text{C}$, which means that there is no tissue damage with this ultrasonic exposure. These images show, that in every of the nine firings, there is good penetration, since heating is observed (dark spot of 1-2 mm diameter). Therefore, this proves that the ultrasound penetration to this target is excellent in all nine locations. Following this diagnostic scan, the intensity was increased to 1500 W/cm^2 (with 5 s duration) and the nine locations were ablated once more. Figure 10.7 shows the MRI image in a plane perpendicular to the beam by using T2-weighted FSE (same parameters as in Figure 10.5).

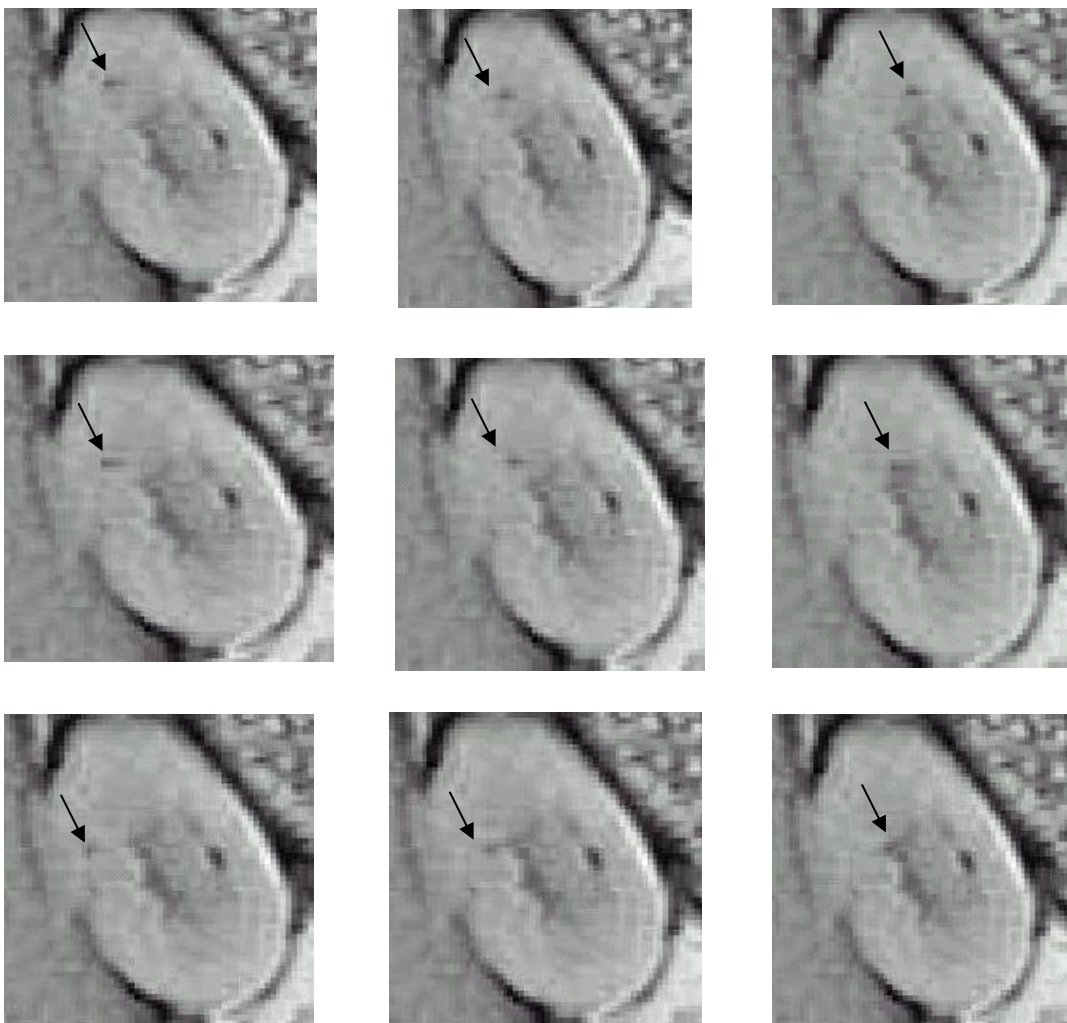


Figure 10.6: MR images showing the focal beam during a 3 X 3 scanning using low intensity ultrasound using T1 weighted FSPGR.

Note that spatial necrosis is continuous, thus resulting in absolutely no untreated spaces. The continuous necrosis coverage was visually confirmed after gross examination of the kidney. On the same tissue, a single lesion (reference) was created using the same exposure (1500 W/cm^2 for 5 s) in order to show the size of a discrete lesion for this specific exposure. Note that, by using this intensity none of the lesions were created under the mechanism of cavitation (confirm by the cavitation detector).

A good indicator of the contrast between necrotic tissue and normal tissue is the contrast-to-noise ratio (CNR). CNR was obtained by dividing the signal intensity difference between the necrotic and normal tissue by the standard deviation of the noise in the normal tissue. In Figure 10.7 the CNR was around 30 indicating the excellent contrast between necrotic and normal tissue.

Figure 10.8 shows the MRI image using T2-weighted FSE of a large lesion in the kidney in a plane perpendicular to the beam. This lesion was created by using a 4x5 grid of lesions. The intensity used was 2000 W/cm^2 at 5 s and the spacing between the lesions was 3 mm. Note that the necrosis coverage is incomplete, resulting to some untreated spots (CNR was around 30). The diagnostic scan of this result has shown that the penetration at the location of the untreated area was poor, since no detectable temperature elevation was observed.

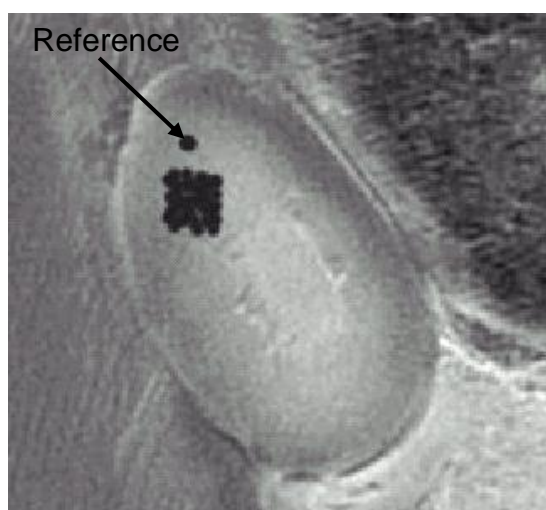


Figure 10.7: MR images (in plane perpendicular to the transducer beam) of large lesions (full coverage of the intended target) using T2-Weighted FSE with $TE = 32\text{ms}$. The spatial average intensity was $1,500 \text{ W/cm}^2$ for 5s

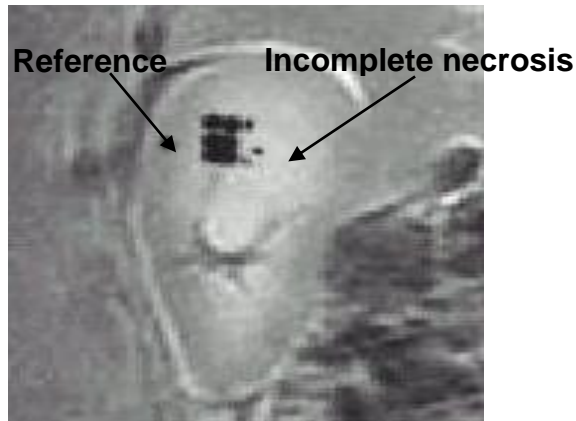


Figure 10.8: MR images (in plane perpendicular to the transducer beam) of large lesions (partial coverage of the intended target) using T2-Weighted FSE with TE = 32ms. The spatial average intensity was 2,000 W/cm² for 5s

10.2.6 Discussion

The robot version 1 presented here is utilized in the research setting for performing experiments either *in vitro* tissue or *in vivo* animals.

The positioning system employs piezoelectric motors and various materials (sheets, rods, angles, pulleys and belts) in order to move the transducer in 3 dimensions. The rotational motion of the piezoelectric motors is coupled to a timing belt which is supported by a fixed plastic pulley. The belt is coupled to a plastic rectangular sheet and thus the rotation of the belt results in a linear motion of the involved sheet. The same principle is applied for every stage. Totally 3 linear axes are implemented for the case of brain ablation. The piezoelectric motor which is the most important element of the positioning device does not affect the quality of imaging of the MRI scanner.

The positioning device is placed on the table of the MRI scanner and access of ultrasound to the brain is achieved either from superior to inferior or laterally. Since the positioning device is placed on the table of the MRI scanner, this device can be used in all the available MRI scanners (i.e. it is a universal positioning device). The existing systems are placed inside the gantry on the table of the MRI scanner, and therefore the dimensions of the system must be adjusted depending on the type of MRI scanner. Also, the existing systems can access the patient from bottom up whereas this positioning device can access patient from the side or from top to bottom.

Another advantage of this device is that it is much simpler and inexpensive than the existing systems, while maintaining high standards of repeatability and readability. Another advantage of this positioning device is that it can be easily reduced or increased in size. This can be adjusted easily by modifying the rod length, sheet length and belt length. All the other components remain fixed in size. Thus, easily any size of positioning device can be designed. There is limitation though based on the diameter of the MRI scanner. Moreover, this positioning device is lightweight (approximately 6 Kg) and therefore it can be transported from one MRI scanner to another (i.e. it is portable and universal).

The positioning device moves the transducer accurately and thus discrete and large thermal lesions can be produced reliably and repeatedly. This has been proven in both *in vitro* and *in vivo* tissues.

The concept of scanning the area to be treated, by applying low intensity ultrasound (diagnostic scan) was shown to be feasible. It is up to the HIFU clinicians whether or not this diagnostic scan is used during clinical work, but certainly this tool can be very useful during research investigations. This concept was demonstrated for a single shot in *in vivo* kidney by Hynynen [14], but was never demonstrated spatially in two dimensions (grid). This diagnostic scan was demonstrated in a plane perpendicular to the beam, but it is possible to demonstrate it in a plane parallel to the beam. When all the points of the grid show decrease of temperature (black spot in the T1-weighted FSPGR), then, during the application of high intensity ultrasound (therapeutic scan), complete necrosis is observed in the targeted area. If ultrasound goes through an interface that includes bubbles, then the diagnostic scan reveals sites with poor ultrasound penetration and, therefore, later in the therapeutic scan, some spaces are left untreated.

10.2.7 Conclusion

A simple, cost effective, portable positioning device has been developed which can be used in virtually any clinical MRI scanner since it can be sited on the scanner's table. The propagation of HIFU can use either a lateral or superior-inferior approach. Discrete and large lesions were created successfully with reproducible results. The quality of MRI imaging is not affected by the presence of the HIFU system.

10.3 Testing the MRI Compatibility of Robot V2 on phantom

The purpose of this experiment was to test the MRI compatibility of positioning device version 2 targeting a gel phantom.

10.3.1 Material and methods

Equipment used

HIFU transducer

- diameter $d = 4$ cm
- focal radius $R = 10$ cm,
- operating at a frequency of 1 MHz.

Tissue: gel phantom (Onda Corp., Sunnyvale, CA).

RF amplifier: LA 100-CE, Kalmus, Bothell, WA, USA

The block diagram and the equipment necessary for a HIFU/MRI system is shown in figures 5.1 and 5.2 respectively and the system is described in chapter 5. Figure 10.9 shows the photograph of the positioning device version 2 placed on the bed of the MRI scanner (Signa 1.5 T, by General Electric, Fairfield, CT, USA). The vertical HIFU transducer is attached on the positioning device and the HIFU transducer was mounted on this holder.

The coupling method of figure 6.14B is used. Therefore, the gel phantom target is immersed in the degassed water saline as shown in the photograph of figure 10.9.

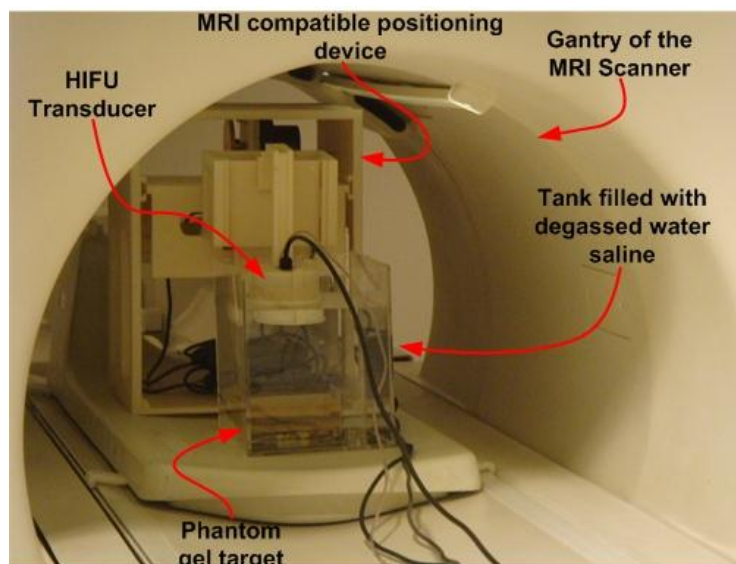


Figure 10.9: Photograph of the positioning device version 2 in the gantry of the MRI scanner. The gel phantom is immersed in the degassed water saline.

The MRI image of figure 10.10 was captured using T2 W FSE and shows the HIFU transducer, the phantom gel and the tank filled with degassed water saline placed in the gantry of the MRI scanner.

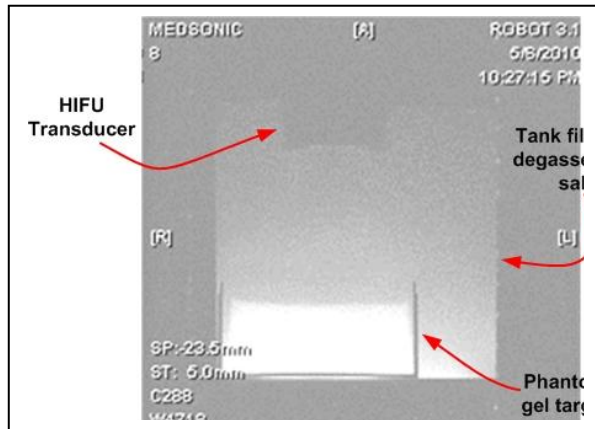


Figure 10.10: The MRI image shows the HIFU transducer, the phantom gel and the tank filled with degassed water saline using T2 W FSE.

The MRI images of Figure 10.11 captured using FSPGR. These images show the phantom gel and the tank filled with degassed water saline. The red arrow of MRI images 10.11A, 10.11B and 10.11C is pointing at the focal spot at three different positions.

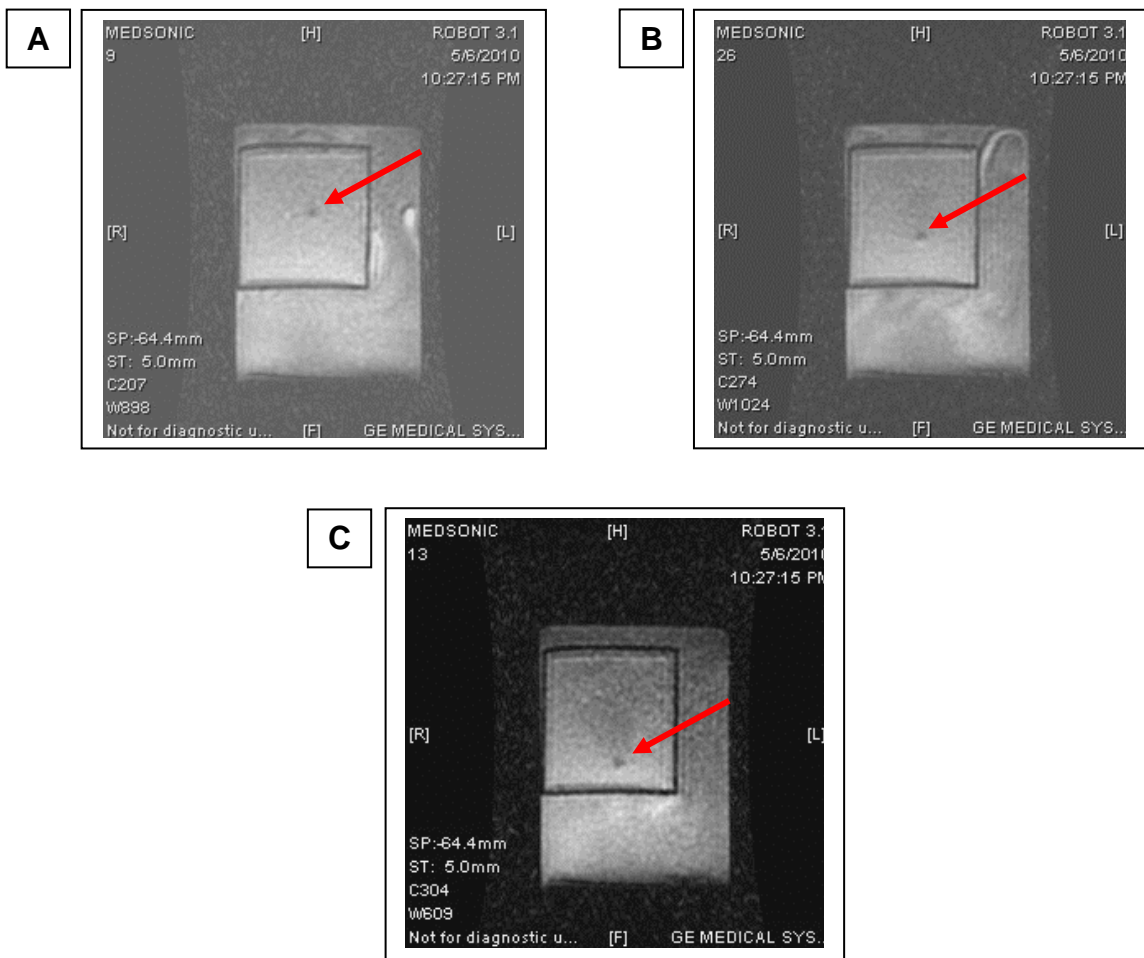


Figure 10.11: The MRI image shows the HIFU transducer, the phantom gel and the tank filled with degassed water saline using FSPGR. The red arrow indicates the focal spot **A.** at position 1 **B.** at position 2 and **C.** at position 3.

This focal spot in different positions achieved by moving the HIFU transducer attached on the vertical transducer holder of the positioning device.

10.3.2 Conclusion

The MRI images captured during this experiment show no significant RF artifact caused by the positioning device, motors, cables and HIFU transducer. Both FSE and FSPGR not affected significantly by the positioning device. This proves the positioning device is MRI compatible.

10.4 Test MRI compatibility of positioning device version 3.

The purpose of this experiment was to test the MRI compatibility of positioning device version 3.

10.4.1 Material and methods

Equipment used

HIFU transducer

- diameter $d = 4$ cm
- focal radius $R = 10$ cm,
- operating at a frequency of 1 MHz.

Tissue: gel phantom (Onda Corp., Sunnyvale, CA) and thrombi inserted in a silicone tube.

RF amplifier: LA 100-CE, Kalmus, Bothell, WA, USA

For this experiment the equipment used for the HIFU/MRI system were the same as for experiment of section 10.4 with the only exception the positioning device version 2 which was replaced with the positioning device version 3. Moreover, the vertical HIFU transducer attached on the positioning device and the HIFU transducer was mounted on this holder.

For this experiment the coupling method of figure 6.14B was also used as for the experiment of section 10.4. Two targets were used for this experiment. The first target was a gel phantom. The second, a silicone tube with the inserted thrombi fixed between two polyethylene corners mounted on the base of the tank. The tank was then filled with degassed water saline as shown in the

photograph of figure 10.12A. The photograph of figure 10.12A also shows the positioning device and the water tank placed on the table of the MRI scanner. The photograph of figure 10.12B shows the positioning device and the subject target in the gantry of the MRI.

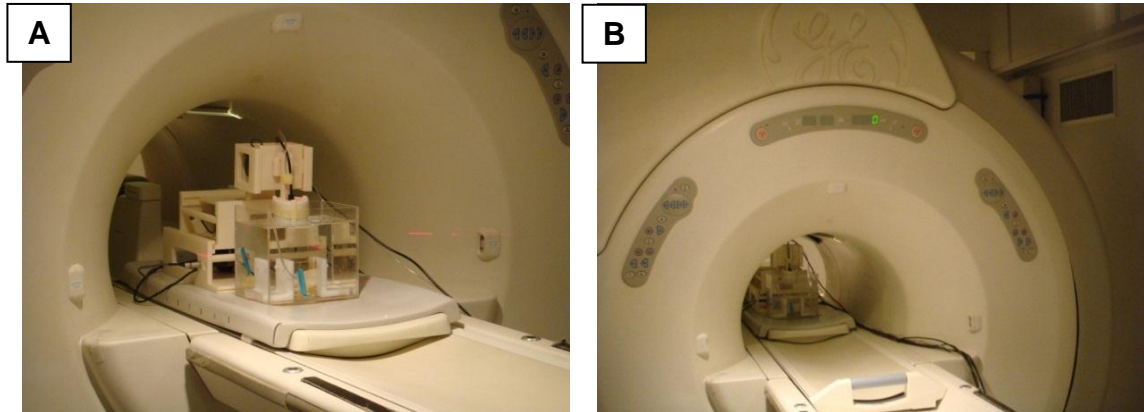


Figure 10.12: A Photograph of the positioning device version 3 on the table of the MRI scanner, B the positioning device version 3 in the gantry of the MRI scanner.

Figure 10.13A shows the MRI image of the HIFU transducer and the phantom gel this image captured using T1 W FSE, and Figure 10.13B shows the MRI image of the phantom gel and the tube passes through the gel. The image was also captured using T1 W FSE.

The MRI image of Figure 10.14 shows the phantom gel mounted within the plastic holders. The image captured using FSPGR in a plane inside the gel.

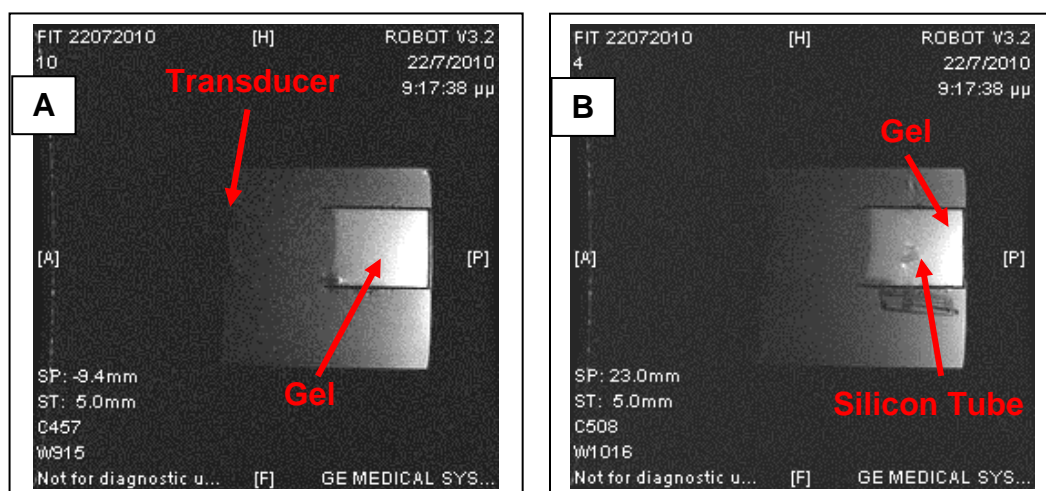


Figure 10.13: A the MRI image shows the HIFU transducer, and the phantom gel this image was captured using T1 W FSE, B the MRI image shows the phantom gel and the tube passes through the gel. The image was also captured using T1 W FSE.

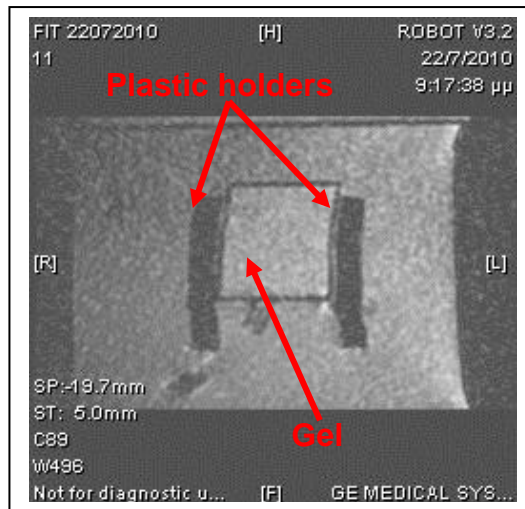


Figure 10.14: The MRI image shows the phantom gel mounted within the plastic holders. The image captured using FSPGR in a plane inside the gel.

10.4.2 Conclusion

The MRI images capture during this experiment show no significant RF artifact caused by the presence of the positioning device version 3, the PUM motors, the cables and the transducer in the gantry of the MRI scanner. FSE and FSPGR not affected significantly by the positioning device. This proves as expected, that the positioning device version 3 is also MRI compatible.

10.5 Ablate a porcine muscle tissue using the positioning device version 3.

The purpose of this experiment is to create lesions in porcine muscle tissue using the positioning device version 3. The HIFU transducer mounted on the vertical transducer holder using the coupling method of figure 6.14A, i.e. the porcine muscle was placed at the bottom of the tank filled with degassed water saline.

10.5.1 Material and methods

Equipment used

Tissue: porcine muscle

RF amplifier: 250 W, AR, Souderton, PA, USA

Positioning Device version 3 (without a HIFU transducer attached)

Two transducers were used for the exposures A and B:

Transducer T1: $f=2$ MHz, $R=4$ cm, $d=4$ cm, 100 W, 2 minutes,
Tissue depth: 2 cm.

Transducer T2: $f=1$ MHz, $R=4$ cm, $d=4$ cm, 100 W, 1 minute,
Tissue depth: 3 cm.

The photograph of figure 10.15 shows the robot version 3 with the vertical transducer holder attached to it. The photograph also shows the target, the porcine muscle placed under the tank filled with degassed water saline.

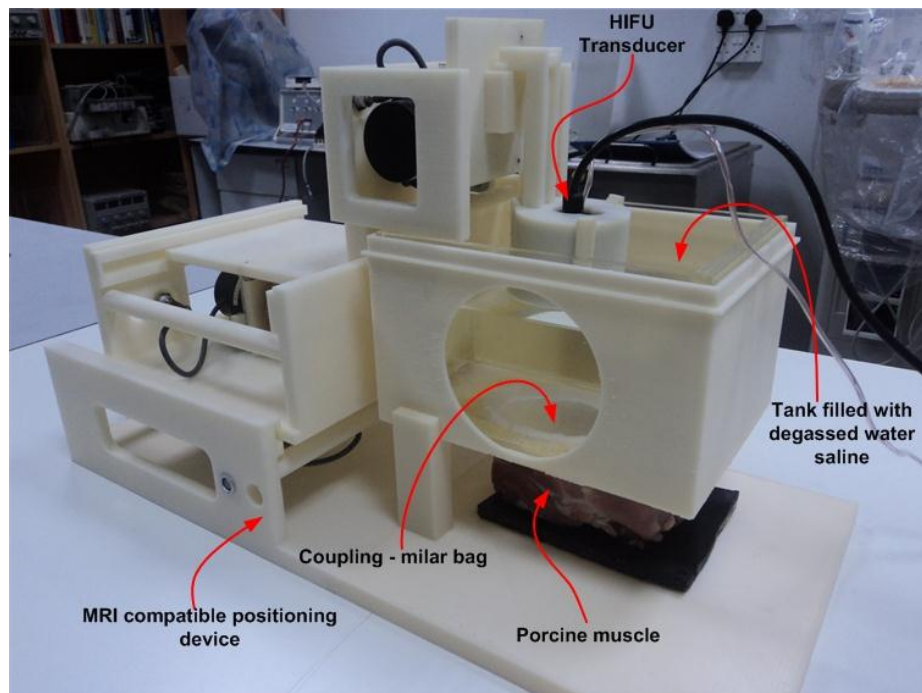


Figure 10.15: Photograph shows the positioning device version 3 with the porcine muscle placed under the tank filled with degassed water saline.

A milar bag is fixed inside the tank which is pushed downwards tangential on the surface of the porcine muscle with the weight of the degassed water saline. That's how the coupling is achieved. For both exposures the tissue was ablated.

The photograph of figure 10.16 shows the lesion achieved with the first exposure and the photographs of figures 10.17A and 10.17B show the lesion from the top and the cross section respectively.

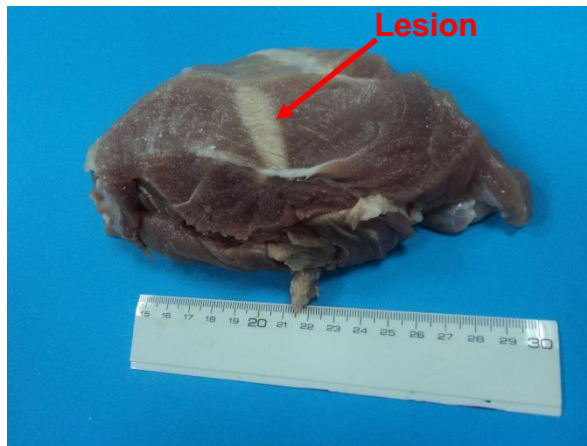


Figure 10.16: Exposure A, the cross section – depth.

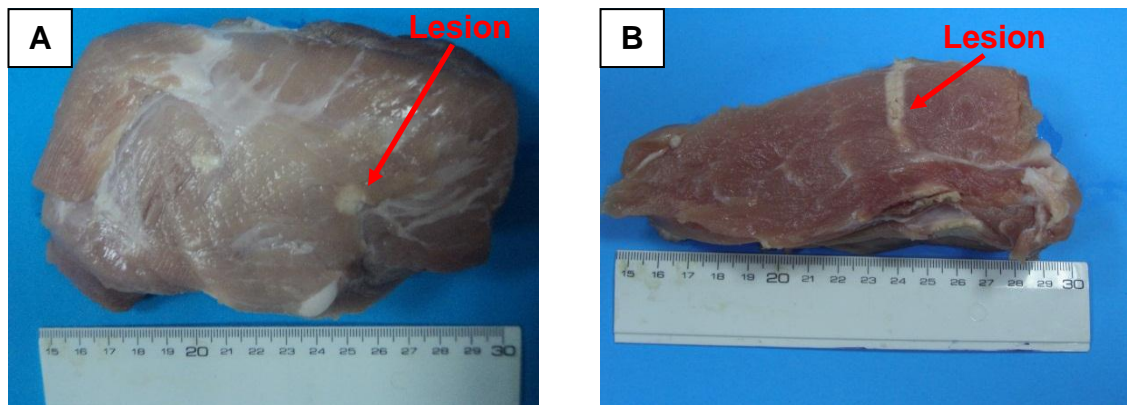


Figure 10.17: Exposure **A.** is the top view of the lesion, **B.** cross section showing the depth of the lesion.

Conclusion

The photographs of figure 10.16 and 10.17 show that for both exposures well penetrated lesions were achieved. Therefore the coupling method is considered successful.

10.6 Visualize the coupling method of robot V3 using MRI.

The purpose of this experiment is to visualize the coupling method of the positioning device version 3 using MRI.

10.6.1 Material and methods

Equipment used

Tissue: Gel phantom (Onda Corp., Sunnyvale, CA).

Positioning Device version 3 (without a HIFU transducer attached)

For this experiment the positioning device version 3 is used without the HIFU transducer. The HIFU transducer is not required for this experiment since the purpose of this experiment is to visualize the effectiveness of the coupling. The coupling method is described in the previous section (10.6). The photograph of figure 10.18A shows the positioning device on the table of the MRI scanner with the tank filled with degassed water saline and the gel phantom at the bottom of the tank. Figure 10.18B show a photograph of the positioning device after the table slide in to the gantry of the MRI.

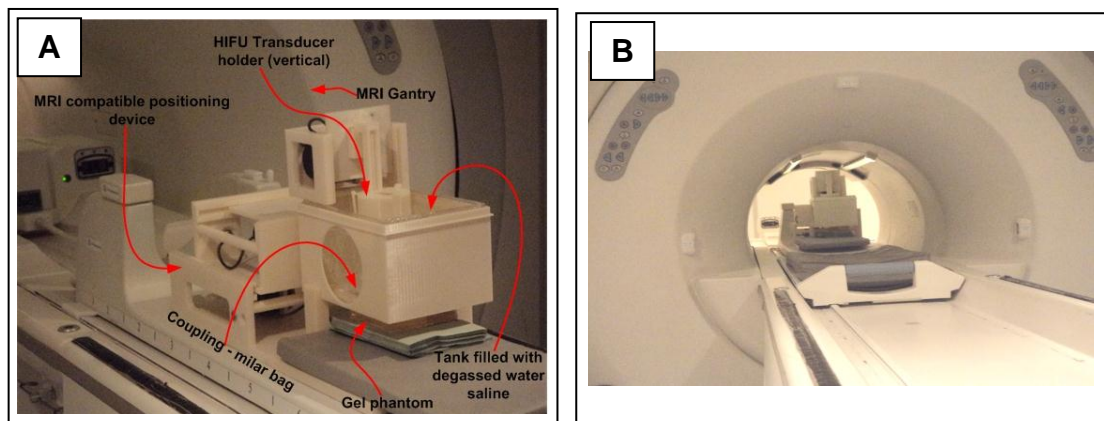


Figure 10.18: **A.** photograph of the positioning device on the table of the MRI with the tank filled with degassed water saline and the gel phantom at the bottom of the tank, **B.** photograph of the positioning device inside the gantry of the MRI scanner.

The MRI image of figure 10.19 shows the coupling between the milar bag fitted in the tank and filled with degassed water saline and the target used (gel phantom).

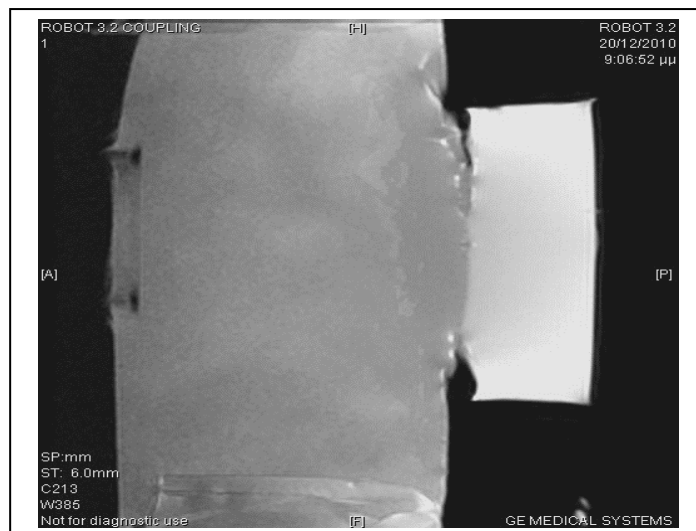


Figure 10.19: An MRI image showing the coupling between the milar bag which is filled with degassed water saline and the gel phantom.

10.6.2 Conclusions

The MRI image of figure 10.19 is an excellent visualization of coupling. This image proves and verifies the results of the experiment described on section 10.6, that the coupling method is successful.

10.7 MRI Compatible Camera using gel

The purpose of this experiment was to investigate the effect of an MRI compatible camera on the quality of MR images and the effect of the MRI scanner on the quality of the camera images.

10.7.1 Material and methods

Equipment used

Tissue: MRI Gel.

MRI compatible camera (12M, MRC Systems GmbH, Heidelberg, Germany)

Positioning Device version 3 (without a HIFU transducer attached) was used as a subject for the MRI compatible camera.

The setup of this experiment is shown in the photograph of figure 8.21A in chapter 8 with the table of the MRI scanner out of the gantry and the photograph of figure 10.20 show the positioning device version 3 with the MRI compatible camera in the gantry of the MRI. The positioning device in this experiment was used as a target of the MRI compatible camera.

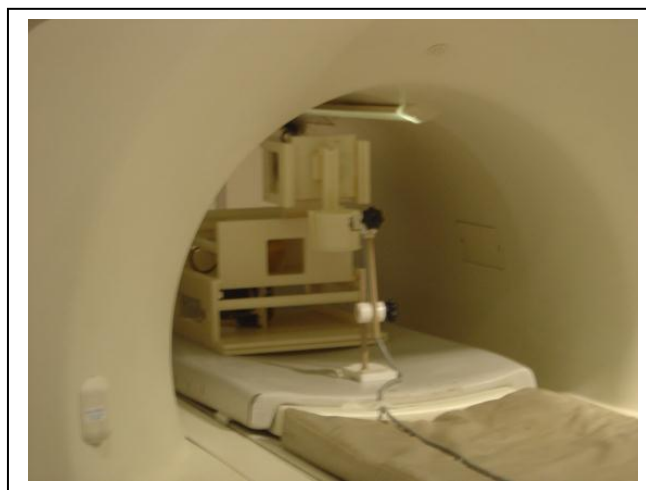


Figure 10.20: Photograph of the experiment setup showing the positioning device version 3 and the MRI compatible camera.

The photographs of figures 8.22A and B in chapter 8 and the photographs of figures 10.21 and 10.22 were captured from the MRI compatible camera. Photograph of figure 8.22B shows the positioning device on the table of the MRI scanner outside the gantry and the photographs of figures 8.22A and 10.21 shows the positioning device in the gantry of the MRI. Furthermore, the photograph of figure 10.22 shows the MRI gel in a plastic container.

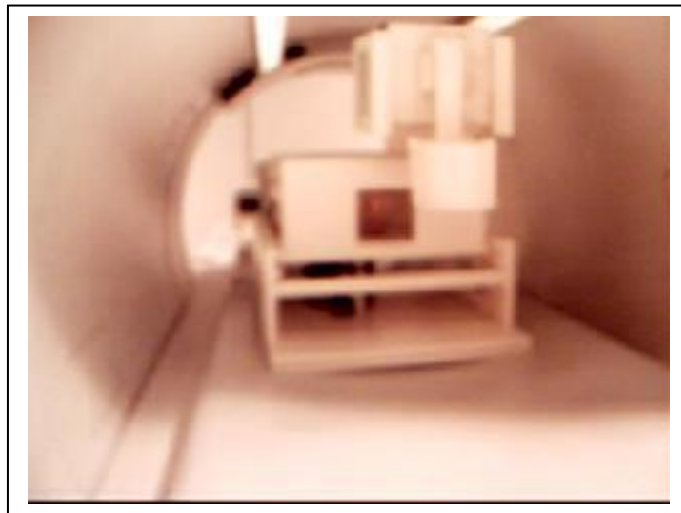


Figure 10.21: Photograph of the positioning device version 3 inside the gantry of the MRI scanner, taken from the MRI compatible camera.



Figure 10.22: Photograph of the MRI Gel inside the gantry of the MRI scanner taken from the MRI compatible camera.

The MRI image of figure 10.23 A was captured using T1 FSE with the MRI compatible camera in the gantry of the MRI and the MRI image of figure 10.23 B was also captured using T1 FSE but without the presence of the MRI compatible camera.

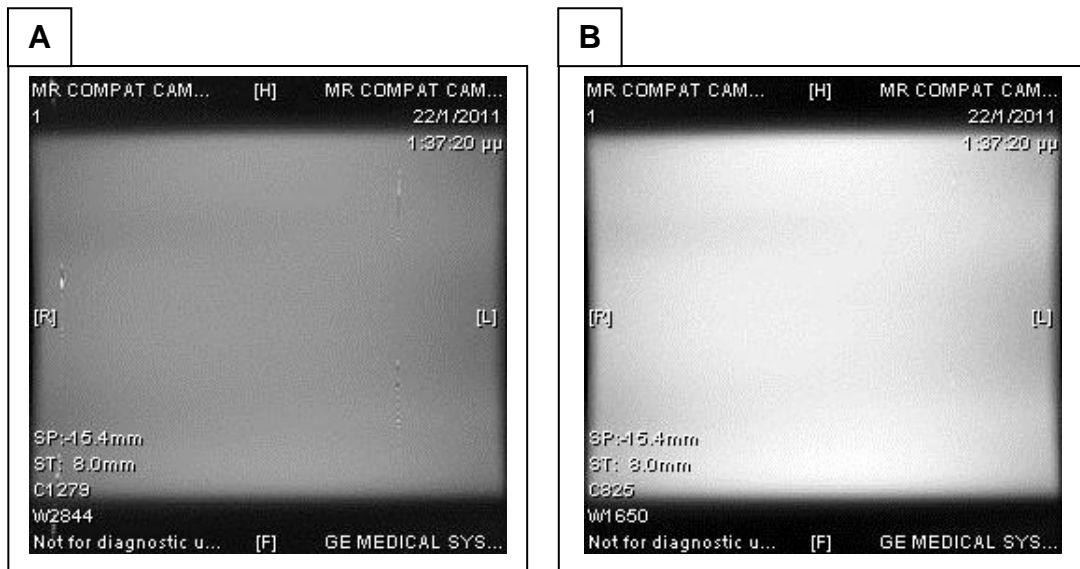


Figure 10.23: **A.** MRI image with T1 FSE with the MRI camera in the gantry of the MRI scanner, **B.** MRI image with T1 FSE without the MRI compatible camera.

10.7.2 Conclusions

The photographs captured from the MRI compatible camera show that there is no effect of the MRI scanner on the images, although, the photograph of figure 10.21 it seems to be dull, most probably this is due to the fact that the camera was out of focus.

Moreover, there were some RF artifacts on the MRI image due to the presence of the MRI camera and some loss of signal.

11 Experiments using HIFU/MRI system

11.1 HIFU ablation of porcine liver guided by MRI

In this section several experiments using gel phantom and in freshly excised pig liver are explained and the results are discussed.

11.1.1 *In vitro* experiments

Before creating lesions in a tissue the system is tested in a gel phantom (Onda Corp., Sunnyvale, CA). Figure 11.1A shows a photograph of the lesion created in the phantom at a plane perpendicular to the transducer beam axis. Figure 11.1B shows the corresponding photograph in a parallel plane. Figure 11.1C shows the MRI image of the result of Figure 11.1A using T2–W FSE (for MRI parameters see Table 11.1, row 2), and Figure 11.1D shows the same result using T1–W FSE.

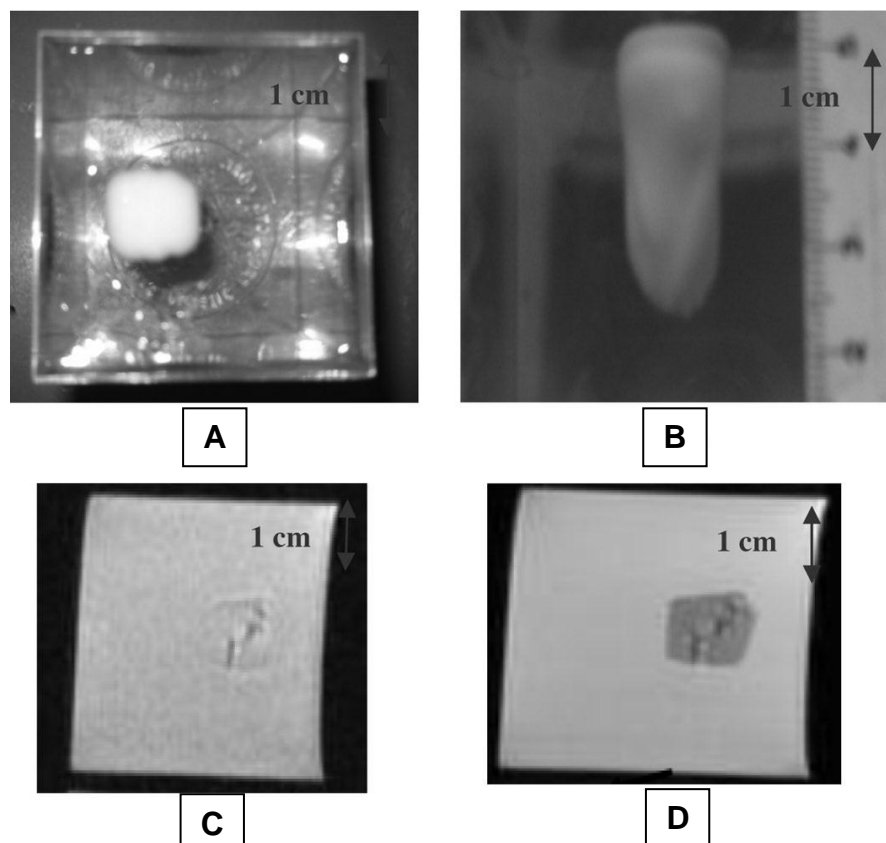


Figure 11.1: **A.** show a photograph of large lesion created in the phantom at a plane perpendicular to the transducer beam axis. **B.** shows the corresponding photograph in a parallel plane. **C.** shows the MRI image of the result of A using T2–W FSE (for MRI parameters see Table 11.1, row 2), and **D.** shows the same result using T1–W FSE.

Note that with T2-W, the contrast is poor because the T2 value of gel and lesion is similar, whereas the relaxation time T1 of the lesion and gel is sufficiently different, and thus, the contrast using T1-W FSE is satisfactory.

11.1.2 Experiments on liver

High intensity focused ultrasound (HIFU) is a thermal modality which is mainly utilised to destroy tumours. HIFU transducers are guided either by ultrasonic imaging or magnetic resonance imaging (MRI). For the clinical application of prostate Foster et al. 1994 [156] and Gelet et al. 1998 [157] utilized ultrasonic imaging. For the clinical application of breast [24], [149], [150] MRI was utilised for guidance and monitoring. For the case of uterine leiomyomas, Tempany et al. 2003 [158] utilized MRI. At the moment there is only one HIFU clinical system for liver cancer [159]. Liver metastases and primary liver cancer are one of the main causes of death [160]. The traditional surgical methods may be curative for some cases, but they are not effective for all cases [161]. Therefore research efforts in the area of HIFU ablation of liver guided by MRI is essential.

A lot of work has been done in many directions earlier in the area of liver ablation using HIFU. The threshold of intensity that is needed to cause irreversible damage in liver was suggested by Frizell 1987 [34] and Frizell 1988 [35]. The first attempt to monitor the effect of HIFU using MRI was reported by Rowland et al. 1997 [162], who demonstrated that monitoring of thermal lesions in liver is feasible.

In this experiment the goal was to investigate the effectiveness of MRI to monitor therapeutic protocols of HIFU in liver *in vitro*. Several MRI pulse sequences are investigated. For high quality imaging which can be used at the end of a therapeutic protocol or at some instances of the protocol, T1-weighted FSE, and T2-weighted FSE are investigated. For fast imaging, the T1-weighted fast spoiled gradient echo (FSPGR) pulse sequence was used. The goal was to create large lesions that included both thermal and cavitation lesions. Therefore, MRI pulse sequences are investigated in order to discriminate between liver and lesion and between thermal and cavitation lesions.

a. *Materials and methods*

HIFU system guided by MRI with cavitation detection.

Figure 11.2 shows the block diagram of the system with photos of the actual instruments. The ultrasonic system consists of a signal generator (HP 33120A Hewlett Packard, now Agilent technologies), a RF amplifier (LA 100-CE, Kalmus, Bothell, WA, USA), and a spherically shaped bowl transducer made from piezoelectric ceramic of low magnetic susceptibility (Etalon, Lebanon, IN, USA). The transducer operates at 4 MHz, has focal length of 10 cm and diameter of 3 cm. The efficiency of the transducer was 55%. The transducer was rigidly mounted on the MRI compatible positioning system. The serial port of a personal computer (PC) controlled the signal generator, whereas the 2-d robotic system (slave robotic system) was controlled by the master robotic system, which is controlled by the parallel port. The slave positioning device was moved by the master positioning device by means of non-magnetic wires.

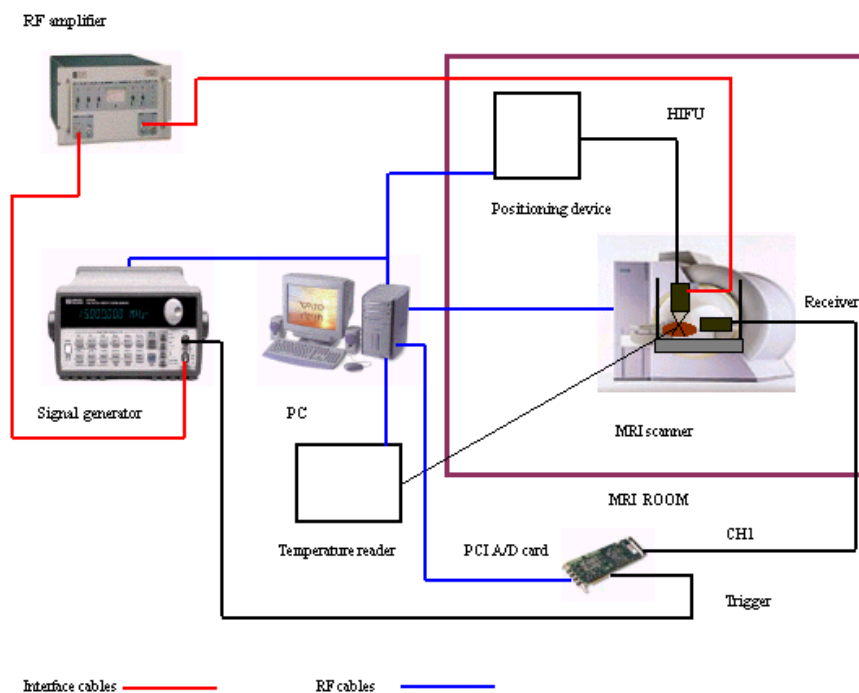


Figure 11.2: MRI guided HIFU system with cavitation detection system using the actual photos of the instruments.

The slave positioning device and the transducer were placed inside a MRI scanner (Signa 1.5 T, General Electric). The coil used was the one used commercially for spinal imaging. The signal generator, the RF amplifier, master robotic system and the PC were placed outside the MRI scanner.

In order to detect cavitation the acoustical method used by [163] was used. This method includes a receiver, which is placed perpendicularly to the beam of the HIFU transducer. Since the HIFU protocol is applied inside the magnet of an MRI scanner, the receiver was MRI compatible. The receiver diameter was 10 mm, its radius of curvature was 10cm and operated with a bandwidth of 10 MHz. The receiver was mechanically coupled to the HIFU transducer. The signal from the receiver was fed to an A/D PCI card (CS1250, A/D 12 bit, 50 MHz, from GAGE, Lachine, Canada). The A/D card was synchronised to receive the signal when the HIFU transducer was activated. The received signal was stored in a PC.

b. Acoustical Field

The size of the focal region produced by this transducer was obtained by mapping the acoustic pressure field with a needle hydrophone (Specialty Engineering Associates, San Jose, CA, USA) having an active element 1 mm. The transducer under test was driven by a pulse/receiver (Panametrics 5050R, Waltham, MA, USA). The hydrophone was connected to the receiver input of the pulse/receiver. The output of the pulse/receiver was connected through an A/D card (GAGE) to the PC for signal processing. The transducer was moved automatically by a robotic system (MD-2, Arrick Robotics, Hurst, TX, USA). The total power delivered by the transducer was measured before the beginning of each experiment with an ultrasound power meter (Model UPM-DT-100N, Ohmic Instruments, Easton, MD, USA) shown in figure 10.1. The error of the power measurement is approximately 2%. The estimation of the acoustical field was based on the principles presented by Raum and O'Brien 1997 [164]. More details of the above system can be found in [165].

c. In Vitro Experiments

The tissue under ablation was placed in a degassed water tank. The water tank was placed on top of the flat MRI coil. The tissue was placed on top of an absorbing material in order to eliminate reflections coming from the bottom of the plastic water tank. The transducer was placed on the arm of the 2-D positioning device and was immersed in the water tank, thus providing good acoustical coupling between tissue and transducer. Any bubbles that may have collected under the face of the transducer face were removed in order to

eliminate any reflections. In all experiments, the liver used, was extracted from freshly killed pigs. The sample was cut down to a size of 60 mm x 60 mm with thickness of 40-50 mm. Totally 18 samples were ablated, creating one large lesion in each liver.

d. HIFU parameters

The in situ spatial average intensity used for creating lesions was 2000 and 2500 W/cm² for 5s; an exposure that creates both thermal and cavitation lesions. In order to create large lesions, a grid pattern of 4x4 overlapping lesions was used. The spacing between successive transducer movements was 3mm, which creates overlapping lesions for the intensity and pulse duration used [165]. The delay between successive ultrasound firings was 10s. Although, the study by McDannold et al. 1999 [166], recommends a delay around 50-60 sec in order to avoid build up in front of the target, for this application and transducer geometry using 10 s delay eliminated most of the built up heating (the lesion length was extended by 2mm).

If in a grid of let say 4x4 lesions of a specific exposure, one lesion was created under the mechanism of cavitation, then the probability of cavitation (POC) is 1/16 or 6.25%.

e. MRI analysis

The MRI parameters used for the various pulse sequences are listed in table 11.1. The signal intensity was measured by placing a circular region of interest (ROI) of approximately 10mm in diameter. The contrast to noise ratio (CNR) was obtained by dividing the signal intensity difference between the ROI in the lesion and in the ROI of normal liver tissue by the standard deviation of the noise in the ROI of normal liver tissue.

f. Experimental Protocol

The following protocol was used during all experiments:

- i. A freshly killed liver was used 1 hour after the sacrifice of the animal
- ii. The sample was degassed and then placed inside the container that contains degassed water

- iii. The slave positioning device, transducer and water container that include the tissue sample were placed inside the MRI scanner
- iv. The signal generator, RF amplifier, master robotic system, and PC were placed outside the MRI room
- v. The sample was ablated using the parameters indicated earlier. During the experiment the water bath, had the same temperature as the room temperature
- vi. The therapeutic protocol was evaluated by using various MRI pulse sequences
- vii. The sample was sliced and photos were taken using a digital camera.

g. Results

Figure 11.3 shows the POC as a function of in situ spatial average intensity for a 5s pulse duration in liver. Note that by using intensity between 2000 and 3500 W/cm², it is possible to create both thermal and cavitation lesions.

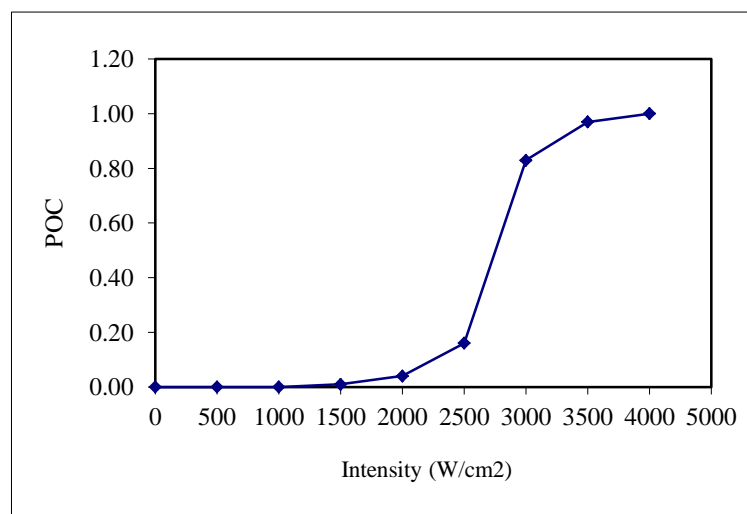


Figure 11.3: POC as a function of in situ spatial average intensity for 5s pulse duration in liver.

Initially, the two traditional FSE techniques (T1-weighted, and T2-weighted) were evaluated. T1-weighted FSE was explored by using different TR (100, 200, 300, 400, 500, 700 and 1000 ms). Figure 11.4A shows the CNR between lesion and liver plotted against TR. All the parameters used are shown in table 11.1 row 1. T2-weighted FSE was explored by using seven different TE (10, 15, 20 30, 40, 45, and 60 ms). Figure 11.4B shows the CNR between lesion and liver plotted against TE. All the parameters used are shown in table 11.1

(row 2). 11.4C shows the CNR between lesion and liver plotted against TR using T1-weighted FSPGR. All the parameters used are shown in table 11.1 (row 3).

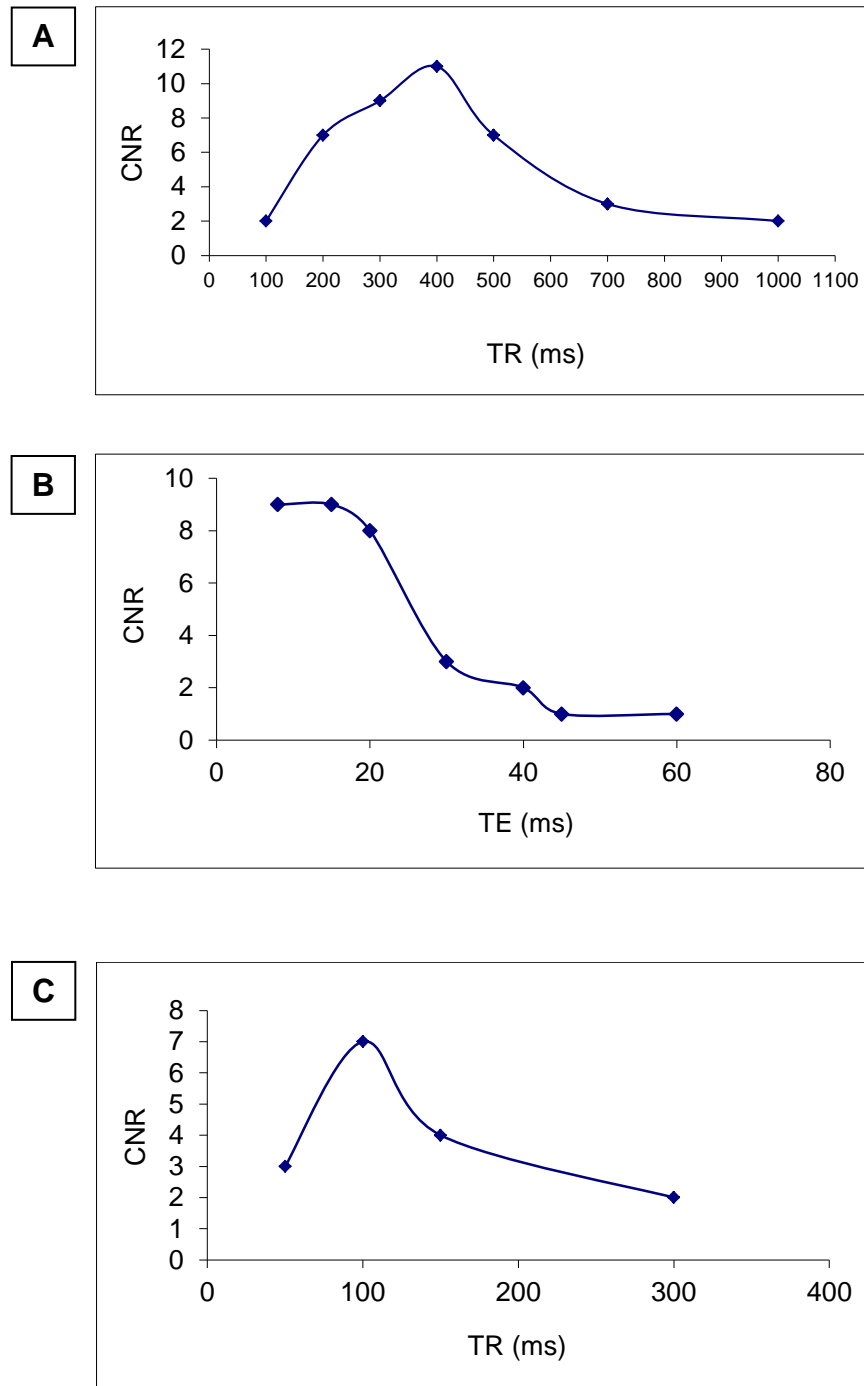
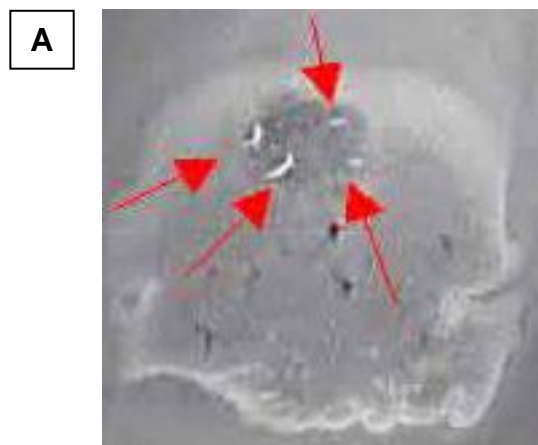


Figure 11.4 **A.** CNR between lesion and liver plotted against TR using T1-weighted FSE, **B.** CNR between lesion and liver plotted against TE using T2-weighted FSE, **C.** CNR between lesion and liver plotted against TR using T1-weighted FSPGR.

Figure 11.5A shows the MR image (in a plane perpendicular to the transducer beam) using T2-weighted FSE with TE=15 ms. This large lesion was created using spatial average in situ intensity of 2500 W/cm² for 5s. By using this intensity, 4 out of the 16 lesions (POC=0.25) were created under the mechanism of cavitation. Figure 11.5B shows a cavitation map, which shows in specific grid of single lesions (volume lesion or large lesion) having 4 lesions, which are created under the mechanism of cavitation. A lesion was classified as cavitation if during the firing of the ultrasonic transducer, the frequency spectrum included subharmonic emissions.

Figure 11.5C shows a typical frequency spectrum during the creation of a cavitation lesion. The cavitation map was also verified using MRI imaging (figure 11.5A) and using gross examination. With T2-weighted FSE the contrast of the cavitation lesion within the large thermal lesion is excellent. The cavitation lesion appears as a scattered bright spot.

Figure 11.6A shows the lesion in a plane parallel to the transducer beam using T2-weighted FSE. This large lesion was created using spatial in situ intensity of 2500 W/cm² for 5s. With this pulse sequence, it is possible to identify the lesion created under the mechanism of cavitation. Figure 11.6B shows the photograph after slicing. In this photograph, the void indicates a site influenced by the mechanism of cavitation (already confirm with harmonic emission and MRI).



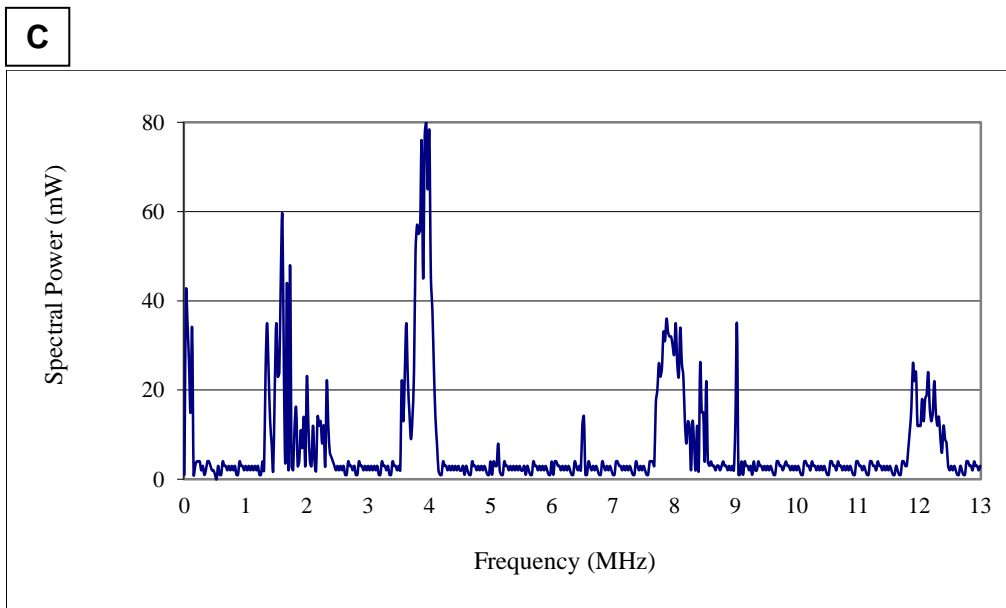
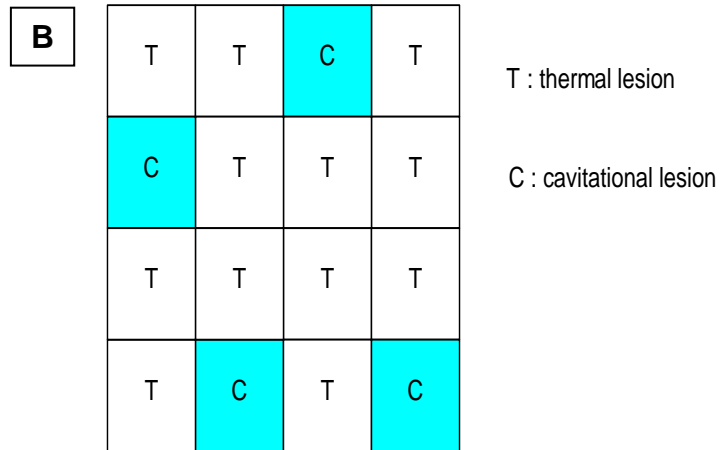


Figure 11.5: **A** MR images (in a plane perpendicular to the transducer beam) of large lesion using T2-weighted FSE showing cavitation lesions, **B** cavitation map of the above large lesion, **C** typical frequency spectrum acquired during the occurrence of a cavitation lesion.

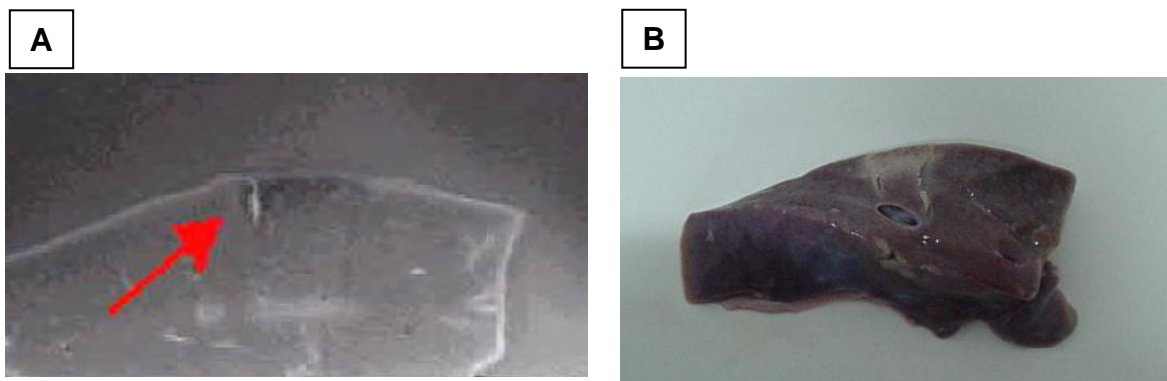


Figure 11.6: MR images (in a plane parallel to the transducer beam) of large lesion using **A.** T2-weighted FSE with TE=15ms. **B.** Photograph after slicing.

h. Discussion

It was concluded so far by several studies (for example [5], [167], and [168]) that MR-guidance of ultrasound serves mainly 4 purposes:

- i. localisation of the focus,
- ii. imaging of the dynamic build-up of necrosis,
- iii. Imaging at the end of the treatment protocol, in order to evaluate the necrosis and possibly re-planned the treatment protocol in the event of incomplete coverage of the target (tumour for the case of oncology applications) and
- iv. Follow-up imaging, evaluating the effectiveness of HIFU ablation, several days after the treatment. This research includes information that will be useful for cases i and iv.

The results of this study indicate that:

- i. The contrast between lesion and normal liver tissue is acceptable when T1-weighted FSE is used.
- ii. Best contrast is observed for TR between 200 and 400 ms. This was proved by evaluating the CNR between lesion and liver as a function of TR. The difference in the signal of the lesion and liver is significant in this range. The window that maximises contrast in liver is much smaller than the case of kidney [48]. MRI could detect the lesion 1-2 minutes after the ablation. In the study by Chen [169], the lesions in the brain appeared in MRI in 15 minutes to 60 minutes using T2-weighted FSE.

Similar evaluation was followed for T2-weighted FSE pulse sequence. Best contrast can be achieved for TE up to 20 ms, with better contrast at lower TE, indicating that PD might be the best pulse sequence for the case of liver *in vitro*. Similar to what was seen in T1-weighted FSE, the window of TE that maximizes contrast is narrow in liver compared to kidney [48]. T2-weighted FSE was proven as the best pulse sequence that can detect cavitation activity. This advantage is attributed to the significant difference in signal intensity between the water-filled air spaces and necrotic tissue. Water-filled air spaces appear brighter than thermal lesions. Therefore for therapeutic protocols created using

the cavitation mode, T2-weighted FSE maybe the optimum pulse sequence to be used.

The T1-weighted FSPGR was investigated as a fast imaging pulse sequence. FSPGR is the most widely accepted fast pulse sequence, used by many researchers (for example [95], [167]). From this pulse sequence the parameter proton resonant frequency shift can be extracted, which allows relative small temperature elevation to be detected [95], [170]. The estimation of temperature can be used to identify the location of the focus using low intensity, which does not cause any irreversible damage to the tissue [95]. It can also be used to estimate the thermal dose during the application of ultrasound [95]. In this study it was found that with TR around 100 ms the CNR between lesion and liver is maximized.

Mack et al. 2001 [171], and Morrison et al. 1998 [45] have shown that T1 and T2-weighted FSE and gradient-echo sequences can effectively monitor lesions created by laser-induced thermotherapy in patients with liver cancer. Therefore we anticipate that the pulse sequences evaluated in this study will be successful also for treatments *in vivo*. In the *in vivo* case the CNR between the thermal lesion and normal liver tissue will be improved by using contrast-enhanced techniques (Aschoff et al. 2000 [172]). Because of the motion artifacts, other techniques should be evaluated (for example fast low-angle shot (FLASH)). Tsuda et al. 2003 [109] used T1-W and T2-W FSE to monitor lesion created in rabbit liver *in vivo* using radiofrequency ablation. In their study they found that the contrast was optimised at TR of 500 ms, which is close to what was found in our study.

Sibille et. al 1993 [39] reported incomplete coverage of implanted tumours with necrosis and therefore the importance of MR imaging is enhanced, because it provides feedback and therefore the treatment protocols can be redesigned so as to eliminate such problems. Follow-up of treatment in liver using MRI is very important since [95] showed that large areas of ultrasonically damaged tumour cells are identified one day after the treatment.

Preferential location of cavitation lesions is at interfaces between liver and the water-filled blood vessels (figure 11.6) an effect also seen by [34] and [173]. The threshold of 100 % cavitation in liver, which is about 3500 W/cm², is similar to what was found in kidney [73]. This observation is in agreement with [34] who stated that whatever constitutes the nuclei for the cavitation events may be common to most soft tissues. The POC increases with intensity and above a certain threshold the POC is 1. Significant POC (above 20%) is caused with intensity above 2500 W/cm² at 5s. For the case of porcine liver *in vitro* this threshold of 100% cavitation is about 3500 W/cm² at 5 s. The trend of POC as a function of spatial in situ intensity is similar to what was found in the study of kidney ablation [73]. Also the length of a single lesion in liver at the intensity of 2000 W/cm² for 5s which is around 20 mm, is very close to the lesion measured in kidney [165]. This is not surprising since liver and kidney have similar absorption [174].

Finally, here a useful research tool is presented for evaluating cavitation, which we call cavitation map. In the cavitation map, lesions are marked as thermal or cavitation. A lesion was classified as cavitation if during the firing of the ultrasonic transducer, the frequency spectrum included subharmonic emissions. The cavitation map was also verified using MRI imaging and using gross examination. This tool can be very useful for evaluating cavitation at different exposures (frequency, intensity and pulse duration) and at different locations (close to blood vessels, interfaces, tissue type). At the moment we cannot think of any significant use of the cavitation map in the clinical setting, but it may be a very important research tool especially for cavitation studies.

NAME	TR (ms)	TE (ms)	Slice thickness (mm)	Matrix	FOV (cm)	NEX	BW (KHz)	ETL	Flip angle
T1-weighted FSE	100, 200, 300, 400, 500, 700, 1000	9.1	3 (gap 0.3 mm)	256x256	16	1	31.25	8	-
T2-weighted FSE	2500	10, 15, 20, 30, 40, 45, 60	3 (gap 0.3 mm)	256x256	16	1	31.25	8	-
FSPGR T1-weighted	50,100, 150,300	2.8	3 (gap 0.3 mm)	256x256	16	1	62.50	-	50°

Table 11.1: Parameters used for the various MRI pulse sequences.

11.2 Evaluation of fast spin echo MRI sequence for an MRI guided high intensity focused ultrasound system for *in vivo* rabbit liver ablation.

Here, in this section the effectiveness of magnetic resonance imaging (MRI) to monitor thermal lesions created by High Intensity Focused Ultrasound (HIFU) in rabbit liver *in vivo* is investigated. The MRI sequences of T1-weighted, and T2-weighted fast spin echo (FSE) were evaluated. The main goal in this research was to find the range of repetition time (TR) and range of echo time (TE) which maximizes the contrast to noise ratio (CNR). An ultrasonic transducer operating at 2 MHz was used, which is navigated using the proposed positioning device version 1.

11.2.1 Introduction

Surgical resection is considered the therapy of choice for liver cancer. However, the percentage of patients who are good candidates for surgery is low [175]. Surgical resection is only feasible in 10–20% of the patients resulting to 5-year survival rates in the region of 40% [175]. Moreover, the incidence of new metastases after resection is high, and the success rate after multiple resections is low [175]. Because of the above disadvantages of surgical resection the development of several less invasive local ablative therapies for liver tumours is imperative. These approaches have included percutaneous ethanol injection [176], cryotherapy [177], radiofrequency [108]-[112], microwave [115]-[117], [178], and laser ablation [101], [102]. These local therapies have produced survival rates similar to those with surgical resection in the treatment of metastases [179], but unfortunately high local recurrence rate is also reported [180].

Therefore, thermal ablation methods could possibly become a main treatment option for liver cancer, especially if recurrence rate is minimized. Another ablative method that could be used for liver cancer treatment is High Intensity Focused Ultrasound (HIFU). HIFU is the only non-invasive local therapy to be proposed to date. If HIFU is proven equivalent to surgical resection, this minimally invasive approach may be able to replace surgery as the treatment of choice.

Since the 90's clinical work has been initiated for liver cancer. Vallancien et al. [181] treated two patients with solitary liver metastases prior to surgical resection. The team headed by Wu in 1999 reported a clinical study for treating 68 patients with liver malignancies [182]. The same group reported a clinical study with 474 patients with Hepatocellular Carcinoma (HCC) treated using HIFU in combination with transarterial chemo-embolization [89]. HIFU ablation has also been used for palliation in 100 patients with advanced-stage liver cancer [183]. Following treatment, symptoms, such as pain and lethargy, were relieved in 87% of the patients.

Without an imaging system that allows for online monitoring of the deposition of ultrasound energy or the creation of induced lesion, it is impossible to predict the precise location of the HIFU beam, to monitor the temperature changes, or to control the deposited thermal dose. In the past, these major constraints limited the development of HIFU as a non-invasive surgical technique. In recent years, however, integration of HIFU with MRI, which allows high-sensitivity tumour detection and the ability to monitor temperature in real time, has increased the potentials of HIFU. MRI-guided HIFU has generally been reserved for the treatment of uterine fibroids [184] and breast adenomas [185]. However, it is very likely that this mode of treatment monitoring and delivery will have a role in the treatment of liver tumours. Recently, a non-randomised clinical trial is under way [186] to assess the safety and efficacy of the MRI guided HIFU system ExAblate 2000 (InSightec, Haifa, Israel) in the treatment of liver tumours. It was reported that a small number of patients has been treated to date with promising results [186].

The first attempt to monitor the effect of HIFU using MRI in liver was reported by Rowland et al. 1997 [162], who demonstrated that monitoring of thermal lesions in liver is feasible. The MRI appearance of lesions in liver created using HIFU was also studied by Jolesz et al. 2004 [187] and Kopelman et al. 2006 [188]. In this study the goal is to investigate the effectiveness of MRI to monitor therapeutic protocols of HIFU in rabbit liver *in vivo*. The two basic and most important MRI sequences of T1-weighted fast spin echo (FSE) and T2-weighted FSE are investigated. The goal was to create large lesions and use MRI to discriminate between liver tissue and lesion. With T1W FSE the signal intensity

vs. repetition time (TR) is evaluated and based on this analysis, the contrast to noise ratio (CNR) is estimated, in order to find the range of TR that produces maximum contrast. Similarly for T2W FSE the range of echo time (TE) is found that maximizes the contrast. A spherically focused transducer operating at 2 MHz was used, which is navigated inside MRI using an MRI compatible robot.

11.2.2 Methods

a. HIFU/ MRI system

The HIFU/MRI system is analysed and described in chapter 5. Figure 5.1 shows the block diagram of a typical HIFU/MRI system and figure 5.2 shows the setup of the actual devices of the HIFU/MRI system.

b. HIFU system

The HIFU system for this study consists of a signal generator (HP 33120A, Agilent technologies, Englewood, CO, USA), an RF amplifier (250 W, AR, Souderton, PA, USA), and the HIFU transducer (Etalon, Lebanon, IN, USA). The transducer operates at 2 MHz, has focal length of 10 cm and diameter of 5 cm. The transducer is rigidly mounted on the MRI-compatible positioning device version 1.

c. MRI Imaging

The positioning device and the transducer were placed inside a MRI scanner (Signa 1.5 T, by General Electric, Fairfield, CT, USA). A spinal coil (USA instruments, Cleveland, OH, USA) was used to acquire the MRI signal for all tissues.

d. Positioning Device

The positioning device is described in details in chapter 6. The enclosure hosting the motor drivers shown in figures 9.2 and 9.3 is placed outside the MRI room since magnetic materials are involved. The DC supply (24 V, 6 A) used to drive the Shinsei drivers is also placed outside of the MRI room.

e. MRI compatible camera

In order to monitor the condition of the animal or humans (future use), an MRI compatible camera (MRC Systems GmbH, Heidelberg, Germany) was mounted on the system. The camera was interfaced by means of a video card. With the aid of the MRI compatible camera, the researcher can monitor the welfare of the animal.

11.2.3 *In vivo* experiments

For the *in vivo* experiments, New Zealand adult rabbits were used weighting approximately 3.5-4 kg. Totally 7 rabbits were used in the experiments. The rabbits were anaesthetized using a mixture of 500 mg of ketamine (100 mg/mL, Aveco, Ford Dodge, IA), 160 mg of xylazine (20 mg/mL, Loyd Laboratories, Shenandoah, IA), and 20 mg of acepromazine (10 mg/mL, Aveco, Ford Dodge, IA) at a dose of 1 mL/kg. The animal experiments protocol was approved by the national body in Cyprus responsible for animal studies (Ministry of Agriculture, Animal Services).

a. HIFU parameters

The *in situ* spatial average intensity was estimated based on the applied power and the half-power width of the beam of the transducer. The attenuation used was 4 Np/m-MHz. The half-power length of the beam is 15.6mm and the half-power width is 1.2 mm. The details of the intensity estimation can be found in [48]. In order to create large lesions, a square grid pattern of 4x4 overlapping lesions was used. The spacing between successive transducer movements was 2 mm, which creates overlapping lesions for the intensity and pulse duration used. In all the exposures the ultrasound was turn on for 5s. The *in situ* spatial average intensity used was $1000\text{W}/\text{cm}^2$. The delay between successive ultrasound firings was 10s.

b. MRI processing

The following parameters were used for T1-W FSE: TR was variable from 100-1000 ms, TE=9 ms, slice thickness=3 mm (gap 0.3 mm), matrix=256x256, FOV=16cm, NEX=1, and ETL=8. For T2-W FSE: TR=2500 ms, TE was variable from 10 ms to 160 ms, slice thickness=3mm (gap 0.3 mm), matrix=256x256, FOV=16 cm, NEX=1, and ETL=8.

The contrast to noise ratio (CNR) was obtained by dividing the signal intensity difference between the Region of Interest (ROI) in the lesion and in the ROI of normal liver tissue by the standard deviation of the noise in the ROI of normal liver tissue. The ROI was circular with diameter of 3 mm.

The tissue temperature change (ΔT) has been estimated using the proton resonance frequency method given by the equation stated in Chung et al. 1996 [189]:

$$\Delta\phi = \gamma * B_0 * \alpha * \Delta T * TE,$$

where $\Delta\phi$ is the temperature-dependent phase shift which is the phase acquired before and during temperature elevation and which accumulates during the echo time TE using fast spoiled gradient (FSPGR). The other terms are γ which is the gyromagnetic ratio of proton, 42.58MHz/T, α is the average proton resonance frequency coefficient, and B_0 is the flux density of the static magnetic field. The measured temperature elevation can be added to the base-line temperature to obtain the absolute temperature. The average proton resonance frequency coefficient α for the frequency shift was taken to be -0.0105ppm/°C as determined by the method described by Vykhodtseva et al 2000 [191].

11.2.4 Results

The goal in this study was to use T1W FSE using different TR (from 100 to 1000 ms) and then evaluate the effect of TR on the CNR. Figure 11.7 shows a large lesion in liver *in vivo* using T1-w FSE (TR=400 ms). This lesion was created using *in situ* spatial average intensity of 1000 W/cm² for 5 s. Since the step size of this 4x4 lesion was 2mm, the size of this lesion is approximately 8mm x 8mm. The MRI estimated maximum temperature in this lesion was 65 °C. Since the estimated temperature is below 100 °C, the occurrence of boiling was excluded. The thermal lesion appears bright and the contrast with liver tissue is excellent.

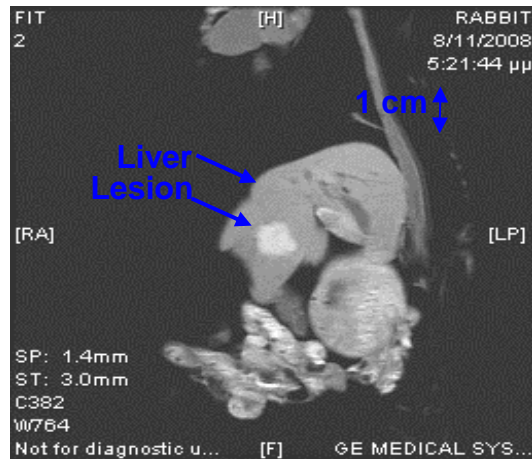


Figure 11.7: Large lesion in liver *in vivo* using T1-w FSE

Figure 11.8 shows the photograph of the lesion of Figure 3 after the animal was sacrificed in a plane perpendicular to the transducer face.

Figure 11.9 shows the CNR between lesion and liver plotted against TR for the MRI image of Figure 11.7. The same trend of CNR was seen in all the remaining 6 rabbits.

Also the maximum CNR between liver and lesion of the other 6 rabbits was also close to 25, and thus we are confident that this typical graph represents the behaviour of CNR vs. TR for rabbit liver ablation *in vivo*. The relaxation time T1 of the lesion is 250ms, and relaxation time T1 of the liver is 600ms. The proton density of the lesion increases by 20 % compared to the host tissue.

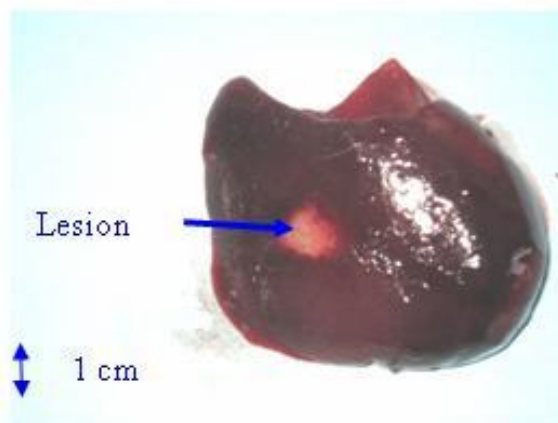


Figure 11.8: Photograph of the lesion shown in Figure 11.7

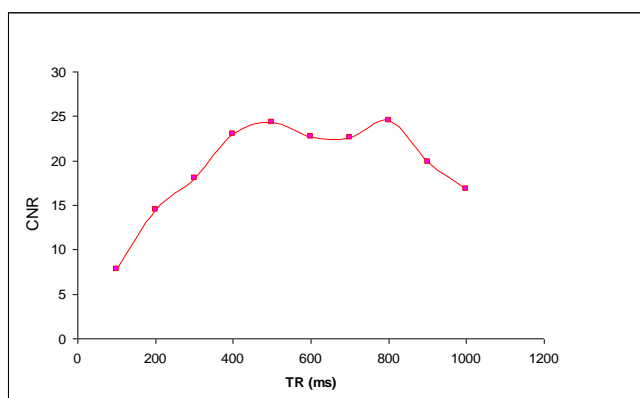


Figure 11.9: CNR vs TR

Figure 11.10 shows the MRI image of the lesion of Figure 11.7 using T1W FSE demonstrating the excellent propagation deep in the liver (i.e. in plane parallel to the transducer beam axis).



Figure 11.10: MRI image of the lesion of Figure 11.7 using T1W FSE

The second goal in this study was to explore T2W FSE using different TE (from 10 to 140 ms) and then evaluate the effect of TE on the CNR. Figure 11.11 shows the MRI images of the same lesion as in Figure 11.7 using T2W FSE (TE=60 ms).

Figure 11.12 shows the CNR between lesion and liver plotted against TE for the liver and lesion of the MRI image of Figure 11.11. The relaxation time T2 of lesion is 35ms and the relaxation time T2 of the liver is 50ms. The proton density of the lesion decreases by 5% compared to the host tissue.

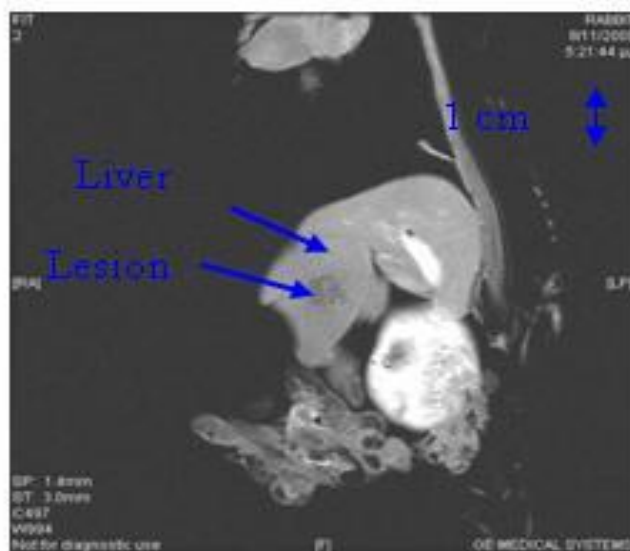


Figure 11.11: MRI images of the same lesion as in Figure 11.7 using T2W FSE.

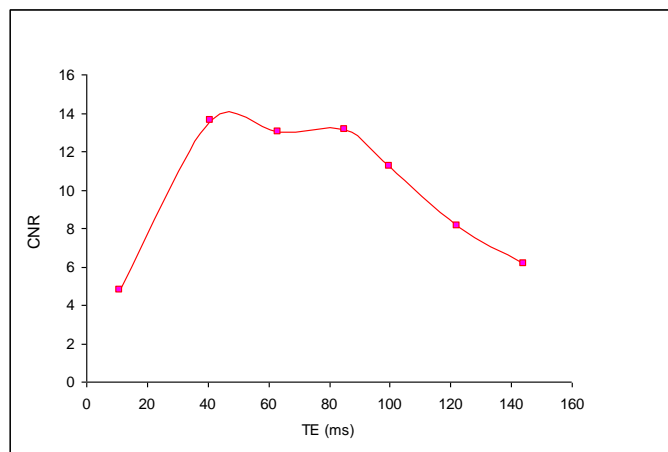


Figure 11.12: CNR vs TE for the MRI image shown in 11.11

11.2.5 Discussion

In this paper the goal was to measure the CNR of FSE MRI sequences in detecting thermal lesions created by HIFU in rabbit liver *in vivo*. Both T1-W FSE and T2-W FSE have been proven successfully for providing excellent contrast between liver and thermal lesion in rabbit *in vivo*.

The CNR with T1W FSE is significantly higher than T2W FSE (25 with T1W compared to 14 with T2W). With T1W FSE the range of TR under which CNR is high and ranges from 400 to 900 ms. Obviously one should use TR of 400

ms in order to minimize the imaging time. Thus, the optimum TR to be used is 400 ms. The maximum contrast measured is approximately 25. The window that maximises contrast in liver is much wider than the case of kidney [189].

The maximum CNR obtained for liver is the highest we measured after 17 years of experience in this field. The relaxation time T1 of lesion (250 ms) is much lower than the T1 of the host tissue (liver) which is 600 ms. The greater the difference, the greater the CNR. However, one might not ignore the significant role that the value of proton density plays in the CNR. The proton density of the lesion is increased by 20%.

The trend of CNR vs TR starts to increase then it becomes flat and then at high TRs it starts to decrease again. This trend is justified because at low TR, the difference in signal intensity between lesion and liver is low at the beginning and therefore CNR is lower. At higher TR the signal intensity of lesion and tissue reaches their maxima and therefore the signal difference is lower and hence the CNR drops again.

With T2W the range of TE that establishes maximum contrast is between 40 ms and 80 ms. This range was estimated by assuming that a CNR value of 10 is acceptable. Similar to what was seen in T1-weighted FSE, the window of TE that maximizes contrast is wider in liver compared to kidney [189]. Note that the maximum CNR value with T2W FSE is around 14 which is much lower than the value obtained with T1W FSE. The relaxation time T2 of lesion (35 ms) is lower than the T2 of the host tissue (liver) which is 50 ms. Therefore, in T2 W FSE the variation of signal intensity between lesion and liver is small (5%) and therefore the factor dominating the CNR in T2-W FSE is the T2 relaxation time. The trend of CNR vs TE starts to increase then it becomes flat and then at high TEs it starts to decrease again. The same explanation holds as in the case of T1-W FSE.

11.3 MRI monitoring of lesions created at temperature below the boiling point and of lesions created above the boiling point using High Intensity Focused ultrasound.

This research evaluates lesions created at temperatures above the boiling point during HIFU exposures using MRI. The evaluation was performed in kidney, and liver.

Kidney and liver were chosen for this study because there is currently a lot of on-going research either in animal models or in humans for both of these tissues. In the area of kidney ablation with HIFU Watkin et al. 1997 [198] used a large animal model and proved the feasibility of this treatment method. Recently Roberts et al. 2006 [199] have performed ablations in the normal rabbit kidneys and they suggested that the mechanical effects of ultrasound, can be used to homogenize tissue.

HIFU ablation of renal tumours in humans remains in the early stages of clinical trials. In the early 1990s, Vallancien et al. [200] reported the first clinical feasibility study in kidney using extracorporeal HIFU. Susani et al 1993 [201], Wu et al. 2003 [202] and Marberger et al. 2005 [203] conducted clinical trials in patients with renal tumours and proved that HIFU may have a place in the treatment of renal tumours.

Hacker et al. 2006 [204] performed also ablation of 43 kidneys (porcine and human), using an experimental handheld extracorporeal technology. Finally Klingler et al. 2008 [205] use laparoscopic methods to treat kidney tumours.

Small animal models [206]-[207] were used to establish the feasibility of HIFU to create lesions in liver tissue. The thresholds for liver tissue destruction at varying exposure parameters were established in the 70s and 80s [35].

Basic research in the area of liver continued during the 1990s; for example the histological effects of HIFU [208], the effects of blood perfusion on during liver

ablation [209], and the relationship between tissue depth and the required intensity levels [36].

Several tumour models have been used to predict the effects of HIFU on liver tumours in humans (for example [38], [210]) and to destroy VX2 liver tumours in rabbits [39], [40]. Hooded Sarcoma N (HSN) fibrosarcoma has been also used as a tumour model in rats with some success [211]. HIFU was also used for the treatment of metastatic melanoma in liver in a cat [212] and Wu et al. 2005 [213] use HIFU in combination with TACE for the treatment of HCC.

MRI was a great enhancement for the HIFU systems because the therapeutic protocols can be accurately guided. Therefore the interest of using MRI as the diagnostic modality of guiding HIFU was increased. This study focuses in the detection of lesions above boiling using MRI. Several MRI sequences are investigated. For high quality imaging, which can be used at the end of a therapeutic protocol or at some instances of the protocol, the fast spin echo (FSE) techniques T1, and T2-weighted are investigated in both tissues under investigation. For fast imaging, the T1-weighted fast spoiled gradient (FSPGR) MRI sequence was used. Fast imaging can be used to monitor the dynamic increase of tissue temperature during the application of an ultrasonic exposure.

In order to prove whether a lesion is created at temperature below boiling or above, it is necessary to estimate the temperature at the focus. The proton resonance frequency (PRF) shift has been proven to be best pulse sequence for estimating temperature, because with this sequence the temperature is less dependent on the physiological changes of tissue during high-temperature HIFU exposures [134]. The temperature dependence of the PRF shift was measured to be linear above 50 °C [134]. This linearity of the PRF shift above the tissue necrosis threshold allows the tissue temperature to be estimated during the therapeutic ultrasound exposures.

The task with high quality imaging was to find an optimum technique that can discriminate thermal from boiling lesions. Discriminating between lesion and normal tissue involves two types of tissues. Discriminating between thermal and boiling lesions involves three types of layers (normal tissue, lesion and cavity).

Therefore the signal intensity vs. MR parameters needs to be evaluated for the above layers in order to optimise the contrast among tissue of interest, lesion and cavity. The other main task was to monitor the temperature elevation using a fast MRI technique in order to observe the shape of the beam during HIFU exposures.

The growth of vapour bubbles due to boiling occurs due to the temperature induced by HIFU. Boiling is different from cavitation which occurs due to pressure oscillations induced by HIFU. Vapour bubbles created by boiling can grow rapidly to a size of few millimetres (Khokhlova et. al. 2006 [214]). This growth can be explosive due to the super heating caused by HIFU. Therefore the cavities produced of few mms can be easily monitored by MRI.

There are two reasons for studying the MRI appearance of boiling lesions that could be of importance:

- i. Since boiling provides enhanced heating, it could be possible for large tumours (for example giant fibroadenomas) to use this type of heating (especially in the centre of the tumour) in order to accelerate the ablation,
- ii. Since the rabbit model is used extensively by many researchers in MRI animal experiments, then it is very useful for them to know the appearance of boiling lesions.

11.3.1 Materials and Methods

a. HIFU/ MRI system

The HIFU/MRI system is analysed and described in chapter 5. Figure 5.1 shows the block diagram of a typical HIFU/MRI system and figure 5.2 shows the setup of the actual devices of the HIFU/MRI system.

b. HIFU system

The HIFU system for this study consists of a signal generator (HP 33120A, Agilent technologies, Englewood, CO, USA), a RF amplifier (250 W, AR, Souderton, PA, USA), and a spherically shaped bowl transducer (Etalon, Lebanon, IN, USA). The transducer used for the kidney and liver ablation

operates with frequency of 4 MHz. The transducer is rigidly mounted on the MRI-compatible positioning device version 1.

c. MRI Imaging

The positioning device and the transducer were placed inside a MRI scanner (Signa 1.5 T, by General Electric, Fairfield, CT, USA). The spinal coil (USA instruments, Cleveland, OH, USA) was used to acquire the MRI signal for the case of kidney and liver.

d. Temperature measurement

Temperature was measured in few experiments in order to confirm that the temperature estimated using the PRF method was accurate enough. Temperature is measured using a data acquisition system (HP 34970A, Agilent technologies, Englewood, CO, USA). Temperature is sensed using a 50- μm diameter T-type copper-costantan thermocouple (Physitemp Instruments, Inc. New Jersey, USA) which is MRI compatible. The thermocouple is placed in the tissue by means of a catheter. The thermocouple measures the temperature at the focus. This is achieved by applying low-intensity (low enough not to cause tissue damage) and during the application of ultrasound the transducer is scanned accordingly in order to detect the maximum temperature. This establishes positioning of the thermocouple in the focus of the transducer. The temperature error of the thermocouple is in the order of 0.1 $^{\circ}\text{C}$.

e. Cavitation detector

From a scientific point of view it will be useful to separate lesions developed based on thermal and based on cavitation mechanisms. In this system we use a passive MRI compatible cavitation detector (Etalon, Lebanon, IN, USA), which is placed perpendicularly to the beam of the HIFU transducer (method described in [215]). Since the HIFU protocol is applied inside the magnet of an MRI scanner, the detector must be MRI compatible. The diameter of the detector was 1 cm, its radius of curvature was 10 cm and operated between 1 and 13 MHz (centre frequency is 7 MHz). The detector was mechanically coupled to the HIFU transducer. The voltage from the detector was fed to an

analogue to digital (A/D) card (CS1250, A/D 12 bit, 50 MHz, from GAGE, Lachine, Canada). The A/D card was synchronised to receive the signal when the HIFU transducer was activated. The received signal was stored in a storage device of a PC. The signal was then displayed using EXCEL (Microsoft Corporation, Redmond, WA USA) in order to visualize whether cavitation occurs or not.

11.3.2 *In vitro* experiments

The tissue was placed on top of an absorbing material in order to shield adjacent tissue from stray radiation from the bottom. The transducer was placed on the arm of the positioning device and was immersed in the water tank, thus providing good acoustical coupling between tissue and transducer. Any bubbles that may have collected under the face of the transducer face were removed in order to eliminate any reflections. In all experiments the tissues used (kidney and liver) were extracted from freshly killed lamb, and the experiment was conducted in the same day. Totally 22 kidneys and 8 liver were ablated for investigating various issues.

11.3.3 *In vivo* experiments

For the *in vivo* experiments, adult rabbits from Cyprus were used weighting approximately 3.5-4 kg. Totally 8 rabbits were used in the experiments. The rabbits were anaesthetized using a mixture of 500 mg of ketamine (100 mg/mL, Aveco, Ford Dodge, IA), 160 mg of xylazine (20 mg/mL, Loyd Laboratories, Shenandoah, IA), and 20 mg of acepromazine (10 mg/mL, Aveco, Ford Dodge, IA) at a dose of 1 mL/kg.

The animal experiments protocol was approved by the national body in Cyprus responsible for animal studies (Ministry of Agriculture, Animal Services).

a. HIFU parameters

In order to create large lesions, a grid pattern of 3x3 or 4x4 overlapping lesions was used. The spacing between successive transducer movements was 2 mm, which creates overlapping lesions for the intensity and pulse duration used. In all the exposure, unless stated otherwise the ultrasound was turn on for 5 s.

The delay between successive ultrasound firings was 10 s for the scanned ablation. The intensity indicated through this paper is in situ spatial average intensity.

b. MRI parameters

The various MRI parameters used for the various pulse sequences are listed in table 11.2. The Region of Interest (ROI) was circular with diameter of nearly 2 mm.

The temperature change (ΔT) has been estimated using the equation stated in Chung et al. 1996 [189] and Ishihara et al. 1995 [190] which is as follows:

$$\Delta\phi=\gamma*B_0*\alpha*\Delta T*TE,$$

Where $\Delta\phi$ is the temperature-dependent phase shift which is the phase acquired before and during temperature elevation and which accumulates during the echo time TE using the gradient-echo pulse sequence FSPGR. The other terms are γ which is the gyromagnetic ratio of proton, 42.58 MHz/T, α is the average proton resonance frequency coefficient and B_0 is the flux density of the static magnetic field. The measured temperature elevation can be added to the base-line temperature to obtain the absolute temperature. The average temperature coefficient for the frequency shift was taken from the study of Vykhodtseva et al 2000 [191].

11.3.4 Results

Figure 11.13 shows an MRI image of 4 lesions *in vitro* kidney (plane perpendicular to the beam) resulting from intensities ranging from 1000 to 2500 W/cm² using T1-weighted FSE (Figure 11.13A), T2-weighted FSE (Figure 11.13B) and T1-weighted FSPGR (Figure 11.13C) with pulse duration of 5s. The MRI parameters used are shown in table 1(row 1, 2 and 4). The MRI estimated maximum temperature at the focus was 55 °C for the intensity of 1000 W/cm², 83 °C for 1500 W/cm², 105 °C for 2000 W/cm² and 123 °C for 2500 W/cm². The temperature measured using the thermocouple for the 1000

W/cm^2 was $53\text{ }^\circ C$, which is very close to the temperature estimated using the PRF method.

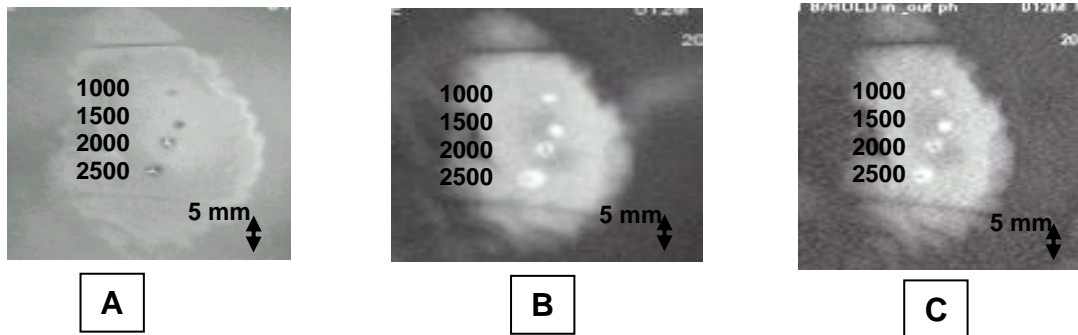


Figure 11.13: MR images (in a plane perpendicular to the beam) of four lesions (intensities 1000, 1500, 2000 and $2500\text{ }W/cm^2$) in kidney *in vitro* using **A.** T1-weighted FSE, **B.** T2-weighted FSE, **C.** T1-weighted FSPGR. With intensities above $2000\text{ }W/cm^2$ the lesions exhibit boiling activity. The discrimination between boiling and non-boiling lesion is best monitored using T2-W FSE

Note that with T2-weighted FSE (Figure 11.13B) white spots (cavity) within the dark thermal lesion are seen for intensities higher than $2000\text{ }W/cm^2$. T1-W FSE and FSPGR show some indication of these cavities, but the resolution is weaker than T2-w FSE.

Figure 11.14 shows MRI images (in a plane parallel to the transducer beam) of 3 lesions in kidney *in vitro* at intensities of 1000, 2000 and $3000\text{ }W/cm^2$. Again T2-weighted FSE shows cavities (due to boiling) within the thermal lesion. T1-W FSE and T1-W FSPGR fail to provide good resolution in this axis.

Having observed that T2-W FSE was probably a successful MRI sequence to detect boiling lesions, this pulse sequence was investigated further by evaluating the Contrast to Noise Ratio (CNR) vs. Echo Time (TE).

Figure 11.15 shows the plot of CNR vs. TE for kidney tissue, lesion and cavity of the lesion of Figure 11.14B (intensity of $3000\text{ }W/cm^2$) demonstrating that good contrast between lesion and cavity is achieved using T2-weighted FSE between 20 and 50 ms.

Figure 11.16 shows a T2-weighted FSE image of 3 lesions in rabbit kidney *in vivo* using different intensities

Ser.	NAME	TR (ms)	TE (ms)	Slice thickness (mm)	Matrix	FOV (cm)	NEX	BW (KHz)	ETL	Other
1	T1-weighted FSE	500	9.2	3, (gap 0.3 mm)	256x256	16	1	31.25	8	-
2	T2-weighted FSE	2500	8,16,3 2,48,6 4,80	3, (gap 0.3 mm)	256x256	16	1	31.25	8	-
3	PD	2500	7.2	3, (gap 0.3 mm)	256x256	16	1	31.25	8	-
4	FSPGR T1-weighted	50	2.7	3, (gap 0.3 mm)	256x256	16	1	62.50	-	Flip angle 500
5	FLAIR	8000	80	3, (gap 0.3 mm)	256x256	16	1	6.9	8	Inversion Time 1200-2200

Table 11.2: Parameters used for the various MRI pulse sequences

The lesion created using 2500 W/cm^2 appears to have a white spot (cavity). These temperatures are lower than the corresponding temperatures *in vitro* (Figure 11.14) for the same intensity due to the removal of heat due to blood flow or possibly due to reflection from various interfaces.

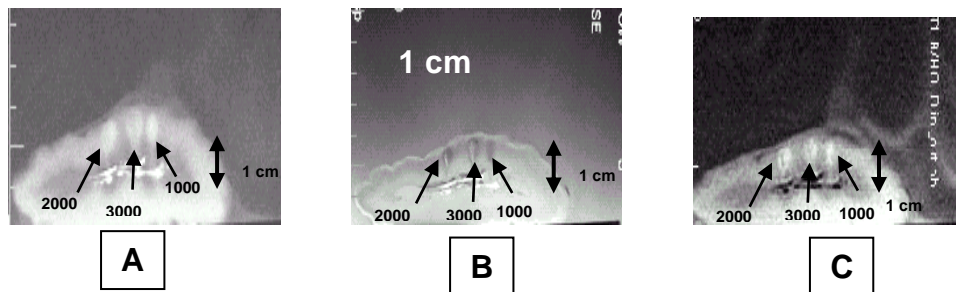


Figure 11.14: MR images (in a plane parallel to the beam) of 3 lesions in kidney *in vitro* using **A.** T1-weighted FSE, **B.** T2-weighted FSE, **C.** T1-weighted FSPGR. With intensities above 2000 W/cm^2 the lesions exhibit boiling activity. The discrimination between boiling and thermal lesion is best monitored using T2-W FSE.

Figure 11.17A shows an MR image of a lesion acquired using T1-weighted FSPGR (for MRI parameters see table 11.2, row 4). Figure 11.17B shows the photograph of the kidney showing cavity within the large thermal lesion.

Note that this large lesion was created using a matrix of 4x4 single lesions with intensity of 1500 W/cm^2 . Out of these 16 lesions, one lesion was created possibly due to the mechanism of cavitation, which results to tissue evaporation

or boiling. The estimated temperature during the creation of this lesion was 120 °C, whereas the temperature for the rest of the lesions (non-boiling) varied from 80 to 85 °C.

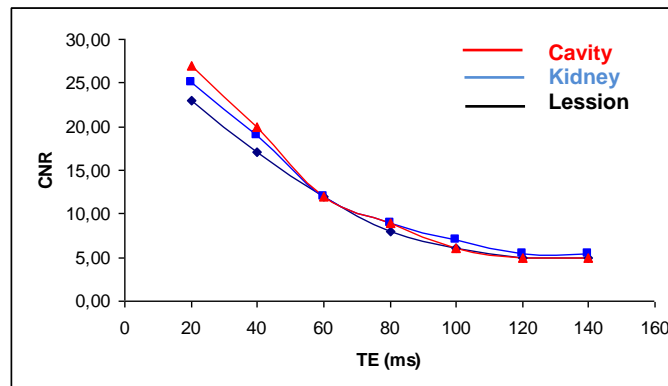


Figure 11.15: CNR vs. TE for the lesion, kidney and cavity for the lesion of Figure 11.18B with intensity of 3000 W/cm²

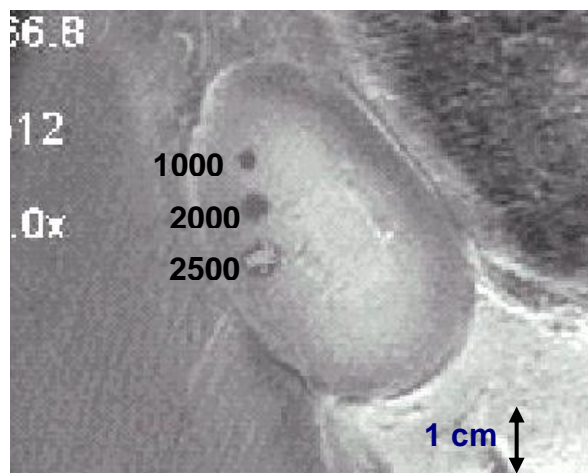


Figure 11.16: MRI image using T2-weighted FSE of 3 lesions in rabbit kidney *in vivo* at different intensities (1000, 2000, and 2500 W/cm²) for a 5 s pulse. The lesion with intensity of 2500 W/cm² is affected by tissue boiling

This bubbly lesion exhibits low-signal lesion (dark spot) and lies inside the large lesion (white spot within the kidney tissue). At the location of the boiling lesion, the passive cavitation detector confirmed the occurrence of cavitation since broadband emission was detected (see figure 11.17C which shows the frequency spectrum of the HIFU transducer). Although with this intensity bubbly lesions should not be produced, the high temperature estimated for this one lesion, should be attributed to cavitation. Cavitation was possibly initiated by

bubbles that are trapped in the *in vitro* tissue due to the absence of blood in the vasculature.

Figure 11.18 demonstrates the temperature increase *in vitro* kidney using HIFU and MRI monitoring. The MRI images were acquired using the dynamic sequence T1-weighted FSPGR. Each image was acquired in 5s. In image 11.18a ultrasound was OFF. In the next 5 images the applied spatial average intensity was 1000 W/cm^2 (for 25 s), and in the last 2 images ultrasound is turned OFF. Due to the heating a dark spot is observed (see arrows). The estimated maximum temperature was $55 \text{ }^\circ\text{C}$.

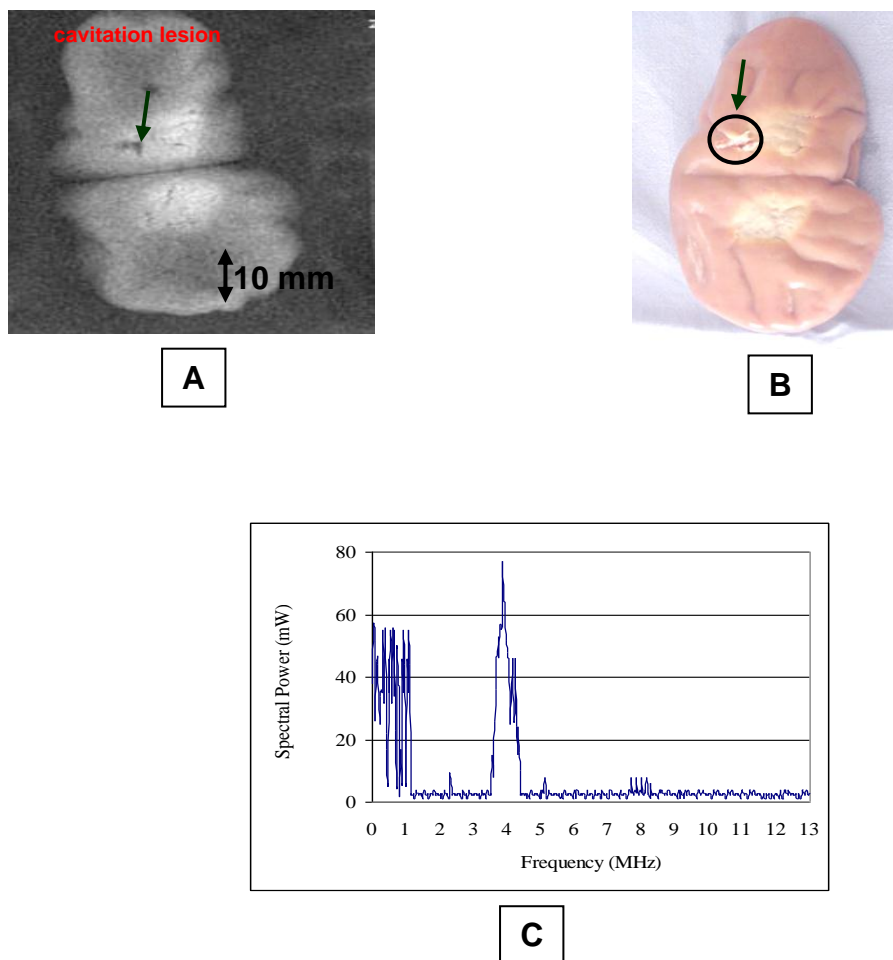


Figure 11.17: **A.** MR image (in a plane perpendicular to the beam) of large lesion in kidney *in vitro* using T1-weighted FSPGR (TR=50 ms), showing one cavitation lesion. **B.** Photograph of the kidney showing the cavitation lesion within the large thermal lesion, **C.** Frequency spectrum of the HIFU transducer exhibiting cavitation activity

Figure 11.19 shows the corresponding temperature increase using T1-weighted FSPGR influenced by boiling. In figure 11.19A ultrasound was OFF. In the next 5 images the applied spatial average intensity was 3500 W/cm² (for 25 s). Note that compared to figure 11.17 where the focal beam is circular, the focal beam in this figure is distorted, which is attributed to the occurrence of boiling confirmed also by the temperature of 112 °C measured.

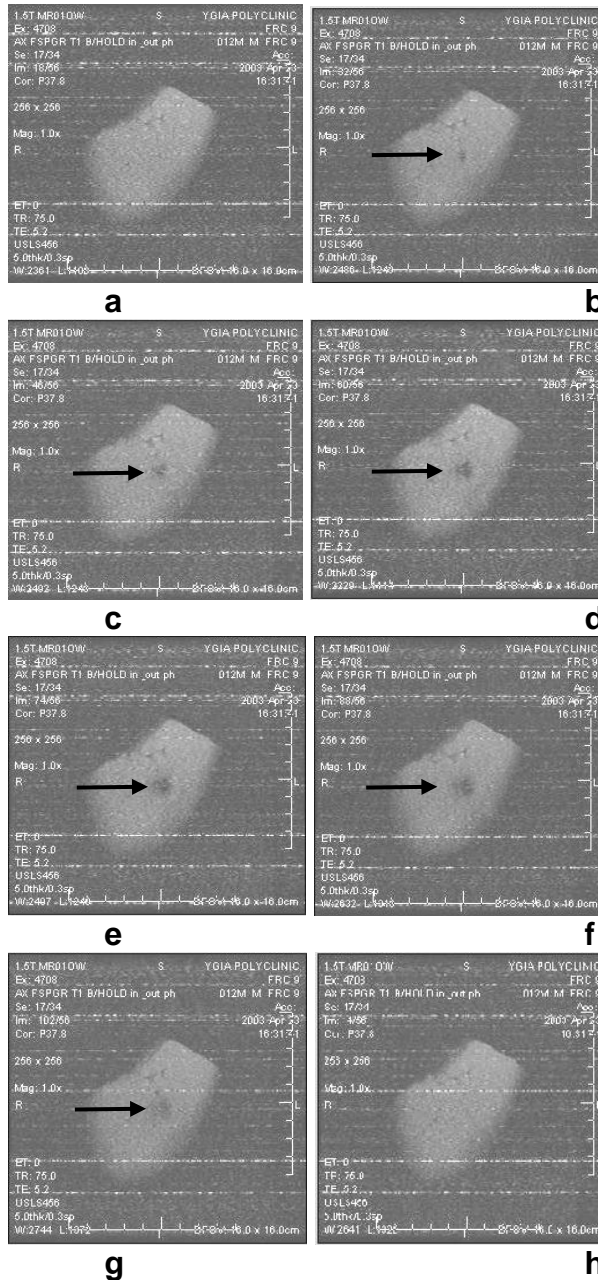


Figure 11.18: Temperature evolution *in vitro* kidney using T1-weighted FSPGR (thermal mechanism). Each image was acquired in 5s. **a.** Ultrasound is OFF **b.-f.** applied spatial average intensity: 1000 W/cm² (for 25s), **g.-h.** ultrasound is OFF

Figure 11.20 shows MRI image of lesion in liver. The image was acquired using Proton density. The lesion was created using low intensity (1000 W/cm^2) for long time (30s). These ultrasonic parameters produce temperature elevation which is above the boiling point ($120 \text{ }^\circ\text{C}$). Thus, the evaporation of tissue causes a cavity that follows the shape of the beam.

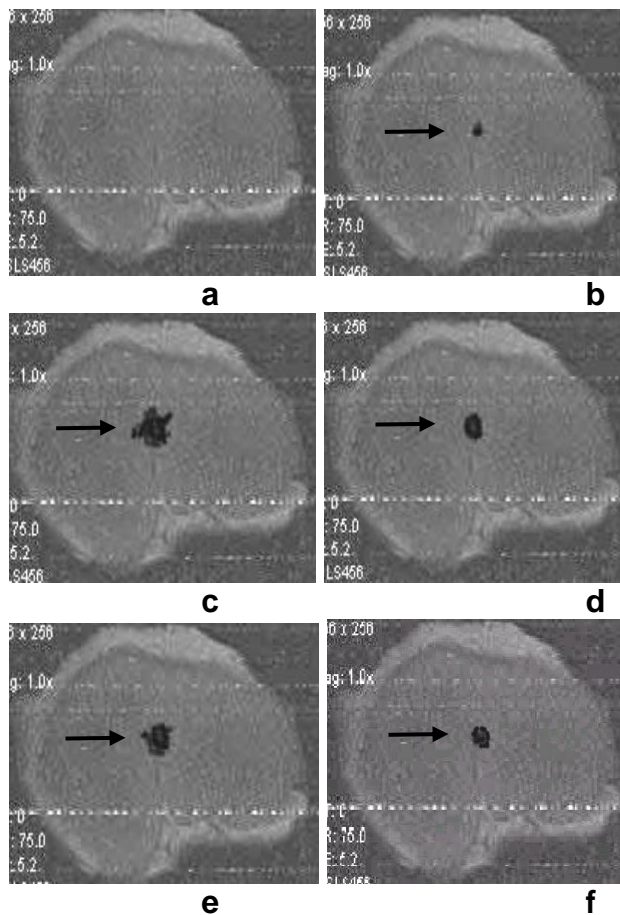


Figure 11.19: Temperature elevation *in vitro* kidney using T1-weighted FSPGR (boiling). **a.** Ultrasound is OFF **b.-f.** applied spatial average intensity: 3500 W/cm^2 (for 25s)

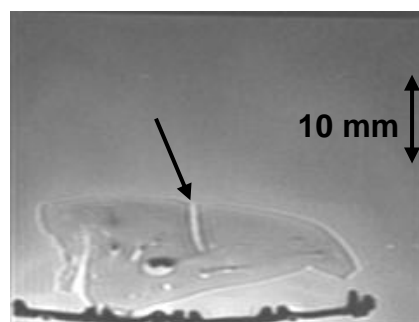


Figure 11.20: MR image using proton density of lesion in liver created under the influence of boiling. The lesion was created using low intensity (1000 W/cm^2) for long time (30 s)

The methodology applied for kidney which evaluates T1-W FSE, T2-W FSE and FSPGR (Figure 11.13 and 11.15) was also applied for liver. It was found that for liver the best pulse sequence to evaluate boiling lesions was T2-w FSE with minimum TE (i.e. proton density). Table 11.3 summarizes the recommended MRI sequence according to our experience for monitoring boiling lesions.

Tissue type	Contrast between lesion below boiling and tissue	Contrast between lesion below boiling, tissue, and lesion above boiling
Kidney	T1-W FSE, T2-W FSE	T2-W FSE
Liver	T1-W FSE, T2-W FSE	T2-W FSE

Table 11.3: Recommended pulse sequences for discriminating between a) normal and thermal lesions and b) normal tissue, lesions created with temperature below boiling and lesions created with temperature above boiling

11.3.5 Discussion

So far it was concluded by several studies (for example Quesson et al. 2000 [167], Salomir et al. 2000 [216], McDannold et al. 2000 [168] that MRI-guidance of HIFU serves mainly 4 purposes:

- i. localisation of the focus,
- ii. imaging of the temperature elevation,
- iii. imaging at the end of the treatment protocol, in order to evaluate the necrosis and possibly re-planning the treatment protocol in the event of incomplete coverage of the target and
- iv. follow-up imaging, evaluating the effectiveness of HIFU ablation, several days after the treatment.

This study enhances the role of MRI guidance in HIFU because it provides techniques to discriminate between non-boiling and boiling lesions.

In kidney the best MRI sequence to detect boiling lesions was T2-W FSE. T2-W FSE was evaluated further by plotting the CNR vs. TE for the three regions of interest (kidney, lesion and cavity). It was concluded that between TE's of 20 and 50 ms, the signal difference, and hence the contrast between the three regions of interest (kidney, lesion and cavity) is maximum (Figure 11.15). According to figure 11.15, the cavity, which appears inside the lesion, has stronger signal and decays slower.

T1-weighted FSE and T1-weighted FSPGR do not consistently show boiling lesions in kidney, and even when cavities are visible the contrast is not very good.

In liver T2-W FSE with low TE (i.e. Proton density) is recommended as an MRI sequence to detect non-boiling lesions and boiling lesions.

Boiling bubbles scatter and reflect ultrasound. These reflections result in shielding the HIFU focus and thus increased prefocal heating is observed. Therefore boiling bubbles, similar to cavitation bubbles, result to distortion of the lesion from a cigar shape into a tadpole shape (Figure 11.14). In addition to this the growth of the lesion is shifted towards the transducer. This phenomenon which is attributed to bubbles, either due to ultrasound-induced cavitation or to boiling has been observed also in the study by ter Haar [217], and by Chavier et al 2000 [72]. For the scanned lesions the focus is not shifted towards the transducer, because while boiling begins in a very short time in both single and scanned lesions, it cannot distort the lesion for scanned exposures because the focus of the transducer moves away from the boiling site. This speculation is also supported in the paper by Khokhlova [214]

This study also showed by means of MRI images that focal beam is distorted during the occurrence of boiling. Initially low intensity was used (1000 W/cm^2) and the temperature elevation was monitored using T1-weighted FSPGR. The shortest acquisition time that we could achieve with our system was 5s. Modifying any MRI parameter to decrease the time resulted to poor contrast or low signal to noise ratio (SNR). If we had achieved faster acquisitions (less than 5s), then it would have possible to see more drastic changes. A decrease in the signal (black spot) demonstrated the increase in the temperature (also observed by Hynynen et al 1995 [14]. The shape of the black spot was circular. The black spot increased gradually with increased temperature, and the shape remains circular at all times (Figure 11.18). When the intensity was increased to 3500 W/cm^2 , the shape of the black spot was irregular indicating that boiling occurred (Figure 11.19).

12 Conclusion and future enhancements

HIFU seems to be the most promising technology in non-invasive procedures in medicine. A technology evolved in the 1950s by the Fry brothers, Francis and William. Back then, fry brothers had introduced the first HIFU system as a non-invasive procedure in medicine. The first application of this system was the treatment of neurologic disorders like Parkinson's disease. However this methodology remained unutilized due to the lack of necessary imaging technology devices. The road towards a major breakthrough innovation opened wide four decades later by Jolesz and Jakab and Ronald Watkins at the GE Corporate R&D lab. Jolesz and Jakab provided a solution for visualization of this non-invasive procedure. They demonstrated that an ultrasonic transducer can be used inside a MRI scanner. That was the beginning of a new era in medicine and non-invasive procedures. Since then more and more researchers joined forces and today two decades after the Jolesz, Jakab successful and revolutionary idea, physicians provided with an enhanced tool which it appears to be applicable for unlimited medical processes. HIFU started as a scalpel ablating any applicable target. Applications include ablating tumours of the brain, breast, uterine fibroids, prostate, liver, kidney and pancreas or even treat cardiac arrhythmia. Meanwhile, researchers are currently study applications of lower energy HIFU for drug delivery, trigger system to restore function like stimulating nerves, ischemic stroke by removing blood clod or thrombus, revive heart operation or even trigger the immune system. Moreover, clinical trials some of which they have receive an FDA approval and/or CE marking, proved that HIFU can be applied for neurological disorders including neuropathic pain, Parkinson's disease and essential tremor.

The innovation of HIFU has brought many benefits to medicine for both the physicians and the patients. The most important benefit is the effect on the patient. Since HIFU procedures are non-invasive the patients can walk out of the surgery room without passing through the intensive care unit (ICU) or by minimizing the number of days in the ICU. This implies that patient have to undergo much less pain, the recovery period is minimized and patients are back to normal life at no time, the cost of the operations is also reduced since the patients to not need to recover in the ICU and the psychological effects on the

patients are also minimized. Furthermore, the treatment can stop any time during the process if the patient feels pain or uncomfortable, something that cannot be done with classical surgery and the treatment can be repeated any number of times if necessary without any effect on the patient. Last but not least, the physicians perform the operation using a mouse and therefore, these procedures are becoming much like an electronic game. On the other hand HIFU is not applicable to all organs, on the lungs for example where there is air, HIFU cannot be applied since ultrasound does not propagate through the air. Although, MRI is the only modality available today for monitoring and receiving feedback on where the focal spot is and on what damage has been achieved on the targeted tissue, there must be a major improvement on MRI scanners in order to be able to track moving organs in real time and keep the focal spot on target all the time. Another weaknesses of this technology is that it cannot take place in normal surgery room since it involves the MRI and this adds to the cost of the operation

Convinced that HIFU is an optimistic and beneficial alternative to traditional surgery the aim of this research concentrates on the treatment of tumours of the abdominal organs liver, kidney, and pancreas, as well as thyroid tumours. Moreover, this study focuses on the design and development of an MR compatible robot which will operate in the gantry of an MRI scanner and guide the HIFU transducer which will ablate the tumours under study. Also, the MR compatible robot will have the ability to be used in experiments on animals.

To achieve the main goal of this study three versions of positioning devices were designed, developed and evaluated. The first version of positioning device proved to be suitable for the guidance of the HIFU transducer in the gantry of an MR scanner. In addition, this first version of positioning device is simple, small to operate in the gantry of the MR, lightweight (approximately 6 Kg) and therefore, portable, and can be used in virtually any clinical MRI scanner since it can be sited on the scanner's table. Moreover, this positioning device is flexible since it can be easily reduced or increased in size. This can be adjusted easily by varying the lengths of the rods, sheets and belts. All the other components remain fixed in size. Thus, easily any size of positioning device can be designed. This positioning device includes a flexible coupling

system, and thus it can be used in all the anatomies considered in this study (brain, liver, kidney, pancreas and thyroid).

The positioning device proved to be functional and discrete and large lesions were created successfully with reproducible results. Finally, the results also show that the quality of MRI imaging is not affected by the presence of the HIFU system.

However, this positioning device is driven with the timing belts and hence there is a possibility for these timing belts to loosen and as a result this will lessen robot's accuracy and stability. Another weakness of this robot is that it cannot be reproduced precisely. These weaknesses brought the idea for the design and development of the second version of positioning device.

The second version of positioning device since it was based on the experience gained from the first version, inherited all the benefits of the first version and in addition the weaknesses were resolved. The timing belts were replaced with racks and pinions and as a result both stability and accuracy of the robot were enhanced. Furthermore, the second robot was designed on CAD software and manufactured by the 3D printer and gave the robot smoother edges more accurate design and made the robot reproducible. A major enhancement in the second version is that it was designed to be as flexible as possible. All the parts of this robot are detachable and this contributed to the portability but even more important any part of the robot can be replaced with no effect on the rest of the parts of the robot. Also, different transducer holders designed for different applications and different transducers can be attached on the robot. Furthermore, this robot can be easily modified and attached on the top of the MRI's gantry providing top-to-bottom access to patients. In addition to the benefit inherited from version one, this robot is durable robust, and reliable. The flexibility added to this robot made the robot applicable for several organs such as liver, kidneys, pancreas and thyroid and also for experiments on animals.

The disadvantage of this second version of positioning device is that at this moment it is not feasible to attach it on the top of the gantry of the MR scanner.

Therefore, at present will only be used for experiments *in vitro* tissues and gel phantom or on animals.

The third version of positioning device inherited all of the characteristic advantages of the previous versions. Moreover, this positioning device is principally influenced by and therefore replaces the first version.

The third version of positioning device can be used for brain tumours as shown in figure 8.19 with the horizontal HIFU transducer holder. Furthermore the water container holder shown in figure 8.12.B, is suitable for *in vitro* targets placed inside or underneath the water tank (kidney, liver, turkey fillet, porcine muscle etc.) by attaching the appropriate vertical HIFU transducer holder and also for *in vivo* targets (small animals like rabbits and rats).

The software developed to guide the robot outside the MRI room is user friendly and enriched with useful features that can be used by the physician during or after the procedure. The user interface proved to be reliable, stable and accurate. The software is flexible and adaptable and therefore, it can be easily updated and modified to fulfil any future requirements.

Evaluation procedures show that the presence of the positioning device in the gantry of the MRI does not affect the quality of MRI imaging. Therefore, all three versions of positioning devices are proved to be MR compatible. In addition discrete and large lesions were created successfully with reproducible results.

The quality of the images captured from the MR compatible camera was not affected by the strong magnetic field of the MR. However, the MRI image slightly affected by the presence of the MRI compatible camera.

In this study several experiments were conducted to evaluate the HIFU/MRI system and the effectiveness of MRI to monitor therapeutic protocols of HIFU. Detection of large lesions using MRI and the best contrast between different tissues and lesions using different MRI sequences were evaluated. The range of repetition time (TR) and range of echo time (TE) which maximizes the contrast to noise ratio (CNR) was also investigated and evaluated. MRI was also utilized to monitor lesions created at temperature below the boiling point

and lesions created at temperature above the boiling point using HIFU in freshly excised tissues and *in vivo* rabbit kidney. T2-weighted fast spin echo (FSE) was proven to be an excellent MRI sequence that can detect lesions with temperature above the boiling point in kidney. This advantage is attributed to the significant difference in signal intensity between the cavity and the thermal lesion. Moreover, in liver the MRI sequence of Proton Density to detect lesions above boiling proved to be a suitable choice.

Finally the MRI compatible positioning devices developed with resolution for all three axes of 0.1 mm will offer a valuable multi-tool for the physicians for a variety of applications. The user will be able to control and monitor the process through a user friendly interface. Furthermore, this HIFU system can be setup at no time and also accepts different HIFU transducer holders of different length, height, and pointing direction or angle as well as HIFU transducers from different manufacturers or with different focal length and therefore different diameter that can be used for almost every accessible organ in the body.

12.1 Future enhancements

The plans for this study are to be able in the near future to acquire an approval for clinical trials. The following steps are to be followed in order to obtain approval for clinical trials:

- i. Obtain CE marking for the HIFU system.
- ii. Apply for clinical trials through the Cyprus Medical device agency. This is the national body for approving clinical trials when a medical device is involved. The Cyprus Medical device agency will consult the Cyprus Bioethic committee and if all the necessary information is submitted satisfactorily, an approval will be given for conducting clinical trials.

Additionally, the directives below will be considered:

- i. Directive 2001/20/EEC of the European Parliament and of the Council of 4th April 2001 on the approximation of the laws, regulations and administrative provisions of the Member States relating to the implementation of good clinical practice in the conduct of clinical trials on medicinal products for human use.

http://europa.eu.int/eur-lex/pri/en/oj/dat/2001/l_121/l_12120010501en00340044.pdf

- ii. Guidelines as suggested by the European Science foundation, in European science foundation policy briefing May 2001, on Controlled clinical trials.

www.esf.org/publication/90/ESPB13.pdf.

Although, the encoders of the motor drivers were utilized to return the location of the motor at any time this location may not directly reflect the actual position of the transducer. Therefore a localization system has to be employed in order to get in real time the actual position of the transducer. This can be achieved by engaging three optical sensors acting like beacons to detect the position of the transducer and send it back to the system. This will be used as a real time feedback to evaluate and correct the process.

Furthermore, the flexible design of the positioning devices will easily allow modifications to target and ablate other organs accessible by HIFU and not consider here such as prostate, uterine fibroids, breast, brain and more. Also, it may be employed in treating other diseases like Parkinson's, ischemic stroke, drug delivery, reviving heart operation and many more.

Also, the software can be enhanced by automating the process further. Engaging in the software image processing will enable the physician to use the mouse to cover the area of the tumour, lineate three dimensional the tumour and hence the software will develop a three dimensional treatment plan. The treatment plan should be editable enabling the physician to add or remove tissue in the treatment plan. However, this implies a closer collaboration with the MRI manufacturer.

Moreover, the database of patient treatments should be expanded to keep more data about the patients and their treatments as well as for the physician which can be utilised to derive useful conclusions for medicine through statistics.

The valuable thermometry property of the MRI should also being embedded in the software and this will give the necessary for a non-invasive procedure,

feedback which will help to visualize the effect (damage) of the ultrasound to the targeted tissue and prevent damage to healthy tissues.

Through the evaluation the lack of rotational motion was appreciated so that the transducer does not only manoeuvre in the XYZ dimensions, but also in an angular direction, thus ablating tissues through the appropriate angle.

The results through the evaluation are very optimistic and with the future enhancements described here the positioning devices developed will drive this research to clinical trials for treating brain, kidney, liver, pancreas, and thyroid tumours.

13 Appendix

13.1 Journal and conferences publications

13.1.1 Journal papers

1. C .Damianou, K. Ioannides, V. HadjiSavas, N. Milonas, A. Couppis, D. Iosif, M. Komodromos F. Vrionides, 'Thermal ablation system using high intensity focused ultrasound (HIFU) and guided by MRI' , Therapeutic Ultrasound, Vol. 6, pp. 123-128, 2006.
2. Damianou, C., Ioannides, K., Milonas, "Positioning device for MRI-guided high intensity focused ultrasound system," Computer-Assisted Radiology and Surgery, vol.2(6), pp. 335-345, 2008.
3. C. Damianou, Ioannides K., Hadjisavas V., Milonas N., Couppis A, Iosif D, 'In vitro and in vivo brain ablation created by high intensity focused ultrasound and monitored by MRI', IEEE Transaction on Ultrasonics, Ferroelectrics and Frequency Control, 56(6), pp. 1189-1198, 2009.
4. Mylonas N., Ioannides K., Hadjisavvas V., Iosif D., Kyriacou P., Damianou C.'Evaluation of fast spin echo MRI sequence for an MRI guided high intensity focused ultrasound system for *in vivo* rabbit liver ablation' J. Biomedical Science and Engineering, 2010, 3, 241-246
5. Christakis Damianou, Kleanthis Ioannides, Venediktos Hadjisavvas, Nikos Mylonas, Andreas Couppis, Demetris Iosif, Panayiotis A. Kyriacou. MRI monitoring of lesions created at temperature below the boiling point and of lesions created above the boiling point using high intensity focused ultrasound. J. Biomedical Science and Engineering, 2010, 8, 763-775.
6. Venediktos Hadjisavvas, Kleanthis Ioannides, Michalis Komodromos, Nikos Mylonas, Christakis Damianou. Evaluation of the contrast between tissues and thermal lesions in rabbit *in vivo* produced by high intensity focused ultrasound using fast spin echo MRI sequences. J. Biomedical Science and Engineering, 2011, 4, 51-61.

Submitted and accepted

7. "Positioning device for MRI-guided high intensity focused ultrasound system", International Journal of medical robotics and computer assisted surgery.

Submitted

8. "A prototype MR compatible positioning device for guiding a Focused ultrasound system for the treatment of abdominal and thyroid cancer."

13.1.2 Conference papers

1. C. Damianou, N. Milonas, V. HadjiSavas, A. Couppis, D. Iosif, K. Ioannides, 'Thermal ablation system using High Intensity Focused Ultrasound (HIFU) and guided by MRI' **CARS 2008** Computer Assisted Radiology and Surgery, June 25 - 28, Barcelona, Spain ,2008.
2. C. Damianou, K. Ioannides, V. HadjiSavas, N. Milonas, A. Couppis, D. Iosif, M. Komodromos F. Vrionides, 'Thermal ablation system using high intensity focused ultrasound (HIFU) and guided by MRI' , International Society of Therapeutic Ultrasound, Minneapolis, 10-13 September, 2008.
3. C.Damianou, K. Ioannides, V. HadjiSavas, N. Milonas, A. Couppis, D. Iosif, M. Komodromos, F. Vrionides, 'High intensity focused ultrasound (HIFU) system guided by MRI'. 12th World Congress of the World Federation for Ultrasound in Medicine and Biology, 30 August – 3 September 2009, Sydney Convention & Exhibition Centre, Sydney, Australia.
4. C.Damianou, N. Milonas, V. HadjiSavas, A. Couppis, D. Iosif, K. Ioannides, Evaluation of the contrast between tissues in rabbit *in vivo* and thermal lesions produced by HIFU using fast spin echo MRI sequences in liver, kidney, heart, brain and pancreas. International Society of Therapeutic Ultrasound, Aux En Provence, France, 23-26 September, 2009.
5. C. Damianou, K. Ioannides, N. Mylonas, V. HadjiSavvas, A. Couppis, D. Iosif 'Liver ablation using a high intensity focused ultrasound system and MRI guidance', 9th International Conference on Information Technology and Applications in Biomedicine, November 5-7, 2009, Larnaca, Cyprus.
6. V. HadjiSavvas, C. Damianou, K. Ioannides, N. Mylonas, , A. Couppis, P. Kyriakou, D. Iosif, , T. Hadji Charambous, G. Parea, 'Penetration of high intensity focused ultrasound *in vitro* and *in vivo rabbit brain* using MR imaging. ', 9th International Conference on Information Technology and Applications in Biomedicine, November 5-7, 2009, Larnaca, Cyprus.
7. N. Mylonas, V. Hadjisavvas, C. Damianou, An MR compatible positioning device for treating brain cancer and stroke using high intensity focused ultrasound (HIFU) under MRI guidance, 10th meeting of the International Society of Therapeutic Ultrasound, ISTU10, Tokyo, Japan, June 9-12, 2010.
8. A. Couppis, K. Ioannides, N. Mylonas, D. Iosif, P. Kyriakou,C.Lafon, F. Chavier J. Chapelon, M. Komodromos, C. Damianou, Evaluation of an MRI guided planar rectangular high intensity focused ultrasound transducer for thermal ablation of cardiac tissue, 10th meeting of the International Society of Therapeutic Ultrasound, ISTU10, Tokyo, Japan, June 9-12, 2010.
9. N. Mylonas, C. Damianou MR-guided focused ultrasound robot for performing experiments on large animals, 10th meeting of the International Society of Therapeutic Ultrasound, ISTU10, Tokyo, Japan, June 9-12, 2010.

13.2 Animal Experiments Issues

FUC has been approved by the Ministry of agriculture of Cyprus to conduct experiments with animals. The Cyprus's authority has revised the regulations regarding animal experiments in 2000 as part of the harmonisation process. The revised regulations follow exactly the EU directives 86/609/EEC (Directive title: "*On the approximation of laws, regulations and administrative provisions of the Member States regarding the protection of animals used for experimental and other scientific purposes*"). In order to obtain the approval to perform animal experiments we have responded to the following issues:

a. Authorised persons.

Experiments will be performed solely by a veterinarian who is a competent persons authorized with the provisions of national legislation. Persons who carry out experiments or take part in them and persons who take care of animals used for experiments, have appropriate education and training.

b. Investigator responsibilities.

The task leader involved in animal experiments is responsible for the standard of animal care and use by all other persons involved in the experiment. It will be ensured that the extent of supervision is compatible with the level of competence of each person and the responsibilities they are given.

c. Previous Work

We will investigate others studies performed earlier in the brain in order to reduce the number of animals used.

d. Pain and distress

If animals develop signs of severe pain or distress despite the precautions outlined above, they will have the pain or distress alleviated promptly or will be killed humanely and without delay. If in doubt, we will always seek the veterinarian's opinion before continuing an experiment.

Unexpected deaths occurring during a project will be properly investigated by the veterinarian to determine the cause and initiate remedial action. If the deaths are due to manipulations, these will cease. The national authority will be notified and the project protocol resubmitted with appropriate modification.

e. Signs of pain or distress

We are familiar with the normal behavior of the animal species chosen, the signs of pain or distress specific to that species, and will monitor the animals for these signs. Animals will be monitored during the experiment appropriately for clinical signs of acute pain or distress. These may include one or more of the following: a. Abnormal stance or movements, b. Abnormal sounds, c. Altered cardiovascular and/or respiratory function, d. Vomiting and abnormal defecation or urination.

f. Animals species

We will use New Zealand rabbits.

g. Repeated use of animals in experiments

Since each animal is sacrificed after the experiment then the issue of using the same animal does not exist.

h. Anaesthesia

The animals will be totally anesthetized. The anesthesia protocol is as follows: 142 mg (1.42 mL) of xylazine is mixed into a 1000 mg vial of Ketamine (10 mL). Each animal receives 1 mL of this cocktail per 10 lbs via an intramuscular injection. The doses administered after that is half the initial dose every 30-40 min. The anesthesia will be monitored by measuring the heart rate and respiration and by visual inspection

i. Euthanasia

The chosen Euthanasia will produce rapid loss of consciousness without pain until death occurs. The animals will be euthanised using 1 ml per 10 lbs of Bethanasia-D special. The route of euthanasia is IV. Following the administration of this drug, a scalpel will be used to create a bilateral pneumothorax.

j. Pre-operative Planning

Surgical success can be improved by careful attention to the following:

- a. The use of healthy, disease-free animals will ensure more reliable research data. We will consult a veterinarian to assist in obtaining such animals.
- b. Surgical time will be reduced by practice on cadavers. This will familiarize us with anatomical landmarks, streamline the experimental surgical procedures and thereby reduce the quantity of anesthetic required. This will promote animal well being.

k. Post-operative care

Not applicable for this type of experiments because the animals will be euthanized at the end of the experiment.

l. Supplying establishments

Since at FUC there are no other researchers doing experiments with animals, we will pick up animals from supplying establishments. The supplying establishment is approved by the national authority.

m. User establishments

Our establishments are registered with and approved by the national authority. Arrangements are made to have installations and equipment suited to the species of animals used and the performance of the experiments conducted there. The design, construction and method of functioning is such as to ensure that the experiments are performed as effectively as possible, with the object of obtaining consistent results with the minimum number of animals and the minimum degree of pain, suffering, and distress harm.

n. Report of results

We will keep records of all animals used and produce them whenever required to do so by the authority. In particular, these records will show the number and species of all animals acquired, from whom they were acquired and the date of their arrival. Such records will be kept for a minimum of three years and shall be submitted to the authority upon request.

o. Animal protocols

Ablate tissue using high intensity ultrasound. The maximum temperature in the brain will never exceed 3 °C. The experiments will demonstrate the ability of the ultrasonic source to dissolve clots in the brain. Power levels and pulse duration that optimize the treatment will be derived

13.2.1 Licenses from Ministry of Agriculture, animal services

a. Lab license for experiments on rabbits

ΚΥΠΡΙΑΚΗ  ΔΗΜΟΚΡΑΤΙΑ

ΥΠΟΥΡΓΕΙΟ ΓΕΩΡΓΙΑΣ, ΦΥΣΙΚΩΝ
ΠΟΡΩΝ ΚΑΙ ΠΕΡΙΒΑΛΛΟΝΤΟΣ
ΚΤΗΝΙΑΤΡΙΚΕΣ ΥΠΗΡΕΣΙΕΣ

ΠΙΣΤΟΠΟΙΗΤΙΚΟ ΕΓΚΡΙΣΗΣ

(Άρθρο 8, Ν.30(I)95 - Κανονισμός 5(3), Κ.Α.Π. 18/2000)

Αρ. Εγγραφής: **CY.EXP.107**

Δια του παρόντος ο Διευθυντής του Τμήματος Κτηνιατρικών Υπηρεσιών, ασκώντας τις εξουσίες που του παρέχονται δυνάμει του περί Ζώων (Επιστημονικά Πειράματα) Νόμου του 1995 και των περί Ζώων (Επιστημονικά Πειράματα) Κανονισμών του 2000 χορηγεί κατόπιν σχετικής αίτησης ημερομηνίας 19 Ιανουαρίου 2009 του **Δρ. Χριστάκη Δαμιανού** της εταιρείας **MEDSONIC LTD.** (Ποντίδος 6, Άγιος Αθανάσιος, 4103 Λεμεσός), Πιστοποιητικό Έγκρισης του Εργαστηρίου Θεραπευτικών Υπερήχων για να διεξάγονται ελεγχόμενα πειράματα σε κουνέλια (εφαρμογή υπερήχων) κάτω από τους ακόλουθους όρους:

- (α) Υπεύθυνος για τη φροντίδα των ζώων είναι ο Δρ. Χριστάκης Δαμιανού.
- (β) Σύμβουλος κτηνίατρος αναφορικά με την Υγεία και Ευημερία των ζώων είναι ο Δρ. Δημήτρης Ιωσήφ
- (γ) Απαγορεύεται η θανάτωση των ζώων με διαφορετική μέθοδο από την κατάλληλη για τα ζώα δυνάμει του Παραρτήματος Ι του Νόμου 30(I)95
- (δ) Να υπάρχει διαθέσιμο πρόσωπο ικανό να θανατώνει τα ζώα κατά τον καθοριζόμενο τρόπο
- (ε) Να τηρείται βιβλίο για την καταγραφή στοιχείων σχετικά με την πηγή, χρησιμοποίηση και καταστροφή των ζώων που χρησιμοποιούνται στα ελεγχόμενα πειράματα
- (στ) Να τηρούνται οι προδιαγραφές, οι όροι και οι διαδικασίες λειτουργίας σύμφωνα με το Παράρτημα 2 των Κανονισμών Κ.Δ.Π. 18/2000.

Το παρόν πιστοποιητικό Υποστατικού Επιστημονικών Πειραμάτων δύναται να ανακληθεί οποτεδήποτε από το Διευθυντή, εφόσον δεν τηρούνται οι διατάξεις του Νόμου και των Κανονισμών.

Σφραγίδα



Υπογραφή: 

Δρ. Χαρ. Κακογιάννης (DVM, PhD)
Διευθυντής
Κτηνιατρικών Υπηρεσιών

Ημερομηνία: **22.05.2009**

F18: 299968 ημερομηνίας: 22.05.2009

Pistopoitiko egrisis piraamatou CY.EXP.107

b. *Approval of the Ministry of Agriculture, animal services for experiments on rabbits*



ΚΥΠΡΙΑΚΗ ΔΗΜΟΚΡΑΤΙΑ

ΥΠΟΥΡΓΕΙΟ ΓΕΩΡΓΙΑΣ ΦΥΣΙΚΩΝ
ΠΟΡΩΝ ΚΑΙ ΠΕΡΙΒΑΛΛΟΝΤΟΣ

ΚΤΗΝΙΑΤΡΙΚΕΣ ΥΠΗΡΕΣΙΕΣ
1417 ΛΕΥΚΩΣΙΑ

Αρ. Φακ.: 8/95/12
Αρ. Τηλ.: + 357 22805 200 - 201
Αρ. Φαξ: + 357 22332803
e.mail: director@vs.moa.gov.cy

22 Μαΐου 2009

Δρ. Χριστάκη Δαμιανού ✓
Ποντίδος 6, Άγιος Αθανάσιος
4103 Λεμεσός

**Διεξαγωγή Επιστημονικών Πειραμάτων σε κουνέλια στο Εργαστήριο
Θεραπευτικών Υπερήχων της Εταιρείας MEDSONIC LTD. στη Λεμεσό**

Αναφέρομαι στο πιο πάνω θέμα και τη σχετική αίτησή σας προς τις Κτηνιατρικές Υπηρεσίες με ημερομηνία 19 Ιανουαρίου 2009 και σας πληροφορώ τα ακόλουθα:

1. Εγκρίνεται ως χώρος διεξαγωγής των πειραμάτων το Εργαστήριο Θεραπευτικών Υπερήχων της εταιρείας MEDSONIC LTD. στη Λεμεσό. Το εργαστήριο είναι ειδικά διαμορφωμένο και φέρει τον απαραίτητο εξοπλισμό για τη διεξαγωγή των πειραμάτων. Έχει επιβεβαιωθεί από τις Κτηνιατρικές Υπηρεσίες στις 8 Μαρτίου 2009.
2. Εγκρίνεται το αίτημά σας για χορήγηση άδειας σχεδίου. Θα εκδοθεί ξεχωριστή άδεια για κάθε πρόγραμμα εργασίας και τα πειράματα θα διεξάγονται στα πλαίσια των υποβληθέντων προγραμμάτων.
3. Εγκρίνεται το αίτημά σας για χορήγηση προσωπικής άδειας.

Για την έκδοση των πιο πάνω αδειών και του πιστοποιητικού καταβάλλονται στο Διευθυντή Κτηνιατρικών Υπηρεσιών τα τέλη που καθορίζονται στο Παράρτημα 3 των Κανονισμών Κ.Δ.Π. 18/2000 (επισυνάπτεται):

- (α) για την έκδοση προσωπικής άδειας € 34,17
(β) για την έκδοση πιστοποιητικού έγκρισης του υποστατικού διεξαγωγής των πειραμάτων €170,86
(γ) για την έκδοση της άδειας σχεδίου για το πρόγραμμα «θεραπεία ισχαιμικού εγκεφαλικού» €170,86 (διάρκεια 5 χρόνια)
(δ) για την έκδοση της άδειας σχεδίου για το πρόγραμμα «θεραπεία όγκων εγκαψάλου» €102,52 (διάρκεια 3 χρόνια).

Η πληρωμή των τελών γίνεται στο Επαρχιακό Κτηνιατρικό Γραφείο Λεμεσού, αφού παρουσιάσετε αντίγραφο της παρούσας επιστολής.

Δρ. Χαρ. Κακογιάννης (DVM, PhD)
Διευθυντής Κτηνιατρικών Υπηρεσιών

Κοιν.: Προϊστάμενο Τομέα Υγείας και Ευημερίας Ζώων
Επαρχιακό Κτηνιατρικό Λειτουργό Λεμεσού
ΦΠ/ΜΑ 22050920Π

Κτηνιατρικές Υπηρεσίες 1417 Λευκωσία
Τηλ. 22805200-201 φαξ 22332803 Ιστοσελίδα: <http://www.moa.gov.cy/vs>

13.3 Cancer Statistics

13.3.1 Liver cancer Statistics

It is estimated that 22,620 men and women (16,410 men and 6,210 women) will be diagnosed with and 18,160 men and women will die of cancer of the liver and intrahepatic bile duct in 2009.

The following information is based on National Cancer Institute's (NCI) Surveillance Epidemiology and End Results (SEER) Cancer Statistics Review.

Incidence & Mortality with liver cancer

SEER Incidence with liver cancer

From 2002-2006, the median age at diagnosis for cancer of the liver and intrahepatic bile duct was 64 years of age. Approximately 1.1% was diagnosed under age 20; 1.0% between 20 and 34; 3.7% between 35 and 44; 20.3% between 45 and 54; 24.6% between 55 and 64; 23.5% between 65 and 74; 19.8% between 75 and 84; and 5.9% 85+ years of age.

The age-adjusted incidence rate was 6.6 per 100,000 men and women per year. These rates are based on cases diagnosed in 2002-2006 from 17 SEER geographic areas.

Incidence Rates by Race		
Race/Ethnicity	Male	Female
All Races	10.2 per 100,000 men	3.6 per 100,000 women
White	8.6 per 100,000 men	3.0 per 100,000 women
Black	13.4 per 100,000 men	4.2 per 100,000 women
Asian/Pacific Islander	21.4 per 100,000 men	8.3 per 100,000 women
American Indian/Alaska Native	13.6 per 100,000 men	6.6 per 100,000 women
Hispanic	15.2 per 100,000 men	5.9 per 100,000 women

Table 13.1: Incidence rates by race of cancer of the liver and intrahepatic bile duct (NCI) [51].

US Mortality with liver cancer

From 2002-2006, the median age at death for cancer of the liver and intrahepatic bile duct was 70 years of age. Approximately 0.3% died under age 20; 0.7% between 20 and 34; 2.5% between 35 and 44; 15.0% between 45 and 54; 20.5% between 55 and 64; 24.1% between 65 and 74; 26.2% between 75 and 84; and 10.7% 85+ years of age.

The age-adjusted death rate was 5.1 per 100,000 men and women per year. These rates are based on patients who died in 2002-2006 in the US.

Death Rates by Race		
Race/Ethnicity	Male	Female
All Races	7.5 per 100,000 men	3.2 per 100,000 women
White	6.8 per 100,000 men	2.9 per 100,000 women
Black	10.8 per 100,000 men	3.9 per 100,000 women
Asian/Pacific Islander	15.0 per 100,000 men	6.6 per 100,000 women
American Indian/Alaska Native	10.3 per 100,000 men	6.5 per 100,000 women
Hispanic	11.3 per 100,000 men	5.1 per 100,000 women

Table 13.2: Death rates by race of cancer for the liver and intrahepatic bile duct (NCI) [51].

13.3.2 Kidney cancer statistics

The following information was taken from National Cancer Institute (NCI) [51].

It is estimated that 57,760 men and women (35,430 men and 22,330 women) will be diagnosed with and 12,980 men and women will die of cancer of the kidney and renal pelvis in 2009

The following information is based on NCI's SEER Cancer Statistics Review.

Incidence & Mortality with kidney cancer (SEER)

SEER Incidence with kidney cancer

From 2002-2006, the median age at diagnosis for cancer of the kidney and renal pelvis was 64 years of age. Approximately 1.3% was diagnosed under age 20; 1.5% between 20 and 34; 6.1% between 35 and 44; 16.4% between 45 and 54; 24.6% between 55 and 64; 24.3% between 65 and 74; 20.0% between 75 and 84; and 5.7% 85+ years of age.

The age-adjusted incidence rate was 13.6 per 100,000 men and women per year. These rates are based on cases diagnosed in 2002-2006 from 17 SEER geographic areas.

Incidence Rates by Race		
Race/Ethnicity	Male	Female
All Races	18.6 per 100,000 men	9.5 per 100,000 women
White	19.2 per 100,000 men	9.9 per 100,000 women
Black	21.3 per 100,000 men	10.3 per 100,000 women
Asian/Pacific Islander	9.6 per 100,000 men	4.8 per 100,000 women
American Indian/Alaska Native	21.7 per 100,000 men	14.1 per 100,000 women
Hispanic	17.6 per 100,000 men	9.6 per 100,000 women

Table 13.3: Incidence rates by race of cancer for the kidney and renal pelvis in 2009 (NCI) [51].

US Mortality with kidney cancer

From 2002-2006, the median age at death for cancer of the kidney and renal pelvis was 71 years of age. Approximately 0.5% died under age 20; 0.5% between 20 and 34; 2.4% between 35 and 44; 10.2% between 45 and 54; 20.0% between 55 and 64; 25.4% between 65 and 74; 27.9% between 75 and 84; and 13.2% 85+ years of age.

The age-adjusted death rate was 4.1 per 100,000 men and women per year. These rates are based on patients who died in 2002-2006 in the US.

Death Rates by Race		
Race/Ethnicity	Male	Female
All Races	6.0 per 100,000 men	2.7 per 100,000 women
White	6.1 per 100,000 men	2.8 per 100,000 women
Black	6.0 per 100,000 men	2.7 per 100,000 women
Asian/Pacific Islander	2.4 per 100,000 men	1.2 per 100,000 women
American Indian/Alaska Native	9.0 per 100,000 men	4.2 per 100,000 women
Hispanic	5.2 per 100,000 men	2.4 per 100,000 women

Table 13.4: Death rates by race of cancer for kidney and renal pelvis in 2009 (NCI) [51].

13.3.3 Pancreatic cancer statistics

The following information was taken from National Cancer Institute (NCI) [51].

It is estimated that 42,470 men and women (21,050 men and 21,420 women) will be diagnosed with and 35,240 men and women will die of cancer of the pancreas in 2009

The following information is based on NCI's SEER Cancer Statistics Review.

Incidence & Mortality with pancreatic cancer

SEER Incidence with pancreatic cancer

From 2002-2006, the median age at diagnosis for cancer of the pancreas was 72 years of age. Approximately 0.0% was diagnosed under age 20; 0.4% between 20 and 34; 2.4% between 35 and 44; 9.6% between 45 and 54; 19.2% between 55 and 64; 26.1% between 65 and 74; 29.4% between 75 and 84; and 12.8% 85+ years of age.

The age-adjusted incidence rate was 11.7 per 100,000 men and women per year. These rates are based on cases diagnosed in 2002-2006 from 17 SEER geographic areas.

Incidence Rates by Race		
Race/Ethnicity	Male	Female
All Races	13.1 per 100,000 men	10.4 per 100,000 women
White	13.1 per 100,000 men	10.2 per 100,000 women
Black	16.6 per 100,000 men	14.6 per 100,000 women
Asian/Pacific Islander	10.1 per 100,000 men	8.2 per 100,000 women
American Indian/Alaska Native	10.2 per 100,000 men	9.3 per 100,000 women
Hispanic	11.1 per 100,000 men	10.2 per 100,000 women

Table 13.5: Incident rates by race of pancreatic cancer 2009 (NCI) [50].

US Mortality with pancreatic cancer

From 2002-2006, the median age at death for cancer of the pancreas was 73 years of age. Approximately 0.0% died under age 20; 0.2% between 20 and 34; 1.7% between 35 and 44; 8.2% between 45 and 54; 17.9% between 55 and 64; 25.9% between 65 and 74; 31.1% between 75 and 84; and 14.9% 85+ years of age.

The age-adjusted death rate was 10.7 per 100,000 men and women per year. These rates are based on patients who died in 2002-2006 in the US.

Death Rates by Race		
Race/Ethnicity	Male	Female
All Races	12.3 per 100,000 men	9.3 per 100,000 women
White	12.2 per 100,000 men	9.1 per 100,000 women
Black	15.4 per 100,000 men	12.4 per 100,000 women
Asian/Pacific Islander	8.1 per 100,000 men	7.0 per 100,000 women
American Indian/Alaska Native	9.1 per 100,000 men	7.8 per 100,000 women
Hispanic	9.1 per 100,000 men	7.5 per 100,000 women

Table 13.6: Death rates by race of pancreatic cancer 2009 (NCI) [51].

13.3.4 Thyroid cancer statistics

It is estimated that 56,460 men and women (13,250 men and 43,210 women) will be diagnosed with and 1,780 men and women will die of cancer of the thyroid in 2012.

The following information is based on NCI's SEER Cancer Statistics Review.

Incidence & Mortality with thyroid cancer

SEER Incidence with thyroid cancer

From 2005-2009, the median age at diagnosis for cancer of the thyroid was 50 years of age. Approximately 1.8% was diagnosed under age 20; 15.5% between 20 and 34; 20.4% between 35 and 44; 24.3% between 45 and 54; 19.0% between 55 and 64; 11.7% between 65 and 74; 5.9% between 75 and 84; and 1.4% 85+ years of age.

The age-adjusted incidence rate was 11.6 per 100,000 men and women per year. These rates are based on cases diagnosed in 2005-2009 from 18 SEER geographic areas.

Incidence Rates by Race		
Race/Ethnicity	Male	Female
All Races	5.9 per 100,000 men	17.3 per 100,000 women
White	6.2 per 100,000 men	18.3 per 100,000 women
Black	3.3 per 100,000 men	10.1 per 100,000 women
Asian/Pacific Islander	5.3 per 100,000 men	17.7 per 100,000 women
American Indian/Alaska Native	3.2 per 100,000 men	10.9 per 100,000 women
Hispanic	4.2 per 100,000 men	16.0 per 100,000 women

Table 13.7: Incident rates by race of thyroid cancer 2009 (NCI) [50].

US Mortality with thyroid cancer

From 2005-2009, the median age at death for cancer of the thyroid was 73 years of age. Approximately 0.1% died under age 20; 0.8% between 20 and 34; 2.2% between 35 and 44; 8.3% between 45 and 54; 16.9% between 55 and 64; 24.7% between 65 and 74; 29.8% between 75 and 84; and 17.3% 85+ years of age.

The age-adjusted death rate was 0.5 per 100,000 men and women per year. These rates are based on patients who died in 2005-2009 in the US.

Death Rates by Race		
Race/Ethnicity	Male	Female
All Races	0.5 per 100,000 men	0.5 per 100,000 women
White	0.5 per 100,000 men	0.5 per 100,000 women
Black	0.4 per 100,000 men	0.6 per 100,000 women
Asian/Pacific Islander	0.5 per 100,000 men	0.8 per 100,000 women
Hispanic	0.5 per 100,000 men	0.6 per 100,000 women

Table 13.8: Death rates by race of thyroid cancer 2009 (NCI) [51].

Lifetime Risk

Based on rates from 2007-2009, 1.03% of men and women born today will be diagnosed with cancer of the thyroid at some time during their lifetime. This number can also be expressed as 1 in 97 men and women will be diagnosed with cancer of the thyroid during their lifetime. These statistics are called the lifetime risk of developing cancer. Sometimes it is more useful to look at the probability of developing cancer of the thyroid between two age groups. For example, 0.24% of men will develop cancer of the thyroid between their 50th and 70th birthdays compared to 0.60% for women.

13.3.5 Brain and other nervous system

It is estimated that 22,910 men and women (12,630 men and 10,280 women) will be diagnosed with and 13,700 men and women will die of cancer of the brain and other nervous system in 2012.

The following information is based on NCI's SEER Cancer Statistics Review Brain and Other Nervous System Section

Incidence & Mortality with brain cancer and other nervous system

SEER Incidence with brain and other nervous system.

From 2005-2009, the median age at diagnosis for cancer of the brain and other nervous system was 57 years of age. Approximately 13.0% were diagnosed under age 20; 8.8% between 20 and 34; 9.2% between 35 and 44; 14.8% between 45 and 54; 19.0% between 55 and 64; 16.7% between 65 and 74; 13.8% between 75 and 84; and 4.7% 85+ years of age.

The age-adjusted incidence rate was 6.5 per 100,000 men and women per year. These rates are based on cases diagnosed in 2005-2009 from 18 SEER geographic areas.

Incidence Rates by Race		
Race/Ethnicity	Male	Female
All Races	7.7 per 100,000 men	5.4 per 100,000 women
White	8.4 per 100,000 men	5.9 per 100,000 women
Black	4.7 per 100,000 men	3.6 per 100,000 women
Asian/Pacific Islander	4.1 per 100,000 men	3.1 per 100,000 women
American Indian/Alaska Native	3.9 per 100,000 men	3.8 per 100,000 women
Hispanic	5.9 per 100,000 men	4.7 per 100,000 women

Table 13.9: Incident rates by race of brain and nervous system 2009 (NCI) [50].

US Mortality

From 2005-2009, the median age at death for cancer of the brain and other nervous system was 64 years of age. Approximately 3.9% died under age 20; 3.7% between 20 and 34; 6.5% between 35 and 44; 14.6% between 45 and 54; 22.5% between 55 and 64; 22.5% between 65 and 74; 19.4% between 75 and 84; and 6.9% 85+ years of age. The age-adjusted death rate was 4.3 per 100,000 men and women per year. These rates are based on patients who died in 2005-2009 in the US.

Trends in Rates

Trends in rates can be described in many ways. Information for trends over a fixed period of time, for example 1996-2009, can be evaluated by the annual percentage change (APC). The average annual percent change over several years. The APC is used to measure trends or the change in rates over time. For information on how this is calculated, go to Trend Algorithms in the SEER*Stat Help system. The calculation involves fitting a straight line to the natural logarithm of the data when it is displayed by calendar year. (See Fast Stats for trends over fixed time intervals) . If there is a negative sign before the number, the trend is a decrease; otherwise it is an increase. If there is an asterisk after the APC then the trend was significant, that is, one believes that it is beyond chance, i.e. 95% sure, that the increase or decrease is real over the period 1996-2009.

A statistical model for characterizing cancer trends which uses statistical criteria to determine how many times and when the trends in incidence or mortality rates have changed. The results of joinpoint are given as calendar year ranges, and the annual percent change (APC) in the rates over each period can be used over a long period of time to evaluate when changes in the trend have occurred along with the APC which shows how much the trend has changed between each of the joinpoints.

13.3.6 World Health Organization: International Agency for research on Cancer; World statistics for liver, pancreas, kidney and thyroid cancer.

Lung cancer is the most common cancer worldwide, accounting for 1.2 million new cases annually; followed by cancer of the breast, just over 1 million cases; colorectal, 940,000; stomach, 870,000; liver, 560,000; cervical, 470,000; esophageal, 410,000; head and neck, 390,000; bladder, 330,000; malignant non-Hodgkin lymphomas, 290,000; leukemia, 250,000; prostate and testicular, 250,000; pancreatic, 216,000; ovarian, 190,000; kidney, 190,000; endometrial, 188,000; nervous system, 175,000; melanoma, 133,000; thyroid, 123,000; pharynx, 65,000; and Hodgkin disease, 62,000 cases.

The three leading cancer killers are different than the three most common forms, with lung cancer responsible for 17.8 per cent of all cancer deaths, stomach, 10.4 per cent and liver, 8.8 per cent [55].

Liver Cancer	Incidence			Mortality			5-year prevalence		
	Number	(%)	ASR (W)	Number	(%)	ASR (W)	Number	(%)	Prop.
Men	523432	7.9	16.0	478134	11.3	14.5	433207	3.2	17.6
Women	226312	3.7	6.0	217592	6.5	5.7	180006	1.2	7.3
Both sexes	749744	5.9	10.8	695726	9.2	9.9	613213	2.1	12.5
All cancers excl. non-melanoma skin cancer (men)	6617844	100.0	202.8	4219626	100.0	127.9	13514868	100.0	550.6
All cancers excl. non-melanoma skin cancer (women)	6044710	100.0	164.4	3345176	100.0	87.2	15288300	100.0	620.8
All cancers excl. non-melanoma skin cancer (both sexes)	12662554	100.0	180.8	7564802	100.0	105.6	28803166	100.0	585.8
<i>Incidence and mortality data for all ages. 5-year prevalence for adult population only. ASR (W) and proportions per 100,000.</i>									

Table 13.10: Estimated incidence, mortality and 5-year prevalence: Liver Cancer [55]

Pancreatic Cancer	Incidence			Mortality			5-year prevalence		
	Number	(%)	ASR (W)	Number	(%)	ASR (W)	Number	(%)	Prop.
Men	144859	2.2	4.4	138377	3.3	4.2	91997	0.7	3.8
Women	133825	2.2	3.3	128292	3.8	3.1	80495	0.5	3.3
Both sexes	278684	2.2	3.9	266669	3.5	3.7	172492	0.6	3.5
All cancers excl. non-melanoma skin cancer (men)	6617844	100.0	202.8	4219626	100.0	127.9	13514868	100.0	550.6
All cancers excl. non-melanoma skin cancer (women)	6044710	100.0	164.4	3345176	100.0	87.2	15288300	100.0	620.8
All cancers excl. non-melanoma skin cancer (both sexes)	12662554	100.0	180.8	7564802	100.0	105.6	28803166	100.0	585.8
<i>Incidence and mortality data for all ages. 5-year prevalence for adult population only. ASR (W) and proportions per 100,000.</i>									

Table 13.11: Estimated incidence, mortality and 5-year prevalence: Pancreatic Cancer [55]

Kidney Cancer	Incidence			Mortality			5-year prevalence		
	Number	(%)	ASR (W)	Number	(%)	ASR (W)	Number	(%)	Prop.
Men	169155	2.6	5.2	72019	1.7	2.2	466631	3.5	19.0
Women	104363	1.7	2.8	44349	1.3	1.1	277559	1.8	11.3
Both sexes	273518	2.2	4.0	116368	1.5	1.6	744190	2.6	15.1
All cancers excl. non-melanoma skin cancer (men)	6617844	100.0	202.8	4219626	100.0	127.9	13514868	100.0	550.6
All cancers excl. non-melanoma skin cancer (women)	6044710	100.0	164.4	3345176	100.0	87.2	15288300	100.0	620.8
All cancers excl. non-melanoma skin cancer (both sexes)	12662554	100.0	180.8	7564802	100.0	105.6	28803166	100.0	585.8
<i>Incidence and mortality data for all ages. 5-year prevalence for adult population only. ASR (W) and proportions per 100,000.</i>									

Table 13.12: Estimated incidence, mortality and 5-year prevalence: Kidney Cancer [55].

Thyroid Cancer	Incidence			Mortality			5-year prevalence		
	Number	(%)	ASR (W)	Number	(%)	ASR (W)	Number	(%)	Prop.
Men	49211	0.7	1.5	11206	0.3	0.3	195097	1.4	7.9
Women	163968	2.7	4.7	24177	0.7	0.6	667377	4.4	27.1
Both sexes	213179	1.7	3.1	35383	0.5	0.5	862474	3.0	17.5
All cancers excl. non-melanoma skin cancer (men)	6617844	100.0	202.8	4219626	100.0	127.9	13514868	100.0	550.6
All cancers excl. non-melanoma skin cancer (women)	6044710	100.0	164.4	3345176	100.0	87.2	15288300	100.0	620.8
All cancers excl. non-melanoma skin cancer (both sexes)	12662554	100.0	180.8	7564802	100.0	105.6	28803166	100.0	585.8
<i>Incidence and mortality data for all ages. 5-year prevalence for adult population only. ASR (W) and proportions per 100,000.</i>									

Table 13.13: Estimated incidence, mortality and 5-year prevalence: Thyroid Cancer [55].

Brain and nervous system Cancer	Incidence			Mortality			5-year prevalence		
	Number	(%)	ASR (W)	Number	(%)	ASR (W)	Number	(%)	Prop.
Men	126815	1.9	3.8	97251	2.3	2.9	171827	1.3	7.0
Women	111098	1.8	3.1	77629	2.3	2.2	145212	0.9	5.9
Both sexes	237913	1.9	3.5	174880	2.3	2.5	317039	1.1	6.4
All cancers excl. non-melanoma skin cancer (men)	6617844	100.0	202.8	4219626	100.0	127.9	13514868	100.0	550.6
All cancers excl. non-melanoma skin cancer (women)	6044710	100.0	164.4	3345176	100.0	87.2	15288300	100.0	620.8
All cancers excl. non-melanoma skin cancer (both sexes)	12662554	100.0	180.8	7564802	100.0	105.6	28803166	100.0	585.8
<i>Incidence and mortality data for all ages. 5-year prevalence for adult population only. ASR (W) and proportions per 100,000.</i>									

Table 13.14: Estimated incidence, mortality and 5-year prevalence: Brain and nervous system Cancer [55].

Summary statistics (2008)

WORLD	Male	Female	Both sexes
Population (thousands)	3414566	3358715	6773281
Number of new cancer cases (thousands)	6617.8	6044.7	12662.6
Age-standardised rate (W)	202.8	164.4	180.8
Risk of getting cancer before age 75 (%)	21.1	16.5	18.6
Number of cancer deaths (thousands)	4219.6	3345.2	7564.8
Age-standardised rate (W)	127.9	87.2	105.6
Risk of dying from cancer before age 75 (%)	13.4	9.1	11.1
5-year prevalent cases, adult population (thousands)	13514.9	15288.3	28803.2
Proportion (per 100,000)	550.6	620.8	585.8
5 most frequent cancers (ranking defined by total number of cases)			
	Lung	Breast	Lung
	Prostate	Colorectum	Breast
	Colorectum	Cervix uteri	Colorectum
	Stomach	Lung	Stomach
	Liver	Stomach	Prostate

Methods of estimation (summary)
Incidence: Population weighted average of the area-specific country rates applied to the 2008 area population.
Mortality: Population weighted average of the area-specific country rates applied to the 2008 area population.
Prevalence: Sum of area-specific prevalent cases

Glossary
<p>Age-standardised rate (W): A rate is the number of new cases or deaths per 100 000 persons per year. An age-standardised rate is the rate that a population would have if it had a standard age structure. Standardization is necessary when comparing several populations that differ with respect to age because age has a powerful influence on the risk of cancer.</p>
<p>Risk of getting or dying from the disease before age 75 (%): The probability or risk of individuals getting/dying from cancer. It is expressed as the number of new born children (out of 100) who would be expected to develop/die from cancer before the age of 75 if they had cancer rates (in the absence of other causes of death).</p>

Table 13.15: Summary cancer statistics [55]

13.4 Software Coding

The code below is written using MATLAB (The Mathworks Inc., Natick, MA) and is the code for reading the temperature at the focal point of the HIFU Transducer.

```
function varargout = Interface_09_25_08(varargin)
%29/01/09
%INTERFACE_09_25_08 M-file for Interface_09_25_08.fig
%   INTERFACE_09_25_08, by itself, creates a new INTERFACE_09_25_08
or raises the existing
%   singleton*.
%
%   H = INTERFACE_09_25_08 returns the handle to a new
INTERFACE_09_25_08 or the handle to
%   the existing singleton*.
%
%   INTERFACE_09_25_08('CALLBACK',hObject,eventData,handles,...)
calls the local
%   function named CALLBACK in INTERFACE_09_25_08.M with the given
input arguments.
%
%   INTERFACE_09_25_08('Property','Value',...) creates a new
INTERFACE_09_25_08 or raises the
%   existing singleton*. Starting from the left, property value
pairs are
%   applied to the GUI before Interface_09_25_08_OpeningFunction
gets called. An
%   unrecognized property name or invalid value makes property
application
%   stop. All inputs are passed to Interface_09_25_08_OpeningFcn
via varargin.
%
%   *See GUI Options on GUIDE's Tools menu. Choose "GUI allows
only one
%   instance to run (singleton)".
%
% See also: GUIDE, GUIDATA, GUIHANDLES

% Edit the above text to modify the response to help
Interface_09_25_08

% Last Modified by GUIDE v2.5 30-Sep-2008 15:45:23

% Begin initialization code - DO NOT EDIT
gui_Singleton = 1;
gui_State = struct('gui_Name',       mfilename, ...
                  'gui_Singleton',  gui_Singleton, ...
                  'gui_OpeningFcn', @Interface_09_25_08_OpeningFcn,
                  ...
                  'gui_OutputFcn',  @Interface_09_25_08_OutputFcn,
                  ...
                  'gui_LayoutFcn',   [] , ...
                  'gui_Callback',    []);
if nargin && ischar(varargin{1})
    gui_State.gui_Callback = str2func(varargin{1});
end

if nargout
    [varargout{1:nargout}] = gui_mainfcn(gui_State, varargin{:});
```

```

else
    gui_mainfcn(gui_State, varargin{:});
end
% End initialization code - DO NOT EDIT

daqregister('c:\MATLAB7\toolbox\daq\daq\private\mwnidaq.dll')
% --- Executes just before Interface_09_25_08 is made visible.
function Interface_09_25_08_OpeningFcn(hObject, eventdata, handles,
varargin)
% This function has no output args, see OutputFcn.
% hObject    handle to figure
% eventdata  reserved - to be defined in a future version of MATLAB
% handles    structure with handles and user data (see GUIDATA)
% varargin   command line arguments to Interface_09_25_08 (see
VARARGIN)

% Choose default command line output for Interface_09_25_08
handles.output = hObject;

% Update handles structure
guidata(hObject, handles);

% UIWAIT makes Interface_09_25_08 wait for user response (see
UIRESUME)
% uiwait(handles.figure1);

% --- Outputs from this function are returned to the command line.
function varargout = Interface_09_25_08_OutputFcn(hObject, eventdata,
handles)
% varargout  cell array for returning output args (see VARARGOUT);
% hObject    handle to figure
% eventdata  reserved - to be defined in a future version of MATLAB
% handles    structure with handles and user data (see GUIDATA)

% Get default command line output from handles structure
varargout{1} = handles.output;

% --- Executes on button press in Btnstart.
function Btnstart_Callback(hObject, eventdata, handles)
% hObject    handle to Btnstart (see GCBO)
% eventdata  reserved - to be defined in a future version of MATLAB
% handles    structure with handles and user data (see GUIDATA)

%tcount = intmin;
for tcount = 0:1:1000
    t = timer('TimerFcn', 'stat=false;
disp(''Timer!'')', 'StartDelay', 0.01);
    start(t)
    wait(t)
    disp(tcount);
    set(handles.txttime, 'string', num2str(tcount/100));
end
%stat=true;
%while(stat==true)

    %txttime.string = tcount;
    %set(handles.txttime, 'string', int2str(tcount));
    % tcount =tcount +1

```

```

    %if (tcount == 20000)
    % stat=false
        %stop(t);
    % end

    %disp('.');
%end %END WHILE

function txttime_Callback(hObject, eventdata, handles)
% hObject    handle to txttime (see GCBO)
% eventdata  reserved - to be defined in a future version of MATLAB
% handles    structure with handles and user data (see GUIDATA)

% Hints: get(hObject,'String') returns contents of txttime as text
%        str2double(get(hObject,'String')) returns contents of txttime
as a double

% --- Executes during object creation, after setting all properties.
function txttime_CreateFcn(hObject, eventdata, handles)
% hObject    handle to txttime (see GCBO)
% eventdata  reserved - to be defined in a future version of MATLAB
% handles    empty - handles not created until after all CreateFcns
called

% Hint: edit controls usually have a white background on Windows.
%        See ISPC and COMPUTER.
if ispc && isequal(get(hObject,'BackgroundColor'),
get(0,'defaultUiControlBackgroundColor'))
    set(hObject,'BackgroundColor','white');
end

% --- Executes on button press in txtExit.
function txtExit_Callback(hObject, eventdata, handles)
% hObject    handle to txtExit (see GCBO)
% eventdata  reserved - to be defined in a future version of MATLAB
% handles    structure with handles and user data (see GUIDATA)
close

% --- Executes on button press in BtnStop.
function BtnStop_Callback(hObject, eventdata, handles)
% hObject    handle to BtnStop (see GCBO)
% eventdata  reserved - to be defined in a future version of MATLAB
% handles    structure with handles and user data (see GUIDATA)

stop(t)

function txttemper_Callback(hObject, eventdata, handles)
% hObject    handle to txttemper (see GCBO)
% eventdata  reserved - to be defined in a future version of MATLAB
% handles    structure with handles and user data (see GUIDATA)

% Hints: get(hObject,'String') returns contents of txttemper as text

```

```

%         str2double(get(hObject,'String')) returns contents of
txttemper as a double

% --- Executes during object creation, after setting all properties.
function txttemper_CreateFcn(hObject, eventdata, handles)
% hObject    handle to txttemper (see GCBO)
% eventdata  reserved - to be defined in a future version of MATLAB
% handles    empty - handles not created until after all CreateFcns
called

% Hint: edit controls usually have a white background on Windows.
%         See ISPC and COMPUTER.
if ispc && isequal(get(hObject,'BackgroundColor'),
get(0,'defaultUiControlBackgroundColor'))
    set(hObject,'BackgroundColor','white');
end

% --- Executes on button press in btnTemper.
function btnTemper_Callback(hObject, eventdata, handles)
% hObject    handle to btnTemper (see GCBO)
% eventdata  reserved - to be defined in a future version of MATLAB
% handles    structure with handles and user data (see GUIDATA)

TFileName = ''
%while TfileName == ''
TFileName = get(handles.txttempfile , 'string' );
%end % WHILE

filename = txttempfile.String
fid = fopen(TFileName, 'wt');
%Open file <lblfilename>, the mode wt is to open a text file for
writing

TempRead = 1;
% Keep on measuring the temperature as lon as tempRead is true.
TempRead
% will become false if the stop reading button is pressed

ai=analoginput('nidaq','dev2')
%Create analog input object
%ai = analoginput('adaptor')
%ai = analoginput('adaptor',ID)
%Arguments'adaptor'The hardware driver adaptor name. The supported
adaptors are advantech, hpe1432, keithley, mcc, nidaq, and winsound.
%ID The hardware device identifier. ID is optional

chans = addchannel(ai,1)
% Add hardware channels to analog input or analog output object

tic
%tic starts the clock toc is the ellapsed time since tic was initiated
TSamplesCount = 0;
while TempRead == 1
    % Keep on measuring the temperature as lon as tempRead is true.
    TempRead
    TSamplesCount = TSamplesCount + 1;
start(ai);
inter = 100;

```

```

data = getdata(ai,inter)
stop(ai);
%data is an array which in this case will get 100 values of temperature
in
%1/10 of a second

Sumtemp = 0;
%The for loop below will calculate the average temperature of 100
readings
for dcount = 1:1:inter
    Sumtemp = Sumtemp + data(dcount);

% 1000 samples per second - the average of 100 inter, sample in 1/10
of a second is calculated
end % FOR
fprintf(fid, '%10.4f\n', data(dcount)* 1000);
% Write each temperature reading in to the file
% 1mV per 1 degree celcius
AvgTemp = 1000*(Sumtemp / inter);
toc;
t= toc;
fprintf(fid, '%4.0f\t %10.4f\t %10.4f\n',TSamplesCount, AvgTemp, t);
%write the average of inter readings into the file
%disp(AvgTemp);

set(handles.txttemper, 'string',num2str(AvgTemp));
set(handles.txttime, 'string',num2str(t));
%Display tcount/100 on the txttime on GUI

end %WHILE

fclose(fid)
% --- Executes on button press in txtStopTempRead.
function txtStopTempRead_Callback(hObject, eventdata, handles)
% hObject    handle to txtStopTempRead (see GCBO)
% eventdata  reserved - to be defined in a future version of MATLAB
% handles    structure with handles and user data (see GUIDATA)

TempRead = 0

function txttempfile_Callback(hObject, eventdata, handles)
% hObject    handle to txttempfile (see GCBO)
% eventdata  reserved - to be defined in a future version of MATLAB
% handles    structure with handles and user data (see GUIDATA)

% Hints: get(hObject,'String') returns contents of txttempfile as text
%        str2double(get(hObject,'String')) returns contents of
txttempfile as a double

% --- Executes during object creation, after setting all properties.
function txttempfile_CreateFcn(hObject, eventdata, handles)
% hObject    handle to txttempfile (see GCBO)
% eventdata  reserved - to be defined in a future version of MATLAB
% handles    empty - handles not created until after all CreateFcns
called

% Hint: edit controls usually have a white background on Windows.
%        See ISPC and COMPUTER.

```

```

if ispc && isequal(get(hObject,'BackgroundColor'),
get(0,'defaultUiControlBackgroundColor'))
    set(hObject,'BackgroundColor','white');
end

```

The code below is written using MATLAB (The Mathworks Inc., Natick, MA) and is the code for that provides the graphical user interface for the end user and drives the motors of the robot. Other features added to this user interface are explained in chapter 9.

```

function varargout = sonomri_main_page(varargin)
% SONOMRI_MAIN_PAGE_NEW M-file for sonomri_main_page.fig
%     SONOMRI_MAIN_PAGE_NEW, by itself, creates a new
SONOMRI_MAIN_PAGE or raises the existing
%     singleton*.
%
%     H = SONOMRI_MAIN_PAGE returns the handle to a new
SONOMRI_MAIN_PAGE or the handle to
%     the existing singleton*.
%
%     SONOMRI_MAIN_PAGE('CALLBACK',hObject,eventData,handles,...)
calls the local
%     function named CALLBACK in SONOMRI_MAIN_PAGE.M with the given
input arguments.
%
%     SONOMRI_MAIN_PAGE('Property','Value',...) creates a new
SONOMRI_MAIN_PAGE or raises the
%     existing singleton*. Starting from the left, property value
pairs are
%     applied to the GUI before sonomri_main_page_OpeningFunction
gets called. An
%     unrecognized property name or invalid value makes property
application
%     stop. All inputs are passed to
sonomri_main_page_new_OpeningFcn via varargin.
%
%     *See GUI Options on GUIDE's Tools menu. Choose "GUI allows
only one
%     instance to run (singleton)".
%
% See also: GUIDE, GUIDATA, GUIHANDLES

% Copyright 2002-2003 The MathWorks, Inc.

% Edit the above text to modify the response to help sonomri_main_page

% Last Modified by GUIDE v2.5 31-May-2007 10:40:50

% Begin initialization code - DO NOT EDIT
gui_Singleton = 1;
gui_State = struct('gui_Name',       mfilename, ...
                  'gui_Singleton',  gui_Singleton, ...
                  'gui_OpeningFcn', @sonomri_main_page_OpeningFcn,
                  ...
                  'gui_OutputFcn',  @sonomri_main_page_OutputFcn, ...
                  'gui_LayoutFcn',  [] , ...
                  'gui_Callback',   []);
if nargin && ischar(varargin{1})
    gui_State.gui_Callback = str2func(varargin{1});
end

```

```

if nargout
    [varargout{1:nargout}] = gui_mainfcn(gui_State, varargin{:});
else
    gui_mainfcn(gui_State, varargin{:});
end
% End initialization code - DO NOT EDIT

% --- Executes just before sonomri_main_page is made visible.

function sonomri_main_page_OpeningFcn(hObject, eventdata, handles,
varargin)
% This function has no output args, see OutputFcn.
% hObject    handle to figure
% eventdata  reserved - to be defined in a future version of MATLAB
% handles    structure with handles and user data (see GUIDATA)
% varargin   command line arguments to sonomri_main_page_new (see
VARARGIN)

% The statemnt below is needed to register the NI DAQ drivers. It is
done
% only once.

% Choose default command line output for sonomri_main_page_new
handles.output = hObject;

% Update handles structure
guidata(hObject, handles);

initial_dir='C:\matlab7\dicom';
load_listbox(initial_dir,handles)

% UIWAIT makes sonomri_main_page_new wait for user response (see
UIRESUME)
% uiwait(handles.figure1);

% --- Outputs from this function are returned to the command line.

function varargout = sonomri_main_page_OutputFcn(hObject, eventdata,
handles)
% varargout  cell array for returning output args (see VARARGOUT);
% hObject    handle to figure
% eventdata  reserved - to be defined in a future version of MATLAB
% handles    structure with handles and user data (see GUIDATA)

% Get default command line output from handles structure
varargout{1} = handles.output;

% --- Executes on selection change in power.
function power_Callback(hObject, eventdata, handles)
% hObject    handle to power (see GCBO)
% eventdata  reserved - to be defined in a future version of MATLAB
% handles    structure with handles and user data (see GUIDATA)

```

```

% Hints: contents = get(hObject,'String') returns power contents as
cell array
%         contents{get(hObject,'Value')} returns selected item from
power

volt=str2double(get(hObject,'String')) %reads voltage frpm command
line.

handles.voltage=volt    %Stores V(1) to handle structure which is
accessible in all
% objects

guidata(hObject,handles) % Saves new structure of handles

% --- Executes during object creation, after setting all properties.
function power_CreateFcn(hObject, eventdata, handles)
% hObject    handle to power (see GCBO)
% eventdata  reserved - to be defined in a future version of MATLAB
% handles    empty - handles not created until after all CreateFcns
called

% Hint: popmenu controls usually have a white background on Windows.
%         See ISPC and COMPUTER.
if ispc
    set(hObject,'BackgroundColor','white');
else

set(hObject,'BackgroundColor',get(0,'defaultUicontrolBackgroundColor')
);
end

% --- Executes on selection change in frequency.
function frequency_Callback(hObject, eventdata, handles)
% hObject    handle to frequency (see GCBO)
% eventdata  reserved - to be defined in a future version of MATLAB
% handles    structure with handles and user data (see GUIDATA)

% Hints: contents = get(hObject,'String') returns frequency contents
as cell array
%         contents{get(hObject,'Value')} returns selected item from
frequency

freq=str2double(get(hObject,'String')); %reads frequency

handles.frequency=freq;    %Stores V(1) to handle structure which is
accessible in all
% objects

guidata(hObject,handles);

% --- Executes during object creation, after setting all properties.
function frequency_CreateFcn(hObject, eventdata, handles)
% hObject    handle to frequency (see GCBO)
% eventdata  reserved - to be defined in a future version of MATLAB

```

```

% handles      empty - handles not created until after all CreateFcns
called

% Hint: popupmenu controls usually have a white background on Windows.
%      See ISPC and COMPUTER.
if ispc
    set(hObject,'BackgroundColor','white');
else

set(hObject,'BackgroundColor',get(0,'defaultUiControlBackgroundColor')
);
end

% --- Executes on button press in powerON.

function powerON_Callback(hObject, eventdata, handles)
% hObject      handle to powerON (see GCBO)
% eventdata    reserved - to be defined in a future version of MATLAB
% handles      structure with handles and user data (see GUIDATA)

% s = serial('COM1');          % Creates a serial port interface
% fopen(s);                    % Opens the serial port.

f=handles.frequency;          % Calls the frequency handle
f=f*1000000;                   % Converts MHz to HZ.

fstring=int2str(f); % Converts integer to string
fstringnew=['frequency ',fstring]; % Concatanates frequency and
frequency                                     % value in the format required
by Agilent generator.

%fprintf(s,fstringnew); % Sent frequency to generator.

v=handles.voltage;            % Calls handle voltage which is
in mV.
v=int2str(v);

Vstring=['VOLtage ',v,'E-3']; % Concatanates voltage and
voltage                                     % value in the format required by
Agilent generator.
%fprintf(s,Vstring); % Sent voltage to generator.

timing(handles.timeON,handles) % Duration that power is ON.

%fclose(s);
%delete(s);
%clear s;

% --- Executes on button press in PowerOFF.
function PowerOFF_Callback(hObject, eventdata, handles)
% hObject      handle to PowerOFF (see GCBO)
% eventdata    reserved - to be defined in a future version of MATLAB
% handles      structure with handles and user data (see GUIDATA)
%Global s

```

```

%s = serial('COM1');
%fopen(s);

v=55; % Sent a low-voltage (ie power OFF).
Vstring=int2str(v); % Converts integer to string
Vstringnew=['VOLTage ',Vstring,'E-3']; % Concatanates voltage and
voltage
% value in the format required by Agilent generator.

fprintf(s,Vstringnew); % Sent voltage to generator.

timing(handles.timeOFF,handles)

fclose(s);
delete(s);
clear s;

function duration_Callback(hObject, eventdata, handles)
% hObject handle to duration (see GCBO)
% eventdata reserved - to be defined in a future version of MATLAB
% handles structure with handles and user data (see GUIDATA)

% Hints: get(hObject,'String') returns contents of duration as text
% str2double(get(hObject,'String')) returns contents of
duration as a double

% Duration ultrasound is ON.
handles.timeON=str2double(get(hObject,'String'))
guidata(hObject,handles);

% --- Executes during object creation, after setting all properties.
function duration_CreateFcn(hObject, eventdata, handles)
% hObject handle to duration (see GCBO)
% eventdata reserved - to be defined in a future version of MATLAB
% handles empty - handles not created until after all CreateFcns
called

% Hint: edit controls usually have a white background on Windows.
% See ISPC and COMPUTER.
if ispc
set(hObject,'BackgroundColor','white');
else

set(hObject,'BackgroundColor',get(0,'defaultUicontrolBackgroundColor')
);
end

function xaxisdist_Callback(hObject, eventdata, handles)
% This function read x distance from an edit box.
% hObject handle to xaxisdist (see GCBO)
% eventdata reserved - to be defined in a future version of MATLAB
% handles structure with handles and user data (see GUIDATA)

% Hints: get(hObject,'String') returns contents of xaxisdist as text

```

```

%         str2double(get(hObject,'String')) returns contents of
xaxisdist as a double

xdist=str2double(get(hObject,'String')); %reads x distance to be
moved

handles.xdistance=xdist; %Stores x distance to handle structure
which is accesible in all
% objects

guidata(hObject,handles);

% --- Executes during object creation, after setting all properties.
function xaxisdist_CreateFcn(hObject, eventdata, handles)
% hObject    handle to xaxisdist (see GCBO)
% eventdata reserved - to be defined in a future version of MATLAB
% handles    empty - handles not created until after all CreateFcns
called

% Hint: edit controls usually have a white background on Windows.
%         See ISPC and COMPUTER.
if ispc
    set(hObject,'BackgroundColor','white');
else

set(hObject,'BackgroundColor',get(0,'defaultUicontrolBackgroundColor')
);
end

function yaxisdist_Callback(hObject, eventdata, handles)
% This function read y distance from an edit box.
% hObject    handle to yaxisdist (see GCBO)
% eventdata reserved - to be defined in a future version of MATLAB
% handles    structure with handles and user data (see GUIDATA)

% Hints: get(hObject,'String') returns contents of yaxisdist as text
%         str2double(get(hObject,'String')) returns contents of
yaxisdist as a double

ydist=str2double(get(hObject,'String')); %reads z distance to be
moved

handles.ydistance=ydist; %Stores y distance to handle structure
which is accesible in all
% objects

guidata(hObject,handles);

% --- Executes during object creation, after setting all properties.
function yaxisdist_CreateFcn(hObject, eventdata, handles)
% hObject    handle to yaxisdist (see GCBO)
% eventdata reserved - to be defined in a future version of MATLAB

```

```

% handles      empty - handles not created until after all CreateFcns
called

% Hint: edit controls usually have a white background on Windows.
%      See ISPC and COMPUTER.
if ispc
    set(hObject,'BackgroundColor','white');
else

set(hObject,'BackgroundColor',get(0,'defaultUiControlBackgroundColor')
);
end

function zaxisdist_Callback(hObject, eventdata, handles)
% This function read z distance from an edit box.
% hObject      handle to zaxisdist (see GCBO)
% eventdata    reserved - to be defined in a future version of MATLAB
% handles      structure with handles and user data (see GUIDATA)

% Hints: get(hObject,'String') returns contents of zaxisdist as text
%      str2double(get(hObject,'String')) returns contents of
zaxisdist as a double

zdist=str2double(get(hObject,'String')); %reads z distance to be
moved

handles.zdistance=zdist      %Stores z distance to handle structure
which is accesible in all
% objects

guidata(hObject,handles);

% --- Executes during object creation, after setting all properties.
function zaxisdist_CreateFcn(hObject, eventdata, handles)
% hObject      handle to zaxisdist (see GCBO)
% eventdata    reserved - to be defined in a future version of MATLAB
% handles      empty - handles not created until after all CreateFcns
called

% Hint: edit controls usually have a white background on Windows.
%      See ISPC and COMPUTER.
if ispc
    set(hObject,'BackgroundColor','white');
else

set(hObject,'BackgroundColor',get(0,'defaultUiControlBackgroundColor')
);
end

% --- Executes on button press in xmove.

function xmoveforward_Callback(hObject, eventdata, handles)
% hObject      handle to xmove (see GCBO)

```

```

% eventdata reserved - to be defined in a future version of MATLAB
% handles structure with handles and user data (see GUIDATA)

nx=handles.xdistance;
nx=16000000*nx;

%Creates a Digital output object
%dio=digitalio('nidaq',1); PCI 6602
dio=digitalio('nidaq','dev2')% USB 6251

% Creates output lines for port 0, line 0 (CW)
% terminal of the Shinsei driver.
addline(dio,0:7,0,'out');

% CW is initially set to logical high and since the ground is logical
low
% (zero) the motor does not move yet.
boarddata=logical([1 1 1 1 1 1 1 1]);

% Sends the above logical word to output port.
putvalue(dio,boarddata);

% The motor goes logical zero and since the Ground terminal of the
Shinsei driver is
% connected to ground, the motor starts to move.
boarddata(3)=0;
putvalue(dio,boarddata);

% Loop that establishes motion in the X forward axis.
for n = 1:nx
end

% To stop the motor you need to set the CW or CCW terminal to high

boarddata(3)=1; % High

% Puts the terminal CW or CCW to logical high and thus motor stops
putvalue(dio,boarddata);

% When you no longer need dio, you should remove it from
% memory and from the MATLAB workspace.
delete(dio)
clear dio

handles.x=handles.x+handles.xdistance;
guidata(hObject,handles);

%Sends the x position to the position display (text box)
set(handles.xposition,'String',handles.x)

% --- Executes on button press in xmoverreverse.
function xmoverreverse_Callback(hObject, eventdata, handles)
% hObject handle to xmoverreverse (see GCBO)
% eventdata reserved - to be defined in a future version of MATLAB
% handles structure with handles and user data (see GUIDATA)

```

```

nx=handles.xdistance;
nx=16000000*nx;

%Creates a Digital output object
%dio=digitalio('nidaq',1);    PCI 6602
dio=digitalio('nidaq','dev2')% USB 6251

% Creates output lines for port 0, line 0 (CCW)
% terminal of the Shinsei driver.
addline(dio,0:7,0,'out');

% CCW is initially set to logical high and since the ground is logical
low
% (zero) the motor does not move yet.
boarddata=logical([1 1 1 1 1 1 1 1]);

% Sends the above logical word to output port.
putvalue(dio,boarddata);

% The motor goes logical zero and since the Ground terminal of the
Shinsei driver is
% connected to ground, the motor starts to move.
boarddata(4)=0;
putvalue(dio,boarddata);

% Loop that establishes motion in the X reverse axis.
for n = 1:nx
end

% To stop the motor you need to set the CW or CCW terminal to high

boarddata(4)=1;          % High

% Puts the terminal CW or CCW to logical high and thus motor stops
putvalue(dio,boarddata);

% When you no longer need dio, you should remove it from
% memory and from the MATLAB workspace.
delete(dio)
clear dio

handles.x=handles.x-handles.xdistance;
guidata(hObject,handles);

%Sends the x position to the position display (text box)
set(handles.xposition,'String',handles.x)

% --- Executes on button press in ymoveleft.
function ymoveleft_Callback(hObject, eventdata, handles)
% hObject      handle to ymove (see GCBO)
% eventdata    reserved - to be defined in a future version of MATLAB
% handles      structure with handles and user data (see GUIDATA)

ny=handles.ydistance;
ny=9000000*ny;

```

```

%Creates a Digital output object
%dio=digitalio('nidaq',1);    PCI 6602
dio=digitalio('nidaq','dev2')% USB 6251

% Creates output lines for port 0, line 0 (CW)
% terminal of the Shinsei driver.
addline(dio,0:7,0,'out');

% CW is initially set to logical high and since the ground is logical
low
% (zero) the motor does not move yet.
boarddata=logical([1 1 1 1 1 1 1 1]);

% Sends the above logical word to output port.
putvalue(dio,boarddata);

% The motor goes logical zero and since the Ground terminal of the
Shinsei driver is
% connected to ground, the motor starts to move.
boarddata(1)=0;
putvalue(dio,boarddata);

% Loop that establishes motion in the Y left axis.
for n = 1:ny
end

% To stop the motor you need to set the CW or CCW terminal to high

boarddata(1)=1;          % High

% Puts the terminal CW or CCW to logical high and thus motor stops
putvalue(dio,boarddata);

% When you no longer need dio, you should remove it from
% memory and from the MATLAB workspace.
delete(dio)
clear dio

handles.y=handles.y+handles.ydistance;
guidata(hObject,handles);

%Sends the y position to the position display (text box)
set(handles.yposition,'String',handles.y)
set(handles.historylist,'String','yleft')

% --- Executes on button press in ymoveright.
function ymoveright_Callback(hObject, eventdata, handles)
% hObject      handle to ymoveright (see GCBO)
% eventdata    reserved - to be defined in a future version of MATLAB
% handles      structure with handles and user data (see GUIDATA)

ny=handles.ydistance;
ny=9000000*ny;

%Creates a Digital output object
%dio=digitalio('nidaq',1);    PCI 6602
dio=digitalio('nidaq','dev2')% USB 6251

```

```

% Creates output lines for port 0, line 0 (CCW)
% terminal of the Shinsei driver.
addline(dio,0:7,0,'out');

% CCW is initially set to logical high and since the ground is logical
low
% (zero) the motor does not move yet.
boarddata=logical([1 1 1 1 1 1 1 1]);

% Sends the above logical word to output port.
putvalue(dio,boarddata);

% The motor goes logical zero and since the Ground terminal of the
Shinsei driver is
% connected to ground, the motor starts to move.
boarddata(2)=0;
putvalue(dio,boarddata);

% Loop that establishes motion in the Y right axis.
for n = 1:ny
end

% To stop the motor you need to set the CW or CCW terminal to high

boarddata(2)=1;          % High

% Puts the terminal CW or CCW to logical high and thus motor stops
putvalue(dio,boarddata);

% When you no longer need dio, you should remove it from
% memory and from the MATLAB workspace.
delete(dio)
clear dio

handles.y=handles.y-handles.ydistance;
guidata(hObject,handles);

%Sends the y position to the position display (text box)
set(handles.yposition,'String',handles.y)
set(handles.historylist,'String','yright')

% --- Executes on button press in zmoveup.
function zmoveup_Callback(hObject, eventdata, handles)
% hObject      handle to zmove (see GCBO)
% eventdata    reserved - to be defined in a future version of MATLAB
% handles      structure with handles and user data (see GUIDATA)

nz=handles.zdistance;
nz=4000000*nz;

%Creates a Digital output object
%dio=digitalio('nidaq',1);    PCI 6602
dio=digitalio('nidaq','dev2')% USB 6251

% Creates output lines for port 0, line 0 (CCW)
% terminal of the Shinsei driver.
addline(dio,0:7,0,'out');

```

```

% CW is initially set to logical high and since the ground is logical
low
% (zero) the motor does not move yet.
boarddata=logical([1 1 1 1 1 1 1 1]);

% Sends the above logical word to output port.
putvalue(dio,boarddata);

% The motor goes logical zero and since the Ground terminal of the
Shinsei driver is
% connected to ground, the motor starts to move.
boarddata(5)=0;
putvalue(dio,boarddata);

% Loop that establishes motion in the Z up axis.
for n = 1:nz
end

% To stop the motor you need to set the CW or CCW terminal to high

boarddata(5)=1;          % High

% Puts the terminal CW or CCW to logical high and thus motor stops
putvalue(dio,boarddata);

% When you no longer need dio, you should remove it from
% memory and from the MATLAB workspace.
delete(dio)
clear dio

handles.z=handles.z+handles.zdistance;

%Sends the z position to the position display (text box)
set(handles.zposition,'String',handles.z)
guidata(hObject,handles);

% --- Executes on button press in zmovedown.
function zmovedown_Callback(hObject, eventdata, handles)
% hObject      handle to zmovedown (see GCBO)
% eventdata    reserved - to be defined in a future version of MATLAB
% handles      structure with handles and user data (see GUIDATA)

nz=handles.zdistance;
nz=4000000*nz;

%Creates a Digital output object
%dio=digitalio('nidaq',1);    PCI 6602
dio=digitalio('nidaq','dev2')% USB 6251

% Creates output lines for port 0, line 0 (CCW)
% terminal of the Shinsei driver.
addline(dio,0:7,0,'out');

% CCW is initially set to logical high and since the ground is logical
low
% (zero) the motor does not move yet.
boarddata=logical([1 1 1 1 1 1 1 1]);

```

```

% Sends the above logical word to output port.
putvalue(dio,boarddata);

% The motor goes logical zero and since the Ground terminal of the
Shinsei driver is
% connected to ground, the motor starts to move.
boarddata(6)=0;
putvalue(dio,boarddata);

% Loop that establishes motion in the Z down axis.
for n = 1:nz
end

% To stop the motor you need to set the CW or CCW terminal to high

boarddata(6)=1;          % High

% Puts the terminal CW or CCW to logical high and thus motor stops
putvalue(dio,boarddata);

% When you no longer need dio, you should remove it from
% memory and from the MATLAB workspace.
delete(dio)
clear dio

handles.z=handles.z-handles.zdistance

%Sends the z position to the position display (text box)
set(handles.zposition, 'String',handles.z)
guidata(hObject,handles);

function edit10_Callback(hObject, eventdata, handles)
% hObject    handle to edit10 (see GCBO)
% eventdata  reserved - to be defined in a future version of MATLAB
% handles    structure with handles and user data (see GUIDATA)

% Hints: get(hObject,'String') returns contents of edit10 as text
%        str2double(get(hObject,'String')) returns contents of edit10
as a double

% --- Executes during object creation, after setting all properties.
function edit10_CreateFcn(hObject, eventdata, handles)
% hObject    handle to edit10 (see GCBO)
% eventdata  reserved - to be defined in a future version of MATLAB
% handles    empty - handles not created until after all CreateFcns
called

% Hint: edit controls usually have a white background on Windows.
%       See ISPC and COMPUTER.
if ispc
    set(hObject,'BackgroundColor','white');
else

set(hObject,'BackgroundColor',get(0,'defaultUicontrolBackgroundColor')
);
end

```

```

function edit11_Callback(hObject, eventdata, handles)
% hObject      handle to edit11 (see GCBO)
% eventdata    reserved - to be defined in a future version of MATLAB
% handles      structure with handles and user data (see GUIDATA)

% Hints: get(hObject,'String') returns contents of edit11 as text
%         str2double(get(hObject,'String')) returns contents of edit11
as a double

% --- Executes during object creation, after setting all properties.
function edit11_CreateFcn(hObject, eventdata, handles)
% hObject      handle to edit11 (see GCBO)
% eventdata    reserved - to be defined in a future version of MATLAB
% handles      empty - handles not created until after all CreateFcns
called

% Hint: edit controls usually have a white background on Windows.
%         See ISPC and COMPUTER.
if ispc
    set(hObject,'BackgroundColor','white');
else

set(hObject,'BackgroundColor',get(0,'defaultUicontrolBackgroundColor')
);
end

function nxgrid_Callback(hObject, eventdata, handles)
% hObject      handle to nxgrid (see GCBO)
% eventdata    reserved - to be defined in a future version of MATLAB
% handles      structure with handles and user data (see GUIDATA)

% Hints: get(hObject,'String') returns contents of nxgrid as text
%         str2double(get(hObject,'String')) returns contents of nxgrid
as a double

handles.nxgrid=str2double(get(hObject,'String'));
guidata(hObject,handles);

% --- Executes during object creation, after setting all properties.
function nxgrid_CreateFcn(hObject, eventdata, handles)
% hObject      handle to nxgrid (see GCBO)
% eventdata    reserved - to be defined in a future version of MATLAB
% handles      empty - handles not created until after all CreateFcns
called

% Hint: edit controls usually have a white background on Windows.
%         See ISPC and COMPUTER.
if ispc
    set(hObject,'BackgroundColor','white');
else

set(hObject,'BackgroundColor',get(0,'defaultUicontrolBackgroundColor')
);

```

```
end
```

```
function nygrid_Callback(hObject, eventdata, handles)
% hObject    handle to nygrid (see GCBO)
% eventdata  reserved - to be defined in a future version of MATLAB
% handles    structure with handles and user data (see GUIDATA)

% Hints: get(hObject,'String') returns contents of nygrid as text
%        str2double(get(hObject,'String')) returns contents of nygrid
as a double
```

```
handles.nygrid=str2double(get(hObject,'String'));
guidata(hObject,handles);
```

```
% --- Executes during object creation, after setting all properties.
function nygrid_CreateFcn(hObject, eventdata, handles)
% hObject    handle to nygrid (see GCBO)
% eventdata  reserved - to be defined in a future version of MATLAB
% handles    empty - handles not created until after all CreateFcns
called
```

```
% Hint: edit controls usually have a white background on Windows.
%       See ISPC and COMPUTER.
```

```
if ispc
    set(hObject,'BackgroundColor','white');
else
    set(hObject,'BackgroundColor',get(0,'defaultUicontrolBackgroundColor')
);
end
```

```
function nxstep_Callback(hObject, eventdata, handles)
% hObject    handle to nxstep (see GCBO)
% eventdata  reserved - to be defined in a future version of MATLAB
% handles    structure with handles and user data (see GUIDATA)

% Hints: get(hObject,'String') returns contents of nxstep as text
%        str2double(get(hObject,'String')) returns contents of nxstep
as a double
```

```
handles.xstep=str2double(get(hObject,'String'));
guidata(hObject,handles);
```

```
% --- Executes during object creation, after setting all properties.
function nxstep_CreateFcn(hObject, eventdata, handles)
% hObject    handle to nxstep (see GCBO)
% eventdata  reserved - to be defined in a future version of MATLAB
% handles    empty - handles not created until after all CreateFcns
called
```

```
% Hint: edit controls usually have a white background on Windows.
%       See ISPC and COMPUTER.
```

```
if ispc
    set(hObject,'BackgroundColor','white');
else
```

```

set(hObject,'BackgroundColor',get(0,'defaultUicontrolBackgroundColor')
);
end

```

```

function nystep_Callback(hObject, eventdata, handles)
% hObject    handle to nystep (see GCBO)
% eventdata  reserved - to be defined in a future version of MATLAB
% handles    structure with handles and user data (see GUIDATA)

% Hints: get(hObject,'String') returns contents of nystep as text
%        str2double(get(hObject,'String')) returns contents of nystep
as a double

```

```

handles.ystep=str2double(get(hObject,'String'));
guidata(hObject,handles);

```

```

% --- Executes during object creation, after setting all properties.

```

```

function nystep_CreateFcn(hObject, eventdata, handles)
% hObject    handle to nystep (see GCBO)
% eventdata  reserved - to be defined in a future version of MATLAB
% handles    empty - handles not created until after all CreateFcns
called

% Hint: edit controls usually have a white background on Windows.
%       See ISPC and COMPUTER.
if ispc
    set(hObject,'BackgroundColor','white');
else

set(hObject,'BackgroundColor',get(0,'defaultUicontrolBackgroundColor')
);
end

```

```

% --- Executes on button press in startGrid.

```

```

function startGrid_Callback(hObject, eventdata, handles)
% hObject    handle to startGrid (see GCBO)
% eventdata  reserved - to be defined in a future version of MATLAB
% handles    structure with handles and user data (see GUIDATA)

```

```

    handles.ydistance=handles.ystep;
    handles.xdistance=handles.xstep;
    %guidata(hObject,handles);

```

```

for i=1:handles.nxgrid
    r=rem(i,2);

```

```

    for j=1:handles.nygrid

```

```

        if r == 0
            ymoveleft_Callback(hObject, eventdata, handles)
            powerON_Callback(hObject, eventdata, handles)
            PowerOFF_Callback(hObject, eventdata, handles)
        %elseif r == 0
        else
            ymoveright_Callback(hObject, eventdata, handles)

```

```

        powerON_Callback(hObject, eventdata, handles)
        PowerOFF_Callback(hObject, eventdata, handles)

    end

end

    xmoveforward_Callback(hObject, eventdata, handles)
    powerON_Callback(hObject, eventdata, handles)
    PowerOFF_Callback(hObject, eventdata, handles)

end

% --- Executes on button press in loadmri.
function loadmri_Callback(hObject, eventdata, handles)
% hObject    handle to loadmri (see GCBO)
% eventdata  reserved - to be defined in a future version of MATLAB
% handles    structure with handles and user data (see GUIDATA)

% File must be in the current directory or you may specify directory.

% info = dicominfo('IM000000') % Displays dicom contents
cd c:\MATLAB7 % Directory where the Dicom file is stored.
%scrsz = get(0,'ScreenSize');
%figure('Position',[10 scrsz(4)/2 scrsz(3)/2 scrsz(4)/2])
figure('position', [450,180,300,150])%left, bottom, width, height
I = dicomread('IM000000'); % Reads image data
image (I); %displays image in colour map
colormap(gray); % Converts to gray scale

% --- Outputs from this function are returned to the command line.
function varargout = lbox2_OutputFcn(hObject, eventdata, handles)
% varargout  cell array for returning output args (see VARARGOUT);
% hObject    handle to figure
% eventdata  reserved - to be defined in a future version of MATLAB
% handles    structure with handles and user data (see GUIDATA)

% Get default command line output from handles structure
varargout{1} = handles.output;

% -----
% Callback for list box - open .fig with guide, otherwise use open
% -----
function varargout = listbox1_Callback(h, eventdata, handles)
% hObject    handle to listbox1 (see GCBO)
% eventdata  reserved - to be defined in a future version of MATLAB
% handles    structure with handles and user data (see GUIDATA)

% Hints: contents = get(hObject,'String') returns listbox1 contents as
cell array
%         contents{get(hObject,'Value')} returns selected item from
listbox1

%figure('position', [450,180,300,150])%left, bottom, width, height

get(handles.figure1, 'SelectionType');

%Compares two strings. If the strings are the same it returns
% a one, otherwise zero.

```

```

% If you double click an item in the listbox you get an open stringn
% for selection type, and therefore strcmp results to logical one.
if strcmp(get(handles.figure1, 'SelectionType'), 'open');

% If you select for examle third item in the list you get a value of
3.
    index_selected = get(handles.listbox1, 'Value');

    % Read all strings from the list.
    file_list = get(handles.listbox1, 'String');

    % Selection of 3 rd string in the list.
    filename = file_list{index_selected};
    if handles.is_dir(handles.sorted_index(index_selected));

        %If item selected is a directory then go one level down this
        direcrory
            cd (filename)

                load_listbox(pwd,handles)

    %Load items of this directory
    file_list = get(handles.listbox1, 'String');

    %Get number of total files in the directory
    nimage=length(file_list);

    % Display all images
    for k=3:nimage
        j=k-2;
        I{k} = dicomread(file_list{k}); % Reads image data
        image (I{k}); %displays image in colour map
        colormap(gray); % Converts to gray scale
        F(j) = getframe; % Gets frames of the figure
    end

        %movie(F)

    end
end

% -----
% Read the current directory and sort the names, and displays
% files in the listbox.
% -----
function load_listbox(dir_path,handles)

%Move to the selected directory
cd (dir_path);

%Gets name, date, bytes and isdir of the current directory.
% perharps date is usefull for date sorting.
dir_struct = dir(dir_path);

% Sorts name, First dot, then two dots, then numbers and then
% alphavetically.
[sorted_names,sorted_index] = sortrows({dir_struct.name}');

```

```

% Stores file names in handles.
handles.file_names = sorted_names;

%If directory stores a 1, if a file it stores a 0.
handles.is_dir = [dir_struct.isdir];

% Stores index in handle
handles.sorted_index = [sorted_index];

%Saves handles data
guidata(handles.figure1,handles)

%Puts file names in the listbox
set(handles.listbox1, 'String',handles.file_names,...
    'Value',1)

% Outputs the current directory to the text
%Pwd prints or displays working directory
set(handles.text1, 'String',pwd)

% --- Executes during object creation, after setting all properties.
function listbox1_CreateFcn(hObject, eventdata, handles)
% hObject    handle to listbox1 (see GCBO)
% eventdata  reserved - to be defined in a future version of MATLAB
% handles    empty - handles not created until after all CreateFcns
called

% Hint: listbox controls usually have a white background, change
%       'usewhitebg' to 0 to use default. See ISPC and COMPUTER.

usewhitebg = 1;
if usewhitebg
    set(hObject, 'BackgroundColor', 'white');
else

set(hObject, 'BackgroundColor',get(0,'defaultUiControlBackgroundColor')
);
end

% --- Executes on button press in zeroxyz.
function zeroxyz_Callback(hObject, eventdata, handles)
% hObject    handle to zeroxyz (see GCBO)
% eventdata  reserved - to be defined in a future version of MATLAB
% handles    structure with handles and user data (see GUIDATA)

%Zeros x,y,z
handles.x=0;
handles.y=0;
handles.z=0;

%Sends the x or y or z position (zero) to the position display (3
texts
%boxes)
set(handles.xposition, 'String',handles.x)
set(handles.yposition, 'String',handles.y)
set(handles.zposition, 'String',handles.z)

guidata(hObject,handles);

```

```

function xposition_Callback(hObject, eventdata, handles)
% hObject      handle to xposition (see GCBO)
% eventdata    reserved - to be defined in a future version of MATLAB
% handles      structure with handles and user data (see GUIDATA)

% Hints: get(hObject,'String') returns contents of xposition as text
%         str2double(get(hObject,'String')) returns contents of
xposition as a double

% --- Executes during object creation, after setting all properties.
function xposition_CreateFcn(hObject, eventdata, handles)
% hObject      handle to xposition (see GCBO)
% eventdata    reserved - to be defined in a future version of MATLAB
% handles      empty - handles not created until after all CreateFcns
called

% Hint: edit controls usually have a white background on Windows.
%         See ISPC and COMPUTER.
if ispc
    set(hObject,'BackgroundColor','white');
else

set(hObject,'BackgroundColor',get(0,'defaultUicontrolBackgroundColor')
);
end

function yposition_Callback(hObject, eventdata, handles)
% hObject      handle to yposition (see GCBO)
% eventdata    reserved - to be defined in a future version of MATLAB
% handles      structure with handles and user data (see GUIDATA)

% Hints: get(hObject,'String') returns contents of yposition as text
%         str2double(get(hObject,'String')) returns contents of
yposition as a double

% --- Executes during object creation, after setting all properties.
function yposition_CreateFcn(hObject, eventdata, handles)
% hObject      handle to yposition (see GCBO)
% eventdata    reserved - to be defined in a future version of MATLAB
% handles      empty - handles not created until after all CreateFcns
called

% Hint: edit controls usually have a white background on Windows.
%         See ISPC and COMPUTER.
if ispc
    set(hObject,'BackgroundColor','white');
else

set(hObject,'BackgroundColor',get(0,'defaultUicontrolBackgroundColor')
);
end

function zposition_Callback(hObject, eventdata, handles)
% hObject      handle to zposition (see GCBO)
% eventdata    reserved - to be defined in a future version of MATLAB
% handles      structure with handles and user data (see GUIDATA)

```

```

% Hints: get(hObject,'String') returns contents of zposition as text
%         str2double(get(hObject,'String')) returns contents of
zposition as a double

% --- Executes during object creation, after setting all properties.
function zposition_CreateFcn(hObject, eventdata, handles)
% hObject    handle to zposition (see GCBO)
% eventdata  reserved - to be defined in a future version of MATLAB
% handles    empty - handles not created until after all CreateFcns
called

% Hint: edit controls usually have a white background on Windows.
%         See ISPC and COMPUTER.
if ispc
    set(hObject,'BackgroundColor','white');
else

set(hObject,'BackgroundColor',get(0,'defaultUicontrolBackgroundColor')
);
end

function timing(periodON,handles)

c=fix(clock);           %Reads time based on PC clock(integer format)
tinit=c(4)*3600+c(5)*60+c(6);           % Sixth element is time in
seconds

t=c(4)*3600+c(5)*60+c(6);           % Current time
while t-tinit<periodON           % If difference between current time and
    %initial time is less than timeON then
    % increase time
    c=fix(clock);           % Get new time within the WHILE loop
    t=c(4)*3600+c(5)*60+c(6);           % Get seconds.
end

% --- Executes on selection change in historylist.
function historylist_Callback(hObject, eventdata, handles)
% hObject    handle to historylist (see GCBO)
% eventdata  reserved - to be defined in a future version of MATLAB
% handles    structure with handles and user data (see GUIDATA)

% Hints: contents = get(hObject,'String') returns historylist contents
as cell array
%         contents{get(hObject,'Value')} returns selected item from
historylist

% --- Executes during object creation, after setting all properties.
function historylist_CreateFcn(hObject, eventdata, handles)
% hObject    handle to historylist (see GCBO)
% eventdata  reserved - to be defined in a future version of MATLAB
% handles    empty - handles not created until after all CreateFcns
called

% Hint: listbox controls usually have a white background on Windows.
%         See ISPC and COMPUTER.
if ispc

```

```

        set(hObject,'BackgroundColor','white');
    else

set(hObject,'BackgroundColor',get(0,'defaultUicontrolBackgroundColor')
);
end

function delay_Callback(hObject, eventdata, handles)
% hObject    handle to delay (see GCBO)
% eventdata  reserved - to be defined in a future version of MATLAB
% handles    structure with handles and user data (see GUIDATA)

% Hints: get(hObject,'String') returns contents of delay as text
%        str2double(get(hObject,'String')) returns contents of delay
as a double

handles.timeOFF=str2double(get(hObject,'String'))
guidata(hObject,handles);

% --- Executes during object creation, after setting all properties.
function delay_CreateFcn(hObject, eventdata, handles)
% hObject    handle to delay (see GCBO)
% eventdata  reserved - to be defined in a future version of MATLAB
% handles    empty - handles not created until after all CreateFcns
called

% Hint: edit controls usually have a white background on Windows.
%        See ISPC and COMPUTER.
if ispc
    set(hObject,'BackgroundColor','white');
else

set(hObject,'BackgroundColor',get(0,'defaultUicontrolBackgroundColor')
);
end

% -----
function enter_patient_data_Callback(hObject, eventdata, handles)
% hObject    handle to enter_patient_data (see GCBO)
% eventdata  reserved - to be defined in a future version of MATLAB
% handles    structure with handles and user data (see GUIDATA)

open ('save_patient_data.fig')

% -----
function retrieve_patient_data_Callback(hObject, eventdata, handles)
% hObject    handle to retrieve_patient_data (see GCBO)
% eventdata  reserved - to be defined in a future version of MATLAB
% handles    structure with handles and user data (see GUIDATA)

open ('retrieve.fig')

% --- Executes on button press in exit_button.
function exit_button_Callback(hObject, eventdata, handles)
% hObject    handle to exit_button (see GCBO)
% eventdata  reserved - to be defined in a future version of MATLAB

```

```

% handles      structure with handles and user data (see GUIDATA)

%close all;

exit

%delete(gcf);

% --- Executes on button press in startcamera.
function startcamera_Callback(hObject, eventdata, handles)
% hObject      handle to startcamera (see GCBO)
% eventdata    reserved - to be defined in a future version of MATLAB
% handles      structure with handles and user data (see GUIDATA)

IMAQMEM(50000000000);
vid = videoinput('winvideo',1);

handles.camera=vid;
guidata(hObject,handles);

set(handles.camera,'TriggerRepeat',Inf);
%set(vid,'FramesPerTrigger',8000);
start(handles.camera);
preview(handles.camera);

% --- Executes on button press in stopcamera.
function stopcamera_Callback(hObject, eventdata, handles)
% hObject      handle to stopcamera (see GCBO)
% eventdata    reserved - to be defined in a future version of MATLAB
% handles      structure with handles and user data (see GUIDATA)

flushdata(handles.camera);
delete(handles.camera)
clear handles.camera

% --- Executes on button press in savecamera.
function savecamera_Callback(hObject, eventdata, handles)
% hObject      handle to savecamera (see GCBO)
% eventdata    reserved - to be defined in a future version of MATLAB
% handles      structure with handles and user data (see GUIDATA)

function edit20_Callback(hObject, eventdata, handles)
% hObject      handle to edit20 (see GCBO)
% eventdata    reserved - to be defined in a future version of MATLAB
% handles      structure with handles and user data (see GUIDATA)

% Hints: get(hObject,'String') returns contents of edit20 as text
%        str2double(get(hObject,'String')) returns contents of edit20
as a double

% --- Executes during object creation, after setting all properties.
function edit20_CreateFcn(hObject, eventdata, handles)
% hObject      handle to edit20 (see GCBO)

```

```

% eventdata reserved - to be defined in a future version of MATLAB
% handles empty - handles not created until after all CreateFcns
called

% Hint: edit controls usually have a white background on Windows.
% See ISPC and COMPUTER.
if ispc
    set(hObject,'BackgroundColor','white');
else

set(hObject,'BackgroundColor',get(0,'defaultUiControlBackgroundColor')
);
end

function edit21_Callback(hObject, eventdata, handles)
% hObject handle to edit21 (see GCBO)
% eventdata reserved - to be defined in a future version of MATLAB
% handles structure with handles and user data (see GUIDATA)

% Hints: get(hObject,'String') returns contents of edit21 as text
% str2double(get(hObject,'String')) returns contents of edit21
as a double

% --- Executes during object creation, after setting all properties.
function edit21_CreateFcn(hObject, eventdata, handles)
% hObject handle to edit21 (see GCBO)
% eventdata reserved - to be defined in a future version of MATLAB
% handles empty - handles not created until after all CreateFcns
called

% Hint: edit controls usually have a white background on Windows.
% See ISPC and COMPUTER.
if ispc
    set(hObject,'BackgroundColor','white');
else

set(hObject,'BackgroundColor',get(0,'defaultUiControlBackgroundColor')
);
end

```

14 References and Bibliography

- [1] J.G. Lynn, R.L. Zwemer, A.J Chick., A.E. Miller, "A new method for the generation and use of focused ultrasound in experimental biology," *J. Gen. Phys.*, 26, pp.179–193. 1942.
- [2] W. Fry, W. Mosberg, J. Barnard, F. Fry, "Production of focal destructive lesions in the central nervous system with ultrasound," *J. Neurosurg* 11, pp.471–478. 1954.
- [3] F.A. Jolesz, P.D. Jakab, "Acoustic pressure wave generation within a magnetic resonance imaging system: potential medical applications," *J. Magn. Reson. Imag.*, vol.1, pp.609-13. 1991.
- [4] K. Hynynen, A. Darkazanli, C. Damianou, E. Unger, J.F. Schenck, "MRI-guided ultrasonic hyperthermia," RSNA meeting, 1992.
- [5] K. Hynynen, A. Darkazanli, E. Unger, J.F. Schenck, "MRI-guided noninvasive ultrasound surgery," *Med. Phys.*, vol.20(1), pp.107-115. 1993.
- [6] H.E. Cline, J.F. Schenck, K. Hynynen, R.D. Watkins, S.P. Souza, F.A. Jolesz, "MR-guided focused ultrasound surgery," *J. Comput. Assist. Tomogr.* vol.16, pp. 956–965. 1992.
- [7] K. Hynynen, A. Darkazanli, C.A Damianou, E. Unger, J.F. Schenck, "The usefulness of a contrast agent and gradient-recalled acquisition in a steady-state imaging sequence for magnetic resonance imaging-guided noninvasive ultrasound surgery," *Invest. Radiol.*, vol.29(10), pp. 897–903. 1994.
- [8] J.Y. Chapelon, J. Margonari, F. Vernier, F. Gorry, R. Ecochard, A. Gelet "In vivo effects of high-intensity ultrasound on prostatic adenocarcinoma," Dunning R3327. *Cancer Res.* Vol.52(22), pp.6353-7. 1992.
- [9] G.R. ter Haar, D. Sinnett, I. Rivens, "High intensity focused ultrasound – a surgical technique for the treatment of discrete liver tumours," *Phy. Med. Biol.* vol. 34(11), pp.1743-50. 1989.
- [10] P.P. Lele, "A simple method for production of trackless focal lesions with focused ultrasound," *J. Physiol.* 160, pp. 494-512. 1962.
- [11] N.I. Vykhodtseva, K. Hynynen, C. Damianou, "Pulse duration and peak intensity during focused ultrasound surgery: theoretical and experimental effects in rabbit brain *in vivo*," *Ultrasound Med Biol.* vol.20(9), pp. 987-1000. 1994.
- [12] F. Lizzi, J. Coleman, J. Driller, L. Franzen, F. Jakobiec, "Experimental, ultrasonically induced lesions in the retina, choroid, and sclera," *Invest. Ophthalmol. Visual Sci.* vol.205, pp.350-360. 1978.
- [13] C. Linke, E.L. Carteensen, L.A. Frizzell, A. Elbdawi, C.W. Fridd, "Localized Tissue destruction by High Intensity Focused Ultrasound," *Arch. Surg.* vol.107, pp. 887-891. 1973.
- [14] K. Hynynen, C. Damianou, V. Colucci, E. Unger, H.H. Cline, F.A. Jolesz, "MR monitoring of focused ultrasonic surgery of renal cortex: experimental and simulation studies," *J. Magn. Reson. Imag.*, vol. 5(3), pp. 259-66. 1995.
- [15] B. Xie, J. Ling, W. Zhang, X. Huang, J. Zhen, Y. Huang, "The efficacy of high-intensity focused ultrasound (HIFU) in advanced pancreatic cancer". *Journal of Chinese Journal of Clinical Oncology*, vol. 5(3), pp.183-186. 2008.

- [16] B. Xie, Y.Y. Li, L. Jia, Y.Q. Nie, H. Du, S.M. Jiang. "Experimental ablation of the pancreas with high intensity focused ultrasound (HIFU) in a porcine model," *Int J Med Sci* 2011; 8(1):9-15. Available from <http://www.medsci.org/v08p0009.htm>
- [17] F. Wu, Z.B. Wang, H. Zhu, W.Z. Chen, J.Z. Zou, J. Bai, K.Q. Li, C.B. Jin, F.L. Xie, H.B. Su, "Extracorporeal high intensity focused ultrasound treatment for patients with breast cancer," vol. 92(1), pp.51-60. 2005. DOI: 10.1007/s10549-004-5778-7.
- [18] Theraclion, the sound therapy, <http://www.theraclion.com/>
- [19] Theraclion, the therapeutic HiFu specialist, raises 3.5 million Euros from Truffle Venture [news release]. Paris: Theraclion SAS; 2007 Feb 21. Available: <http://www.genopole.net/media/pdf/eng/presse/050502-comm-theraclion-en.pdf>Add to My Files
- [20] O. Esnault, A. Rouxel, E. Le Nestour, G. Gheron, L. Leenhardt, "Minimally Invasive Ablation of a Toxic Thyroid Nodule by High-Intensity Focused Ultrasound," *American Journal of Neuroradiology*, doi: 10.3174/ajnr.A1979. 2010.
- [21] O. Esnault, B. Franc, J.P. Monteil, J.Y. Chapelon, "High-intensity focused ultrasound for localized thyroid-tissue ablation: preliminary experimental animal study," *Thyroid*, vol.14(12), pp.1072–76. 2004.
- [22] O. Esnault, B. Franc, F. Ménégau, A. Rouxel, E. De Kerviler, P. Bourrier, F. Lacoste, J.Y. Chapelon, L. Leenhardt, "High-intensity focused ultrasound ablation of thyroid nodules: first human feasibility study," *Thyroid*. vol.21(9), pp.965-73. Aug. 2011.
- [23] R. Bihrl, R.S. Foster, N.T. Sanghvi, F.J. Fry, J.P. Donohue, "High-intensity focused ultrasound in the treatment of prostatic tissue," *Urology*, vol.43(2 Suppl), pp. 21-6. 1994.
- [24] K. Hynynen, O. Pomeroy, D.N. Smith, P.E. Huber, N.J. McDannold, J. Kettenbach, J. Baum, S. Singer, and F.A. Jolesz, "MR imaging-guided focused ultrasound surgery of fibroadenomas in the breast: a feasibility study," *Radiology* 219(1), pp. 176-185. 2001.
- [25] W.A. Kaiser, H. Fischer, J. Vagner, M. Selig, "Robotic system for biopsy and therapy of breast lesions in a high-field whole-body magnetic resonance tomography" unit. *Invest Radiol* vol.35, pp.513–519. 2000.
- [26] Felden, A., Vagner, J., Hinz, A., Fischer, H., Pfleiderer, S. O., Reichenbach, J. R., and Kaiser, W. A. (2002) ROBITOM-Robot for Biopsy and Therapy of the Mamma. *Biomed. Tech.* 47:2–5.
- [27] N.V. Tsekos, J. Shudy, E. Yacoub, P. V. Tsekos, I. G. Koutlas, "Development of a Robotic Device for MRI-Guided Interventions in the Breast", 2nd IEEE International Symposium on Bioinformatics and Bioengineering, Washington, DC. 2001.
- [28] B.T. Larson, A.G. Erdman, N.V. Tsekos, E. Yacoub, P.V. Tsekos, I.G. Koutlas, "Design of an MRI-compatible robotic stereotactic device for minimally invasive interventions in the breast," *ASME J. Biomech. Eng.* vol.126, pp.458–465. 2004.
- [29] K. Masamune, E. Kobayashi, Y. Masutani, M. Suzuki, T. Dohi, H. Iseki, K. Takakura, "Development of an MRI compatible needle insertion manipulator for stereotactic neurosurgery," *J. Image. Guid. Surg.* vol. 1(4), pp.242–248. 1995.
- [30] K. Chinzei, K. Miller, "Towards MRI guided surgical manipulator," *Med. Sci. Monit*, vol. 7, pp. 153–163. 2001.

- [31] A. Krieger, R.C. Susil, C. Menard, J.A. Coleman, G. Fichtinger, E. Atalar, L.L. Whitcomb, "Design of a novel MRI compatible manipulator for image guided prostate interventions," *Biomedical Engineering, IEEE Transactions*, vol. 52(2), pp. 306-313. 2005
- [32] R.C. Susil, A. Krieger, J.A. Derbyshire, A. Tanacs, L.L. Whitcomb, G. Fichtinger, E. Atalar, "System for MR image-guided prostate interventions: canine study," *Radiology* vol.228, pp.886–894. 2003.
- [33] F.A. Jolesz, P.R. Morrison, S.J. Koran, R.J. Kelley, S.G. Hushek, R.W. Newman, M.P. Fried, A. Melzer, R.M. Seibel, H. Jalahej, "Compatible Instrumentation for Intraoperative MRI: Expanding Resources," *J. Magn. Reson. Imag.*, vol.8(1), pp.8–11. 1998.
- [34] L. Frizzell, C. Linke, E. Carstensen, C. Fridd, "Thresholds for focal ultrasound lesions in rabbit kidney, liver and testicle," *IEEE Trans on Biomed. Eng. BME*, vol.24(4), pp.393-6. 1987.
- [35] L. Frizzell, "Threshold dosages for damage to mammalian liver by high intensity focused ultrasound," *IEEE Trans. Ultrasonics, Ferroelectrics, and Frequency Control, UFFC* vol.35(5), pp.578-581. 1988
- [36] A. Sibille, F. Prat, J.Y. Chapelon, F.A. Fadil, L. Henry, Y. Theillere, T. Ponchon, D. Cathignol, "Extracorporeal ablation of liver tissue by high-intensity focused ultrasound," *Oncology*, vol.50(5), pp.375-9. 1993.
- [37] L. Chen, G.R. ter Haar, D. Robertson, J.P. Bensted, C.R. Hill, "Histological study of normal and tumour-bearing liver treated with focused ultrasound," *Ultrasound Med. Biol.*, vol.25(5), pp.847-56. 1999.
- [38] R. Yang, C.R. Reilly, F.J. Rescorla, P.R. Faught, N.T. Sanghvi, F.J. Fry, Jr T.D. Franklin, L. Lumeng, J.L. Grosfeld, "High-intensity focused ultrasound in the treatment of experimental liver cancer," *Arch Surg.*, vol.126(8), pp.1002-10. 1991.
- [39] A. Sibille, F. Prat, J.Y. Chapelon, F. abou el Fadil, L. Henry, Y. Theilliere, T. Ponchon, D. Cathignol, "Characterization of extracorporeal ablation of normal and tumour-bearing liver tissue by high intensity focused ultrasound," *Ultrasound Med. Biol.*, vol.19(9), pp.803-13. 1993.
- [40] F. Prat, M. Centarti, A. Sibille, F.A. Fadil, L. Henry, J.Y. Chapelon, D. Cathignol, "Extracorporeal high-intensity focused ultrasound for VX2 liver tumours in the rabbit," *Hepatology*, vol.21(3), pp.832-6. 1995.
- [41] S.Q. Cheng, Z.D. Zhou, Z.Y. Tang, Y. Yu, H.Z. Wang, S.S. Bao, D.C. Qian. "High-intensity focused ultrasound in the treatment of experimental liver tumour", *J. Cancer Res. Clin. Oncol.*, vol.123(4), pp.219-23. 1997.
- [42] J.E. Kennedy, F. Wu, G.R. ter Haar, F.V. Gleeson, R.R. Phillips, M.R. Middleton, D. Cranston, "High-intensity focused ultrasound for the treatment of liver tumours," *Ultrasonics* vol.42, pp.931–935. 2004.
- [43] L. Chen, G.R. ter Haar, C.R. Hill, S.A. Eccles, G. Box, "Treatment of implanted liver tumours with focused ultrasound," *Ultrasound Med. Biol.*, vol.24(9), pp.1475-88. 1998.
- [44] L. Chen, I. Rivens, G.R. ter Haar, S. Riddler, C.R. Hill, JP. Bensted, "Histological changes in rat liver tumours treated with high-intensity focused ultrasound," *Ultrasound Med Biol*, vol.19(1), pp.67-74. 1993.
- [45] P.R. Morrison, F.A. Jolesz, D. Charous, R.V. Mulkern, S.G. Hushek, R. Margolis, M.P. Fried, "MRI of laser-induced interstitial thermal injury in an *in vivo* animal liver model with histologic correlation," *J. Magn. Reson. Imaging*. Vol.8(1), pp.57-63. 1998.

- [46] T.A. Leslie, J.E. Kennedy. High intensity focused ultrasound in the treatment of abdominal and gynaecological diseases," *Int. F. Hyperthermia*, vol.23(2), pp. 173-182. 2007.
- [47] R.O. Illing, J.E. Kennedy, F. Wu, G.R. ter Haar, A.S. Protheroe, P.J. Friend, F.V. Gleeson, D.W. Cranston, R.R. Phillips, M.R. Middleton, "The safety and feasibility of extracorporeal high-intensity focused ultrasound (HIFU) for the treatment of liver and kidney tumours in a Western population," *British Journal of Cancer*, vol.93(8), pp.890-895. 2005.
- [48] C. Damianou, M. Pavlou, O. Velev, K. Kyriakou, M. Trimikliniotis, "High intensity focused ultrasound ablation of kidney guided by MRI. Ultrasound," *Med. Biol. Vol.30(3)*, pp.397-404. 2004.
- [49] C. Damianou. MRI monitoring of the effect of tissue interfaces in the penetration of high intensity focused ultrasound in kidney *in vivo*," *Ultrasound in Med. Biol. Vol.30(9)*, pp.1209-1215. 2004.
- [50] University of Virginia Health System, <http://uvahealth.com/services/cancer-center/>
- [51] National Cancer Institute, <http://www.cancer.gov>
- [52] Surveillance Epidemiology and end Results (SEER), <http://seer.cancer.gov/statfacts/>
- [53] Urology Channel, <http://www.urologychannel.com/>
- [54] Foyo Herb, <http://www.4uherb.com/cancer/>
- [55] World Health Organization. International Agency for research on Cancer, <http://globocan.iarc.fr/factsheet.asp>
- [56] ABC Health & wellbeing, <http://www.abc.net.au/health/library/stories/2005/06/16/1831822.htm>
- [57] PubMed Health - U.S. National Library of Medicine, <http://www.ncbi.nlm.nih.gov/pubmedhealth/>
- [58] MedlinePlus-Trusted Health Information for you, <http://www.nlm.nih.gov/medlineplus/thyroiddiseases.html>
- [59] American Cancer Society, <http://www.cancer.org/Cancer/ThyroidCancer/>
- [60] American Thyroid Association, <http://www.thyroid.org/index.html>
- [61] Memedicine health experts for everyday emergencies, <http://www.emedicinehealth.com/>
- [62] National Institute of Health – NIH...Turning Discovery Into Health, <http://www.nih.gov/>
- [63] C.M. Pacella, G. Bizzarri, S. Spiezia, A. Bianchini, R. Guglielmi, A. Crescenzi, S. Pacella, V. Toscano, E. Papini, "Thyroid tissue: US-guided percutaneous laser thermal ablation," *Radiology*, vol.232(1), pp.272-80. May, 2004.
- [64] Elaine N. Marieb, "Human Anatomy and Physiology", Fifth Edition., Benjamin/Cummings. 4 Aug 2000.
- [65] John Nolte "The Human Brain: An Introduction to Its Functional Anatomy", Fifth Edition., Mosby. 21 Nov 2001.
- [66] Stanford Medicine, <http://cancer.stanford.edu/>
- [67] American Brain Tumor Association, <http://www.abta.org/>
- [68] M. Gautherie, "Methods of External Hyperthermic Heating (Clinical Thermology)," Springer-Verlag Berlin and Heidelberg GmbH & Co. K. New York, London, Paris, Tokyo, Hong Kong, 1990, ISBN-10: 3540509763, ISBN-13: 978-3540509769

- [69] A.J. Zagzebski, "Essentials of Ultrasound Physics," Mosby, 1996. ISBN-10: 0815198523, ISBN-13: 978-0815198529
- [70] V. Gibbs, D. Cole, A. Sassano, "Ultrasound Physics and Technology: How, Why and When," 1st edition. Churchill Livingstone; Edinburgh, London, New York, Oxford, Philadelphia, St Louis, Sydney and Toronto 2009. ISBN-10: 0702030414, ISBN-13: 978-0702030413
- [71] D.L. Hykes, W.R. Hedrick, D.E. Starchman, "Ultrasound physics and instrumentation," Churchill Livingstone, New York, Edinburg, London, and Melbourne. 1985.
- [72] F. Chavrier, J.Y. Chapelon, A. Gelet, D. Cathignol, "Modeling of high-intensity focused ultrasound-induced lesions in the presence of cavitation bubbles", J. Acoust. Soc. Am. vol.108(1), pp. 432-440, 2000.
- [73] C. Damianou, "MRI monitoring of cavitation produced by High Intensity Focused ultrasound," submitted in IEEE Trans. Ultrasonics Ferroelectric Freq control. 2003.
- [74] T.J. Dubinsky, C. Cuevas, M.K. Dighe, O. Kolokythas, J.H. Hwang. "High intensity focused ultrasound: current potential and oncologic applications", Am J Roentgenol 2008;190:191-199.
- [75] K.D. Evans, B. Weiss, M. Knopp, "High-Intensity Focused Ultrasound (HIFU) for Specific Therapeutic Treatments: A Literature Review," Journal of Diagnostic Medical Sonography, vol.23(6), pp.319-327. Nov. 2007.
- [76] F. W. Kremkau, "Diagnostic Ultrasound: Principles and Instruments 7th ed, Saunders Elsevier, Philadelphia, PA, 2006,
- [77] J.V. Frangioni, "New Technologies for Human Cancer Imaging" Journal of Clinical Oncology Biology of Neoplasia Vol.26, pp.4012-4021, Aug. 2008.
- [78] Insightec-Bring therapy in to focus,
<http://www.insightec.com/InSightec>AboutUs.html>
- [79] R. Gassert, E. Burdet, K. Chinzei, "Opportunities and challenges in MR-Compatible Robotics," IEEE Engineering in Medicine and Biology, Vol. 27(3), pp.15-22. 2008.
- [80] M. Li, D. Mazilu, A. Kapoor, K. A. Horvath, "MRI Compatible Robot Systems for Medical Intervention, Advances in Robot Manipulators," Ernest Hall (Ed.), ISBN: 978-953-307-070-4, InTech, pp.443-458. 2010. Available from: <http://www.intechopen.com/books/advances-in-robot-manipulators/mri-compatible-robot-systems-for-medical-intervention>
- [81] J.E. Kennedy, G.R. ter Haar, D. Cranston, "High intensity focused ultrasound: surgery of the future?" Br J Radiol vol.76, pp.590–599. 2003.
- [82] C. Damianou, N. Milonas, K. Ioannides, "Positioning Device for MRI-guided high intensity focus ultrasound system," CARS, vol.2, pp.335-345. 2008.
- [83] C. Damianou, K. Ioannides, V. Hadjisavvas, N. Mylonas, A. Couppis, D. Iosif, "*In vitro* and *in vivo* brain ablation created by high intensity focused ultrasound and monitored by MRI," IEEE Transactions on Ultrasonics, Ferroelectrics, and Frequency Control, Vol.56(6), 1189-1198. Jun. 2009.
- [84] K. Chinzei, R. Kikinis and A. Jolesz, "MR Compatibility of Mechatronic Devices: Design Criteria," in Proc., 2nd Int. Conf. Medical Image Computing and Computer Assisted Interventions (MICCAI), vol.1679, pp.1020-1030. 1999.

- [85] F. Gérard, B. Rémi, C.J. Yves, G.R. ter Haar, L. Cyril, L.B. Olivier, C. Laurent, P. Fabrice; L. Jérôme. "Safety Issues for HIFU Transducer Design," 4th International Symposium on Therapeutic Ultrasound. AIP Conference Proceedings, Vol.754, pp. 233-241. 2005.
- [86] M. Thompson, "Image-Guided Focused Ultrasound gains ground as noninvasive therapeutic tool," Medtech Insight, vol. 13(9), pp.1-11. 2011.
- [87] F.J. Murat, L. Poissonier, A. Gelet, "Recurrent prostate cancer after radiotherapy-salvage treatment by High Intensity Focused Ultrasound," European Renal & Genito Urinary Disease. 2006.
- [88] F. Wu, Z.B. Wang, W.Z. Chen, J.Z. Zou, "Extracorporeal High-Intensity Focused Ultrasound for treatment of solid carcinomas: Four-year Chinese clinical experience," In Proceedings of the 2nd International Symposium on Therapeutic Ultrasound, Seattle, USA. 2002.
- [89] F. Wu, Z.B. Wang, W.Z. Chen, J.Z. Zou, J. Bai, H. Zhu, K.Q. Li, F.L. Xie, C.B. Jin, H.B. Su, G.W. Gao, "Extracorporeal focused ultrasound surgery for treatment of human solid carcinomas: early Chinese clinical experience. Ultrasound Med Biol vol.30, pp.245–260. 2004.
- [90] F.W. Kermakau, "Cancer therapy with ultrasound: a historical review," J Clin Ultrasound vol.7(4), pp.287-300. 1979.
- [91] K. Hynynen, C. Damianou, A. Darkazanli, E. Unger, J.F. Schenck, "The feasibility of using MRI to monitor and guide noninvasive ultrasound surgery," Ultrasound Med Biol. vol.19(1), pp.91-2. 1993.
- [92] K. Hynynen, A. Darkazanli, C.A. Damianou, E. Unger, J.F. Schenck, "Tissue thermometry during ultrasound exposure," Eur. Urol., vol.23(suppl 1), pp.12-6. 1993.
- [93] H.E. Cline, J.F. Schenck, R.D. Watkins, K. Hynynen, F.A. Jolesz, "Magnetic resonance guided thermal surgery," Magn. Reson. Med., vol.30(1), pp.98-106. 1993.
- [94] C. Damianou, "MRI positioning system for ultrasound brain surgery," WO/2007/082495.
- [95] K. Hynynen, N.I. Vykhodtseva, A.H. Chung, V. Sorrentino, V. Colucci, F.A. Jolesz, "Thermal effects of focused ultrasound on the brain: determination with MR imaging", Radiology, vol.204(1), pp.247-53. 1997.
- [96] M. Li, D. Mazilu, K. Horvath, "Robotic system for transapical aortic valve replacement with MRI guidance," Proc. of MICCAI '08 Lecture Notes in Computer Science. Vol.5242, pp.476-484. 2008.
- [97] A. Couppis, K. Ioannides, N. Mylonas, D. Iosif, P. Kyriakou, C. Lafon, F. Chavier J. Chapelon, M. Komodromos, C. Damianou, "Evaluation of an MRI guided planar rectangular high intensity focused ultrasound transducer for thermal ablation of cardiac tissue," 10th meeting of the International Society of Therapeutic Ultrasound, ISTU10, Tokyo, Japan, June 9-12, 2010.
- [98] N. Mylonas, V. Hadjisavvas, C. Damianou, "An MR compatible positioning device for treating brain cancer and stroke using high intensity focused ultrasound (HIFU) under MRI guidance," 10th meeting of the International Society of Therapeutic Ultrasound, ISTU10, Tokyo, Japan, June 9-12, 2010.
- [99] Wright C., Hynynen K., D. Goertz, "An *in vitro* and *in vivo* investigation of high intensity focused ultrasound thrombolysis," Ultrasound Med Biol.

- Submitted. Imaging Research, Sunnybrook Health Sciences Centre, Toronto, ON, Canada. 2012.
- [100] A.V. Alexandrov, C.A. Molina, J.C. Grotta, Z. Garami, S.R. Ford, J. Alvarez-Sabin, J. Montaner, M. Saqqur, A.M. Demchuk, L.A. Moyer, M.D. Hill, A.W. Wojner, CLOTBUST Investigators, "Ultrasound-enhanced systemic thrombolysis for acute ischemic stroke. *N. Engl. J. Med.*, vol.351, pp.2170-8. 2004.
- [101] E.A. Dick, R. Joarder, M. de Jode, S.D. Taylor-Robinson, H.C. Thomas, G.R. Foster, W.M. Gedroyc, "MR-guided laser thermal ablation of primary and secondary liver tumours," *Clin Radiol.*;58(2), pp.112-20. 2003.
- [102] T.J. Vogl, R. Straub, K. Eichler, D. Woitaschek, M.G. Mack, "Malignant liver tumours treated with MR imaging-guided laser-induced thermotherapy: experience with complications in 899 patients (2,520 lesions)," *Radiology*, vol. 225(2), pp.367-77. 2002.
- [103] M.G. Mack, R. Straub, K. Eichler, K. Engelmann, A. Roggan, D. Woitaschek, M. Böttger, T.J. Vogl, "Percutaneous MR imaging-guided laser-induced thermotherapy of hepatic metastases," *Abdom Imaging*, vol.26, pp.369–374. 2001.
- [104] M.G. Mack, R. Straub, K. Eichler, et al. "MR-guided laser-induced thermotherapy in recurrent extrahepatic abdominal tumors," *Eur Radiol*; vol.11, pp.2041–2046. 2001.
- [105] J.K. Seifert, T. Junginger, "Cryotherapy for liver tumors: current status, perspectives, clinical results, and review of literature," *Technol Cancer Res Treat.* vol.3, pp.151-63. 2004.
- [106] T. Mala, B. Edwin, Ø. Mathisen, T. Tillung, E. Fosse, A. Bergan, O. Søreide, I. Gladhaug, "Cryoablation of colorectal liver metastases: minimally invasive tumour control," *Scand J Gastroenterol*, vol.39(6), pp.571-578. 2004.
- [107] K.C. Xu, L.Z. Niu, W.B. He, W.B. He, Y.Z. Hu, J.S. Zuo, "Percutaneous cryosurgery for the treatment of hepatic colorectal metastases," *World J Gastroenterol.* vol. 14(9), pp.1430-436. 2008.
- [108] D. Elias, T. De Baere, T. Smayra, J.F. Ouellet, A. Roche, P. Lasser, "Percutaneous radiofrequency thermoablation as an alternative to surgery for treatment of liver tumour recurrence after hepatectomy," *Br J Surg.* vol. 89(6), pp.752-6. 2002.
- [109] M. Tsuda, H. Rikimaru, K. Majima, T. Yamada, H. Saito, T. Ishibashi, S. Takahashi, H. Miyachi, M. Endoh, S. Yamada, "Time-related changes of radiofrequency ablation lesion in the normal rabbit liver: findings of magnetic resonance imaging and histopathology," *Invest Radiol.* vol. 38(8), pp.525-31. 2003.
- [110] T. Livraghi, S.N. Goldberg, F. Monti, A. Bizzini, S. Lazzaroni, F. Meloni, S. Pellicanò, L. Solbiati, G.S. Gazelle, "Saline-enhanced radiofrequency tissue ablation in the treatment of liver metastases," *Radiology*, vol. 202, pp.205–210. 1997.
- [111] J.P. McGahan, G.D. Dodd III, "Radiofrequency Ablation of the Liver Current Status," *AJR* January vol. 176(1), pp. 3-16. 2001.
- [112] D.A. Gervais, F.J. McGovern, R.S. Arellano, W.S. McDougal, P.R. "Mueller Renal cell carcinoma: clinical experience and technical success with radiofrequency ablation of 42 tumors," *Radiology* 226, pp. 417–424. 2003.

- [113] D.W. Kim, M.H. Rho, H.J. Kim, J.S. Kwon, Y.S. Sung, S.W. Lee, "Percutaneous Ethanol Injection for Benign Cystic Thyroid Nodules: Is Aspiration of Ethanol-Mixed Fluid Advantageous?" *AJNR* vol. 26(8), pp. 2122-2127. Sep. 2005
- [114] T. Livraghi, A. Giorgio, G. Marin, A. Salmi, I. de Sio, L. Bolondi, M. Pompili, F. Brunello, S. Lazzaroni, G. Torzilli, "Hepatocellular carcinoma and cirrhosis in 746 patients: long-term results of percutaneous ethanol injection," *Radiology* vol. 197, pp. 101–108. 1995.
- [115] T. Seki, M. Wakabayashi, T. Nakagawa, T. Itho, T. Shiro, K. Kunieda, M. Sato, S. Uchiyama, K. Inou, "Ultrasonically guided percutaneous microwave coagulation therapy for small hepatocellular carcinoma," *Cancer*, vol. 74(3), pp.817–825. Aug. 1994.
- [116] R. Murakami, S. Yoshimatsu, Y. Yamashita, T. Matsukawa, M. Takahashi, K. Sagara, "Treatment of hepatocellular carcinoma: value of percutaneous microwave coagulation," *AJR Am J Roentgenol*; vol. 164(5), pp.1159–1164. May 1995.
- [117] M. Sato, Y. Watanabe, S. Ueda, S. Iseki, Y. Abe, N. Sato, S. Kimura, K. Okubo, M. Onji, "Microwave coagulation therapy for hepatocellular carcinoma. *Gastroenterology*," vol. 110(5), pp.1507–1514. May 1996.
- [118] T. Livraghi, S.N. Goldberg, S. Lazzaroni, F. Meloni, L. Solbiati, G.S. Gazelle, "Small hepatocellular carcinoma: treatment with radio-frequency ablation versus ethanol injection," *Radiology*; vol. 210, pp.655–661. 1999.
- [119] T. Seki, M. Wakabayashi, T. Nakagawa, M. Imamura, T. Tamai, A. Nishimura, N. Yamashiki, A. Okamura, K. Inoue, "Percutaneous microwave coagulation therapy for patients with small hepatocellular carcinoma: comparison with percutaneous ethanol injection therapy," *Cancer*, vol. 85(8), pp.1694–1702. Apr. 1999.
- [120] G. Gravante, J. Overton, R. Sorge, N. Bhardwaj, M.S. Metcalfe, D.M. Lloyd, A.R. Dennison, "Radiofrequency ablation versus resection for liver tumours: an evidence-based approach to retrospective comparative studies," *J Gastrointest Surg*. vol.15(2), pp.378-87. Feb 2011
- [121] T. Shibata, Y. Iimuro, Y. Yamamoto, Y. Maetani, F. Ametani, K. Itoh, J. Konishi, "Small hepatocellular carcinoma: comparison of radio-frequency ablation and percutaneous microwave coagulation therapy," *Radiology* vol. 223, pp. 331–337. 2002.
- [122] Express Healthcare,
<http://www.expresshealthcare.in/200910/knowledge01.shtml>
- [123] Wu F., Z.B. Wang, P. Lu, Z.L. XU, W.Z Chen, H. ZHU, C.B. Jin, "Activated anti-tumor immunity in cancer patients after high intensity focused ultrasound ablation," *Ultrasound Med Biol*; vol. 30(9), pp.1217-22. Sep. 2004.
- [124] Z.L. Xu, X.Q. Zhu, P. Lu, Q. Zhou, J. Zhang, F. Wu, "Activation of tumor-infiltrating antigen presenting cells by high intensity focused ultrasound ablation of human breast cancer," *Ultrasound Med Biol*. vol. 35(1), pp.50-7. Oct. 2009.
- [125] F. Wu, Z.B. Wang, Y.D. Cao, Q. Zhou, Y. Zhang, Z.L. Xu, X.Q. Zhu, "Expression of tumor antigens and heat-shock protein 70 in breast cancer cells after high-intensity focused ultrasound ablation," *Ann Surg Oncol*. 2007 Mar, vol. 14(3), pp.1237-42. Epub 2006 Dec 24.

- [126] Z. Jie, Z. Chun-liang, T. Jian-wen, Z. Ling, W. Hua, "Focal target controlling during high intensity focused ultrasound therapy based on respiratory gating," *Journal of Clinical Rehabilitative Tissue Engineering Research* vol. 15(43). Oct. 2011.
- [127] V. Auboiroux, L. Petrusca, M. Viallon, T. Goget, C.D. Becker, R. Salomir, "Ultrasonography-based 2D motion-compensated HIFU sonication integrated with reference-free MR temperature monitoring: a feasibility study ex vivo," *Physics in Medicine and Biology*, vol. 57(10), pp.159-171. May 2012.
- [128] R. Gassert, E. Burdet, K. Chinzei, "MRI-Compatible robotics– A Critical Tool for Image Guided Interventions, *Clinical Diagnostics and Neuroscience*," *IEEE Engineering in Medicine and Biology*, vol. 27, pp. 12-14. 2008.
- [129] J.F. Schenck, "The role of magnetic susceptibility in magnetic resonance imaging: MRI magnetic compatibility of the first and second kinds," *Med Phys.* vol. 23(6), pp. 815-850. 1996.
- [130] H. Fankhauser, D.H. Fankhauser, D. Glauser, P. Flury, Y. Piguet, M. Epitoux, J. Favre, R.A. Meuli, "Robot for CT-guided stereotactic neurosurgery," *Stereotactic and Functional Neurosurgery*, vol. 63(1-4), pp. 93-98. 1994.
- [131] T. Verghese, V. Palathinkara, M.B. Massat, J. McGill, M. Weichelt, "Innovation and Achievement in Advancing MR-guided Therapeutics," GE Signa Pulse, a GE Healthcare MR publication, pp. 64-68. 2011.
- [132] H. Cline, R. Ettinger, K. Rohling, R. Watkins, inventors, General Electric Company, assignee, Magnetic resonance guided focussed ultrasound surgery, United States patent, US 5247935. 1993.
- [133] R. Ettinger, H. Cline, R. Watkins, K. Rohling, inventors, General Electric Company, assignee, Magnetic resonance guided ultrasound therapy system with inclined track to move transducers in a small vertical space. United States patent, US 5275165. 1994.
- [134] K. Hynynen, W.R. Freund, H.E. Cline, A.H. Chung, R.D. Watkins, J.P. Vetro, F.A. Jolesz, "A clinical, noninvasive, MR imaging-monitored ultrasound surgery method," *Radiographics*, vol. 16(1), pp.185-195. 1996.
- [135] H. Cline, K. Rohling, W. Abeling, inventors, General Electric Company, assignee, Mechanical positioner for magnetic resonance guided ultrasound therapy United States patent, US5443068. 1995.
- [136] O. Yehezkeili, D. Freundlich, N. Magen, C. Marantz, Y. Medan, S. Vitek, A. Weinreb, inventors, INSIGHTEC-TXSONICSLTD, assignee, Mechanical positioner for MRI guided ultrasound therapy system WO0209812. 2002.
- [137] K. Chinzei, N. Hata, F.A. Jolesz, R. Kikinis, "MR Compatible Surgical Assist Robot: System Integration and Preliminary Feasibility Study," *Int Conf Med Image Comput Comput Assist Interv. (MICCAI)*, Pittsburgh, PA, USA, vol. 1935, pp. 921-930. 2000.
- [138] E. Hempel, H. Fischer, L. Gumb, T. Höhn, H. Krause, U. Voges, H. Breitwieser, B. Gutmann, J. Durke, M. Bock, A. Melzer, "An MRI-compatible surgical robot for precise radiological interventions," *Comput. Aided. Surg.*, vol. 8(4), pp. 180-191. 2003.
- [139] INNOMEDIC - Touch the future –Available: <http://www.innomedic.de/>
- [140] A. Melzer, B. Gutmann, T. Remmele, R. Wolf, A. Lukoscheck, M. Bock, H. Bardenheuer, H. Fischer, "INNOMOTION for percutaneous image-

- guided interventions: principles and evaluation of this MR- and CT-compatible robotic system,” *IEEE Eng Med Biol Mag*, vol. 27, pp. 66–73. 2008.
- [141] M. Moche, D. Zajonz, T. Kahn, B. Harald, “MRI-guided procedures in various regions of the body using a robotic assistance system in a closed-bore scanner: preliminary clinical experience and limitations,” *J. Magn. Reson. Imaging*, vol. 31(4), pp.964–974. 2010.
- [142] K. Cleary, A. Melzer, V. Watson, G. Kronreif, D. Stoianovici, “Interventional robotic systems: Applications and technology state-of-the art,” *Minimally Invasive Therapy & Allied Technologies* vol. 15(2), pp. 101-113. 2006.
- [143] A. Melzer, R. Seibel, “MR-guided treatment of degenerative spinal diseases,” *Minimally Invasive Therapy & Allied Technologies*, vol. 8(5), pp.89–93. 1999.
- [144] A. Melzer, B. Gutmann, A. Lukoscsek, M. Mark, W. Zylka, H. Fischer, “Experimental Evaluation of an MRI compatible Telerobotic System for CT MRI guided Interventions,” *Supplement to Radiology*, vol. 226, pp.409-444. 2003.
- [145] C. Moonen, “MRI-guided high intensity focused ultrasound (HIFU) An alternative form of non-invasive out-patient treatment in oncology,” *OncoSolutions*, vol. 1, pp.22-23. 2008.
- [146] R. Seip, N.T. Sanghvi, R. Carlson, J. Tavakkoli, K. Dines, T.A. Gardner, T. Uchida, “Sonablate 500: A Novel Platform for Transrectal Image-Guided HIFU Treatment of Localized Prostate Cancer,” presented at the 32nd Annual Symposium of the Ultrasonic Industry Association (UIA). Oct. 2002.
- [147] O. Yehezkeli, D. Freundlich, N. Magen, C. Marantz, Y. Medan, S. Vitek, A. Weinreb, inventors, TxSonics Ltd, assignee, Mechanical positioner for MRI guided ultrasound therapy system. United States patent, US 6,582,381. 2003.
- [148] N. Tsekos, inventor, Regents of the University of Minnesota, assignee, MRI-guided interventional mammary procedures. United States patent US 6, 675,037. 2004.
- [149] O.H. Pomeroy, K. Hynynen, S. Singer, et al., “MR-imaging guided focused ultrasound therapy for breast fibroadenomas: a feasibility study,” *Radiology*, vol.197, pp.331. 1995.
- [150] P. Huber, J. Jenne, R. Rastert, I. Simiantonakis, H.P. Sinn, H.J. Strittmatter, D. von Fournier, M. Wannemacher, J. Debus, “A new noninvasive approach in breast cancer therapy using magnetic resonance imaging-guided focused ultrasound surgery,” *Cancer research*, vol. 61, pp.8441-8447. 2001.
- [151] Y. Koseki, T. Washio, K. Chinzei, H. Iseki, “Endoscope manipulator for trans-nasal neurosurgery, optimized for and compatible to vertical field open MRI,” *Proc. Of MICCAI '02 Lecture Notes in Computer Science*. Vol.2488/2002, pp.114–21. 2002.
- [152] N. Hata, R. Hashimoto, J. Tokuda, S. Morikawa, “Needle guiding robot for MR-guided microwave thermotherapy of liver tumor using motorized remote-center-of-motion constraint,” *Proc. of IEEE International Conference on Robotics & Automation*. pp. 1652-1656, Barcelona, Spain. 2005.
- [153] R. Chopra, L. Curiel, R. Staruch, L. Morrison, K. Hynynen, “An MRI-compatible system for focused ultrasound experiments in small animal

- models,” American Association of Physicists in Medicine. DOI: 10.1118/1.3115680. 2009.
- [154] B. James, Dabney, L. Thomas, Harman, “Model-Based Control of Piezoelectric Ultrasonic Motors for Space Robotic Applications,” University of Houston, ISSO Annual Report, pp. 76-79. 2002.
- [155] C. Damianou, “*In vitro* and *in vivo* ablation of porcine renal tissues using High Intensity focused Ultrasound,” *Ultrasound in Med. Biol.* Vol.29 (9), pp.1321-1330. 2003.
- [156] R.S. Foster, R. Bihrlle, N.T. Sanghvi, J.P. Donohue, F.J. Fry, “High intensity focused ultrasound treatment of human BPH,” *Prog. Clin. Biol. Res.*, vol. 386, pp. 463-71. 1994.
- [157] A. Gelet, J.Y. Chapelon, R. Bouvier, C. Pangaud, R. Souchon, E. Blanc, D. Cathignol, J.M. Dubernard, “Preliminary results of the treatment of 44 patients with localized cancer of the prostate using transrectal focused ultrasound,” *Prog. Urol.*, vol. 8(1), pp.68-77. Feb. 1998.
- [158] C. Tempany, E. Stewart, N. McDannold, B. Quade, F. Jolesz, K. Hynynen, “MR imaging-guided focused ultrasound surgery of uterine leiomyomas: a feasibility study,” *Radiology*, vol.226, pp.897-905. 2003.
- [159] F. Wu, W.Z. Chen, J. Bai, J.Z. Zou, Z.L. Wang, H. Zhu, Z.B. Wang, “Pathological changes in human malignant carcinoma treated with high-intensity focused ultrasound,” *Ultrasound Med. Biol.*, vol.27(8), pp.1099-106. 2001.
- [160] A. Di Bisceglie, V. Rustgi, J. Hoofnagle, G. Dusheiko, M. Lotze, Hepatocellular carcinoma. *Ann Intern Med*, vol.108, pp.390-401. 1988.
- [161] J. Bruix, I. Civera, X. Calvet, J. Fuster, C. Bru, C. Ayuso, R. Vilara, L. Biox, J. Visa, J. Rodeg, “Surgical resection and survival in Western patients with hepatocellular carcinoma,” *J Hepatol*, vol.15, pp.350-355. 1992.
- [162] I.J. Rowland, I. Rivens, L. Chen, C.H. Lebozer, D.J. Collins, G.R. ter Haar, M.O. Leach, “MRI study of hepatic tumours following high intensity focused ultrasound surgery,” *British Journal of Radiology*, vol.70, pp.144-53. 1997.
- [163] P. Lele “Effects of ultrasound on solid mammalian tissues and tumours *in vivo*,” Plenum press, New York, pp.275-306. 1987.
- [164] K. Raum, W.D. O'Brien Jr., “Pulse-echo field distribution measurement technique for High-frequency ultrasound devices,” *IEEE Trans. Ultrasonics Ferroelectric Freq. control*, vol.44(4), pp.810-815. 1997.
- [165] C. Damianou, “*In vitro* and *in vivo* ablation of porcine renal tissues using High Intensity focused Ultrasound”, *Ultrasound Med Biol*; vol.29 (9), vol.1321-1330. 2003.
- [166] N.J. McDannold, F.A. Jolesz, K.H. Hynynen, “Determination of the optimal delay between sonications during focused ultrasound surgery in rabbits by using MR imaging to monitor thermal buildup *in vivo*,” *Radiology*, vol.211(2), pp.419-26. 1999.
- [167] B. Quesson, J. Zwart, C. Moonen, “Magnetic Resonance Temperature Imaging for Guidance of Thermotherapy,” *J. Magn. Reson. Imaging*; vol.12, pp.525–533. 2000.
- [168] N. McDannold, K. Hynynen, F. Jolesz, “MRI Monitoring of the Thermal Ablation of Tissue: Effects of Long Exposure Times,” *J. Magn. Reson. Imaging*, vol.13, pp.421–427. 2001.

- [169] L. Chen, D. Bouley, E. Yuh, H. D'Arceuil, K. Butts, "Study of focused ultrasound tissue damage using MRI and histology," *J. Magn. Reson. Imaging*, vol.10(2), pp.146-53. 1999.
- [170] N. McDannold, K. Hynynen, D. Wolf, G. Wolf, F.A. Jolesz, "MRI evaluation of thermal ablation of tumours with focused ultrasound," *J. Magn. Reson. Imaging*, vol.8(1), pp.91-100. 1998.
- [171] M.G. Mack, R. Straub, K. Eichler, K. Engelmann, S. Zangos, A. Roggan, D. Woitaschek, M. Bottger, T.J. Vogl, "Percutaneous MR imaging-guided laser-induced thermotherapy of hepatic metastases," *Abdom Imaging.*, vol.26(4), pp.369-74. 2001.
- [172] A.J. Aschoff, N. Rafie, J.A. Jesberger, J.L. Duerk, J.S. Lewin, "Thermal lesion conspicuity following interstitial radiofrequency thermal tumour ablation in humans: a comparison of STIR, turbo spin-echo T2-weighted, and contrast-enhanced T1-weighted MR images at 0.2 T," *J. Magn. Reson. Imaging.*, vol.12(4), pp.584-9. 2000.
- [173] A.J. Coleman, J.E. Saunders, "A review of the physical properties and biological effects of the high amplitude acoustic fields used in extracorporeal lithotripsy," *Ultrasonics*, vol.3, pp.75-89. 1993.
- [174] C. Damianou, N. Sanghvi, F. Fry, R. Maass, "Dependence of Ultrasonic attenuation and absorption in dog soft tissues on temperature and thermal dose," *Journal of Acoustical Society of America*, vol. 102(2), pp. 628-634. 1997.
- [175] A. Grasso, A.F. Watkinson, J.M. Tibballs, A.K. Burroughs, "Radiofrequency ablation in the treatment of hepatocellular carcinoma- a clinical viewpoint," *J. Hepatol.*, vol.33, pp.667-72. 2000.
- [176] T. Livraghi, S. Lazzaroni, F. Meloni, G. Torzilli, C. Vettori, "Intralesional ethanol in the treatment of unresectable liver cancer," *World J. Surg.*, vol.19, pp.801-806. 1995.
- [177] J.L. McCall, M.W. Booth, D.L. Morris, "Hepatic cryotherapy for metastatic liver tumors," *Br. J. Hosp. Med.* Vol.54, pp.378-381. 1995.
- [178] N. Yamanaka, E. Okamoto, T. Tanaka, T. Oriyama, J. Fujimoto, K. Furukawa, E. Kawamura, "Laparoscopic microwave coagulative necrosis therapy for hepatocellular carcinoma," *Surg. Laparosc. Endosc.*, vol.5, pp.444-449. 1995.
- [179] G.D. Dodd, M.C. Soulen, R.A. Kane, T. Livraghi, W.R. Lees, Y. Yamashita, A.R. Gillams, O.I. Karahan, H. Rhim, "Minimally invasive treatment of malignant hepatic tumors: at the threshold of a major breakthrough," *Radiographics*, vol.20, pp.9-27. 2000.
- [180] L. Solbiati, T. Livraghi, S.N. Goldberg, T. Lerace, F. Meloni, M. Dellanoce, L. Cova, E.F. Halpern, G.S. Gazelle, "Percutaneous radiofrequency ablation of hepatic metastases from colorectal cancer: long-term results in 117 patients," *Radiology*, vol.221, pp.159-166. 2001.
- [181] G. Vallancien, M. Harouni, B. Veillon, A. Mombet, D. Prapotnich, J.M. Brisset, J. Bougaran, "Focused extracorporeal pyrotherapy: Feasibility study in man," *J Endourol*, vol.6, pp.173-181. 1992.
- [182] F. Wu, W. Chen, J. Bai, "Effect of high-intensity focused ultrasound on patients with hepatocellular cancer - preliminary report," *Chinese J Ultrasonog*; vol.8, pp.213-216. 1999.
- [183] Li CX, Xu GL, Jiang ZY, Li JJ, Luo GY, Shan HB, Zhang R, Li Y. Analysis of clinical effect of high-intensity focused ultrasound on liver cancer. *World J Gastroenterol* 2004;10:2201-2204.

- [184] Stewart EA, Rabinovici J, Tempany CM, Inbar Y, Regan L, Gostout B, Hesley G, Kim HS, Hengst S, Gedroyc WM. Clinical outcomes of focused ultrasound surgery for the treatment of uterine fibroids, *Fertil Steril*. 2006; 85(1):22-9.
- [185] Schmitz A., Gianfelice D., Daniel B., Mali W., van den Bosch M. Image-guided focused ultrasound ablation of breast cancer: current status, challenges, and future directions, *Eur Radiol* 2008;18:1431–1441.
- [186] W.M. Gedroyc. Magnetic resonance guided focused ultrasound (MRgFUS) treatment of liver tumours. In: Coussios CC, editor. 6th International Symposium on Therapeutic Ultrasound. Oxford: AIP; 2006.
- [187] F. Jolesz, K. Hynynen, N. McDannold, D. Freundlich, D. Kopelman, “Noninvasive Thermal Ablation of Hepatocellular Carcinoma by Using Magnetic Resonance Imaging–Guided Focused Ultrasound”, *GASTROENTEROLOGY*, vol.127, pp.S242–S247. 2004.
- [188] D. Kopelman, Y. Inbar, A. Hanannel, D. Freundlich, D. Castel, A. Perel, A. Greenfeld, T. Salamon, M. Sareli, A. Valeanu, M. Papa, “Magnetic resonance-guided focused ultrasound surgery (MRgFUS): Ablation of liver tissue in a porcine model,” *European Journal of Radiology*, vol.59, pp.157–162. 2006.
- [189] A.H. Chung, K. Hynynen, V. Colucci, K. Oshio, H.E. Cline, F.A. Jolesz, “Optimization of spoiled gradient-echo phase imaging for *in vivo* localization of a focused ultrasound beam”, *Magn Reson Med.*, vol.36(5), pp.745-52. Nov. 1996.
- [190] Y Ishihara, A Calderon, H Watanabe, et al. “A precise and fast temperature mapping using water proton chemical shift”, *Magn Reson Med*, vol.34, pp.814-23. 1995.
- [191] N. Vykhodtseva, V. Sorrentino, F. Jolesz, R. Bronson, K. Hynynen, “MRI detection of the thermal effects of focused ultrasound on the brain,” *Ultrasound in Med. & Biol.*, Vol.26(5), pp.871–880. 2000.
- [192] *Abdominal Ultrasound: How, Why and When*, 3rd edition. Churchill Livingstone, A.J. Smith, China, 2010. ISBN-10: 0443069190, ISBN-13: 978-0443069192
- [193] C. Damianou, N. Milonas, V. HadjiSavas, A. Couppis, D. Iosif, K. Ioannides, “Thermal ablation system using High Intensity Focused Ultrasound (HIFU) and guided by MRI,” *CARS 2008 Computer Assisted Radiology and Surgery*, Barcelona, Spain , Jun. 25-28, 2008.
- [194] C. Damianou, “*In vitro* and *in vivo* ablation of porcine renal tissues using High Intensity focused Ultrasound *Journal of Ultrasound in Medicine and Biology*,” vol. 29 (9), pp. 1321-1330. 2003.
- [195] N.V. Tsekos, A. Özcan, E. Christoforou, “A Prototype Manipulator for Magnetic Resonance-Guided Interventions inside Standard Cylindrical Magnetic Resonance Imaging Scanners,” *J. Biomech. Eng.*, vol. 127(6), pp.972-981. 2005. doi:10.1115/1.2049339
- [196] E.G. Christoforou, C. Keroglou, I. Seimenis, N.V. Tsekos, E. Andreou, C. Pitris, E. Eracleous, “An approach to MR–guided interventions with a manually–operated manipulator,” 10th IEEE International Conference on Information Technology and Applications in Biomedicine (ITAB 2010), Corfu, Greece, 3-5. Nov.2010
- [197] N. Hata, J. Tokuda, S. Hurwitz, S. Morikawa, “MRI-compatible manipulator with remote-center-of-motion control,” *J. Magn. Reson. Imaging.*, vol. 27, pp. 1130–1138. 2008.

- [198] N.A. Watkin, S.B. Morris, I.H. Rivens, G.R. ter Haar. "High intensity focused ultrasound ablation of the kidney in a large animal model," J Endourol, vol. 11(3), pp. 191–196. 1997.
- [199] W.W. Roberts, T.L. Hall, K. Ives, J.S. Wolf Jr., J.B. Fowlkes, C.A. Cain. "Pulsed cavitation ultrasound: A noninvasive technology for controlled tissue ablation (histotripsy) in the rabbit kidney," J Urol, vol. 175(2), pp.734-738. 2006.
- [200] G. Vallancien, E. Chartier-Kastler, M. Harouni, D. Chopin, J. Bougaran, "Focused extracorporeal pyrotherapy: Experimental study and feasibility in man," Semin Urol. Vol. 11, pp.7-9. 1993.
- [201] M. Susani, S. Madersbacher, C. Kratzik, L. Vingers, M. Marberger "Morphology of tissue destruction induced by focused ultrasound," Eur Urol, vol. 23(Suppl 1), pp.34-38. 1993.
- [202] F. Wu, Z.B. Wang, W.Z. Chen, J. Bai, H. Zhu, T.Y. Qiao, "Preliminary experience using high intensity focused ultrasound for the treatment of patients with advanced stage renal malignancy" J Urol. vol.170(6 Pt 1), pp. 2237-2240. 2003.
- [203] M. Marberger, G. Schatzl, D. Cranston, J.E. Kennedy, "Extracorporeal ablation of renal tumours with high-intensity focused ultrasound," BJU Int, vol. 95(Suppl 2), pp.52-55. 2005.
- [204] A. Hacker, M.S. Michel, E. Marlinghaus, K.U. Kohrmann, P. Alken "Extracorporeally induced ablation of renal tissue by high-intensity focused ultrasound," BJU Int, vol. 97, pp.779-785. 2006.
- [205] C. Klingler, M. Susani, R. Seip, J. Mauermann, N. Sanghvi, M. Marberger "A Novel Approach to Energy Ablative Therapy of Small Renal Tumours: Laparoscopic High-Intensity Focused Ultrasound," European urology vol.53, pp. 810-818. 2008.
- [206] Taylor KJ, Connolly CC. Differing hepatic lesions caused by the same dose of ultrasound. J Pathol 1969; 98:291–293.
- [207] Linke CA, Carstensen EL, Frizzell LA, Elbadawi A, Fridd CW. Localized tissue destruction by high-intensity focused ultrasound. Arch Surg 1973; 107:887–891.
- [208] G.R. ter Haar, D. Robertson, "Tissue destruction with focused ultrasound *in vivo*," Euro Urol. vol. 23, pp. 8-11. 1993.
- [209] L. Chen, G.R. ter Haar, C.R. Hill, M. Dworkin, P. Carnochan, H. Young, J.P. Bensted, "Effect of blood perfusion on the ablation of liver parenchyma with high-intensity focused ultrasound," Phys Med Biol; vol.38, pp.1661-1673. 1993.
- [210] W.E. Moore, R-M Lopez, D.E. Mathews, P.W. Sheets, M.R. Etchison, A.S. Hurwitz, A.A. Chalian, F.J. Fry, D.W. Vane, J.L. Grosfeld "Evaluation of high-intensity therapeutic ultrasound irradiation in the treatment of experimental hepatoma," J Paediatr Surg; vol.24, pp.30–33. 1989.
- [211] G.R. ter Haar, I. Rivens, L. Chen, S. Riddler "High intensity focused ultrasound for the treatment of rat tumours," Phys Med Biol, vol.36, pp.1495-1501. 1991.
- [212] G.R. ter Haar, R.L. Clarke, M.G. Vaughan, C.R. Hill "Trackless surgery using focused ultrasound: Technique and case report," Minimal Invasiv Ther, vol 1, pp.13–19. 1991
- [213] F. Wu, Z.B. Wang, W.Z. Chen, J.Z. Zou, J. Bai, H. Zhu, K.Q. Li, C.B. Jin, F.L. Xie, H.B. Su, "Advanced hepatocellular carcinoma: Treatment with high-intensity focused ultrasound ablation combined with

- transcatheter arterial embolization,” *Radiology*, vol.235, pp.659-667. 2005.
- [214] V. Khokhlova, M. Bailey, J. Reed, B. Cunitz, P. Kaczkowski, L. Crum, “Effects of nonlinear propagation, cavitation, and boiling in lesion formation by high intensity focused ultrasound, in a gel phantom,” *J. Acoust. Soc. Am.* vol.119(3), pp. 1834-1848. March 2006.
- [215] C. Coussios, C. Farny, G.R. ter Haar, R. Roy, “Role of acoustic cavitation in the delivery and monitoring of cancer treatment by high-intensity focused ultrasound (HIFU),” *Int. J. Hyperthermia*, vol.23(2), pp. 105-120. 2007.
- [216] R. Salomir, J. Palussière, F.C. Vimeux, J.A. de Zwart, B. Quesson, M. Gauchet, P. Lelong, J. Pergrale, N. Grenier and C.T.W Moonen, “Local hyperthermia with MR-guided focused ultrasound: spiral trajectory of the focal point optimized for temperature uniformity in the target region.” *J. Magn. Reson. Imaging*, vol. 12, pp. 571-583. 2000.
- [217] G. ter Haar, “Ultrasound focal beam surgery,” *Ultrasound Med. Biol.* vol.21, pp.1089–1100. 1995.